2003-09-18

The Effect of Biopolymer Properties on Bacterial Adhesion: an Atomic Force Microscopy (AFM) Study

Nehal Ibrahim Abu-Lail
Worcester Polytechnic Institute

Worcester Polytechnic Institute

Department of Chemical Engineering

THE EFFECT OF BIOPOLYMER PROPERTIES ON BACTERIAL ADHESION: AN ATOMIC FORCE MICROSCOPY (AFM) STUDY

A Thesis in
Chemical Engineering

By
Nehal Ibrahim Abu-Lail

Submitted in Partial Fulfillment
Of the Requirements
for the Degree of

Doctor of Philosophy

September 12, 2003

Approved:

Terri A. Camesano, Ph.D. Advisor
Assistant Professor of Chemical Engineering
Worcester Polytechnic Institute

Approved:

Robert Thompson, Ph.D. Committee
Professor of Chemical Engineering
Worcester Polytechnic Institute

Approved:

William Clark, Ph.D. Committee
Associate Professor of Chemical Engineering
Worcester Polytechnic Institute

Approved:

John Bergendahl, Ph.D. Committee
Assistant Professor of Civil and
Environmental Engineering
Worcester Polytechnic Institute

Abstract

The effect of bacterial surface biopolymers on bacterial adhesion to surfaces was studied through experiments and modeling. Atomic Force Microscopy (AFM) provided the tool to measure the interaction forces between different bacterial cells and silicon nitride tips under different chemical conditions at a nanoscopic level. Two bacterial strains were considered: *Pseudomonas putida* KT2442 and *Escherichia coli* K-12 JM109. This study addressed the following issues: 1) the effect of solution ionic strength and solvent polarity on adhesion between *Pseudomonas putida* KT2442 and the silicon nitride AFM tip, 2) role of heterogeneity of bacterial surface biopolymers on bacterial adhesion, 3) role of lipopolysaccharides (LPS) on adhesion at three different scales: continuous, batch, and nanoscale, and 4) nature of interactions between *E. coli* JM109 and a model surface (silicon nitride tip).

To address the first issue, formamide, water, and methanol were used to investigate the effect of polarity on surface characteristics of biopolymers on the bacterial surface while a range of salt concentrations between that of water to 1 M KCl were used to study the effect of ionic strength. The adhesion increased with decreasing polarity of the solvent, indicating that the polymers on the bacterial surface are hydrophilic in nature. The adhesion was slightly affected by ionic strength variations up to a concentration of 0.1 M KCl; this may have been due to the fact that the ionic concentration in the solution did not counterbalance the ionic concentration in the biopolymer brush on the bacterial surface. However, a dramatic increase in the adhesion magnitude was observed when the salt concentration increased above 0.1 M KCl. This transition in adhesion with ionic strength from a low to high value induced a transition in the elasticity of the bacterial

surface biopolymers. The biopolymer brush layer did change from rigid to soft with increasing the ionic strength. The elasticity was quantified mainly by the use of the freely jointed chain (FJC) model.

Our interest in investigating the role of heterogeneity on adhesion developed from the results of the first study. The bacterial surface polymers were thought to be different in their chemical and physical nature since they were found to span a range of segment lengths. Analyzing the adhesion forces for *P. putida* KT2442 showed that the bacterial surface is heterogeneous. The heterogeneity was evident on the same cell surface and between different cells from the same population.

To resolve the third issue, approximately, 80% of the surface LPS of *E. coli* K-12 JM109 were removed by treating the cells with 100 mM ethylenediaminetetraacetic acid (EDTA). The effect of LPS removal on the adhesion of the cells to the silicon nitride tip was studied in water and phosphate buffered silane (PBS). The adhesion results from the AFM experiments were compared to batch retention experiments with glass as the substratum and column attachment experiments with columns packed with quartz sand. LPS controlled bacterial adhesion to the different surfaces in the study at three scales: batch, continuous, and nano-scale.

Finally, the nature of interactions between *E. coli* JM109 and a model surface (silicon nitride tip) were investigated in solvents of varying polarity (formamide, water, and methanol). The Young's modulus of elasticity for the bacterial surface was estimated by fitting of the Hertzian model to the force-indentation curves. Young's modulus values increased as the solvent polarity decreased, indicating a stiffer bacterial surface in lower polarity solvents. The average adhesion force in each solvent was negatively correlated

with the dielectric constant of the solvent, suggesting hydrophilic biopolymers. Specific and non-specific interaction forces between the AFM tip and the biopolymers were further characterized by applying a Poisson statistical analysis to the discrete adhesion data. The specific and non-specific interaction forces were the highest in methanol (-4 and -1.48 nN respectively). These values are in accordance with the high adhesion magnitude values measured with AFM in methanol. The results of my different studies emphasized the important role of AFM in studying biological interactions to different surfaces and in characterizing bacterial surface biopolymers.

Table of contents

List of Tables

List of Figures

Acknowledgments

This publication was made possible in part by grant number BES-0238627 from the National Science Foundation (NSF) CAREER Award and in part by grant number PRF #38988-G2 from the American Chemical Society (ACS). Its contents are solely the responsibility of the authors and do not necessarily represent official views of the funding agency.

I would like first to thank god for giving me the power and the support to continue this piece of work.

Next I would like to thank my advisor, Terri Camesano, for her continuous help, support, and understanding and for giving me the freedom to perform the research that I like and guide me throughout all the years of my Ph.D.

I would like to thank my committee members for reviewing the thesis.

I would like deeply to thank my parents, brother, and sisters for their love, unconditional support, trust, worries, and encouragement.

I would like also to thank many of my faithful friends for standing beside me through this period especially: Abhijit, Elizete, Ikram, and Maged.

Finally I would like to thank my labmates Ray, Bhupinder, and Laila for their help always and for many useful discussions.

Chapter 1

Introduction

1.1 Problem Statement and Research Objectives

The attachment of bacteria to surfaces plays an important role in many different applications. Examples of such applications are: environmental soil bioremediation [1, 2], the migration of pathogens in groundwater [3], controlling drinking water quality [4], and biomedical applications such as: adhesion to contact lenses [5] and other implanted or prosthetic devices [6, 7]. Although many researchers extensively studied the attachment of bacteria to different surfaces, predicting whether they will preferably attach to a given surface at a certain set of conditions is still not possible. This is because attachment might occur due to several mechanisms and under a wide range of chemical conditions [8]. The conformational changes in bacterial surface biopolymers [7, 9-11], as well as the effect of different forces such as van der Waals or electrostatic forces [12], steric interactions [13] and hydration forces and hydrogen bonding [14] are important factors influencing the variations in adhesion mechanisms.

Although earlier studies indicated that bacterial adhesion to surfaces might be controlled by polymer interactions [9, 13, 15-17], very little was known regarding the way biopolymer physical and chemical properties affect bacterial adhesion. In the first three chapters, my focus was on studying the adhesion of *Pseudomonas putida* KT2442 to a model surface, an atomic force microscopy (AFM) silicon nitride tip. *Pseudomonas putida* KT2424 was chosen as our first model bacterium due to two main factors. First, it is used widely for bioremediation, and second, it can be used as a model to quantify the effect of extracellular polysaccharides (EPS) on bacterial adhesion [18-20]. The second

model bacterium was *Escherichia coli* JM109 (Chapters five and six). The two models have lipopolysaccharides (LPS) on their surfaces but the surface of *E. coli* JM109 differs from the surface of *Pseudomonas putida* KT2442 because the former lacks the extracellular polysaccharides (EPS) component. *E. coli* JM109 is used in bioremediation and in biomedical applications [21].

With the use of these two bacterial models and atomic force microscopy (AFM) as the primary investigation tool, the first goal of my research (Chapter 2) was to study how the conformation of biopolymers on a bacterial surface changed with changing solution ionic strength and polarity, and to relate these changes to bacterial adhesion. Although earlier AFM studies looked at the change in conformation of model biopolymers [22-24] or synthetic polymers [25-27], very rarely was the conformation of biopolymers on the surface of a living cell considered [28]. Therefore, I studied the conformations of *Pseudomonas putida* KT2442 surface biopolymers under conditions of varying solvent polarity and ionic strength, in order to quantify the relationship between solution chemistry, physiochemical properties of the biopolymers, and bacterial adhesion.

While studying the elasticity of *Pseudomonas putida* KT2442 surface biopolymers, we learned that the bacterial surface is heterogeneous. Earlier studies have speculated that heterogeneity in cell surface LPS or EPS is the reason for a distribution of bacterial adhesion affinities to sand for a monoclonal population [17]. A bimodal distribution in the attachment efficiencies of bacteria with soil for a single population of cells has been observed in several systems [29-31]. Since no direct link between macromolecule heterogeneity and a distribution of attachment affinities has been demonstrated, my second goal (Chapter 3) was to present direct, single-molecule evidence of the

heterogeneity in polysaccharides on bacterial surfaces, at both the level of an individual bacterium and across a population of bacterial cells. This part of my study suggested that heterogeneity plays a key factor in explaining the inability to predict bacterial adhesion with existing models.

An interesting effect was observed during these studies, with respect to the role of ionic strength on the biopolymers. A slight effect of ionic strength on adhesion of *Pseudomonas putida* KT2442 to AFM silicon nitride tip in the range between that of pure water to 0.1 M KCl was observed, despite the negative zeta potential of both surfaces. We would have expected particle-particle repulsion to diminish as the ionic strength of the solution increased. Bulk investigations of bacterial attachment to similarly charged surfaces show that ionic strength usually affects the attachment probability, with less attachment seen in low ionic strength solutions because of increased long range electrostatic repulsion [16]. However in some other studies, the expected trend of increasing adhesion with increasing ionic strength was not observed. For example, cell adhesion or flocculation was seen at a finite salt concentration despite predictions of energy barriers that should have been too large to permit adhesion [32, 33]. Due to the discrepancy associated with effect of ionic strength on bacterial adhesion, the goal of the fourth part of my study was to further investigate the effect of higher salt concentrations (up to 1 M KCl) on the adhesion of *Pseudomonas putida* KT2442 to an AFM silicon nitride tip (Chapter 4). This part of my study suggested that the surface biopolymers of *Pseudomonas putida* KT2442 undergo a salt-induced transition in their flexibility from rigid to soft biopolymers and this was correlated with a transition from low to high adhesion.

LPS and proteins in the outer membrane of gram-negative bacteria, as well as EPS for some strains are the polymers that may influence adhesion. The LPS molecule is composed generally of an inner core, outer core, lipid layer and an O-antigen layer as the outmost portion of the LPS [21]. In previous work, removing the O-antigen portion of the LPS changed the way isogenic mutants attached to hydrophobic or hydrophilic polystyrene culture dishes [31, 34]. In other cases, the presence of LPS can facilitate adhesion through the formation of hydrogen bonds with the surface [35]. Conflicting results regarding whether LPS removal affects steric repulsion were previously reported. The interactions between lawns of *E. coli* K-12 strain *D21* (the parent) and mutant strain *D21f2* (which has truncated LPS) were studied. The presence of the LPS caused steric repulsion with a mica surface while the truncation of the LPS allowed for a hydrophobic attraction to be observed [15]. A second group studied the same mutant strains of *E. coli* plus an additional strain and observed no correlation between the length of the LPS and the amount of steric repulsion [36]. Due to this unresolved issue, my third goal (Chapter 5) was to study the effect of the removal of LPS from the surface of *E. coli* K-12 JM109 strain on bacterial adhesion and relate the AFM adhesion measurements at nano-scale to macroscopic adhesion measurements. Two macroscopic adhesion scales were studied: bacterial retention in a batch system (with glass as a substrate), and bacterial transport in porous media (quartz sand) under flow conditions. Our study was the first in which AFM adhesion forces were related to bacterial attachment at the batch and column scale.

The nature of the interactions between bacteria and surfaces is a function of many factors, including bacterial characteristics such as the type of surface biopolymers and their charge, substrate properties, and solvent properties. Many studies in the literature

addressed the effect of one or more of these factors on adhesion. In our previous manuscript on *E. coli* JM109, the effect of bacterial surface biopolymers on adhesion was investigated. In other studies in literature, changing the surface roughness and topography at the micron and submicron scale was shown to affect the strength of bacterial attachment to substrata [37]. Lateral changes of 0.1 μm in the surface topography were sufficient to affect the strength of bacterial attachment. An increase in applied force from 4 to 8 nN was necessary to move bacteria retained in surface defects of approximately 1 μm wide and 0.2 μm deep compared with cells attached on smooth surfaces [37]. In addition to the substrate roughness, the substrate's water contact angle has an effect on bacterial attachment. Bacterial adhesion was found to decrease with decreasing of contact angle on material substrates (increasing of surface free energy) [38]. Although the effect of bacterial surface properties and the substrate properties on adhesion has been subjected to many studies, many aspects of LPS properties and how they affect bacterial adhesion in different solvents are still unknown. Due to this lack of knowledge, the goal for this part of my study (Chapter six) was to investigate the nature of interactions between the LPS- bearing *E. coli* JM109 as a model bacterium to silicon nitride AFM tip as a model substratum in solvents with various polarities.

1.2 Literature Review

Bacterial adhesion is affected by many factors including the substrate type and charge[38], biopolymer properties, charge and heterogeneity [1, 17], solvent type, and other environmental conditions [39]. Among these factors, a focus is placed on the important role of bacterial surface biopolymers in controlling bacterial adhesion. AFM is used as our investigation tool since AFM can simultaneously provide information on

local surface properties and interaction forces [40]. Among the different biopolymer properties that can be studied with AFM are the conformation of the biopolymers, the hydrophilic/hydrophobic nature of biopolymers, and biopolymer heterogeneity. These properties can either be estimated by applying theoretical models to the AFM data or by statistical analysis of the AFM data. The different theories are briefly discussed below.

1.2.1 Elasticity of Biopolymers

Elastic properties of biopolymers can be estimated by applying biopolymer-stretching models to the AFM data. In the simplest model for polymer conformation, the polymer can be described as a Gaussian chain. The chain in this model is a random coil in which the distribution of the polymer conformation is independent of the microscopic structure of the molecule [41]. However, at higher forces, the sections of the chain are no longer oriented in random fashion, and the molecules become oriented along the direction of the external force. This case can be described using the freely jointed chain (FJC) model. The polymer is described as consisting of n rigid elements, each of length l_k, connected through flexible joints that are free to rotate in any direction (Figure 1.1A). This model takes into account entropic effects only. The FJC model has been successfully used to describe the elasticity of biopolymers such as dextran [22], oligonucleotides [42], and poly (dimethylsiloxane) [27].

The wormlike chain (WLC) can also be used to describe polymer elasticity. In this model, the polymer chain is considered to be continuously curved and the direction of the curvature at any point in the chain is random (Figure 1.1B). The chain in this model is intermediate between a rigid rod and a flexible coil. The WLC takes into account the local stiffness in the chain in terms of the persistence length (L_p) and the

long-range flexibility by adding an enthalpic term to the entropic term. In the WLC model, extension of the polymer is limited to the polymer's contour length. The WLC model has been successfully used to estimate the elasticity of some biopolymers, such as DNA [26, 27, 43].

In some cases, the extensible freely jointed chain (FJC+) model was used to account for elastic deformations of bonds and bond angles (enthalpic effects) that are neglected in the FJC model. The polymer is modeled as n identical springs in series (Figure 1.1C). Due to the enthalpic effects included in this model, the polymers can be stretched beyond their contour lengths. This model was used to estimate polymer elasticity for polymers such as polyvinyl alcohol in aqueous solution [25], and polyethylene glycol in hexadecane [44]. The FJC and WLC models have two fitting parameters, while the FJC+ model has three adjustable parameters. Comparison between the measured force data and the elastic models forces allows us to estimate the elasticity of the bacterial surface polymers.

1.2.2 Steric Interactions between the Biopolymers and the AFM Tip

In addition to the biopolymer's elasticity, two other properties of the bacterial surface biopolymers can be obtained from AFM force measurements. These properties are the brush layer thickness and grafting density of the biopolymers on the bacterial surface. A model developed by Alexander [45] and de Gennes [46] for grafted polymers at relatively high surface coverage and modified by Butt et al. [47] to describe the forces between a spherical AFM tip and a flat surface can be used to model the steric interactions between the AFM tip and cell surface polymers. The force per unit area

between two surfaces, only one of which is coated with polymer, is a function of the brush thickness, grafting density of the biopolymers, temperature, and tip radius.

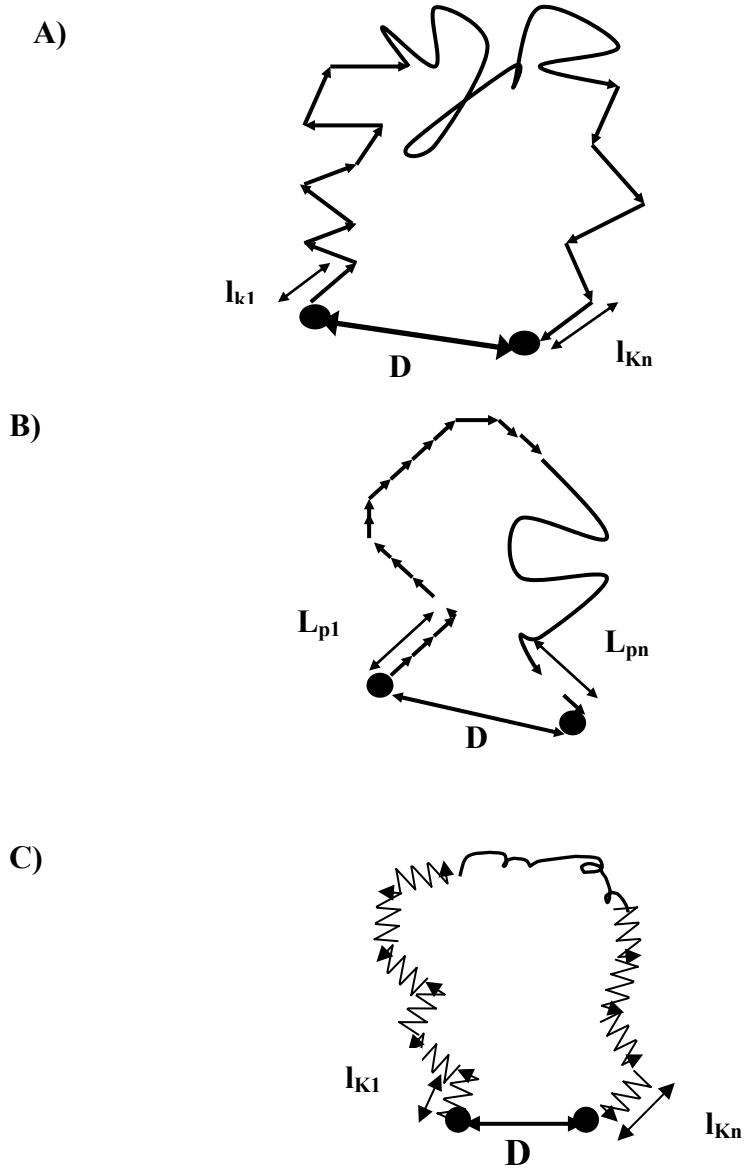

Figure 1.1. Diagrams show the different elastic models of polymers stretching. A) Freely jointed chain (FJC) model, B) Worm like chain (WLC) model, C) Extensible freely jointed chain (FJC+) model

1.2.3 Effect of Bacterial Biopolymers on Adhesion

Characterizing the different bacterial surface biopolymers properties such as their elasticity and conformation is so important. This importance arise from the fact that the presence and properties of bacterial surface biopolymers are known to influence bioadhesion to different surfaces including soil [17, 31, 48], biomaterials [49], and mammalian cells [50]. The properties of these biopolymers change with variations in solution chemistry such as ionic strength and pH. These changes lead to differences in adhesion. A discrepancy was always observed in literature regards the effect of ionic strength on adhesion. In some studies, increasing the ionic strength lead to an increase in the attachment probability of bacteria to similar charged surfaces [16]. However, in other studies, bacterial adhesion was indifferent to electrolyte concentration [33, 51].

Understanding how the biopolymer properties change with solution chemistry requires knowledge about the nature of the bacterial surface biopolymers. Often, the surface of gram negative bacterium is composed of lipopolysaccharides (LPS), proteins, and a layer of extracellular polysaccharides (EPS) in some strains. Lipopolysaccharides (LPS) cover ~ 45% of the surface of gram negative bacteria [52], and many bacterial surfaces have a layer of extracellular polysaccharides (EPS) [53]. For microbes without EPS, the O-antigen of the LPS is believed to be responsible for adhesion because it protrudes into the cell surrounding. Correlations between biopolymer size and adhesion have been observed. For example, the affinity of *E. coli* and *Citrobactor freundii* O-antigens for TiO_2 and Al_2O_3 increased as the molecular mass of the O-antigen increased [35]. A correlation between the size of the LPS molecule and the adhesion forces were found using mutants with varying LPS properties [15]. These studies show that the

conformation of the LPS on the bacterial surface can affect adhesion. The LPS layer on some bacterial types consists of more than one sugar type. These types vary in their conformation, molecular weight, and chemical behavior. For example, *E. coli* JM109's LPS layer consists of at least seven different oligosaccharides [54]. This variation in the LPS composition attributes to the heterogeneity seen on the bacterial surface and among the cell population.

In addition to characterizing the effect of solution chemistry on biopolymer properties, AFM can be used to probe the hydrophobicity of the biopolymers, and biopolymers heterogeneity. Studying the distribution of the adhesion affinities measured between the AFM silicon nitride tip and bacterial surface biopolymers can help in characterizing the heterogeneity. Applying statistical distribution models to the histograms of the adhesion affinities can minimize the effect of the heterogeneity and help in predicting bacterial adhesion. Different statistical models have been used in the literature to describe the heterogeneity in biopolymer characteristics. Previous studies of bacterial heterogeneity within a single population suggested that there may be a bimodal distribution in bacterial adhesion or in the properties of the biopolymers [17, 29, 30]. Other statistical models such as a normal distribution [75], gamma distribution [75], and Poisson distribution [75] can be used to describe the heterogeneity and minimize the effect of biopolymer heterogeneity on predicting bacterial adhesion.

1.2.4 Elasticity of the Cell

The elasticity of the underlying bacterial surface can also be quantified from AFM force measurements. The bacterial surface elasticity can be described by the Young's modulus, which can be evaluated from AFM measurements by applying the Hertzian model of

continuum mechanics of contact to the force-indentation curves [56, 57]. The Hertzian model describes the indentation of a non-deformable conical indenter (the AFM silicon nitride tip) into an infinitely deformable elastic half space (the bacterial surface). This approach of evaluating the Young's moduli from AFM experiments has been applied on multiple locations of *Saccharomyces cerevisiae* MUCL 38475 yeast cells in water. Young's modulus values that range between 0.6 ± 0.4 MPa to 6.1 ± 2.4 MPa were obtained [58]. Higher elastic moduli were reported on collapsed murein sacculi isolated from *E. coli* K-12 in the hydrated state (25 MPa) also using AFM. The high value obtained for the elastic modulus on the peptidoglycan strands in the sacculus was in excellent agreement with theoretical calculations on peptidoglycan network [59]. Measurements on the proteinaceous sheath of the archaebacterium *Methanospirillum hungatei* GP1 gave Young's moduli of 20 to 40 GPa using AFM [60].

1.2.5 Bacterial Adhesion

1.2.5.1 AFM Studies

A study that compared the adhesion of *Lactococcus lactis* in the exponential and stationary growth phases on glass and polystyrene to the adhesion of *L. lactis* to AFM probes showed that bacterial adhesion is influenced by the force applied when the cell comes in contact with the substratum. This may affect the relevance of adhesion tests in laminar conditions with respect to real situations [61]. This study pointed out that the differences between the classical approaches of cell adhesion and the AFM studies should not be ignored. The classical cell adhesion methods, represented by batch retention experiments, column transport experiments, and laminar flow studies, were until recently the main methods to quantify bacterial adhesion. The batch retention of bacterial cells is

simply quantified by counting the number of cells retained on the substratum after a certain amount of time.

1.2.5.2 Attachment during Flow

In column transport experiments, the one dimensional colloid filtration theory [62] is usually used to calculate the collision efficiency. Collision efficiency is the fraction of striking bacteria that attach to the collector surface. The effect of diffusion, neighboring particles, London-van der Waals interactions, interception, and gravitational settling is considered in calculating the collector efficiency [63, 64].

1.2.6 Statistical Analysis of AFM data

Statistical analysis of the AFM force measurements by different techniques can provide a wealth of information on the microscopic and macroscopic quantities that affect bacterial adhesion. The individual strength of bonds formed between the AFM tip and the bacterial surface biopolymers during the contact in liquid medium can be estimated from the discrete pull-off forces. Several approaches that rely either on a quantized distribution of discrete single-bond contact forces or on the histogram distribution of rupture forces have been used in the literature to determine the individual bond forces for different systems including ligand-receptor interactions [65-67]. These approaches require at least several hundreds of force measurements to be performed and hence require a long measurement time and might damage the sample surface due to repetitive contact [68].

Another approach, which does not rely upon the resolution of the measurements and can be used to quantify the individual strength of bond forces, is derived based on Poisson statistics [68-74]. The method is based on statistically analyzing the AFM pull-off events. Applying a Poisson distribution to the data can lead to an accurate estimation

of the individual bond strengths and can provide detailed information on the magnitude of specific and non-specific forces [68-74] that are involved in the interaction between the tip and the bacterial surface.

With knowledge of the magnitude of the specific forces, non-specific forces, and solvent properties, the significance of different interaction forces in controlling bacterial adhesion can be determined. Depending on the solvent type, the specific forces may include van der Waals interactions, acid-base interactions, and hydrogen bonding. Non-specific forces are long range in nature, such as electrostatic interactions.

Besides quantifying individual bond forces, several recent efforts have used statistical approaches to relate micro- and nanoscopic measurements of adhesion and interaction forces to macroscopic properties of the bacterium-substrate system. For example, the repulsive forces probed with AFM upon approach of the tip to the bacterial surface were correlated to the activation barrier that governs the initial attachment of the bacterium to the glass [55]. Furthermore, the maximum distances at which the attractive forces are probed with AFM tip upon retraction as well as the equilibrium lengths of the bacterial surface biopolymers obtained by steric analysis upon approach were in good relation with area blocked by an adhering bacterium [55].

1.2.7 Force Balances and Interaction Energy

As the final step to control bacterial adhesion, an incorporation of the bacterial properties, substrate properties, and solution characteristics in one model to evaluate the role of different types of interaction forces on adhesion is of extreme importance. Typically, bacterial adhesion to a surface has been described by the Derjaguin-Landau-Verwey-Overbeek (DLVO) theory of colloidal stability. The interactions in this theory

are a balance between London-van der Waals (usually attractive forces) and electrostatic (repulsive forces) physiochemical interactions [76]. However, often only qualitative or inconsistent correlations are observed between bacterial adhesion and the van der Waals and /or electrostatic properties of the substrate [77-81]. Other forces that include steric interactions, specific ion effects, non-charge transfer Lewis acid base interactions, hydration forces, hydration pressure, hydrogen bonding, and the hydrophobic effect may also come into play [12, 82]. To include the hydrophobic interactions and hydration forces between the bacteria and the substrate, an extended DLVO theory was proposed by van Oss [83].The theory takes into account the acid-base interactions that arise due to the nature of the solvent in which the interactions take place. Although the DLVO theory was extended with an additional force term, these types of interactions were shown to be negligible in many cases especially for hydrophilic/ substrata combinations [16, 17]. In summary, neither DLVO nor extended DLVO theories showed an ability to fully describe the effect of biopolymers conformation, bacterial softness, or the effect of solvent type on bacterial adhesion.

To overcome the limitations of the DLVO theory, as it is applied to bacteria, Ohshima developed the soft-particle DLVO theory to help explain the interactions between soft biological particles and surfaces [84-90]. The theory assumes the presence of an ion-penetrable, charged polyelectrolyte layer around a rigid core. Since the outer membrane of the bacteria is composed of LPS, proteins, and phospholipids [8], the surface has a non-uniform distribution of charge, and therefore the zeta potential is an inaccurate measure of the surface potential. By fitting the soft-particle theory to the electrophoretic mobility data as a function of ionic strength, a surface potential value can

be obtained. Earlier studies used to rely on Smoluchowski formula to calculate the surface potential of the bacterium. According to the Smoluchowski formula, the surface potential is expressed as zeta potential and depends only on the viscosity of the medium which the measurements took place in. A comparison of the surface potentials from conventional theory (Smoluchowski formula) [85] and soft-particle calculations showed that conventional theory always predicted higher surface potentials for the bacteria. Lower energy barriers were obtained when the energy calculations were performed with surface potentials obtained from the soft-particle calculations than when zeta potential values were used [91].

Only recently, the importance of non-DLVO interactions in influencing colloidal interactions has been recognized [14, 92]. Steric interactions are an important type of interaction; their importance in affecting bacterial adhesion is starting to be recognized now that AFM provides a way to quantify such interactions. Steric interactions between the AFM tip and the bacterial surface polymers are modeled using a scaling relation developed for grafted polymers at relatively high surface coverage. This model has been developed to account for the force per unit area between two surfaces [45, 46]. The model was modified to describe the forces between a spherical AFM tip and a flat surface by integrating the force per unit area over the tip surface [47].

1.3 Organization of the Dissertation

This dissertation represents manuscripts that I have written during the course of my Ph.D. Chapter 2 is a manuscript that has been published in *Langmuir,* **2002***, 18,* 4071-4081, entitled “Elasticity of *Pseudomonas putida* KT2442 Surface Polymers Probed with Single-Molecule Force Microscopy” by N.I. Abu-Lail and T.A. Camesano. My goal

during this study was to probe how the conformation of bacterial surface polymers changed as a function of changing solvent polarity and ionic strength. In addition, I quantified the adhesion magnitudes between silicon nitride tips and *Pseudomonas putida* KT2442 in different solvents. To achieve our goal, the elasticity of *Pseudomonas putida* KT2442 polymers was measured by AFM in solvents spanning a range of polarity (formamide, water, and methanol) and ionic strengths (water, 0.01 M KCl, and 0.1 M KCl). The FJC and WLC models were used to estimate polymer segment or persistence lengths. Adhesion forces between the polymer chains and AFM silicon nitride tips were compared in these solvents. By the end of this study we demonstrated that AFM could be used successfully to probe the elasticity of bacterial surface polymers under different solvents. We found the polymers on the surface of *Pseudomonas putida* KT2442 to be very flexible, hydrophilic in nature, and cellulose-like structures. The adhesion of the bacterial surface biopolymers to the AFM tip was slightly affected by solution ionic strengths up to 0.1 M KCl. This observation directed our attention to the need for studying the effect of salt concentration on bacterial adhesion more thoroughly. We also pointed out the need for bacterial attachment models that can relate bacterial adhesion to polymer properties and polymer heterogeneity. I designed the experiments for this study in conjunction with Dr. Camesano, performed the experiments and analyzed the data, and the paper was written by me and Dr. Camesano.

The heterogeneity of the polymers on the bacterial surface became evident after observing the variations in the properties of the surface polymers of *Pseudomonas putida* KT2442. For example, we observed variations in the estimated persistence lengths (WLC) or segment lengths (FJC) for the polymers in different solvents. We also observed

a distribution of polymer molecular weights, obtained by size exclusion chromatography. This work was published as the manuscript given in Chapter 3, "Heterogeneity in Bacterial Surface Polysaccharides, Probed on a Single-Molecule Basis" in *Biomacromolecules,* **2002***, 3,* 661-667 by T.A. Camesano and N.I. Abu-Lail. I performed the experiments and analyzed the data with Dr. Camesano. The paper was written by me and Dr. Camesano. We presented in our paper quantitative evidence of the heterogeneity in polysaccharides on bacterial surfaces, at both the levels of an individual bacterium and among a population of bacterial cells.

To clarify the role of ionic strength on bacterial adhesion, further AFM measurements between *Pseudomonas putida* KT2442 and AFM silicon nitride tip at higher ionic strength concentrations were performed. This slight effect of low salt concentration on adhesion of *Pseudomonas putida* KT2442 to the AFM tip was hypothesized to be the result of an imbalance between the ion concentrations in the solvent and inside the biopolymer brush. Our hypothesis was confirmed, when a large increase in the adhesion between *Pseudomonas putida* KT2442 and the AFM silicon nitride tip was observed at higher salt concentrations (0.10 M – 1 M KCl). The results of this study showed that the biopolymers on the surface of *P. putida* KT2442 undergo a salt-induced conformational change from a soft random structure in low ionic strength solutions to an ordered, rigid structure in the presence of salt. Accompanying this conformational change, the adhesion behavior of the polymers changes. Greater adhesion forces are observed between the biopolymers and the AFM tip in high ionic strength solutions. A demonstration of the important effect of the conformational changes in biopolymers that occur due to the salt concentration in solution was published in the

manuscript given in Chapter 4, "Role of Ionic Strength on the Relationship of Biopolymer Conformation, DLVO Contributions, and Steric Interactions to Bioadhesion of *Pseudomonas putida* kT2442 in "*Biomacromolecules,* **2003,** *4(4),* 1000-1012 by N.I. Abu-Lail and T.A. Camesano. I performed the experiments and analyzed the data. The paper was written by me and Dr. Camesano. The paper pointed out the need to include the effect of salt concentration on adhesion in bacterial adhesion models.

In the first three manuscripts, I focused on studying bacterial adhesion with *Pseudomonas putida* KT2442 as a model. In the next two manuscripts, *E. coli* JM109 was used as the bacterial model. The first manuscript *E. coli* manuscript developed from my interest in clarifying the effect of LPS on bacterial adhesion. This interest developed after I read a paper about removing LPS from *E. coli* K-12 JM109 (55). My goal for this study was to investigate the effect of LPS on bacterial adhesion at batch and continuous scales. Adhesion measurements by AFM were compared to the extent of transport of the same cells through a quartz sand column and to the degree of retention to glass in batch systems. Experiments were performed on intact *E. coli* and on cells in which the LPS was removed. This work, described in Chapter 5 was published in *Environmental Science & Technology,* **2003***, 37,* 2173-2183. The manuscript is entitled "The Role of Lipopolysaccharides in the Adhesion, Retention, and Transport of *Escherichia Coli* JM109" by N. I. Abu-Lail and T. A. Camesano. I designed and executed the experiments and analyzed the data. The manuscript is written by me and Dr. Camesano. We concluded that LPS controlled the bacterial adhesion on both batch and continuous levels and that the differences in adhesion could be directly measured with AFM.

The second manuscript on *E. coli* JM109 shows our interest to better understand the nature of the interactions between *E. coli* JM109 and a model surface under different types of solvents. Our interest in exploring the nature of these interactions developed after we measured high adhesive forces between *E. coli* JM109 surface polymers (highly charged) and the AFM silicon nitride tip in methanol. My goal for this part was to explain how the type of solvent and the charge of the bacterial surface affect the nature and type of forces that control the attachment of the bacteria to a model surface. The result of this study is described in Chapter 6, as a manuscript that is in preparation for submission to Langmuir. The manuscript is entitled "Nature of the Interaction Forces between *Escherichia coli* JM109 and a Model Surface" by N. I. Abu-Lail and T. A. Camesano. I designed and executed the experiments and analyzed the data. The manuscript is written by me and Dr. Camesano. We concluded from this work that the conformation of bacterial surface biopolymers directly affect bacterial elasticity and adhesion. Increasing the solvent polarity decreased the adhesion of the bacterium to the model surface and decreases the stiffness of the bacterial surface.

Finally, I summarized my work and the main conclusions as well as recommendations for further study in Chapter 7.

1.4 References

1. Decho, A.W., *Exopolymer microdomains as a structuring agent for heterogeneity within microbial biofilms.* Microbial Sediments, 2000: p. 9-15.
2. Schramm, A., L.H. larsen, N.P. Revcbech, N.B. Ramsing, R. Amann, and K.H. Schleifer, *Structure and function of a nitrifying biofilm as determined by in situ hybridization and the use of microelectrodes.* Applied and Environmental Microbiology, 1996. **62**(12): p. 4641-4647.
3. Gerba, C.P. and G. Bitton, *Microbial Pollutants: Their survival and transport pattern to groundwater*, in *Groundwater Pollution Microbiology*, G.B.a.C.P. Gerba, Editor. 1984, Wiley Interscience: New York. p. 65-88.
4. Dawson, D.J. and D.P. Sartory, *Microbiology safety of water.* British Medical bulletin, 2000. **56**(1): p. 74-83.
5. Garcia-Saenz, M.C., A. Arias-Puente, M.J. Fresnadillo-martinez, and B. Paredes-Garcia, *Adherenc of two strains of Staphylococcus epideridis to contact lenses.* Cornea, 2002. **21**(5): p. 511-515.
6. Guo, A., L.L. Rife, N.A. Rao, and R.E. Smith, *Anterior segment prosthesis development:evaluation of expanded polytetrafluorethylene as a sclera-attached prosthetic material.* Cornea, 1996. **15**(2): p. 210-214.
7. Nablo, B.J., T.-Y. Chen, and M.H. Schoenfisch, *Sol-gel derived nitric oxide releasing matrials that reudce bacterial adhesion.* J. Am. Chem. Soc., 2001. **123**: p. 9712-9713.

8. Fletcher, M., *Bacterial attachment in aquatic environments: a diversity of surfaces and adhesion strategies*, in *Bacterial Adhesion: Molecular and Ecological Diversity*, M. Fletcher, Editor. 1996, Wiley-Liss, Inc.: New York.

9. Jucker, B.A., H. Harms, and A.J.B. Zehnder, *Polymer interactions between five gram-negative bacteria and glass investigated using LPS micelles and vesicles as model systems.* Colloids and Surfaces B: Biointerfaces, 1998. **11**: p. 33-45.

10. Jucker, B.A., A.J.B. Zehnder, and H. Harms, *Adsorption of bacterial surface polysaccharides on mineral oxides is mediated by hydrogen bonds.* Environmental Science & Technology, 1998. **32**: p. 2909-2915.

11. Fletcher, M. and A.W. Decho, *Biofilms.* Encyclopedia of Life Sciences, www.els.net, 2001.

12. Israelachvili, J.N., *Intermolecular & Surface Forces (2nd edition)*. 1992, New York: Academic Press.

13. Camesano, T.A. and B.E. Logan, *Probing bacterial electrosteric interactions using atomic force microscopy.* Environmental Science & Technology, 2000. **34**: p. 3354-3362.

14. Grasso, D., K. Subramanian, M. Butkus, K.A. Strevett, and J. Bergendahl, *A review of non-DLVO interactions in environmental colloidal systems.* Re/Views in Environmental Science & Bio/Technology, 2002. **1**: p. 17-38.

15. Ong, Y.-L., A. Razatos, G. Georgiou, and M.M. Sharma, *Adhesion forces between E. coli bacteria and biomaterial surfaces.* Langmuir, 1999. **15**: p. 2719-2725.

16. Rijnaarts, H.H.M., W. Norde, J. Lyklema, and A.J.B. Zehnder, *DLVO and steric contributions to bacterial deposition in media of different ionic strengths.* Colloids and Surfaces B: Biointerfaces, 1999. **14**: p. 179-185.

17. Simoni, S.F., H. Harms, T.N.P. Bosma, and A.J.B. Zehnder, *Population heterogeneity affects transport of bacteria through sand columns at low flow rates.* Environmental Science & Technology, 1998. **32**: p. 2100-2105.

18. Eberl, L., A. Ammendola, M.H. Rothballer, M. Givskov, C. Sternberg, M. Kilstrup, K.-H. Schleifer, and S. Molin, *Inactivation of gltB abolishes expression of the assimilatory nitrate reductase gene (nasB) in Pseudomonas putida KT2442.* Applied and Environmental Microbiology, 2000. **182**: p. 3368-3376.

19. Huijberts, G.N.M., G. Eggink, P. D_E Waard, G.W. Huisman, and B. Withholt, *Pseudomonas putida KT2442 cultivated on glucose accumulates poly(3-Hydroxyalkanoates) consisting of saturated and unsaturated monomers.* Applied and Environmental Microbiology, 1992. **58**(2): p. 536-544.

20. Givskov, M., L. Eberl, S. Møller, L.K. Poulsen, and S. Mølin, *Responses to nutrient starvation in Pseudomonas putida KT2442: Analysis of general cross-protection, cell shape, and macromolecular content.* Journal of Bacteriology, 1994. **176**: p. 7-14.

21. Amro, N.A., L.P. Kotra, K. Wadu-Mesthridge, A. Bulychev, S. Mobashery, and G. Liu, *High resolution imaging atomic force microscopy studies of Escherichia coli outer membrane: Structural basis for permeability.* Langmuir, 2000. **16**: p. 2789-2796.

22. Rief, M., F. Oesterhelt, B. Heymann, and H.E. Gaub, *Single molecule force spectroscopy on polysaccharides by atomic force microscopy.* Science, 1997. **275**(5304): p. 1295-?

23. Marko, J.F., E.D. Siggia, and S. Smith, *Entropic elasticity of lambda-phage DNA.* Science, 1994. **265**: p. 1599-1600.

24. Li, H., M. Rief, F. Oesterhelt, and H. Gaub, *Single-molecule force spectroscopy on xanthan by AFM.* Advanced Materials, 1998. **3**(4): p. 316-319.

25. Li, H., W. Zhang, X. Zhang, J. Shen, B. Liu, C. Gao, and G. Zao, *Single molecule force spectroscopy on poly(vinyl alcohol) by AFM.* Macromol. Rapid. Commun., 1998. **19**: p. 609-611.

26. Ortiz, C. and G. Hadziioannou, *Entropic elasticity of single polymer chains of poly(methylacrylic acid) measured by atomic force microscopy.* Macromolecules, 1999. **32**: p. 780-787.

27. Senden, T.J., J.-M. di Meglio, and P. Auroy, *Anomalous adhesion in adsorbed polymer layers.* Eur. Phys. J. B., 1998. **3**: p. 211-216.

28. Van der Aa, B.C., R.M. Michel, M. Asther, M.T. Zamora, P.G. Rouxhet, and Y.F. Dûfrene, *Stretching cell surface macromolecules by atomic force microscopy.* Langmuir, 2001. **17**: p. 3116-3119.

29. Baygents, J.C., J. Glynn, J. R., O. Albinger, B.K. Biesewmeyer, K.L. Ogden, and R.G. Arnold, *Variation of surface charge density in monoclonal bacterial populations: implications for transport through porous media.* Environmental Science & Technology, 1998. **32**: p. 1596-1603.

30. Bolster, C.H., A.L. Mills, G.M. Hornberger, and J. Herman, *Effect of intra-population heterogeneity on the long distance transport of bacteria.* Ground Water, 2000. **38**: p. 370-375.

31. Williams, V. and M. Fletcher, *Pseudomonas fluorescens adhesion and transport through porous media are affected by lipopolysaccharide composition.* Applied and Environmental Microbiology, 1996. **62**: p. 100-104.

32. Zita, A. and M. Hermansson, *Effects of ionic strength on bacterial adhesion and stability of flocs in a wastewater activated sludge system.* Applied and Environmental Microbiology, 1994. **60**: p. 3041-3048.

33. Smets, B.F., D. Grasso, M.A. Engwall, and B.J. Machinist, *Surface physicochemical properties of Pseudomonas fluorescens and impact on adhesion and transport through porous media.* Colloids and Surfaces B: Biointerfaces, 1999. **14**: p. 121-139.

34. Pringle, J.H. and M. Fletcher, *Influence of substratum hydration and adsorbed macromolecules on bacterial attachment to surfaces.* Appl. Environ. Microbiol., 1986. **51**(6): p. 1321-1325.

35. Jucker, B.A., H. Harms, S.J. Hug, and A.J.B. Zehnder, *Adsorption of bacterial surface polysaccharides on mineral oxides is mediated by hydrogen bonds.* Colloids and Surfaces B: Biointerfaces, 1997. **9**: p. 331-343.

36. Velegol, S.B. and B.E. Logan, *Contributions of bacterial surface polymers, electrostatics, and cell elasticity to the shape of AFM force curves.* Langmuir, 2002. **18**: p. 5256-5262.

37. Boyd, R.D., J. Verran, M.V. Jones, and M. Bhakoo, *Use of the AFM to determine the effect of substratum surface topography on bacterial adhesion.* Langmuir, 2002. **18**(6): p. 2343-2346.

38. Morimoto, M. *The effect of the surface free energy of materials on adhesion of bacterial cells.* in *ACS National Meeting*. 1996. Orlando, Florida, August 25-29: American Chemical Society, Washington, D.C.

39. Marshall, K.C., *Mechanisms of BActerial Adhesion at Solid-Water Interfaces*, in *Bacterial Adhesion: Mechanisms and Physiological Significance*. 1985, Plenum Press: New York. p. 133-161.

40. Dufrêne, Y.F., *Application of atomic force microscopy to microbiological surfaces: from reconstituted cell surface layers to living cells (Review).* Micron, 2001. **32**: p. 152-165.

41. Janshoff, A., M. Neitzert, Y. Oberdorfer, and H. Fuchs, *Force spectroscopy of molecular systems-single molecule spectroscopy of polymers and biomolecules.* Angew. Chem. Int. Ed., 2000. **39**: p. 3212-3237.

42. Lee, G.U., L.A. Chrisey, and R.J. Colton, *Direct measurement of the forces between complementary strands of DNA.* Science, 1994. **266**: p. 771-773.

43. Marko, J.F. and E.D. Siggia, *Stretching DNA.* Macromolecules, 1995. **28**: p. 8759-8770.

44. Oesterhelt, F., M. Rief, and H.E. Gaub, *Single molecule force spectroscopy by AFM indicates helical structure of poly(ethylene-glycol) in water.* New Journal of Physics, 1999. **1**: p. 6.1-6.11.

45. Alexander, S., *Adsorption of chain molecules with a polar head a scaling description.* Journal de Physique (Paris), 1977. **38**(8): p. 983-987.

46. de Gennes, P.G., *Polymers at an interface: A simplified view.* Advances in Colloid and Interface Science, 1987. **27**: p. 189-209.

47. Butt, H.-J., M. Kappl, H. Mueller, and R. Raiteri, *Steric forces measured with the atomic force microscope at various temperatures.* Langmuir, 1999. **15**: p. 2559-2565.

48. D_EFlaun, M.F., A.S. Tanzer, A.L. McAteer, B. Marshall, and S. Levy, *Development of an adhesion assay and characterization of an adhesion-deficinet mutant of Pseudomonas fluorescens.* Applied and Environmental Microbiology, 1990. **56**(1): p. 112-119.

49. Triandafillu, K., D.J. Balazs, B.-O. Aronsson, P. Descouts, P. Tu Quoc, C. van Delden, H.J. Mathieu, and H. Harms, *Adhesion of Pseudomonas aeruginosa strains to untreated and oxygen-plasma treated poly(vinyl chloride) (PVC) from endotracheal intubation devices.* Biomaterials, 2003. **24**(8): p. 1507-1518.

50. Henriksson, A., R. Szewzyk, and P.L. Conway, *Characteristics of the adhesive determinants of Lactobacillus fermentum 104.* APPLIED AND ENVIRONMENTAL MICROBIOLOGY, 1991. **57**(2): p. 499-502.

51. Poortinga, A.T., R. Bos, and H.J. Busscher, *reversibility of bacterial adhesion at an electrode surface.* Langmuir, 2001. **17**: p. 2851-2856.

52. DiRienzo, J.M., K. Nakamura, and M. Inouye, *The outer membrane proteins of gram-negative bacteria:biosynthesis, assembly, and functions.* Ann. Rev. Biochem., 1978. **47**: p. 481-532.

53. Neidhardt, F.C., J.L. Ingraham, and M. Schaechter, *Physiology of the Bacterial Cell: A Molecular Approach*. 1990, Sunderland, MA: Sinauer Associates.

54. Phillips, N.J., T.J. Miller, J.J. Engstrom, W. Melaugh, R. McLaughlin, M.A. Apicella, and B.W. Gibson, *Characterization of chimeric LPS from E. coli strain JM109 Transformed with lipooligasaccharide synthesis genes (lsg) from Haemophilus influenzae.* The Journal of Biological Chemistry, 2000. **275**(7): p. 4747-4758.

55. Vadillo-Rodriguez, V., H.J. Busscher, W. Norde, J. de Vries, and H.C. van der Mei, *On relations between microscopic and macroscopic physiochemical properties of abcterial cell surfaces: An AFM study on Streptococcus mitis strains.* Langmuir, 2003. **19**: p. 2372-2377.

56. Hertz, H.J., Reine Angew. Math., 1882. **92**: p. 156.

57. Johnson, K.L., *Contact Mechanics*. 1985, Cambridge: Cambridge University Press. 452.

58. Touhami, A., B. Nysten, and Y.F. Dufrene, *Nanoscale mapping of the elasticity of microbial cells by AFM.* Langmuir, 2003. **19**: p. 4539-4543.

59. Yao, X., M. Jericho, D. Pink, and T. Beveridge, *Thickness and elasticity of gram-negative murein sacculi measured by atomic force microscopy.* Journal of Bacteriology, 1999. **181**(22): p. 6865-6875.

60. Xu, W., P.J. Mulhern, B.L. Blackford, M.H. Jericho, M. Firtel, and T.J. Beveridge, *Modeling and measuring the elastic properties of an archael surface, the sheath of Methanospirillum hungatei, and the implication for methane production.* Journal of Bacteriology, 1996. **178**: p. 3106-3112.

61. Boonaert, C.J.P., Y.F. Dufrêne, S.R. Derclaye, and P.G. Rouxhet, *Adhesion of Lactococcus lactis to model substra: direct study of the interface.* Colloids and Surfaces B: Biointerfaces, 2001. **22**: p. 171-182.

62. Yao, K.-M., M.T. Habibian, and C.R. O'Melia, *Water and waste water filtration: Concepts and applications.* Environmental Science & Technology, 1971. **5**: p. 1105-1112.

63. Rajagopalan, R. and C. Tien, *Trajectory analysis of deep-bed filtration with the sphere-in-cell porous media model.* AIChE Journal, 1976. **22**: p. 523-533.

64. Jewett, D.G., T.A. Hilbert, B.E. Logan, R.G. Arnold, and R.C. Bales, *Bacterial transport in laboratory columns and filters: influence of ionic strength and pH on collision efficiency.* Water Research, 1995. **29**(7): p. 1673-1680.

65. Hoh, J.H., J.P. Cleveland, C.B. Prater, J.-P. Revel, and P.K. Hansma, *Quantized adhesion detected withAFM.* J. Am. Chem. Soc., 1992. **114**: p. 4917-4918.

66. Lee, G.U., D.A. Kidwell, and R.J. Colton, *Sensing discrete streptavidin-biotin interactions with atomic force microscopy.* Langmuir, 1994. **10**: p. 354-357.

67. Moy, V., T., E.-L. Florin, and H.E. Gaub, *Intermolecular forces and energies between ligands and receptors.* Science, 1994. **266**: p. 257-259.

68. Williams, J.M., T. Han, and J.T.P. Beebe, *Determination of single-bond forces from contact force variances in AFM.* Langmuir, 1996. **12**: p. 1291-1295.

69. Lo, Y.-S., N.D. Huefner, W.S. Chan, F. Stevens, J.M. Harris, and J.T.P. Beebe, *Specific interactions between biotin and avidin studied by AFM using the Poisson statistical analysis method.* Langmuir, 1999. **15**: p. 1373-1382.

70. Lo, Y.-S., Y.-J. Zhu, and J.T.P. Beebe, *Loading-rate dependence of individual ligand-receptor bond-rupture forces studied by AFM.* Langmuir, 2001. **17**: p. 3741-3748.

71. Wenzler, L.A., G.L. Moyes, G.N. Raikar, R.L. Hansen, J.M. Harris, J.T.P. Beebe, L.D. Wood, and S.S. Saavedra, *Measurements of single-molecule bond-rupture forces between self-assembled monolayers of organosilanes with the atomic force microscope.* Langmuir, 1997. **13**: p. 3761-3768.

72. Wenzler, L.A., G.L. Moyes, L.G. Olson, J.M. Harris, and T.B. Beebe, *Single-Molecule Bond-rupture force analysis of interactions between AFM tips and substrates modified with organosilanes.* Anal. Chem., 1997. **69**(14): p. 2855-2861.

73. Stevens, F., Y.-S. Lo, J.M. Harris, and J.T.P. Beebe, *Computer modeling of AFM force measurements: comparisons of Poisson, histogram, and continuum methods.* Langmuir, 1999. **15**: p. 207-213.

74. Han, T., J.M. Williams, and J.T.P. Beebe, *Chemical bonds studied with functionalized AFM tips.* Analytica Chimica Acta, 1995. **307**: p. 365-376.

75. Barlow, R.J., *Statistics. A guide to the use of statistical methods in physical sciences*. 1989, New York: Wiley.

76. Marshall, K.C., R. Stout, and R. Mitchell, *Mechanism of the initial events in the sorption of marine bacteria to surfaces.* Journal of General Microbiology, 1971. **68**: p. 337-348.

77. van Loosdrecht, M.C.M., J. Lyklema, W. Norde, G. Schraa, and A.J.B. Zehnder, *The role of bacterial cell wall hydrophobicity in adhesion.* Applied and Environmental Microbiology, 1987. **53**: p. 1893-1897.

78. van Loosdrecht, M.C.M., J. Lyklema, W. Norde, G. Schraa, and A.J.B. Zehnder, *Electrophoretic mobility and hydrophobicity as a measure to predict the initial steps of bacterial adhesion.* Applied and Environmental Microbiology, 1987. **53**: p. 1898-1901.

79. van Loosdrecht, M.C.M., J. Lyklema, W. Norde, and A.J.B. Zehnder, *Bacterial adhesion: A physicochemical approach.* Microbial Ecology, 1989. **17**: p. 1-5.

80. Vigeant, M.A.S. and R.M. Ford, *Interactions between motile Eschericia coli and glass in media with various ionic strengths, as observed with a three-dimensional-tracking microscope.* Applied and Environmental Microbiology, 1997. **63**: p. 2474-3479.

81. McEldowney, S. and M. Fletcher, *Effect of growth conditions and surface characteristics of aquatic bacteria on their attachment to solid surfaces.* Journal of General Microbiology, 1986. **132**: p. 513-523.

82. Rijnaarts, H.H.M., W. Norde, E.J. Bouwer, J. Lyklema, and A.J.B. Zehnder, *Reversibility and mechanism of bacterial adhesion.* Colloids and Surfaces B: Biointerfaces, 1995. **4**: p. 5-22.

83. van Oss, C.J., *Interfacial Forces in Aqueous Media*. 1994, New York: Marcel Dekker.

84. Hayashi, H., S. Tsuneda, A. Hirata, and H. Sasaki, *Soft particle analysis of bacterial cells and its interpretation of cell adhesion behaviors in terms of DLVO theory.* Colloids and Surfaces B: Biointerfaces, 2001. **22**(2): p. 149-157.

85. Ohshima, H., *Electrophoresis of soft particles.* Advances in Colloid and Interface Science, 1995. **62**: p. 189-235.

86. Ohshima, H. and T. Kondo, *Approximate analytic expression for the electrophoretic mobility of colloidal particles with surface-charge layers.* Journal of Colloid and Interface Science, 1989. **130**(1): p. 281-282.

87. McClaine, J.W. and R.M. Ford, *Characterizing the adhesion of motile and nonmotile Escherichia coli to a glass surface using a parrallel-plate flow chamber.* Biotechnology and Bioengineering, 2002. **78**: p. 179-189.

88. Morisaki, H., S. Nagai, H. Ohshima, E. Ikemoto, and K. Kogur, *The effect of motility and cell-surface polymers on bacterial attachment.* Microbiology, 1999. **145**(10): p. 2797-2802.

89. Bos, R., H.C. van der Mei, and H.J. Busscher, *"Soft particle" analysis of the electrophoretic mobility of a fibrillated and non-fiberillated oral streptococcal strain : Streptococcus salivarius.* Biophysical Chemistry, 1998. **74**(3): p. 251-255.

90. Takashima, S. and H. Morisaki, *Surface characteristics of the microbial cell of Pseudomonas syringae and its relevance to cell attachment.* Colloids and Surfaces B: Biointerfaces, 1997. **9**(3/4): p. 205-212.

91. McLaine, J.W. and R.M. Ford, *Reversal of flagellar rotation is important in initial attachment of Escherichia coli to glass in a dynamic system with high- and*

low-ionic strength buffers. Applied and Environmental Microbiology, 2002. **68**: p. 1280-1289.

92. Bostrom, M., D.R.M. Williams, and B.W. Ninham, *Specific Ion Effects: Why DLVO theory fails for biology and colloid systems.* Physical Review Letters, 2001. **87**(16): p. 168103-1 : 168103-4.

Chapter 2

Elasticity of *Pseudomonas putida* KT2442 Surface Polymers Probed With Single-Molecule Force Microscopy

Abstract

Single-molecule force microscopy was used to study the effect of solvent polarity and ionic strength on the elasticity of bacterial surface polymers. Adhesion forces were measured between *Pseudomonas putida* KT2442 bacterial cells and silicon nitride tips of an atomic force microscope (AFM). Force-extension profiles were analyzed to determine the elasticity of the polymer chains in several solvents (water, formamide, methanol, 0.1 M KCl and 0.01 M KCl). Adhesion peaks were fit to entropic-based, statistical mechanical, random walk formulations (the freely jointed chain (FJC) and the wormlike chain (WLC) models). The experimental data showed better agreement with the FJC (average $R^2 = 0.86 \pm 0.20$) than the WLC model (average $R^2 = 0.76 \pm 0.22$). The segment length was 0.18 - 1.0 nm in all 5 solvents using the FJC model, with about 60% of the chains having a segment length of 0.18 nm. The persistence length was 0.18 - 0.83 nm using the WLC model, with about 78% of chains having a persistence length of 0.18 nm. The WLC model was not able to represent polymer properties for chains < 11 nm (4% of the data), since persistence lengths shorter than the C-C bond were obtained. The WLC model also failed to predict the high magnitude adhesion forces in KCl solutions and methanol. The extensible freely jointed chain model (FJC+) was considered since the latter accounts for enthalpic effects neglected in the FJC model, but it did not represent the data better than the FJC model. Adhesive interactions between the biopolymer and the AFM tip were compared in these solvents. Adhesion was highest in the least polar

solvent, methanol. Adhesion forces in water and formamide were about the same, and less than forces observed in methanol. Although biopolymer contour lengths varied over a wide range (tens to hundreds of nm) in all solvents, shorter lengths were observed when salt was present, indicating that the polymer chains were less extended in the presence of salt.

2.1 Introduction

Understanding bacterial adhesion to surfaces requires knowledge of the conformational properties of bacterial surface polymers [1-5]. Bacterial surface and extracellular polymers play a role in biofilm properties and dynamics, such as the induction of genetic changes [1], the development of microbial consortia [6], the enhanced resiliency of cells to antibiotics, chlorination and other potential disinfectants [7-9], and corrosion [10]. Biofilm formation is also important in environmental bioremediation [11, 12], drinking water quality, and in biomedical applications such as adhesion to contact lenses [13] and other implanted or prosthetic devices [5, 14, 15]. While it is known that bacterial surface macromolecules play a role in bacterial adhesion and biofilm formation, very little is known regarding the physical properties of these biopolymers at a single-molecule basis.

Earlier results indicated that bacterial adhesion to surfaces may be controlled by polymer interactions [16-20]. Lipopolysaccharides (LPS) cover 45% of the surface of Gram-negative bacteria [21] and may protrude 30 nm or more into the surrounding media [4]. Many bacterial surfaces also have a layer of extracellular polysaccharides (EPS)[6]. Some correlation with biopolymer size and adhesion has been observed. For example, the affinity of *Escherichia coli* and *Citrobacter freundii* O-antigens for TiO_2 and Al_2O_3 surfaces increased as the molecular mass of the O-antigen increased [17]. Polymer compressibility and affinity for solids were thought to determine whether polymers enhanced or inhibited adhesion [4]. The elastic and mechanical properties of polymers can be probed via stretching experiments using atomic force microscopy (AFM) or similar instruments. Single-molecule force spectroscopy (SMFS) allows individual

molecules to be temporarily adsorbed to an AFM tip and stretched. Typically, the molecule is bonded or grafted to a substrate on one end, or in the case of cell surface macromolecules, the cell is attached to a substrate and the polymers are free in solution. These stretching experiments are used to provide information on polymer elasticity and other physical and chemical properties.

Quantitative information regarding chain elasticity can be obtained using statistical mechanical, random walk formulations, i.e., the freely jointed chain (FJC), the wormlike chain (WLC), the extensible FJC, or the extensible WLC model [2, 3, 22-39]. In the FJC model, the polymer is considered to be composed of n independent rigid segments, each of segment length *a* [27]. The persistence length in the WLC model is the length of a statistically straight segment in the polymer [27]. By fitting the experimental data to these models, a segment length or persistence length can be estimated. These models predict linear forces at low extensions, where the chains behave like entropic Hookean springs. At moderate extensions, non-linear, non-Gaussian forces will be predicted [40]. At high stretches, the force rapidly diverges as the distance approaches the contour length of the chain. The chain has less possible configurations and hence less entropy at high stretches.

The first extensive studies of this kind were performed with DNA. DNA, a unique biopolymer due to its size and large persistence length (~ 50 nm), has now been extensively studied using single-molecule force spectroscopy [26, 31, 35, 36, 41, 42]. These experiments have demonstrated a strong-stretching regime when the end-to-end distance approaches the DNA contour length, and shows evidence of wormlike chain (WLC) behavior [26, 31]. When the elasticity of λDNA was directly measured by AFM

and laser tweezers[31, 41], a sharp transition was discovered from a low to high extension state at a force of ~0.45 pN for the underwound molecules and ~3 pN for overwound ones, reflecting the formation of alternative structures in stretched, coiled λDNA molecules [41]. In similar experiments, single-stranded DNA molecules were stretched in the presence of salt. Deviations from freely jointed chain (FJC) behavior were observed, suggesting that DNA has significant local curvature in salt solutions [36]. In addition, AFM was used also to directly probe interaction forces between complementary single strands of DNA [42]. Adhesive forces between complementary 20-base strands fell into three distinct distributions at 1.52, 1.11, and 0.83 nN. These forces are associated with the rupture of the interchain interaction between single pairs of molecules involving 20, 16, and 12 base pairs, respectively.

The use of SMFS was extended to elasticity studies on other biopolymers, such as the polysaccharides xanthan [25, 43, 44], and dextran [45, 46], polysaccharides on living cells of *Aspergillus oryzae*[3], and many other biopolymers [3, 22, 30, 33, 34, 47] and synthetic polymers [2, 23, 24, 32, 37, 48-51]. Native xanthan shows a plateau in the force-extension curve at 400 pN that is characteristic of hydrogen bonding and electrostatic interactions stabilizing the double helices of the xanthan structure. The transition is irreversible and is not seen for denatured (single helical) xanthan [25]. Dextran macromolecules show a characteristic transition at 700 nN [45, 52]. Based on Monte Carlo simulations, this transition was attributed to the C_5-C_6 bond of the sugar ring flipping into a new conformation, elongating the monomer by 0.65 Å (~10% of its length) [52].

Recently, AFM was used to identify the components of mixtures of polysaccharides at the single-molecule level. The elasticity of certain polysaccharides is governed by force-induced conformational transitions of the pyranose ring. These transitions produce atomic fingerprints in the force-extension spectrum that are characteristic of the type of the glycosidic linkage [53-55]. The force spectrums of dextran, cellulose, amylose, and pullulan have been identified and serve as chemical fingerprints for these polysaccharides. This method can identify and distinguish individual polysaccharide molecules adsorbed on a surface at single-molecule resolution, which is not possible by any other spectroscopic technique.

In this study, the elasticity of bacterial surface polymers from *Pseudomonas putida* KT2442 was measured by single-molecule force spectroscopy in solvents spanning a range of polarity (water, formamide, methanol) and ionic strengths (water, 0.01 M KCl, 0.1 M KCl). The WLC and FJC models were used to estimate polymer persistence and segment lengths. Adhesion forces between the polymer chains and the AFM silicon nitride tip were compared in these solvents.

2.2 Materials and Methods

2.2.1 Cultures

Bacteria that have been extensively investigated for their use in bioremediation were chosen. D.F. Dwyer (Department of Earth, Ecological and Environmental Sciences, University of Toledo, Ohio) provided the *Pseudomonas putida* KT2442. This strain can degrade substituted aromatic compounds under appropriate conditions [56-59]. KT2442 cultures were grown in M9 buffer containing a mineral salt mixture, 5mM benzoate and 50 μg/L rifampicin [60].

2.2.2 Sample preparation

KT2442 cells were covalently bonded to clean, silanized glass as described elsewhere [16]. Slides were kept hydrated the entire time prior to AFM work under purified water (milli-Q water, Millipore Corp.), which was replaced with the desired solvent (0.1 and 0.01 M KCl solutions were used to investigate the effect of the ionic strength on biopolymer conformation; formamide, water and methanol were used to study the effect of solvent polarity on biopolymer conformation (Table 2.1)).

2.2.3 Polymer Characterization

The polymers were separated from the bacterial cells (grown until late exponential growth phase) by centrifugation for 15 minutes at 6000 RPM (DAMON/IEC HT Centrifuge). The polymers were freeze-dried and kept in the refrigerator until use.

2.2.4 Zeta Potential

The charge density of KT2442 cells and KT2442 surface polymers was measured using a zeta potential analyzer (Zeta PALS, BIC). Measurements were performed ten times and averaged, on late-exponential phase bacterial cells, resuspended in 0.1 mM MES buffer (pH = 6.66). A 1000 ppm solution of the freeze-dried polymers was prepared in 0.1 mM MES buffer. The zeta potential of the polymers was also measured ten times and averaged.

2.2.5 Polarimetery

The optical rotatory dispersion of the polymers was determined using a Perkin Elmer 241 MC polarimeter. A 25,000 ppm polymer water solution was prepared from the freeze-dried polymer. The measurements were run at four different wavelengths using a sodium lamp (589 nm) and a mercury lamp (546 nm, 436 nm, and 365 nm), and the

maximum measured value of optical rotation in degrees was reported. The accuracy in measuring the optical rotation was ± 0.001 degree.

2.2.6 Force Analysis Using AFM

Forces were measured between individual bacterial cells and silicon nitride cantilevers in different solvents using an AFM (Digital Instruments Dimension 3100 with Nanoscope III controller). Silicon nitride tips were purchased from Digital Instruments (DNPS tips). The spring constant for these tips was 0.13 ± 0.02 N/m, measured using the Cleveland method [61] and the correlation equations given in the DI software. To select a cell for analysis, an image was obtained in tapping mode of a portion of the glass slide. The tip was then positioned over the center of a bacterium, the rastering of the cantilever stopped, the tapping turned off, and a force measurement performed. Triplicate measurements were performed on a single area of a bacterial cell. Measurements were made for at least five cells under each solvent.

The data files were treated as described previously [16] to convert them from AFM deflection data to force data, using the constant compliance region of the curves to "zero" the force curves [62]. Force measurements were also made on clean glass before and after force measurements on bacterial cells, to ensure that the tip was not contaminated during the course of the experiment. The measurements on glass were always identical (within the experimental error), confirming that the biopolymers were released as the tip was retracted.

2.2.7 Retraction curves

Forces are recorded while the tip approaches and is retracted from the sample (Figure 2.1). Far from the sample surface, no forces are observed between the tip and

bacterial polymers. As the tip approaches, the polymer brush layer compresses, inducing a repulsive force. Often when contact is made, polymers from the bacterial surface adsorb onto the tip. As the tip is retracted, a force equivalent to the adhesion force is required to pull the tip away from the polymer brush. This force is called the "pull-off force" and the location where it occurs depends on the length of the polymer chain. Multiple adhesion peaks may be observed, depending on the polymer type, the length of the polymer chain, and whether one or multiple chains are adsorbed to the tip.

2.2.8 Modeling

Three models were applied to the force-extension data. In the freely jointed chain (FJC) model, the polymer is considered to be composed of n independent rigid segments, each of length a, and connected by freely rotated pivots with equal probabilities for rotation in all directions. The chain gets more flexible as the segment length *a* gets smaller. The force needed to stretch a FJC to a length D is given by [23]

$$F_{chain} = \frac{-k_B T}{a} L^{-1}\left(\frac{D}{L_c}\right) \tag{2.1}$$

Where k_B is Boltzmann constant (1.38106×10^{-23} J/K), T is absolute temperature; L_c is the polymer contour length, and L^{-1} is the inverse Langevin function, approximated by the first four terms of its series [23]:

$$L^{-1} = 3\left(\frac{D}{L_c}\right) + \frac{9}{5}\left(\frac{D}{L_c}\right)^3 + \frac{297}{175}\left(\frac{D}{L_c}\right)^5 + \frac{1539}{875}\left(\frac{D}{L_c}\right)^7 \tag{2.2}$$

Second, the wormlike chain (WLC) model was applied, in which the polymer chain is considered to be continuously curved and the direction of the curvature at any point in the chain is random. The chain in this model is intermediate between a rigid rod and a flexible coil. The WLC model takes into account the local stiffness of the chain in

terms of the persistence length (L_P) and the long-range flexibility. The force required to stretch a wormlike chain in a solvent to a length D is given by [23]

$$F_{chain} = \frac{-k_B T}{L_P}\left[\frac{D}{L} + \frac{1}{4\left(1-\frac{D}{L_c}\right)^2} - \frac{1}{4}\right] \tag{2.3}$$

The extensible freely jointed chain model (FJC+) was used in some cases to account for elastic deformations of bonds and bond angles that are neglected in the freely jointed chain model. The polymer is modeled according to the FJC+ as n identical springs in series and can be expressed as [33]

$$D(F) = L_c[\coth(\frac{FL_k}{k_B T}) - (\frac{k_B T}{FL_k})][1 + \frac{F}{L_c \kappa}] \tag{2.4}$$

where, L_k is the segment length, L_c is the contour length = n L_k, and κ is the spring constant of a single segment.

The model's ability to fit the experimental data was compared based on the estimated values of R^2 (the coefficient of determination, often used to judge the adequacy of a regression model) using the Tablecurve fitting program.

2.3 Results

2.3.1 Effect of Salt Concentration on Biopolymer Conformation and Adhesive Forces

Pull-off distances and adhesion forces between bacterial polymers and the silicon nitride tip were compared for all solvents. In water, a range of pull-off distances was observed that went up to 850 nm, with the mean at 212 nm (Table 2.1, Figure 2.2). While short polymers (<150 nm) were seen to a significant extent in all solvents, long polymers were not observed when salt was present. Over 70% of the pull-off distances

were < 50 nm in the highest salt solution (0.1 M KCl), while the percentages of polymers this size were ~55% in 0.01 M KCl and ~45% in water. Polymers with pull-off distances > 450 nm were never observed in the salt solutions (Figure 2.2, Figure 2.3). These results indicate that the biopolymer was more elongated in pure water, and could adopt a more coiled conformation when salt was present. The pull-off distances in water were compared to the pull-off distances in the other 4 solvents. In each case, the pull-off distances in water were statistically different from the pull-off distances in the other solvents (methanol, formamide, 0.01 M KCl, and 0.1 M KCl, each considered separately; statistical differences determined by Mann-Whitney Rank Sum Tests, all *P* values were <0.01).

No trend could be observed in the adhesion force with respect to electrolyte concentration (Table 2.1, Figure 2.3). The mean adhesion force was nearly the same in water, 0.1 M KCl, and 0.01 M KCl, within the range of experimental values observed.

2.3.2 Effect of Solvent Polarity on Biopolymer Conformation and Adhesive Forces

The average pull-off distance increased with increasing dielectric constant, with average distances of 137, 212, and 295 nm in methanol, water, and formamide, respectively (Figure 2.4). The polymers were clustered at shorter pull-off distances less in the more polar solvents, with the percentage of pull-off distances < 200 nm being 40% for formamide, 60% for water, and 80% for methanol (these distances were shown to be statistically different among solvents using a Mann-Whitney Rank Sum test, all *P* values were <0.01).

Solvent polarity also affected the adhesion force, with the highest affinity between the biopolymers and the tip observed in the least polar solvent (methanol; Figure 2.4, Figure 2.5). Generally in water and formamide, the adhesive interactions between the biopolymer and the AFM tip were similar, given the wide range of adhesive forces observed (Figure 2.5). However, at short distances (<88 nm), greater adhesion was observed in water compared to formamide (Figure 2.5).

2.3.3 Comparison with Polymer Elasticity Models

2.3.3.1 The Effect of Solution Ionic Strength

Salt solutions with concentrations of 0.01 M and 0.1 M KCl were used to demonstrate the effect of solvent ionic strength on biopolymer conformation, and estimation of elastic parameters was made using the FJC and WLC models. While a range of persistence and segment lengths was observed (Table 2.2), generalizations can be made. The maximum persistence length value increased with increasing ionic strength, from 0.20 nm in 0.01 M KCl to 0.36 nm in 0.1 M KCl, indicating that the polymers become stiffer at higher salt concentrations (Figure 2.6; Table 2.2). The FJC model predicted the same trend, with a segment length up to 0.32 nm in 0.01 M KCl and 0.65 nm in 0.1 M KCl (Figure 2.7; Table 2.2).

The estimated contour lengths from the WLC model were shorter than the pull-off distances (~52 to 92% of the pull-off distance). The estimated contour lengths using the FJC model were longer than the pull-off distances in most cases.

2.3.3.2 Effect of Solvent Polarity

The WLC and FJC models were applied to the data in all solvents. The effect of solvent polarity on polymer conformation was probed by estimating the persistence or

(segment) length, and contour lengths, in solvents with different dielectric constants: methanol, water, and formamide. Again, while a range of values was observed, some general trends are apparent. Using either model, the polymer was stiffer in more polar solvents. The maximum estimated persistence lengths based on the WLC model were 0.82 nm in formamide, 0.28 nm in water, and 0.21 nm in methanol (Figure 2.8). The FJC model predicted segment lengths up to 1.0 nm in formamide, 0.35 nm in water, and 0.18 nm in methanol (Figure 2.9; Table 2.2).

The estimated contour lengths using the WLC model were always less than the experimental pull-off distances (Table 2.2). Contour lengths between 31% and 93% of the pull-off distance were estimated in formamide, 29% to 99.6% in water, and 47% to 97% in methanol. More than 81% of the chains in all solvents were stretched to 85% of their pull-off distance, which is proportional to the contour length of the polymers. [37] Lower stretching capacities were observed at low and high extensions (Figures 2.8A, 2.8B, 2.8C).

2.3.3.3 Comparison of WLC and FJC Models

In comparing the two models for all solvents, the FJC model gives slightly better agreement with the experimental data (R^2 = 0.86 ± 0.20 in FJC, R^2 = 0.76 ± 0.22 in WLC). In addition, there were two cases where the WLC model could not be used. For chain extensions <11 nm, the WLC model was discounted since it predicted persistence length values lower than the C-C bond length (0.154 nm). Also, at high magnitude forces (>0.5 nN) and low chain extensions, the WLC model could not fit the whole range of the data (Figures 2.6A, 2.6B, 2.8B, 2.8C). The FJC model was able to fit all the

experimental data, for all of the solvents. Therefore, the FJC model is preferred since it applies to the whole range of data.

2.3.3.4 Extensible Freely Jointed Chain model

Since the FJC model does not account for bond deformation or stretching of the molecules beyond their contour lengths, the extensible freely jointed chain (FJC+) model was applied to force curves in water, to determine if these additional stretches needed to be accounted for. The FJC+ model has an additional enthalpic term that gives rise to a linear increase in the force for large extensions ($D \sim L_c$), and an additional fitting parameter that takes into account chain elasticity. The resulting fits for the FJC and FJC+ models are compared in water (Figure 2.10). In general, both models are in good agreement with the experimental data. At low extensions, the FJC works better than the FJC+ model, as shown by the higher R^2 values. At mid extensions, both models can fit the data equally well. At high extensions, the FJC+ could not explain the experimental observations, since the experimental measured forces become small in value. The segment lengths estimated with the FJC+ model were 0.21 - 0.93 nm, which are higher than the segment lengths estimated using the FJC model (0.154 – 0.36 nm). The range of contour lengths was comparable using the two models, 7.5 - 838 nm with the FJC+, and 8.7 -802 nm with the FJC model (for the same experimental data). The FJC+ model predicted segment elasticity values between 0.43 N/m to 100 N/m for these biopolymers.

2.4 Discussion

2.4.1 Effect of Polarity and Ionic Strength on Biopolymer Conformation

While a range of segment and persistence lengths was observed in all solvents, the polymers were slightly more rigid in 0.1 M KCl compared to the lower salt or pure water

solutions. The contour length of the biopolymers decreased when salt was added, probably because the macromolecules could adopt a more coiled conformation.

These types of transitions with respect to ionic strength (stiffer and more coiled when salt is present) are not uncommon. Many polysaccharides need some salt to be present in solution to stabilize their structures, and will denature when no salt is present. For example, succinoglycan forms a disordered non-helical structure in pure water but transforms to a gel-like structure in 0.1 M KCl [50]. Gel formation is possible because electrostatic repulsion between polymer chains is reduced in the present of salt. Denatured xanthan will renature into its native double-helix form only when salt is present [63, 64]. Gellan is a double-stranded helix in very dilute aqueous solution containing low molecular weight salts but adopts a disordered; perhaps single-stranded configuration in the absence of added salts [65]. The presence of salts minimizes electrostatic repulsion among charged segments of the polysaccharide chains.

For charged polysaccharides in which electrostatic repulsion among subunits is strong, their conformation may be able to change from extended to coiled upon the addition of salt. For a polysaccharide produced by the marine bacterium *Pseudomonas atlantica*, as the ionic strength was increased to marine salt concentrations (about 0.5 M), adsorbed anionic EPS contracted in its configuration and collapsed onto the solid substrate surface [66]. As another example, the conformation of (negatively-charged) xanthan chains transformed from isolated extended rods to coils and sometimes aggregates when KCl was added to solution [63].

The estimated values of segment and persistence lengths for KT2442 polysaccharides are similar to values observed for other flexible polymers. SMFS

experiments demonstrated a Kuhn length (segment length) of 6 ± 0.5 Å for dextran [45]. Poly (methacrylic acid), polydimethylsiloxane, and polyinosine all have segment lengths between 0.25 and 0.33 nm [22, 42, 49] (measured in SMFS experiments). However, some polysaccharides are much more rigid, such as xanthan [63] (L_P can be hundreds of nm, depending on whether salt was present), succinoglycan [50] (L_P = 36-105 nm, depending on whether salt was present), and scleroglucan [67, 68](L_P = 80 ± 10 nm).

2.4.2 Biopolymer Elastic Properties

Almost 70% of the chains in all solvents have persistence and/or segment lengths of 0.18 nm, which is only slightly higher than the C-C bond length (0.154 nm). This indicates that the polymers are flexible chains under all solvents.

2.4.3 Comparison between Different Models

Three different statistical models were used to fit the experimental data, the freely jointed chain (FJC), the wormlike chain (WLC), and the extensible freely jointed chain (FJC+). The first two models have two fitting parameters (contour length and either segment (FJC) or persistence (WLC) length). The FJC+ also includes a term for segment elasticity. At higher forces, chain segments are no longer oriented in a random fashion, but orient predominately along the direction of the external force. The general polymer models, FJC and WLC, can describe this situation. The FJC model accounts only for entropic behavior. In the WLC model, enthalpic and entropic contributions are included, but extension is limited to the contour length of the polymer [33].

The FJC model describes the experimental data for the KT2442 surface polymers very well, with a mean R^2 value of 0.86 ± 0.20. The FJC model has been successfully applied to many flexible polymers [22, 69, 70]. The WLC model was almost as good as

the FJC model for most of the data, with an average R^2 value of 0.76 ± 0.22. However, the WLC model failed in two instances. At short distances, the WLC model predicted a persistence length shorter than the length of a C-C bond. There is some ambiguity in where to set the zero position in these force-extension curves, since the bacterial cell is slightly deformable. However, we estimate that our accuracy in establishing the zero positions for force and distance are within 10 nm and 0.06 nN, and so only minimal errors would be caused by this problem. In addition, the WLC model was less able to fit high magnitude forces at low extensions (2.6A, 2.6B, 2.8B, 2.8C). Therefore, the FJC model is preferred over the WLC model for these particular biopolymers.

The extensible freely jointed chain model (FJC+) takes into account elastic deformations by adding an enthalpic term to the FJC model. Segment elasticity represents the chains' ability to stretch beyond their contour lengths. This model works well at high forces, when a rupture in the bonds or a change in the structure is expected [33]. We tested the FJC+ model for our polymer chains in water, even though we have never observed plateau regions (indicative of conformational transitions) in our force-extension curves. The FJC+ was successfully applied to the data for the polymer chains in water in the low to mid range extensions, but did not fit our data well at higher extensions (Figure 2.10). Since the FJC+ model did not improve the fit compared to the FJC model, it is suggested that the polymers were not stretched beyond their contour lengths, and hydrogen bond rupture did not occur. The FJC+ model was not applied to the data for the other solvents but we would expect a similar trend in the results.

2.4.4 Biopolymer Adhesion

Surface biopolymers may control bacterial adhesion [1-5, 71]. In the present study, adhesion forces were measured between bacterial cells and an AFM tip in several solvents and adhesion was found to be a weak function of ionic strength. The adhesion forces were about the same in water, 0.01 M KCl, and 0.1 M KCl. The measured values of zeta potential for KT2442 bacterial cells (-17.31 ± 0.06 mV) and for the extracted surface polymers of KT2442 (-3.86 ± 0.04 mV) were quite different, indicating that the polymers have a low charge density. This may explain the weak dependence of the pull-off force on the ionic strength.

The effect of ionic strength on bacterial adhesion has been widely studied [16, 18, 65, 72]. Less adhesion under low ionic strength conditions has been observed as a general trend. The decrease in adhesion is usually described by the classical Derjaguin- Landau-Verwey- Overbeek (DLVO) theory of colloidal stability, in which the total interaction energy between two surfaces is considered as the sum of van der Waals and electrostatic interactions [73]. In bacterial adhesion studies, a transition sometimes occurs between a DLVO-controlled to steric-controlled barrier to adhesion. The transition occurs at an ionic strength high enough for electrostatic interactions to be minimized [18]. Bacterial adhesion to porous media in transport studies has been found to be reduced in low ionic strength solutions [52, 72, 74, 75], although only qualitative agreement with predictions based on DLVO theory have been observed [20].

In solvents with different polarities, adhesion was higher in the least polar solvent, methanol, and lower in the more polar solvents. The biopolymers are probably hydrophilic since they adhere more strongly to the tip under the least hydrophilic conditions. Previous indirect evidence indicated that KT2442 produced hydrophilic

polymers, since the water contact angle on a lawn of bacterial cells is 24.5º [60]. Other research has demonstrated that repulsion due to intrachain interactions decreases in less polar solvents. For example, hydrophobic intrachain interactions were eliminated in hexadecane, which is an entirely apolar solvent [37]. The nature of the solvent affects solvation forces and depends on the dielectric constant (ε) in a complex manner [73].

2.4.5 Heterogeneity of Biopolymers

In our study, a range of values of segment lengths, persistence lengths, and contour lengths were observed, which seems to indicate that more than one type of polysaccharide is present on the bacterial surface. The range of contour lengths is not surprising, and care must be taken in interpreting this data since the tip may make contact with some point along the chain that is not necessarily the end of the chain. The lengths observed cannot be easily related to the actual length of the polymer (Figure 2.11). In other studies on well-defined biopolymers, where the contour length is clearly known, all the data can be normalized to the contour length of the polymer [22, 25, 76]. We cannot normalize the data by the length since the polymer length is not independently known. However, even if we cannot be sure how many different length polymer molecules are present on the bacterial surface, it still appears that we have multiple types of polymers based on the range of different persistence and segment lengths observed. If the biopolymer material were chemically homogeneous, but of different lengths, the persistence length would not be expected to change.

Based on a size exclusion chromatography (SEC) experiment on extracted biopolymers from *P. putida* KT2442, a broad peak was observed near a polymer

molecular weight of 1.8 x 10^5. The broadness of this peak indicated that multiple sized polymers are present (data not shown).

2.4.6 Chemical Nature of the Biopolymers

AFM provides primarily physical information, but has recently been used as a chemical "fingerprinting" technique for certain polysaccharides [53]. Researchers have shown that bond linkages in $\alpha(1\rightarrow4)$ sugars often give rise to characteristic and reproducible transitions in SMFS experiments. For example, amylose and dextran each show single transitions that occur at ~280 and ~850 pN, respectively. Some polysaccharides, such as pectin, show two transitions in their force spectra, due to a two-step chair inversion transition in the α-D-galactopyranuronic acid ring. A technique has now been developed for relating the number of conformational transitions in force spectrograms to the sum of the glycosidic and aglycon bonds in the axial (a) position. One polysaccharide that does not show a force transition is methylcellulose (a sugar with β-linkages), which displays purely entropic behavior. The force spectra we observe for *P. putida* KT2442 biopolymers most closely resemble those of cellulose, since no transition is observed that could be attributed to a conformational transition. Also, the purely entropic FJC model is able to represent the elastic properties of these biopolymers quite well. A polarimetry test run on our polymers confirmed this hypothesis. The negative rotations observed in the measurements indicated that we have a β sugar [77]. Determining detailed chemical information on polysaccharides would require the use of AFM in combination with other methods. However, new techniques such as polysaccharide fingerprinting or the use of chemically modified tips allow AFM to

provide an unprecedented degree of chemical information at a molecular level on microbial and other cell surfaces.

2.5 Summary

Single-molecule force microscopy was successfully used to quantify the elasticity of *Pseudomonas putida* KT2442 polymers in various solvents. The effect of ionic strength on the polymer elasticity was studied through using of 0.1 and 0.01 M KCl solutions. The effect of polarity on polymer elasticity was studied using methanol, water, and formamide. Three different models were used to quantify polymer elasticity from force-extension profiles: the freely-jointed chain, wormlike chain, and extensible freely-jointed chain models. The FJC was found to fit the experimental data better than the WLC model. Enthalpic effects were found to be unimportant; hence the FJC+ was not better than the FJC model. The polymers are found to be very flexible, since more than 70% of the total estimated segment or persistence lengths of the chains is ~0.18 nm, a little higher than the C-C bond length (0.154 nm). The adhesion forces are weakly dependent on ionic strength. This might be due to the low charge density of KT2442's surface polymers. Adhesion forces between the bacteria and the AFM tip increases as the polarity decreased; indicating that the polymers are hydrophilic. The KT2442 polymers were thought to be cellulose-like, based on their optical rotation and characteristic force spectra. This work will be useful to those wishing to develop improved models of bacterial adhesion. We have demonstrated the important effect of surface polymer properties on adhesion forces and point out the need for bacterial adhesion models to account for polymer properties and polymer heterogeneity.

2.6 Acknowledgments

We thank Jayne Morrow and Professor Domenico Grasso (Smith College) for their help in performing the zeta potential measurements, Dr. Rick Stock (WPI) for his help in purifying the bacterial polymers, Professors Lale Burk and Kate Queeney (Smith College) for their help in performing the polarimetry tests, and Professor William Hobey (WPI) for helping us interpret the polarimetry results.

2.7 References

1. Fletcher, M. and A.W. Decho, *Biofilms.* Encyclopedia of Life Sciences, www.els.net, 2001.
2. Courvoisier, A., F. Isel, J. Francois, and M. Maaloum, *End-adsorbed telechelic polymer chains at surfaces:Bridging and elasticity.* Langmuir, 1998. **14**: p. 3727-3729.
3. Van der Aa, B.C., R.M. Michel, M. Asther, M.T. Zamora, P.G. Rouxhet, and Y.F. Dûfrene, *Stretching cell surface macromolecules by atomic force microscopy.* Langmuir, 2001. **17**: p. 3116-3119.
4. Jucker, B.A., A.J.B. Zehnder, and H. Harms, *Adsorption of bacterial surface polysaccharides on mineral oxides is mediated by hydrogen bonds.* Environmental Science & Technology, 1998. **32**: p. 2909-2915.
5. Nablo, B.J., T.-Y. Chen, and M.H. Schoenfisch, *Sol-gel derived nitric oxide releasing matrials that reudce bacterial adhesion.* J. Am. Chem. Soc., 2001. **123**: p. 9712-9713.
6. Davies, D., M.R. Parsek, J.P. Pearson, B.H. Iglewski, J.W. Costerton, and E.P. Greenberg, *The involvement of cell-to-cell signals in the development of bacterial biofilm.* Science, 1998. **280**(5361): p. 295-298.
7. Fletcher, M., *The physiological activity of bacteria attached to solid surfaces.* Advances in Microbial Physiology, 1991. **32**: p. 53-85.
8. Fletcher, M., *Bacterial attachment in aquatic environments: a diversity of surfaces and adhesion strategies*, in *Bacterial Adhesion: Molecular and Ecological Diversity*, M. Fletcher, Editor. 1996, Wiley-Liss, Inc.: New York.

9. Marshall, K.C., *Adhesion as a strategy for access to nutrients*, in *Bacterial Adhesion: Molecular and ecological Diversity*, M. Fletcher, Editor. 1996, John-Wiley & Sons, Inc.: New-York.

10. Dexter, S.C., P. Chandrasekaran, H.-J. Zhang, and S. Wood. *Microbial corrosion in marine environments: Effect of microfouling organisms on corrosion of passive metals*. in *Biocorros. Biofouling Proc.* 1992.

11. Decho, A.W. and D.J.W. Moriarty, *Bacterial exopolymer utilization by a harpacticoid copepod: a methodology and results.* Limnology and Oceanography, 1990. **35**(5): p. 1039-1049.

12. Schramm, A., L.H. Larsen, N.P. Revsbech, N.B. Ramsing, R. Amann, and K.H. Schleifer, *Structure and function of a nitrifying biofilm as determined by in situ hybridization and the use of microelectrodes.* Appl. Environ. Microbiol., 1996. **62**(12): p. 4641-4647.

13. Serry, F.M., I. Revenko, and M.J. Allen, *Application of AFM for contact lens manufacturing*. 1998, Digital Instruments.

14. Matsuzawa, M., R.S. Potember, D.A. Stenger, and V. Krauthamer, *Containment and growth of neuroblastoma cells on chemically patterned substrates.* J. Neurosci Methods, 1993. **50**(2): p. 253-260.

15. Guo, A., L.L. Rife, N.A. Rao, and R.E. Smith, *Anterior segment prosthesis development:evaluation of expanded polytetrafluorethylene as a sclera-attached prosthetic material.* Cornea, 1996. **15**(2): p. 210-214.

16. Camesano, T.A. and B.E. Logan, *Probing bacterial electrosteric interactions using atomic force microscopy.* Environmental Science & Technology, 2000. **34**: p. 3354-3362.

17. Jucker, B.A., H. Harms, S.J. Hug, and A.J.B. Zehnder, *Adsorption of bacterial surface polysaccharides on mineral oxides is mediated by hydrogen bonds.* Colloids and Surfaces B: Biointerfaces, 1997. **9**: p. 331-343.

18. Rijnaarts, H.H.M., W. Norde, J. Lyklema, and A.J.B. Zehnder, *DLVO and steric contributions to bacterial deposition in media of different ionic strengths.* Colloids and Surfaces B: Biointerfaces, 1999. **14**: p. 179-185.

19. Ong, Y.-L., A. Razatos, G. Georgiou, and M.M. Sharma, *Adhesion forces between E. coli bacteria and biomaterial surfaces.* Langmuir, 1999. **15**: p. 2719-2725.

20. Simoni, S.F., H. Harms, T.N.P. Bosma, and A.J.B. Zehnder, *Population heterogeneity affects transport of bacteria through sand columns at low flow rates.* Environmental Science & Technology, 1998. **32**: p. 2100-2105.

21. DiRienzo, J.M., K. Nakamura, and M. Inouye, *The outer membrane proteins of gram-negative bacteria:biosynthesis, assembly, and functions.* Ann. Rev. Biochem., 1978. **47**: p. 481-532.

22. Ortiz, C. and G. Hadziioannou, *Entropic elasticity of single polymer chains of poly(methylacrylic acid) measured by atomic force microscopy.* Macromolecules, 1999. **32**: p. 780-787.

23. Butt, H.-J., M. Kappl, H. Mueller, and R. Raiteri, *Steric forces measured with the atomic force microscope at various temperatures.* Langmuir, 1999. **15**: p. 2559-2565.

24. Hugel, T., M. Grosholz, H. Clausen-Schaumann, A. Pfau, H. Gaub, and M. Seitz, *Elasticity of single polyelectrolyte chains and their desorption from solid supports studied by AFM based single molecule force spectroscopy.* Macromolecules, 2001. **34**: p. 1039-1047.

25. Li, H., M. Rief, F. Oesterhelt, and H. Gaub, *Single-molecule force spectroscopy on xanthan by AFM.* Advanced Materials, 1998. **3**(4): p. 316-319.

26. Marko, J.F. and E.D. Siggia, *Stretching DNA.* Macromolecules, 1995. **28**: p. 8759-8770.

27. Flory, P.J., *Statistical Mechanics of Chain Molecules*. 1988, New York: Wiley.

28. Murphy, E.M., J.M. Zachara, S.C. Smith, J.L. Phillips, and T.W. Wiestma, *Interaction of hydrophobic organic compounds with mineral-bound humic substances.* Environmental Science & Technology, 1994. **28**: p. 1291-1299.

29. Rief, M., M. Gautel, F. Oesterhelt, J.M. Fernandez, and H.E. Gaub, *Reversible unfolding of individual titin immunoglobin domains by AFM.* Science, 1997. **276**: p. 1109-1111.

30. Kellermayer, M.S.Z., S.B. Smith, H.L. Granzier, and C. Bustamante, *Folding-Unfolding Transitions in Single Titin Molecules Characterized with Laser Tweezers.* Science, 1997. **276**(5315): p. 1112-1116.

31. Smith, S.B., Y. Cui, and C. Bustamante, *Overstretching B-DNA: The elastic response of individual double-stranded DNA molecules.* Science, 1996. **271**: p. 795-799.

32. Oberdorfer, Y., H. Fuchs, and A. Janshoff, *Conformational analysis of native fibronectin by means of force spectroscopy.* Langmuir, 2000. **16**(26): p. 9955-9958.

33. Janshoff, A., M. Neitzert, Y. Oberdorfer, and H. Fuchs, *Force spectroscopy of molecular systems-single molecule spectroscopy of polymers and biomolecules.* Angew. Chem. Int. Ed., 2000. **39**: p. 3212-3237.

34. Benoit, M., D. Gabriel, G. Gerisch, and H.E. Gaub, *Discrete interactions in cell adhesion measured by single-molecule force spectroscopy.* Nature Cell Biology, 2000. **6**: p. 313-319.

35. Bustamante, C., J.F. Marko, E.D. Siggia, and S. Smith, *Entropic elasticity of l-phage DNA.* Science, 1994. **265**: p. 1599-1601.

36. Smith, S.B., L. Finzi, and C. Bustamante, *Direct mechanical measurements of the elasticity of single DNA molecules by using magnetic beads.* Science, 1992. **258**: p. 1122-1126.

37. Oesterhelt, F., M. Rief, and H.E. Gaub, *Single molecule force spectroscopy by AFM indicates helical structure of poly(ethylene-glycol) in water.* New Journal of Physics, 1999. **1**: p. 6.1-6.11.

38. Oberhauser, A.F., P.E. Marszalek, H.P. Erikson, and J.M. Fernandez, *The molecular elasticity of the extracellular matrix protein tenascin.* Nature, 1998. **393**: p. 181-185.

39. Oesterhelt, F., D. Oesterhelt, M. Pfeiffer, A. Engel, H.E. Gaub, and D.I. Muller, *Unfolding pathways of individual bacteriorhodopsins.* Science, 2000. **288**(5463): p. 143-146.

40. Haubt, B.J., J. Ennis, and E.M. Sevick, *The detachment of a polymer chain from a weekly adsorbing surface using an AFM tip.* Langmuir, 1999. **15**: p. 3886-3892.

41. Strick, T.R., J.-F. Allemand, D. Bensimon, A. Bensimon, and V. Croquette, *The elasticity of a single supercoiled DNA molecule.* Science, 1996. **271**: p. 1835-1837.

42. Lee, G.U., D.A. Kidwell, and R.J. Colton, *Sensing discrete streptavidin-biotin interactions with atomic force microscopy.* Langmuir, 1994. **10**: p. 354-357.

43. Li, H., M. Rief, F. Oesterhelt, and H. Gaub, *Force spectroscopy on single xanthan molecules.* Appl. phys. A., 1999. **68**: p. 407-410.

44. Capron, I., S. Alexandre, and G. Muller, *An atomic force microscopy study of the molecular organisation of xanthan.* Polymer, 1998. **39**(23): p. 5725-5730.

45. Rief, M., F. Oesterhelt, B. Heymann, and H.E. Gaub, *Single molecule force spectroscopy on polysaccharides by atomic force microscopy.* Science, 1997. **275**(5304): p. 1295-?

46. Rief, M., J.M. Fernandez, and H.E. Gaub, *Elasticity coupled two-level systems as a model for biopolymer extensibility.* Physical Review Letters, 1998. **81**(21): p. 4764-4767.

47. Jucker, B.A., H. Harms, and A.J.B. Zehnder, *Polymer interactions between five gram-negative bacteria and glass investigated using LPS micelles and vesicles as model systems.* Colloids and Surfaces B: Biointerfaces, 1998. **11**: p. 33-45.

48. Razatos, A., Y.-L. Ong, F. Boulay, D.L. Ebert, J.A. Hubbell, M.M. Sharma, and G. Georgiou, *Force measurements between bacteria and poly(ethylene glycol)-coated surfaces.* Langmuir, 2000. **16**: p. 9155-9158.

49. Senden, T.J., J.-M. di Meglio, and P. Auroy, *Anomalous adhesion in adsorbed polymer layers.* Eur. Phys. J. B., 1998. **3**: p. 211-216.

50. Balnois, E., S. Stoll, K.J. Wilkinson, J. Buffle, M. Rinaudo, and M. Milas, *Conformations of succinoglycan as observed by atomic force microscopy.* Macromolecules, 2000. **33**: p. 7440-7447.

51. Li, H., W. Zhang, X. Zhang, J. Shen, B. Liu, C. Gao, and G. Zao, *Single molecule force spectroscopy on poly(vinyl alcohol) by AFM.* Macromol. Rapid. Commun., 1998. **19**: p. 609-611.

52. Jewett, D.G., T.A. Hilbert, B.E. Logan, R.G. Arnold, and R.C. Bales, *Bacterial transport in laboratory columns and filters: influence of ionic strength and pH on collision effeciency.* Water Research, 1995. **29**(7): p. 1673-1680.

53. Marszalek, P.E., H. Li, and J.M. Fernandez, *Fingerprinting polysaccharides with single-molecule force spectroscopy.* Nature Biotechnology, 2001. **19**: p. 258-262.

54. Marszalek, P.E., A.F. Oberhauser, Y.-P. Pang, and J.M. Fernandez, *Polysaccharide elasticity governed by chair-boat transitions of the glucopyranose ring.* Nature, 1998. **396**: p. 661-666.

55. Marszalek, P.E., Y.-P. Pang, H. Li, J. El Yazal, A.F. Oberhauser, and J.M. Fernandez, *Atomic levers control pyranose ring conformation.* Proceedings of the National Academy of Science USA, 1999. **96**: p. 7894-7898.

56. Nüßlein, K., D. Maris, K. Timmis, and D.F. Dwyer, *Expression and transfer of engineered catabolic pathways harbored by Pseudomonas spp. introduced into activated sludge microcosms.* Applied and Environmental Microbiology, 1992. **58**: p. 3380-3386.

57. Lupi, C.G., T. Colangelo, and C.A. Mason, *Two-Dimensional gel electrophoresis analysis of the response of Pseudomonas putida KT2442 to 2-chlorophenol.* Applied and Environmental Microbiology, 1995. **61**(8): p. 2863-2872.

58. van der Meer, J.R., A.R.W. van Neerven, E.J. De Vries, W.M. De Vos, and A.J.B. Zehnder, *Cloning and characterization of plasmid-encoded genes for the degradation of 1,2-dichlorobenzene, 1,4-dichlorobenzene, and 1,2,4-trichlorobenzene of Pseudomonas sp strain P51.* Journal of Bacteriology, 1991. **173**: p. 6-15.

59. Schwartz, A. and R. Bar, *Cyclodextrin-enhanced degradation of toluene and P-toluic by Pseudomonas putida.* Applied and Environmental Microbiology, 1995. **61**(7): p. 2727-2731.

60. Camesano, T.A., K.M. Unice, and B.E. Logan, *Blocking and ripening of colloids in porous media: Implications for bacterial transport.* Colloids and Surfaces A: Physicochemical and Engineering Aspects, 1999. **160**: p. 291-307.

61. Cleveland, J.P., S. Manne, D. Bocek, and P.K. Hansma, *Nondestructive method for determining the spring constant of cantilevers for scanning force microscopy.* Review of Scientific Instruments, 1993. **64**: p. 403-405.

62. Ducker, W.A., T.J. Senden, and R.M. Pashley, *Direct measurement of colloidal forces using an atomic force microscope.* Nature, 1991. **353**: p. 239-241.

63. Camesano, T.A. and K.J. Wilkinson, *Single molecule study of xanthan conformation using atomic force microscopy.* Biomacromolecules, 2001. **2**: p. 1184-1191.

64. Holzwarth, G. and E.B. Prestridge, *Multistranded helix in xanthan polysaccharide.* Science, 1977. **197**: p. 757.

65. McIntire, T.M. and D.A. Brant, *Imaging of individual biopolymers and supermolecular assemblies using noncontact AFM.* Biopolymers, 1997. **42**: p. 133-146.

66. Frank, B.P. and G. Belfort, *Intermolecular forces between extracellular polysaccharides measured with the atomic force microscope.* Langmuir, 1997. **13**: p. 6234-6240.

67. Stokke, B.T. and D.A. Brant, *The reliability of wormlike polysaccharide chain dimensions estimated from electron micrographs.* Biopolymers, 1990. **30**: p. 1161-1181.

68. Vuppu, A.K., A.A. Garcia, and C. Vernia, *Tapping mode AFM of scleroglucan networks.* Biopolymers, 1997. **42**: p. 89-100.

69. Lee, G.U., L.A. Chrisey, and R.J. Colton, *Direct measurement of the forces between complementary strands of DNA.* Science, 1994. **266**: p. 771-773.

70. Senden, T.J. and C.J. Drummond, *Surface chemistry and tip-sample interactions in atomic force microscopy.* Colloids and Surfaces A: Physicochemical and Engineering Aspects, 1994. **94**: p. 29-51.

71. Jucker, B.A., A.J.B. Zehnder, and H. Harms, *Quantification of polymer interactions in bacterial adhesion.* Environmental Science & Technology, 1998. **32**: p. 2909-2915.

72. Camesano, T.A. and B.E. Logan, *Influence of fluid velocity and cell concentration on the transport of motile and non-motile bacteria in porous media.* Environmental Science & Technology, 1998. **34**: p. 2254-3362.

73. Israelachvili, J.N., *Intermolecular & Surface Forces (2nd edition)*. 1992, New York: Academic Press.

74. Gannon, J.T., V.B. Manilal, and M. Alexander, *Relationship between cell surface properties and transport of bacteria through soil.* Applied and Environmental Microbiology, 1991. **57**: p. 190-193.

75. Fontes, D.E., A.L. Mills, G.M. Hornberger, and J.S. Herman, *Physical and chemical factors influencing transport of microorganisms through porous media.* Applied and Environmental Microbiology, 1991. **57**: p. 2483-2481.

76. Hull, R.A., R.E. Gill, P. Hsu, B.H. Minshew, and S. Falkow., *Construction and expression of recombinant plasmids encoding type I or D-mannose-resistant pili from a urinary tract infection.* Infect. Immun., 1981. **33**: p. 933-938.

77. Robyt, J.F. and B.J. White, *Biochemical Techniques:Theory and Practice*. 1990: Waveland Press, Inc.

78. Lide, D.R., *CRC Handbook of Chemistry and Physics*. 77 ed, ed. H.P.R. Frederikse. 1996, New York: CRC Press.

Table 2.1. Effect of Solvent on Average Properties of Adhesion Peaks

Solvent	Dielectric constant (ε)[78]	Mean Pull-off Distance (nm)[a]	Range of Pull-off Distances (nm)	Mean Pull-off Force (nN)
Formamide	111	295 ± 212	<1 – 725	-0.25 ± 0.24
Water	80.1	212 ± 211	<1 – 812	-0.46 ± 1.3
Methanol	33	137 ± 125	<1– 576	-1.1 ± 2.3
0.1 M KCl	-	68 ± 59	<1 – 229	-0.66 ± 1.4
0.01 M KCl	-	119 ± 90	<1 – 440	-0.46 ± 0.50

[a]Caution should be used in interpreting these mean and standard deviation values. The high standard deviation is caused by the polydispersity of the sample, and is not due to experimental "error". In addition to these values, histograms may provide a more meaningful way to examine the trends among the solvents (c.f. Figures 2.2 and 2.4).

Table 2.2 Summary of Model Parameters for Surface Biopolymers of *Pseudomonas putida* KT2442

	FJC			WLC		
Solvent	**L_c (nm)**	**a (nm)**	**Mean R^2**	**L_c (nm)**	**L_P (nm)**	**Mean R^2**
Water	9 - 1500	0.154 – 0.35	0.92 ± 0.13	9 - 1762	0.009 – 0.28	0.84 ± 0.17
Formamide	4 -853	0.154 –1	0.84 ± 0.23	9 - 986	0.006 – 0.82	0.79 ± 0.19
Methanol	8 -1100	0.154 –0.18	0.81 ± 0.22	7 -1248	0.036 – 0.21	0.69 ± 0.21
0.1 M KCl	6 - 259	0.154 – 0.65	0.78 ± 0.32	7 - 300	0.154 –0.36	0.67 ± 0.31
0.01 M KCl	6 - 176	0.154 – 0.32	0.88 ± 0.13	5 - 188	0.154 –0.20	0.73 ± 0.21

2.8 Figure captions

Figure 2.1. Typical AFM force curve. Far from surface, there is no interaction between the polymer brush layer and the tip. As the tip approaches the surface, the polymer brush layer compresses, giving rise to a repulsive force. Often some of the surface polymers will attach to the tip once contact has been made, given rise to the adhesion peaks in the retraction curve. Finally the tip will detach from the polymers and the interaction force will return to zero.

Figure 2.2. Probability distribution of pull-off distances for *Pseudomonas putida* KT2442 biopolymers at different ionic strengths.

Figure 2.3. The pull-off force vs. the pull-off distance for *Pseudomonas putida* KT2442 biopolymers in different solvents, demonstrating the effect of ionic strength.

Figure 2.4. Probability distribution of pull-off distances for *Pseudomonas putida* KT2442 biopolymers in solvents with different polarities.

Figure 2.5. The pull-off force vs. the pull-off distance for *Pseudomonas putida* KT2442 biopolymers in different solvents, demonstrating the effect of solvent polarity.

Figure 2.6. Comparison between experimental data and wormlike chain model (WLC) for KT2442 in A) 0.1 M KCl (L_c = 6.8 nm to 300 nm, L_P = 0.154 nm to 0.36 nm, R^2 = 0.67 ± 0.31. For all of the data in 0.01 M KCl, L_c is 1.16 ± 0.25 of the pull-off distance), B) 0.01 M KCl (L_c = 4.9 nm to 188 nm, L_P = 0.154 nm to 0.20 nm, R^2 = 0.73 ± 0.21. In 0.01 M KCl, L_c is 1.14 ± 0.20 of the pull-off distance). Each solid line presents a

stretching event of a polymer or a part of it, and has its own persistence length and contour length that differs from other solid lines. The same applies to Fig. 2.8.

Figure 2.7. Comparison between experimental data and freely jointed chain model (FJC) for KT2442 in A) 0.1 M KCl (L_c = 5.7 nm to 259 nm, a = 0.154 nm to 0.65 nm, R^2 = 0.78 ± 0.32. L_c in 0.1 M KCl is 0.90 ± 0.2 of the pull-off distance), B) 0.01 M KCl (L_c = 5.6 nm to 176 nm, a = 0.154 nm to 0.32 nm, R^2 = 0.88 ± 0.13. L_c in 0.01 M KCl is 0.81 ± 0.19 of the pull-off distance). Each solid line presents a stretching event of a polymer or a part of it, and has its own segment length and contour length that differs from other solid lines. The same applies to Fig. 2.9.

Figure 2.8. Comparison between experimental data and WLC model for KT2442 in A) Water (L_c = 8.6 nm to 1762 nm, L_P = 0.009 nm to 0.28 nm, R^2 = 0.84 ± 0.18. L_c in for all water lines is 1.18 ± 0.35 of the pull-off distance), B) Methanol (Lc = 6.9 nm to 1248 nm, L_P = 0.04 nm to 0.22 nm, R^2 = 0.68 ± 0.22. L_c for all methanol data is 1.19 ± 0.46 of the pull-off distance), C) Formamide (L_c = 8.6 nm to 986 nm, L_P = 0.006 nm to 0.82 nm, R^2 = 0.79 ± 0.19. L_c for formamide is 1.19 ± 0.36 of the pull-off distance). For clarity, each curve is divided into two parts, showing the comparison between the experimental data and the WLC model at low and high extensions, separately.

Figure 2.9. Comparison between experimental data and FJC model for KT2442 in A) Water (L_c = 8.7 nm to 1500 nm, a = 0.154 nm to 0.35 nm, R^2 = 0.92 ± 0.13. L_c for all the data considered together is 0.91 ± 0.38 of the pull-off distance). B) Methanol (L_c = 7.6 nm to 1100 nm, a = 0.154 nm to 0.18 nm, R^2 = 0.83 ± 0.21. L_c for all the data considered together is 0.82 ± 0.20 of the pull-off distance). C) Formamide (L_c = 3.9 nm to 853 nm, a

= 0.154 nm to 1.0 nm, $R^2 = 0.84 \pm 0.23$. L_c for all of the data considered together is 0.88 ± 0.26 of the pull-off distance). For clarity, each curve is divided into two parts, showing the comparison between the experimental data and the WLC model at low and high extensions, separately.

Figure 2.10. A) Comparison between FJC and FJC+ models at low extensions in water (R^2 values range between 0.47 to 0.97 with FJC, 0.39 to 0.97 with FJC+), B) Comparison between FJC and FJC+ models at mid extensions under water (R^2 values range between 0.94 to 0.99 in FJC model, while they range between 0.97 to 0.99 in FJC+ model) C) a comparison between FJC and FJC+ models at high extensions under water (R^2 values range between 0.58 to 0.98 with FJC model, while the FJC+ was not able to fit the last curve). L_c for all of the data considered together is 0.80 ± 0.19 of the pull-off distance.

Figure 2.11. A) Different polymers apparently exist on the surface of *P. putida* KT2442. More than one type can be attached to the tip at the same time. B) A surface polymer on KT2442 that can be attached to the tip at different locations. Even though multiple polymers (or portions of polymers) may attach to the tip as the tip approaches the surface, the chains will detach at different times. Therefore, when we analyze each adhesion event in our force-extension spectra, we are always examining the detachment (i.e. adhesion) of a single chain.

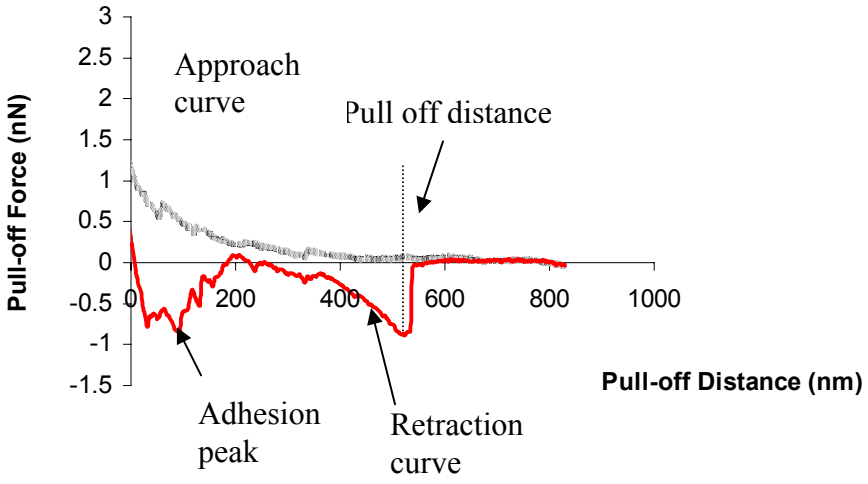
Pull-off Force (nN)
3
2.5
2
1.5
1
0.5
0
-0.5
-1
-1.5
0
200
400
600
800
1000
Pull-off Distance (nm)
Approach curve
Pull off distance
Adhesion peak
Retraction curve

Figure 2.1

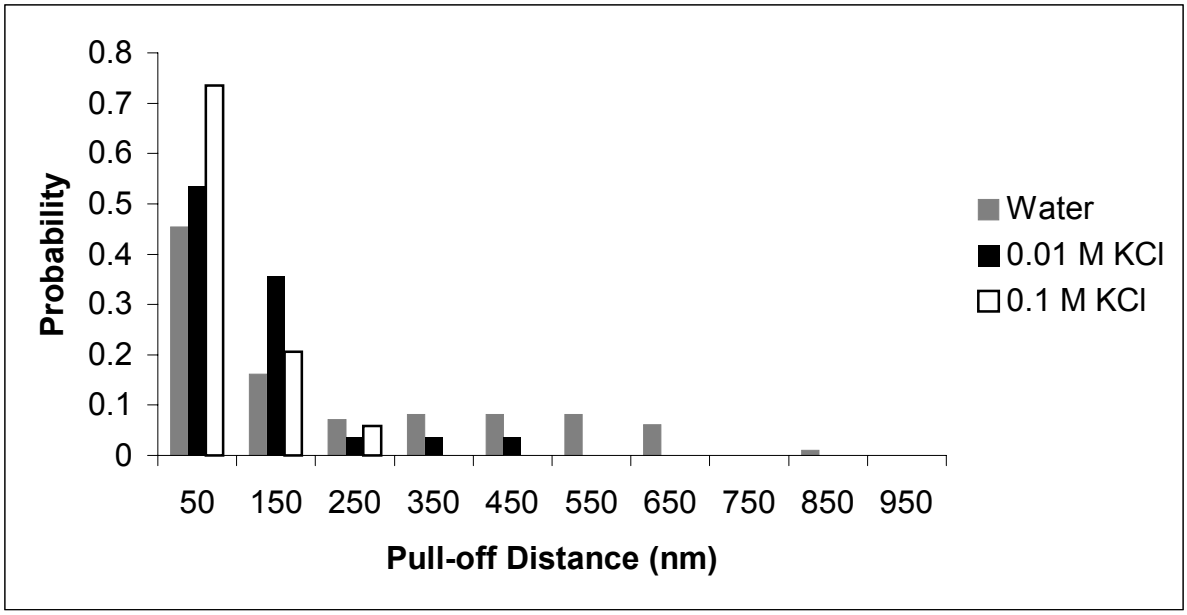
0.8
0.7
0.6
0.5
0.4
0.3
0.2
0.1
0
Probability
50
150
250
350
450
550
650
750
850
950
Pull-off Distance (nm)
Water
0.01 M KCl
0.1 M KCl

Figure 2.2

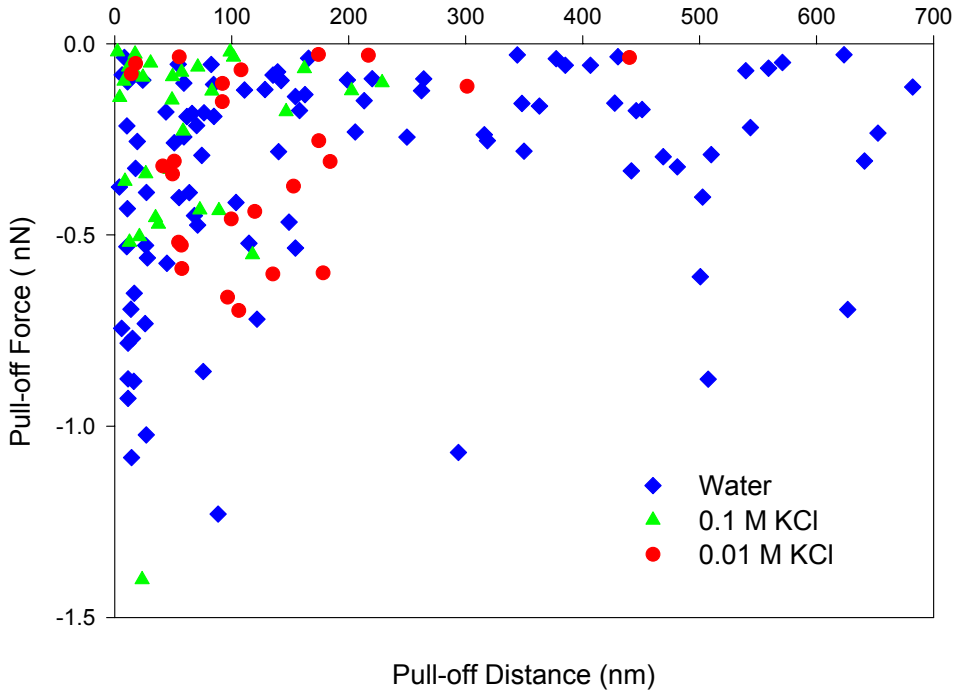
0
100
200
300
400
500
600
700
0.0
-0.5
-1.0
-1.5
Pull-off Force (nN)
Pull-off Distance (nm)
Water
0.1 M KCl
0.01 M KCl

Figure 2.3

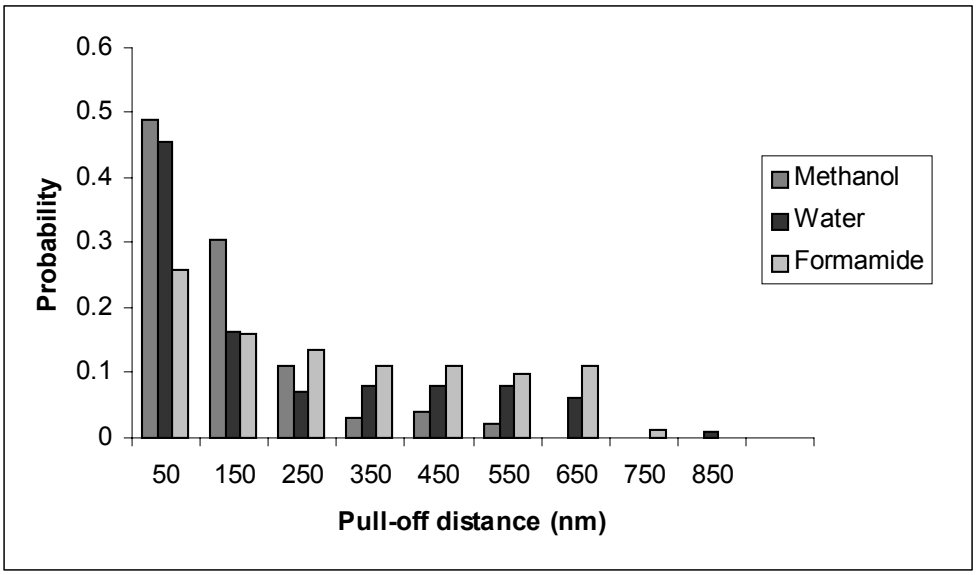
0.6
0.5
0.4
0.3
0.2
0.1
0
Probability
50
150
250
350
450
550
650
750
850
Pull-off distance (nm)
Methanol
Water
Formamide

Figure 2.4

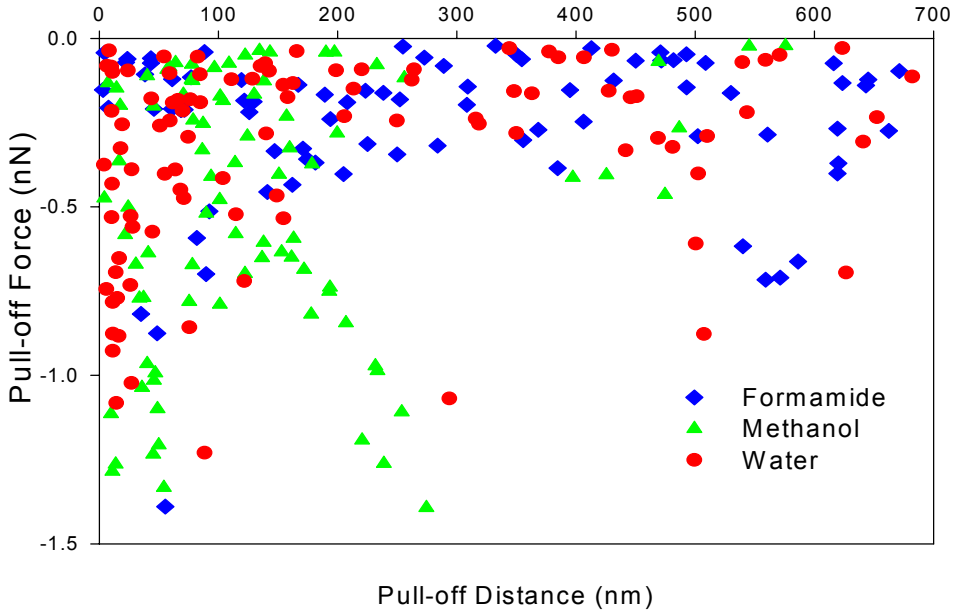
0
100
200
300
400
500
600
700
0.0
-0.5
-1.0
-1.5
Pull-off Force (nN)
Pull-off Distance (nm)
Formamide
Methanol
Water

Figure 2.5

A) 0.1 M KCL

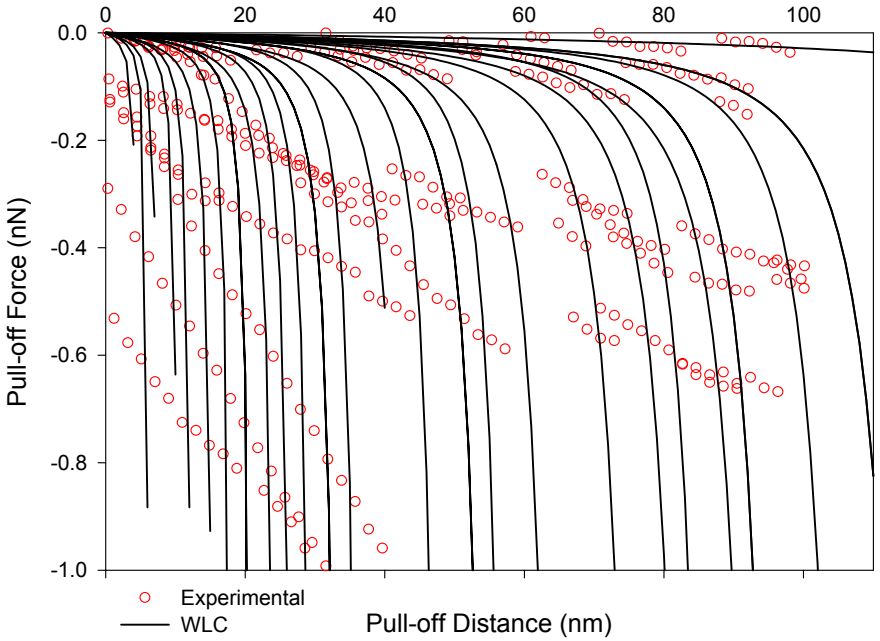

B) 0.01 M KCl

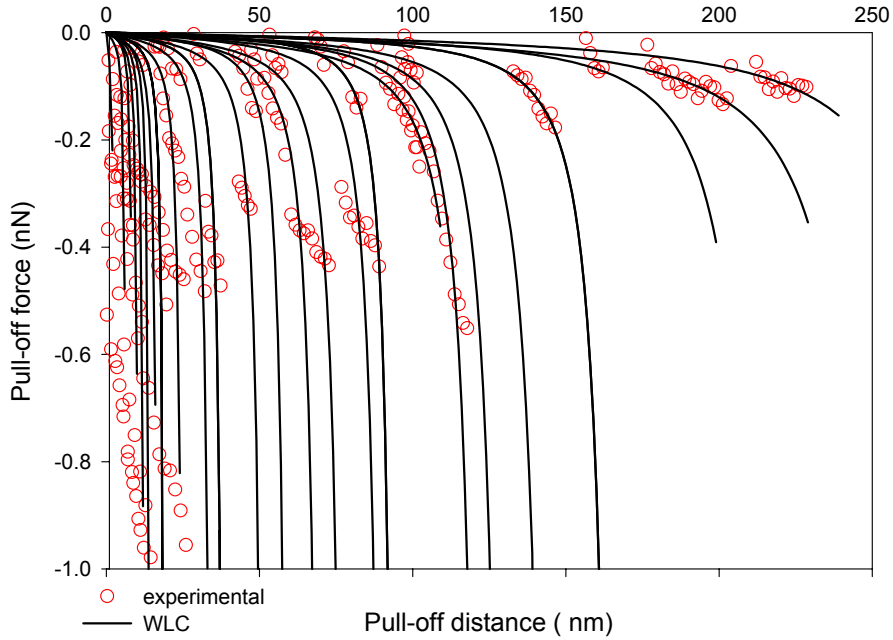

Figure 2.6

A) 0.1 M KCl

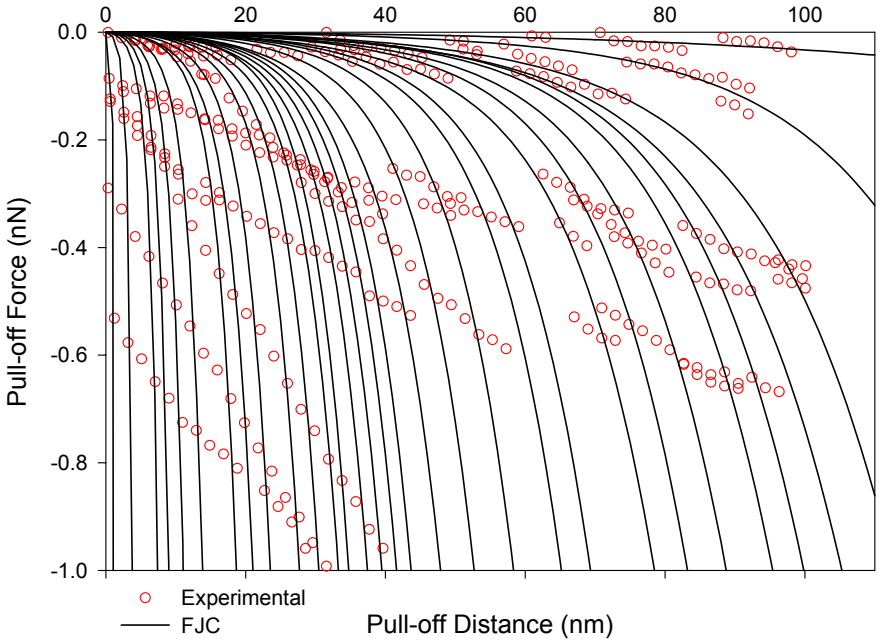

B) 0.01 M KCl

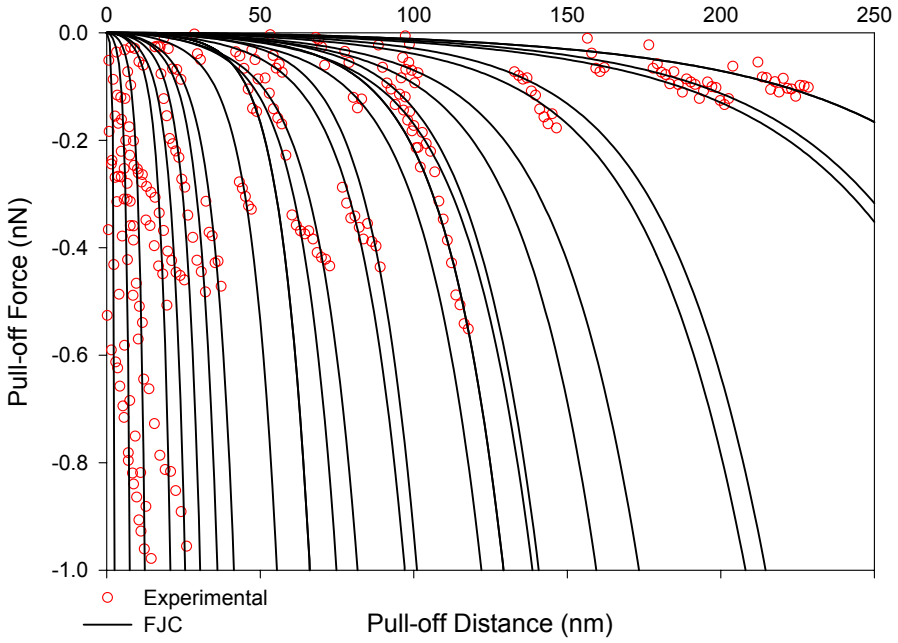

Figure 2.7

A) Water

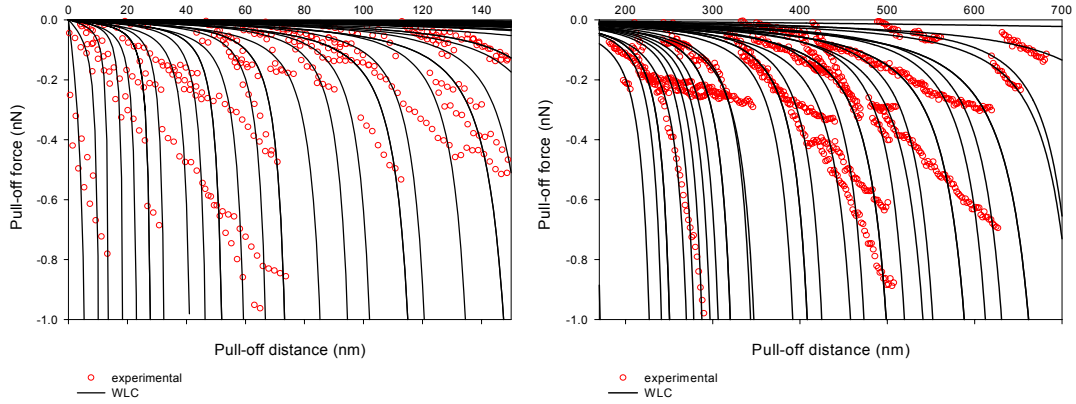

B) Methanol

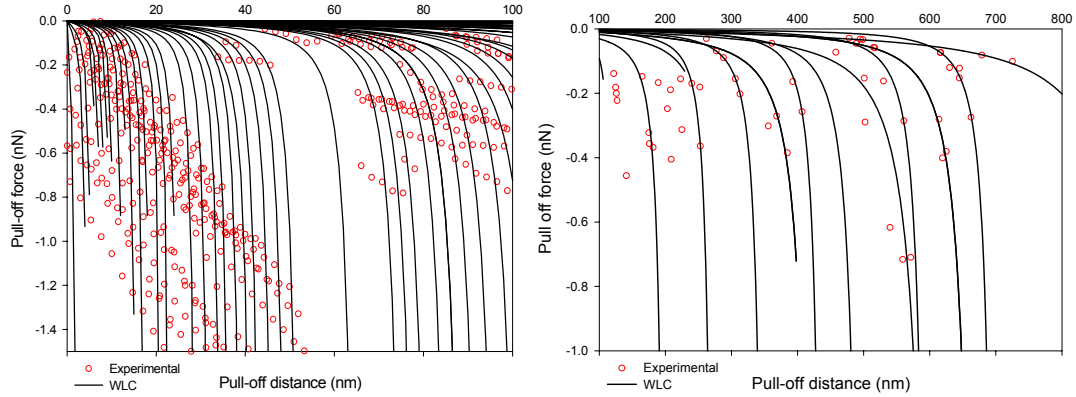

C) Formamide

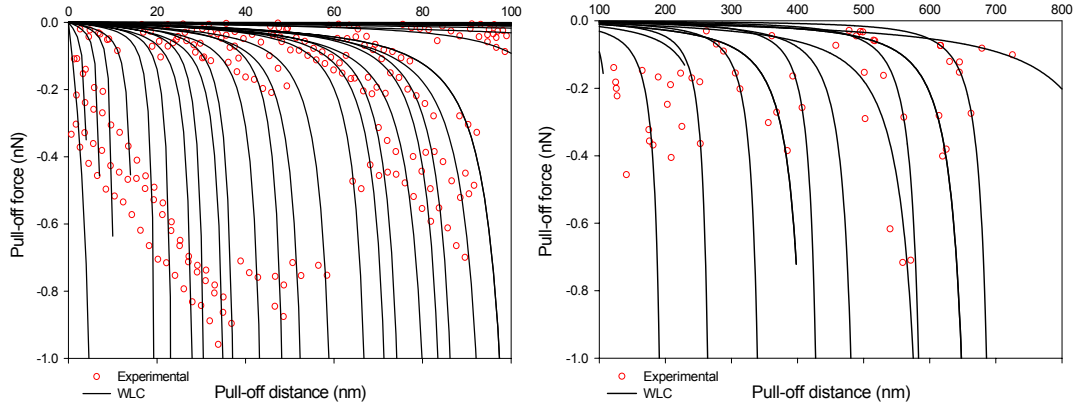

Figure 2.8

A) Water

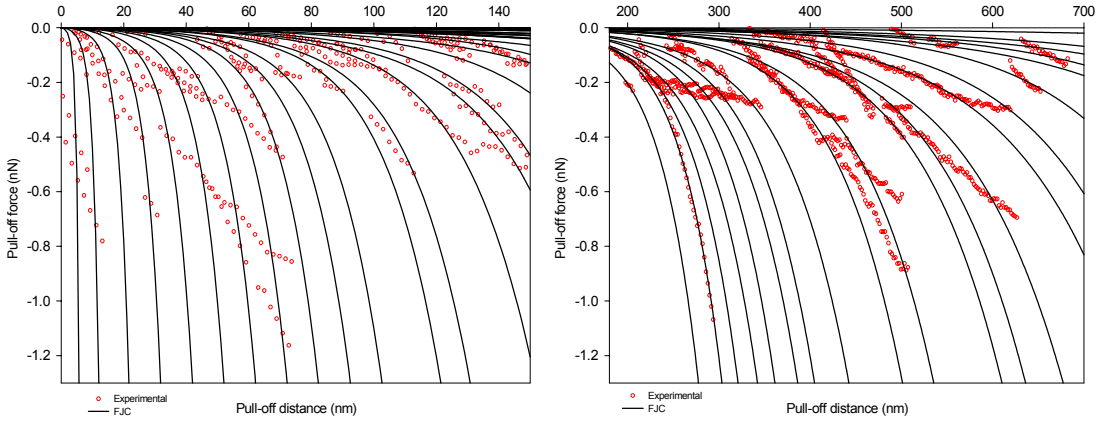

B) Methanol

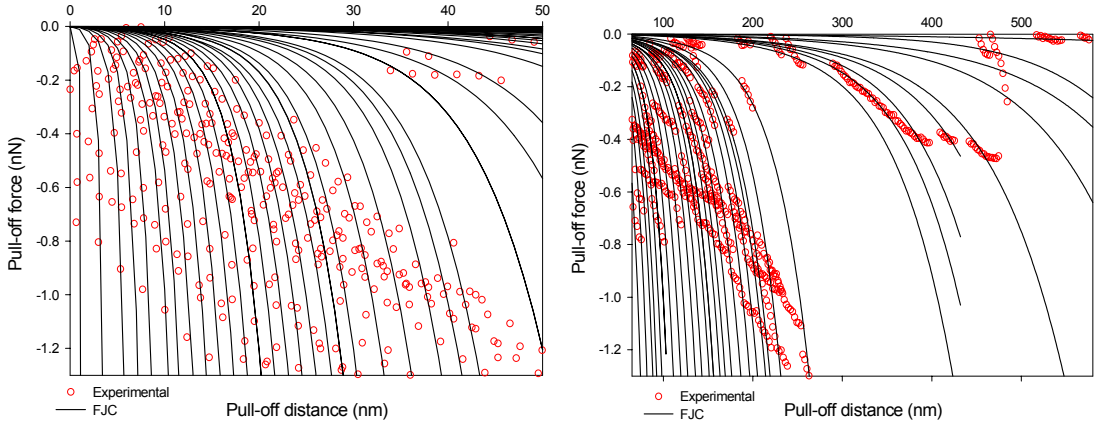

C) Formamide

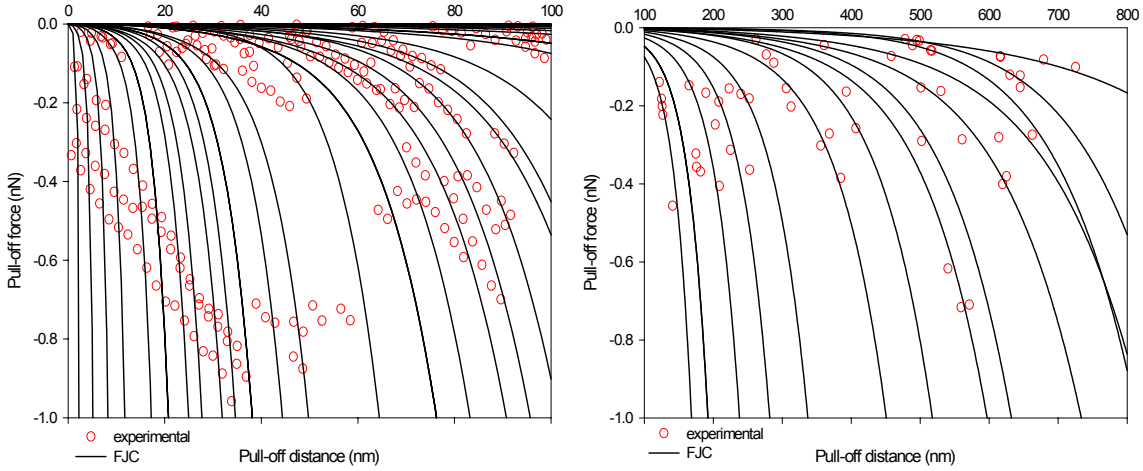

Figure 2.9

A) Short-Range Extensions

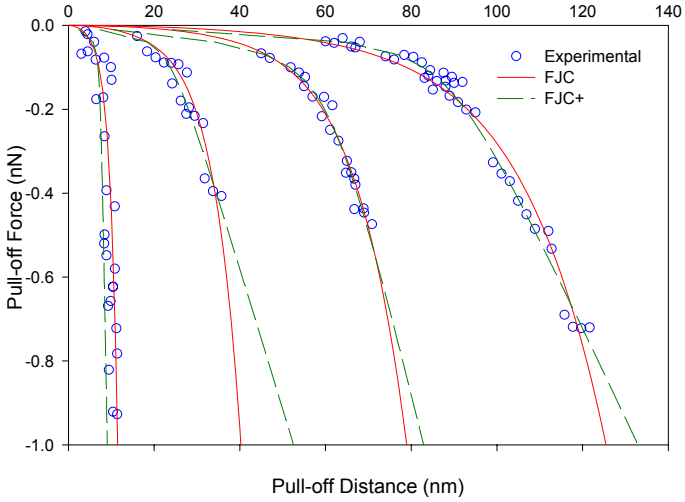

B) Mid-Range Extensions

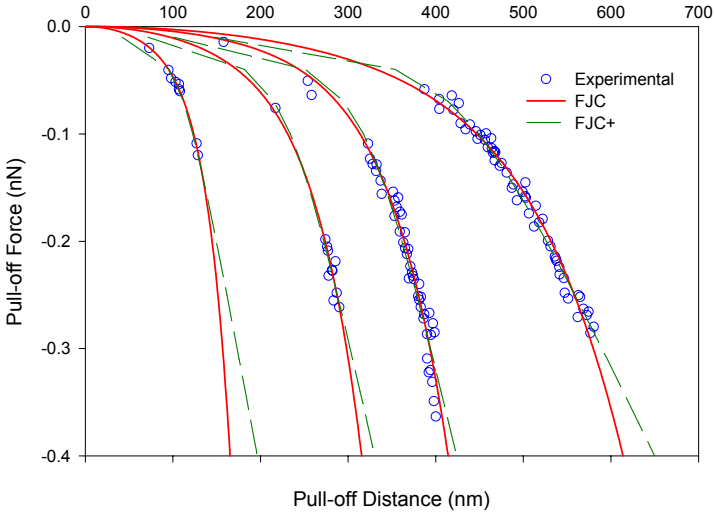

C) Long-Range Extensions

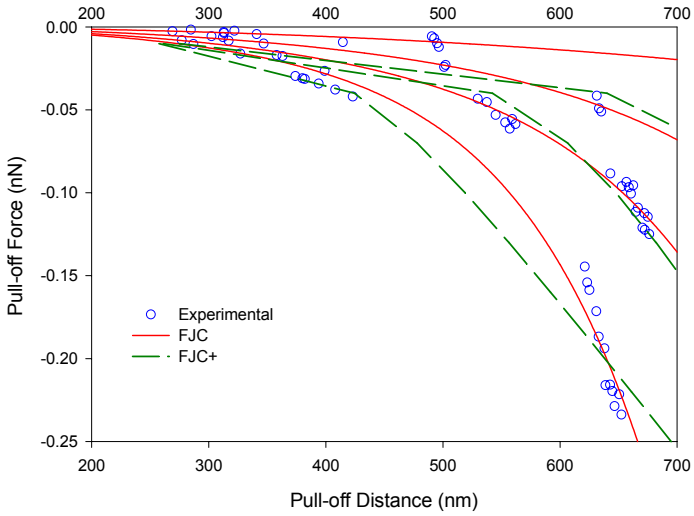

Figure 2.10

A) B)

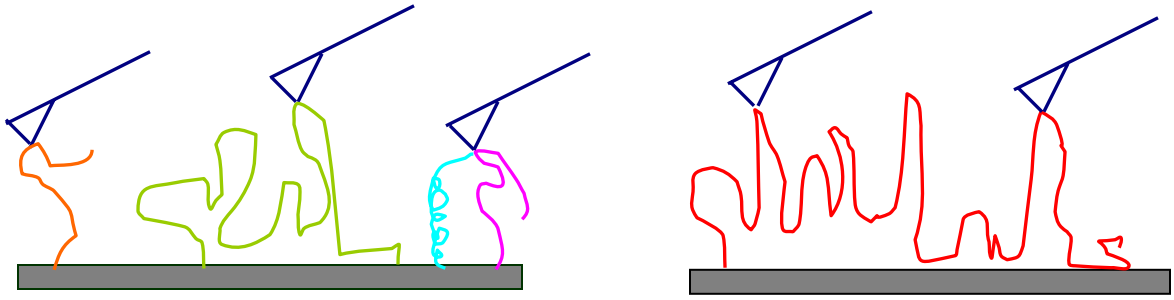

Figure 2.11

Chapter 3

Heterogeneity in Bacterial Surface Polysaccharides, Probed on a Single-Molecule Basis

Abstract

The heterogeneity in bacterial surface macromolecules was probed by examining individual macromolecules on the surface of *Pseudomonas putida* KT2442 via single-molecule force spectroscopy (SMFS). Using an atomic force microscope (AFM), the silicon nitride tip was brought into contact with biopolymer molecules on bacterial cells and these macromolecules were stretched. Force-extension measurements on different bacterial cells showed a range of adhesion affinities and polymer lengths. However, substantial heterogeneity was also observed in the force-extension curves on a single bacterium. A given bacterium has biopolymers that range in size from tens to hundreds of nanometers, and with adhesion affinities for the AFM tip from nearly zero to greater than 1 nN. A distribution of polymer sizes was confirmed by size-exclusion chromatography. The freely jointed chain (FJC) model for polymer elasticity was applied to individual force-extension curves in order to estimate the contour lengths and segment lengths of the polymer chains. A range of segment lengths was obtained using the FJC model, from 0.154 nm up to 0.45 nm in water, 0.154 – 0.65 nm in 0.1 M KCl, and 0.154 – 0.32 nm in 0.01 M KCl. The modeling confirms that the heterogeneity in biopolymers is more than a matter of differences in molecular weights, since a range of stiffnesses (segment lengths) was also observed. The effect of salt concentration on biopolymer conformation and adhesion was also explored. The biopolymers were slightly more

extended in water than in either of the salt solutions (0.01 and 0.1 M KCl). Although the adhesion of polysaccharides with the AFM tip was expected to be dependent on salt concentration, heterogeneity overwhelmed any trends that could be observed in adhesion with respect to solution ionic strength. These experiments indicate that heterogeneity in biopolymer properties on an individual bacterium and within a population of bacterial cells may be much greater than previously believed.

3.1 Introduction

Understanding the fundamental adhesion processes between bacteria and surfaces is important for many environmental and biomedical applications, such as *in situ* bioremediation, microbially-facilitated transport of contaminants, and biofilm formation on biomaterials and implants. Bacterial adhesion depends on the properties of extracellular polymers, but while progress has been made in understanding the role of surface biopolymers on adhesion [1-4], predictions of attachment based on biopolymer properties have not yet been possible.

We hypothesize that heterogeneity in cell surface macromolecules is a key factor in explaining the inability to predict adhesion. A bimodal distribution in the attachment efficiencies of bacteria with soil for a single population of cells has been observed in several systems [5-9]. Heterogeneity in cell surface lipopolysaccharides (LPS) or extracellular polysaccharides (EPS) has been speculated as the reason for a distribution of bacterial affinities [7], but a direct link between macromolecule heterogeneity and different attachment affinities has not yet been demonstrated.

Lipopolysaccharides (LPS) cover ~45% of the surface of Gram-negative bacteria [10], and many bacterial surfaces have a layer of extracellular polysaccharides (EPS [11]). For microbes without EPS, the O-antigen portion of the LPS is believed to be responsible for adhesion because it protrudes into the cell surrounding. Correlations with biopolymer size and adhesion have been observed. For example, Jucker et al. [12] found that the affinity of *Escherichia coli* and *Citrobacter freundii* O-antigens for TiO_2 and Al_2O_3 increased as the molecular mass of the O-antigen increased. Ong et al. [13] found a correlation between the size of the LPS molecule and adhesion forces using mutants

with varying LPS properties. Mean-field calculations for predicting the interaction between a model bacterium and a planar surface demonstrated that a single polymer chain with a persistence length typical for polysaccharides could provide sufficient steric repulsion to prevent bacterial adhesion. These studies illustrate that the conformational behavior of bacterial surface macromolecules affects the likelihood for adhesion.

Techniques are now available to probe the physical and chemical properties of bacterial surface macromolecules at the nanoscale. Single-molecule force spectroscopy (SMFS) experiments involve using an atomic force microscope (AFM) or similar instrument to stretch macromolecules. While these experiments are employed for DNA [14-16], polysaccharides [17-24], proteins [14, 17], and other polymers [25], very few experiments have involved macromolecules on a living cell surface. In the first such study, Benoit et al. [26] probed the surface proteins on cells of *Dictyostelium discoideum* and determined that adhesion between adjacent cells involves discrete interactions. In another very interesting study, van der Aa et al. [27] stretched macromolecules on the surface of fungal spores of *Aspergillus oryzae*, and were able to use the extended freely jointed chain model to account for polymer elastic properties.

In this communication, we present direct, single-molecule evidence of the heterogeneity in polysaccharides on bacterial surfaces, at both the level of an individual bacterium and across a population of bacterial cells. SMFS experiments allowed us to probe the macromolecules on multiple, individual cells. We determined the morphology and mechanical properties of the polysaccharides from these studies. Evidence of physical heterogeneity in cell surface macromolecules and in adhesion properties is presented.

3.2 Materials and Methods

3.2.1 Cultures

Bacteria that have been extensively investigated for use in bioremediation [28, 29] were chosen for experimentation. D.F. Dwyer (Department of Earth, Ecological, and Environmental Sciences, The University of Toledo, Toledo, OH), provided *Pseudomonas putida* KT2442, a microbe that can degrade substituted aromatic compounds [28]. Cultures were grown in M9 buffer containing a mineral salt solution and 5 mM benzoate and 50 μg/l rifampicin [29].

3.2.2 Bacterial Cell Preparation for AFM Measurements

KT2442 cells were bonded to glass slides as previously described [30]. Slides were kept hydrated the entire time prior to AFM work. Experiments were conducted in pure water, 0.01 M KCl, and 0.1 M KCl.

3.2.3 Single-Molecule Force Spectroscopy

Forces were measured between individual bacterial cells and silicon nitride cantilevers in water using an AFM (Digital Instruments Dimension 3100 with Nanoscope III controller). The attachment of bacterial cells to glass slides, selection of a cell for a force measurement, and conversion of deflection data to force-extension curves has been described previously [31]. At least triplicate measurements were performed on a single bacterium. Measurements were made on at least 5 bacterial cells per chemical condition studied. All force measurements were counted individually (no averaging was performed). Silicon nitride AFM tips were used (DNPS, Digital Instruments), with an average spring constant of 0.13 ± 0.02 N/m, measured using the Cleveland method [32].

When contact is made between the AFM tip and a bacterium, surface

macromolecules from the bacterium adsorb onto the tip, leading to an adhesion force. The AFM tip continues to retract, stretching these surface biopolymers until eventually the tip breaks free of the adhesion forces and returns to a force of zero. This process forms a cycle. Contact between the tip and the bacterial surface polymers until maximum adhesion is reached is the first half of the cycle, while the retraction of the tip from the surface polymers and a return to a force of zero is the second part of the cycle. In the analysis of the force curves, only the data from the first part of the cycle was considered. The distance at which the force returns to zero is called the "pull-off distance". The adhesion force between the biopolymer and the tip before breaking free is the "pull-off force".

3.2.4 Modeling Biopolymer Elastic Properties

Elastic properties of the biopolymers were estimated using polymer-stretching models. In the simplest model for polymer stretching, polymer conformation can be described as a Gaussian chain, where the distribution is independent of the microscopic structure of the molecule [33]. However, at higher forces, the sections of the chain no longer orient in a random fashion, and the molecule becomes oriented along the direction of the external force. This case can be described using the freely jointed chain (FJC) model. The polymer is described as consisting of n rigid elements, each with a length l_k, connected through flexible joints that are free to rotate in any direction. The pulling force, F, can be related to the extension of the chain, x.

$$F = \frac{-k_B T}{l_k} \mathbf{L}^{-1}\left(\frac{x}{L}\right) \tag{3.1}$$

$$\mathbf{L}^{-1} = 3\left(\frac{x}{L}\right) + \frac{9}{5}\left(\frac{x}{L}\right)^3 + \frac{297}{175}\left(\frac{x}{L}\right)^5 + \frac{1539}{875}\left(\frac{x}{L}\right)^7 \tag{3.2}$$

where k_B is Boltzmann constant, T is absolute temperature, L is contour length (the length of the linearly extended molecule not including stretching in the backbone), and **L** is the Langevin function. The FJC model has been successfully used to describe the elasticity of such polymers as dextran [34], oligonucleotides [14], polydimethylsiloxane [35], and poly(methacrylic acid) [25]. The model's ability to fit the experimental data was compared based on the estimated values of R^2 (the coefficient of determination, often used to judge the adequacy of a regression model) using the Tablecurve fitting program.

3.2.5 Polymer Characterization

We performed all AFM experiments on intact bacterial cells, but supplemented these investigations with studies on extracted biopolymers from *P. putida* KT2442. For these experiments, the polymers were separated from the bacterial cells (grown until late exponential growth phase) by centrifugation for 15 minutes at 6000 RPM (DAMON/IEC HT Centrifuge). The polymers were freeze-dried and kept in the refrigerator until use.

3.2.6 Size-Exclusion Chromatography

The size distribution and the molecular weights of KT2442 surface polymers were analyzed using two columns (ultrahydrogel 250 and 2000). A Wyatt Technology Cooperator Dawn DSP laser photometer was used to obtain the molecular weights and a Waters Differential Refractometer R401 was used to analyze the mass. A 100 mg/ml solution of the freeze-dried polymer was injected in the column for the analysis (0.2 ml injection).

3.2.7 Polarimetry

The optical rotatory dispersion of the polymers was determined using a Perkin Elmer 241 MC polarimeter. A 25,000 ppm polymer solution (in water) was prepared

from the freeze-dried polymer. The measurements were run at four different wavelengths using a sodium lamp (589 nm) and a mercury lamp (546 nm, 436 nm, and 365 nm), and the maximum measured value of optical rotation in degrees was reported. The accuracy in measuring the optical rotation was ± 0.001 degree.

3.3 Results

3.3.1 Single-Molecule Force Spectroscopy

Force-extension curves were compared to determine intracellular and cell-to-cell variability in biopolymer properties. When examining force measurements on several cells, it is obvious that there is heterogeneity in the amount of adhesion force and in the size of the biopolymers (Figure 3.1). Biopolymer sizes can range from tens to many hundreds of nanometers. On a single bacterium, we also see a range of force-extension curves (Figure 3.2). On bacterial cell #1, the adhesion peak at ~ 500 nm appeared twice, and the adhesion peak at ~600 nm on bacterial cell #2 was also repeated. However, these peaks are generally not reproducible because the AFM tip is more likely to make contact with a different portion of the polymer or a different polymer molecule in subsequent measurements. Most of the adhesion peaks were not repeated.

The amount of adhesion between the AFM tip and the biopolymer is important to quantify for those interested in bacterial adhesion. However, Figure 3.3 shows that a bacterium may have biopolymers with adhesion affinities for the AFM tip that range from nearly zero to > 1 nN. The values of the adhesion peaks (the point at which tip break free from the polymers) in the force curves for different bacterial cells were used to construct Figure 3.3. Intracellular variability appears to be as important as cell-to-cell variability.

Due to this variability, we can only get meaningful information by examining many adhesion events over multiple cells. When many measurements are performed, it is possible to generalize about the polymer properties if polymer elasticity models (like the FJC model) are employed. Although the polymers may have a wide range of sizes and adhesion affinities, the FJC model can be applied to all of the data with reasonable accuracy (Figure 3.4; the average R^2 is 0.95). The results of the FJC modeling (for water) show that the segment length, l_k varied from 0.154 (the lower limit since it is the length of a C-C bond) to 0.45 nm, but 65% of the chains in water have a segment length in the range of 0.154 – 0.20 nm. These segment lengths indicate that very flexible polymers are present on the bacterial surfaces. The histogram showing the segment length distribution for polymers in water clearly shows a peak at an l_k of 0.154 – 0.20 nm. A small portion of chains have l_k values 0.20 – 0.25 nm, 0.30 -0.35, and very few have l_k values higher than 0.4 nm Figure 3.5, Table 3.1.

SMFS experiments were also performed in 0.01 M and 0.1 M KCl, and the FJC model was applied to this data (the full force-extension curves and table of l_k values are shown only for water). The segment length values in the two salt solutions were compared with the corresponding values in water. Figure 3.5 shows that in all solvents, the largest peak is for segment lengths of 0.154 – 0.20 nm, with few chains having higher l_k values.

The pull-off distances were also compared among solvents. In water, the pull-off distances ranged from tens to hundreds of nm (Figure 3.6, Table 3.2). A substantial number of long chains were observed in water, with 38% of the chains having pull-off distances longer than 200 nm (Figure 3.6A). In either of the salt solutions tested, < 10%

of the chains had pull-off distances longer than 200 nm.

Adhesion forces between the biopolymers and the silicon nitride tips were also measured in the three solvents. The heterogeneity in the adhesion affinities of biopolymers is so great that it overwhelms any trend that could be observed with respect to salt concentration (Figure 3.6B). When looking at the results for any one solvent, we see that heterogeneity in the adhesion affinity exists among biopolymers on a single cell, and across cells of a given population.

3.4 Discussion

3.4.1 Physical Heterogeneity

Since we do not have independent knowledge of the contour length of the polymers, it is difficult to relate the pull-off distances to the contour lengths of the biopolymers. It is likely that the pull-off distances are some fraction of the actual contour lengths of the molecules, and these distances should be proportional to the contour lengths if single molecules are probed [24]. Since we cannot say from the AFM experiment if we have polymers of different sizes, a size-exclusion chromatography (SEC) experiment was also performed on polymer extracted from *P. putida* KT2442. The broadness of the SEC peak (Figure 3.7) demonstrates that we do have polymers with a range of molecular weights, and therefore would expect to find polymers of different lengths.

3.4.2 Chemical Heterogeneity

At high forces, the majority of biopolymers show deviations from polymer elasticity models, even with models that include elastic deformations from the backbone [18, 36]. For example, dextran molecules exhibit a plateau in their force-extension curve

at 700 pN [18]. The conformational transition is attributed to the C_5-C_6 bond of the sugar ring flipping into a new conformation, which causes the molecule to elongate by 0.65 Å (~10% of its length). Dextran can be stretched and relaxed again. For native xanthan, an irreversible transition is observed at 400 pN [19]. Xanthan's structure is stabilized by hydrogen bonds and electrostatic interactions. Once the xanthan double helix has been broken apart by the stretching event, the helix cannot reform. The structure of xanthan is like cellulose in that is has (1,4)-β-D-glucose residues and a substituted sugar side chain. These structures can participate in hydrogen bonding because of the β linkages. Marszalek et al. [22-24] demonstrated the link between a plateau region in the force-extension curve and the conformation of the sugar with respect to the pyranose ring. Stretching the polysaccharide with an external force is likely to favor a conformation of the pyranose ring that provides greater separation between the glycosidic oxygens, and this leads to an extension of the molecule. The distance between O_1 and O_4 increases during a chair-boat transition when the glycosidic oxygen is in the axial position, as in amylose. The distance between O_1 and O_4 is already at a maximum when O_1 is in the equatorial position, as in cellulose. In cellulose and similar compounds, no plateau is observed and no enthalpic component of the force-extension curve is present.

In our study, we want to determine if the macromolecules are all the same chemically. If the polymer is chemically homogeneous but of different molecular weights, then we should be able to normalize the data to all fall on one curve, as could be done with a chemically homogeneous sample of poly(methacrylic acid) [25]. This cannot be done in our case because the FJC model yields a range of segment lengths. Therefore, we probably have distinctly different macromolecules present on the bacterial surface.

However, it does seem likely that the polymers on the surface are chemically similar, based on the shape of the SMFS curves. Cellulose and other sugars with β(1→4) linkages do not show force-induced plateaus. The biopolymers on the surface of *P. putida* KT2442 never show a plateau or evidence of a conformational transition in their force-extension measurements. While they may not be identical chemically, they appear to be cellulose-like, or consisting of β(1→4) linkages. A polarimetry test run on our polymers confirmed this hypothesis. The negative rotations observed in the measurements indicated that we do have β-type sugars [37], although further experiments are being performed to determine more precisely the structure of these sugars.

The study of polysaccharide conformation in the presence of stresses is important for many fields besides bacterial adhesion. The range of forces required to trigger these conformational transitions are found naturally in cellular systems, such as the high tensile stress that bacterial and plant cell walls must support in response to changes in turgor pressure. Another example is in the mechanical cellular event, exocytosis. The major steps of exocytosis entail physical movement and the generation of force [38].

3.4.3 Effect of Solution Ionic Strength

Many studies indicate that polysaccharide conformation is affected by the type and amount of salt in solution and those polysaccharides need some salt to stabilize their helical structures. For example, succinoglycan forms a disordered non-helical structure in pure water but is a gel-like structure in 0.1 M KCl [39]. The formation of a gel is possible because electrostatic repulsion between polymer chains is reduced in the presence of KCl. Upon heating to 95ºC, native xanthan can be denatured from a double to single helical structure. Denatured xanthan will renature into its native double-helix

form only when salt is present in solution [40, 41]. Gellan is a double-stranded helix in very dilute aqueous solution containing low molecular weight salts but adopts a disordered, perhaps single-stranded configuration in the absence of added salts [42]. The presence of salts minimizes electrostatic repulsion among charged segments of the polysaccharide chains.

For charged polysaccharides, their conformation can be altered by the addition of salt. Electrostatic repulsion between charged units is decreased when salt is added, allowing the polysaccharide to transform from an extended to coiled shape. For example, in a polysaccharide produced by the marine bacterium *Pseudomonas atlantica*, as the ionic strength was increased to marine salt concentrations (about 0.5 M), adsorbed anionic EPS changed from an extended to contracted configuration and collapsed onto the solid substrate surface [43]. The conformation of xanthan transformed from isolated extended rods to coils and sometimes aggregates when KCl was added to solution [40]. Sometimes this effect is ion specific. For example, intermolecular associations in hyaluronan are stabilized by NaCl and not KCl [44]. Cowman et al. hypothesized this to be due to either counterion bridges or the differences in water structure between the two solvents.

In our study, there is evidence that the polymer chains became more coiled when salt was present, since longer, presumably extended chains were observed only in pure water. However, the heterogeneity of our sample makes it difficult to provide more conclusive evidence of this conformational change.

3.4.4 Adhesion Affinities

With biopolymers having different physical and chemical properties, it is

therefore not surprising that a range of adhesion affinities for the silicon nitride AFM tip was observed. For some microbes, a bimodal distribution in adhesion affinities has been hypothesized, such as for the adhesion of *Pseudomonas sp.* B13 to sand [7], and the adhesion of the Savannah River deep isolate A1264, and the Oyster, VA soil isolate CD1 to glass beads in laboratory column studies [5]. For *P. putida* KT2442, it appears that even a bimodal distribution of adhesion affinities would not be sufficient to explain the observed behavior since many adhesion affinities were observed. Preliminary data from our laboratory indicates that many bacterial strains have multiple polymers on their surfaces, including *Escherichia coli* JM109 and *Burkholderia cepacia* G4. It is perhaps the presence of these multiple polymers with different properties on a bacterial surface that have made it so difficult to predict and explain bacterial adhesion behavior. Preliminary nuclear magnetic resonance (NMR) results suggest that three distinct sugars are present on the surface of *P. putida*. Our future work will involve mapping the polysaccharides on bacterial surfaces at a single-molecule level.

3.5 Acknowledgments

We thank Dave Adams (WPI), Eric Wakshull (Biogen), and Rick Stock (WPI) for experimental assistance in polymer preparation and SEC experiments, Ted Crusberg (WPI) for many helpful discussions, William Winter (SUNY-ESF, Syracuse) for the NMR analysis, Lale Burk and Kate Queeney (Smith College) for their help with the polarimetry tests, and the WPI Research Development Council for partial funding of this work.

3.6 References

1. Rijnaarts, H.H.M., W. Norde, E.J. Bouwer, J. Lyklema, and A.J.B. Zehnder, *Reversibility and mechanism of bacterial adhesion.* Colloids and Surfaces B: Biointerfaces, 1995. **4**: p. 5-22.
2. Rijnaarts, H.H.M., W. Norde, J. Lyklema, and A.J.B. Zehnder, *The isoelectric point of bacteria as an indicator for the presence of cell surface polymers that inhibit adhesion.* Colloids and Surfaces B: Biointerfaces, 1995. **4**: p. 191-197.
3. Rijnaarts, H.H.M., W. Norde, J. Lyklema, and A.J.B. Zehnder, *DLVO and steric contributions to bacterial deposition in media of different ionic strengths.* Colloids and Surfaces B: Biointerfaces, 1999. **14**: p. 179-185.
4. Jucker, B.A., A.J.B. Zehnder, and H. Harms, *Adsorption of bacterial surface polysaccharides on mineral oxides is mediated by hydrogen bonds.* Environmental Science & Technology, 1998. **32**: p. 2909-2915.
5. Baygents, J.C., J. Glynn, J. R., O. Albinger, B.K. Biesewmeyer, K.L. Ogden, and R.G. Arnold, *Variation of surface charge density in monoclonal bacterial populations: implications for transport through porous media.* Environmental Science & Technology, 1998. **32**: p. 1596-1603.
6. Albinger, O., B.K. Biessemeyer, R.G. Arnold, and B.E. Logan, *Effect of bacterial heterogeneity on adhesion to uniform collectors by monoclonal population.* FEMS Microbiology Leters, 1994. **124**(321-326).
7. Simoni, S.F., H. Harms, T.N.P. Bosma, and A.J.B. Zehnder, *Population heterogeneity affects transport of bacteria through sand columns at low flow rates.* Environmental Science & Technology, 1998. **32**: p. 2100-2105.

8. Williams, V. and M. Fletcher, *Pseudomonas fluorescens adhesion and transport through porous media are affected by lipopolysaccharide composition.* Applied and Environmental Microbiology, 1996. **62**: p. 100-104.

9. Bolster, C.H., A.L. Mills, G.M. Hornberger, and J. Herman, *Effect of intra-population heterogeneity on the long distance transport of bacteria.* Ground Water, 2000. **38**: p. 370-375.

10. DiRienzo, J.M., K. Nakamura, and M. Inouye, *The outer membrane proteins of gram-negative bacteria:biosynthesis, assembly, and functions.* Ann. Rev. Biochem., 1978. **47**: p. 481-532.

11. Neidhardt, F.C., J.L. Ingraham, and M. Schaechter, *Physiology of the Bacterial Cell: A Molecular Approach*. 1990, Sunderland, MA: Sinauer Associates.

12. Jucker, B.A., H. Harms, S.J. Hug, and A.J.B. Zehnder, *Adsorption of bacterial surface polysaccharides on mineral oxides is mediated by hydrogen bonds.* Colloids and Surfaces B: Biointerfaces, 1997. **9**: p. 331-343.

13. Ong, Y.-L., A. Razatos, G. Georgiou, and M.M. Sharma, *Adhesion forces between E. coli bacteria and biomaterial surfaces.* Langmuir, 1999. **15**: p. 2719-2725.

14. Lee, G.U., D.A. Kidwell, and R.J. Colton, *Sensing discrete streptavidin-biotin interactions with atomic force microscopy.* Langmuir, 1994. **10**: p. 354-357.

15. Strick, T.R., J.-F. Allemand, D. Bensimon, A. Bensimon, and V. Croquette, *The elasticity of a single supercoiled DNA molecule.* Science, 1996. **271**: p. 1835-1837.

16. Smith, S.B., Y. Cui, and C. Bustamante, *Overstretching B-DNA: The elastic response of individual double-stranded DNA molecules.* Science, 1996. **271**: p. 795-799.

17. Rief, M., M. Gautel, F. Oesterhelt, J.M. Fernandez, and H.E. Gaub, *Reversible unfolding of individual titin immunoglobin domains by AFM.* Science, 1997. **276**: p. 1109-1111.

18. Rief, M., J.M. Fernandez, and H.E. Gaub, *Elasticity coupled two-level systems as a model for biopolymer extensibility.* Physical Review Letters, 1998. **81**(21): p. 4764-4767.

19. Li, H., M. Rief, F. Oesterhelt, and H. Gaub, *Single-molecule force spectroscopy on xanthan by AFM.* Advanced Materials, 1998. **3**(4): p. 316-319.

20. Li, H., M. Rief, F. Oesterhelt, and H. Gaub, *Force spectroscopy on single xanthan molecules.* Appl. phys. A., 1999. **68**: p. 407-410.

21. Ludwig, M., M. Rief, L. Scmidt, F. Oesterhelt, M. Gautel, and H.E. Gaub, *AFM, a tool for single-molecule experiments.* Appl. phys. A., 1999. **68**: p. 173-176.

22. Marszalek, P.E., A.F. Oberhauser, Y.-P. Pang, and J.M. Fernandez, *Polysaccharide elasticity governed by chair-boat transitions of the glucopyranose ring.* Nature, 1998. **396**: p. 661-666.

23. Marszalek, P.E., Y.-P. Pang, H. Li, J. El Yazal, A.F. Oberhauser, and J.M. Fernandez, *Atomic levers control pyranose ring conformation.* Proceedings of the National Academy of Science USA, 1999. **96**: p. 7894-7898.

24. Marszalek, P.E., H. Li, and J.M. Fernandez, *Fingerprinting polysaccharides with single-molecule force spectroscopy.* Nature Biotechnology, 2001. **19**: p. 258-262.

25. Ortiz, C. and G. Hadziioannou, *Entropic elasticity of single polymer chains of poly(methylacrylic acid) measured by atomic force microscopy.* Macromolecules, 1999. **32**: p. 780-787.

26. Benoit, M., D. Gabriel, G. Gerisch, and H.E. Gaub, *Discrete interactions in cell adhesion measured by single-molecule force spectroscopy.* Nature Cell Biology, 2000. **6**: p. 313-319.

27. Van der Aa, B.C., R.M. Michel, M. Asther, M.T. Zamora, P.G. Rouxhet, and Y.F. Dûfrene, *Stretching cell surface macromolecules by atomic force microscopy.* Langmuir, 2001. **17**: p. 3116-3119.

28. Nüßlein, K., D. Maris, K. Timmis, and D.F. Dwyer, *Expression and transfer of engineered catabolic pathways harbored by Pseudomonas spp. introduced into activated sludge microcosms.* Applied and Environmental Microbiology, 1992. **58**: p. 3380-3386.

29. Wagner-Dobler, I., R. Pipike, K.N. Timmis, and D.F. Dwyer, *Evaluation of Aquatic Sediment Microcosms and their use in assessing possible effects of introduced microorganisms on ecosystem parameters.* Applied and Environmental Microbiology, 1992. **58**(4): p. 1249-1258.

30. Camesano, T.A. and B.E. Logan, *Imaging modified bacterial cells using atomic force microscopy.* Langmuir, 2000. **16**: p. 4563-4572.

31. Camesano, T.A. and B.E. Logan, *Probing bacterial electrosteric interactions using atomic force microscopy.* Environmental Science & Technology, 2000. **34**: p. 3354-3362.

32. Cleveland, J.P., S. Manne, D. Bocek, and P.K. Hansma, *Nondestructive method for determining the spring constant of cantilevers for scanning force microscopy.* Review of Scientific Instruments, 1993. **64**: p. 403-405.

33. Janshoff, A., M. Neitzert, Y. Oberdorfer, and H. Fuchs, *Force spectroscopy of molecular systems-single molecule spectroscopy of polymers and biomolecules.* Angew. Chem. Int. Ed., 2000. **39**: p. 3212-3237.

34. Rief, M., F. Oesterhelt, B. Heymann, and H.E. Gaub, *Single molecule force spectroscopy on polysaccharides by atomic force microscopy.* Science, 1997. **275**(5304): p. 1295-?

35. Senden, T.J., J.-M. di Meglio, and P. Auroy, *Anomalous adhesion in adsorbed polymer layers.* Eur. Phys. J. B., 1998. **3**: p. 211-216.

36. Smith, S.B., L. Finzi, and C. Bustamante, *Direct mechanical measurements of the elasticity of single DNA molecules by using magnetic beads.* Science, 1992. **258**: p. 1122-1126.

37. Robyt, J.F. and B.J. White, *Biochemical Techniques:Theory and Practice*. 1990: Waveland Press, Inc.

38. Fisher, T.E., P.E. Marszalek, A.F. Oberhauser, M. Carrion-Vazquez, and J.M. Fernandez, *The micro-mechanics of single molecules studied with AFM.* Journal of Physiology, 1999. **520**(1): p. 5-14.

39. Balnois, E. and K.J. Wilkinson, *Sample preparation techniques for the observation of environmental biopolymers by AFM.* Colloids and Surfaces A: Physicochemical and Engineering Aspects, 2002. **207**: p. 229-242.

40. Camesano, T.A. and K.J. Wilkinson, *Single molecule study of xanthan conformation using atomic force microscopy.* Biomacromolecules, 2001. **2**: p. 1184-1191.

41. Holzwarth, G. and E.B. Prestridge, *Multistranded helix in xanthan polysaccharide.* Science, 1977. **197**: p. 757.

42. McIntire, T.M. and D.A. Brant, *Imaging of individual biopolymers and supermolecular assemblies using noncontact AFM.* Biopolymers, 1997. **42**: p. 133-146.

43. Frank, B.P. and G. Belfort, Langmuir, 1999. **13**: p. 6234-6240.

44. Cowman, M.K., M. Li, and E.A. Balazs, *tapping Mode AFM of Hyaluronan: Extended and intramolecularly interacting chains.* Biophysical Journal, 1998. **75**(October): p. 2030-2037.

Table 3.1. Summary of parameters used to fit the solid lines in Figure 3.4. The average segment length was 0.21 ± 0.08 nm, average contour length was 273 ± 250 nm, and the average R^2 was 0.95 ± 0.07. Values are shown in order of increasing contour length.

L (nm)	l_k (nm)	R^2	L (nm)	l_k (nm)	R^2
3.90	0.154	0.67	195	0.327	1.00
8.80	0.154	0.83	219	0.209	0.98
16.1	0.154	0.88	246	0.154	0.96
23.6	0.154	0.79	263	0.154	0.97
30.6	0.154	0.89	278	0.154	0.96
37.7	0.154	0.95	296	0.154	0.98
45.3	0.154	0.95	306	0.190	0.99
50.4	0.193	0.97	354	0.189	0.98
55.3	0.233	0.97	373	0.193	1.00
66.7	0.178	0.94	412	0.230	0.99
76.8	0.154	0.95	464	0.154	0.99
88.7	0.154	0.99	482	0.163	1.00
91.8	0.191	0.99	545	0.154	0.97
111	0.154	0.99	525	0.254	1.00
123	0.156	0.99	527	0.456	0.99
120	0.232	0.99	730	0.168	0.99
121	0.385	0.95	689	0.265	0.98
155	0.222	0.97	767	0.239	0.99
150	0.336	0.98	772	0.316	0.97
192	0.200	1.00	923	0.400	0.83

Table 3.2. Summary of the mean and standard deviation of pull-off distances and pull-off forces for the data shown in Figure 3.6.

Solvent	Pull-off Distance (nm)	Pull-off Force (nN)
Water	212 ± 211	-0.46 ± 1.3
0.01 m KCl	119 ± 90.0	-0.46 ± 0.50
0.1 M KCl	68.0 ± 59.0	-0.66 ± 1.4

3.6 Figure Captions

Figure 3.1. Force extension curves for five different bacterial cells (*Pseudomonas putida* KT2442). Only one measurement is shown per bacterium. The heterogeneity in adhesion forces and pull-off distances for bacteria from the same initial solution is demonstrated. All measurements were made in water.

Figure 3.2. Heterogeneity in force-extension curves on individual bacteria is demonstrated. Multiple measurements were made on each of three bacterial cells. All measurements were made in water.

Figure 3.3. Summary of the adhesion forces observed for many bacterial cells. Each symbol (not each data point) represents a different bacterium. Examination of any one symbol illustrates that on a given bacterium, many different adhesion affinities and biopolymer pull-off distances were observed. All measurements were made in water with a minimum of 5 measurements per cell.

Figure 3.4. Experimental data (symbols) and freely jointed chain (FJC) model results (solid lines) for biopolymer stretching experiments in water. This figure compiles the data for many individual bacterial cells. Agreement of the data with the FJC model is generally good, with the average R^2 value = 0.95). Each solid line is the result of fitting equation (3.1) to each set of experimental data, and has it is own fitting parameters (segment length and contour length) that differ from other experimental data sets. The fitting parameters and R^2 values for all the curves in this figure are given in Table 3.1.

Figure 3.5. This histogram shows the distribution of segment length values for different polymer chains estimated using the FJC model for KT2442 in water, 0.01 M KCl, and 0.1

M KCl. The highest peak in the three solvents was observed at the range of 0.154 – 0.20 nm. This histogram shows that there is a distribution of polymer segment lengths in all solvents, which indicates that the polymers are heterogeneous. The average value of the segment length was found to be 0.21 ± 0.05 nm in water, 0.20 ± 0.03 nm in 0.01 M KCl, and 0.23 ± 0.11 nm in 0.1 M KCl.

Figure 3.6. Histograms comparing A) pull-off distances in three solvents and B) adhesion force in three solvents. The pull-off distances tend to be lower when salt was present. No trend in adhesion can be seen with respect to the ionic strength of the solvent. The heterogeneity in biopolymer properties overwhelms any trend that could be seen with respect to the ionic strength of the solvent. The mean and standard deviations for the pull-off distances and the pull-off forces in all solvents are given in Table 3.2.

Figure 3.7. Chromatogram from the size-exclusion chromatography experiment on the polymers extracted from *P. putida* KT2442

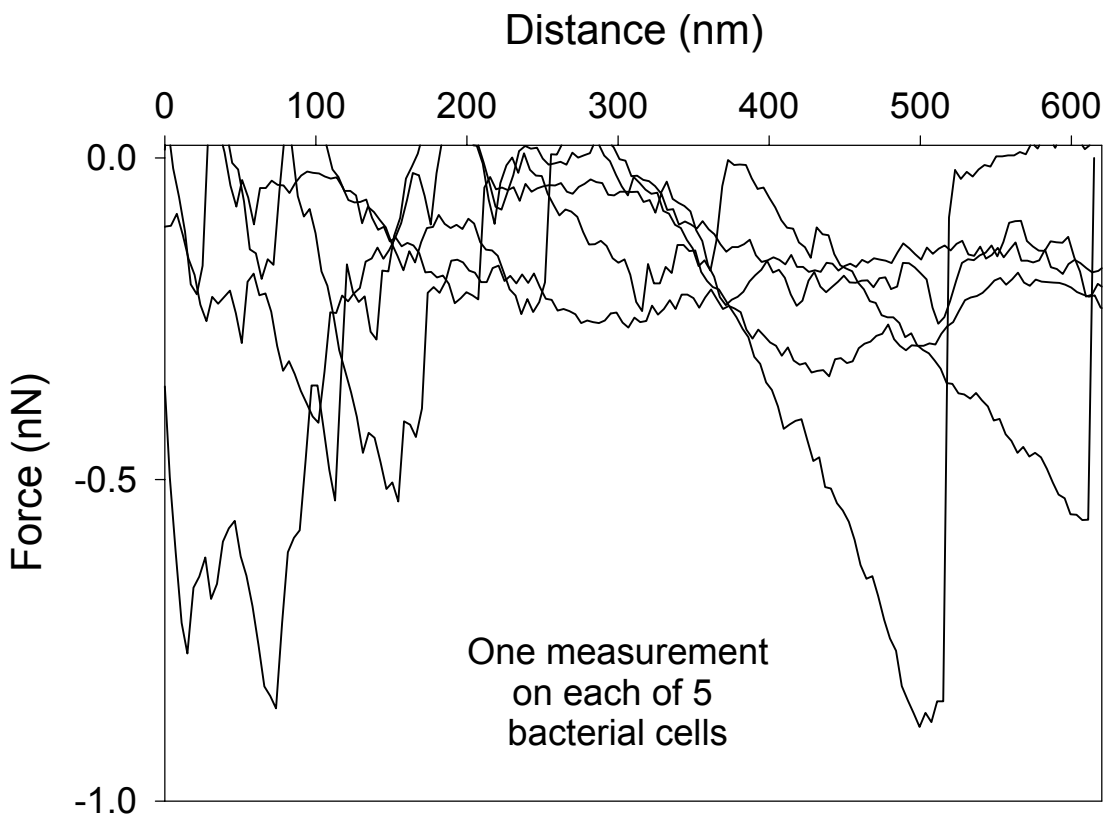
Distance (nm)
0
100
200
300
400
500
600
0.0
-0.5
-1.0
Force (nN)
One measurement
on each of 5
bacterial cells

Figure 3.1

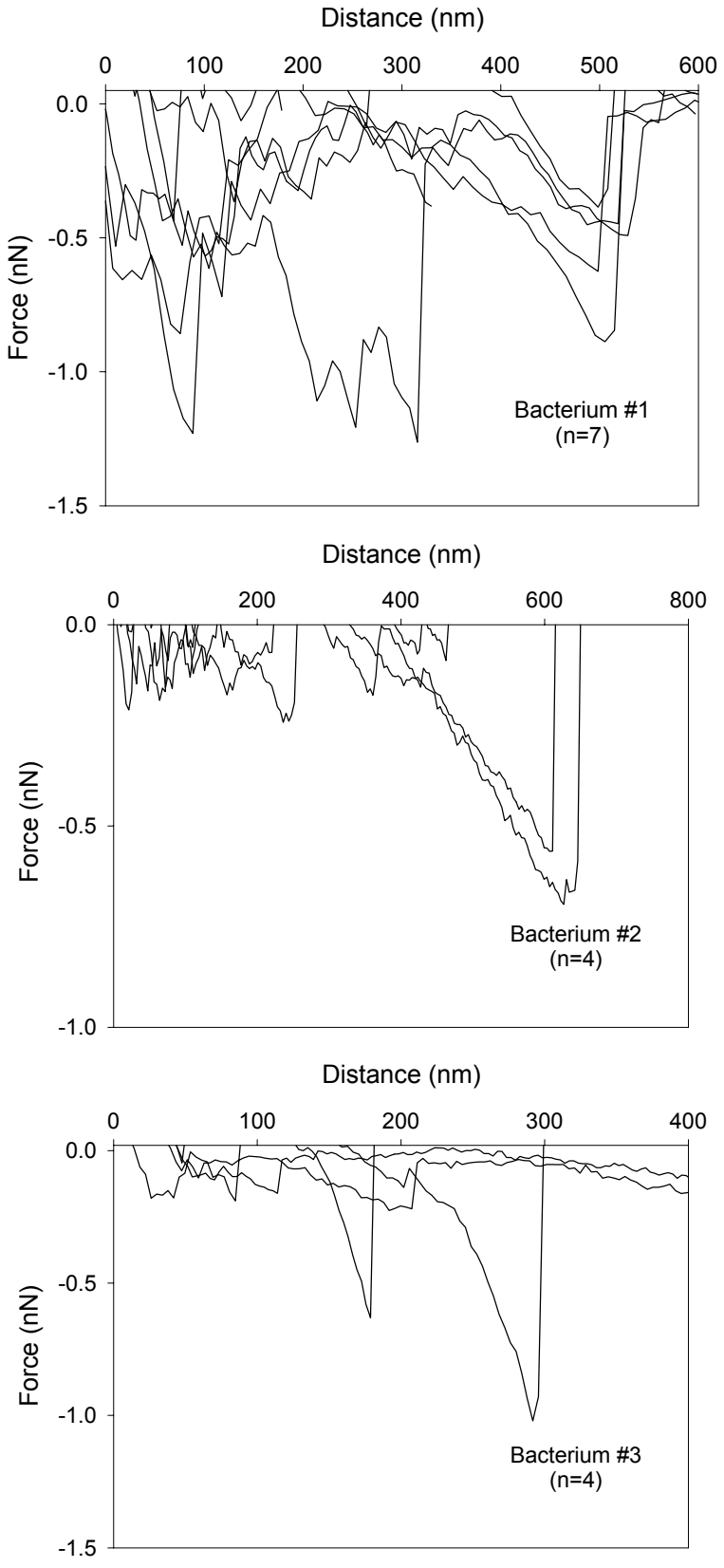
Distance (nm)
0
100
200
300
400
500
600
0.0
-0.5
-1.0
-1.5
Force (nN)
Bacterium #1
(n=7)
Distance (nm)
0
200
400
600
800
0.0
-0.5
-1.0
Force (nN)
Bacterium #2
(n=4)
Distance (nm)
0
100
200
300
400
0.0
-0.5
-1.0
-1.5
Force (nN)
Bacterium #3
(n=4)

Figure 3.2

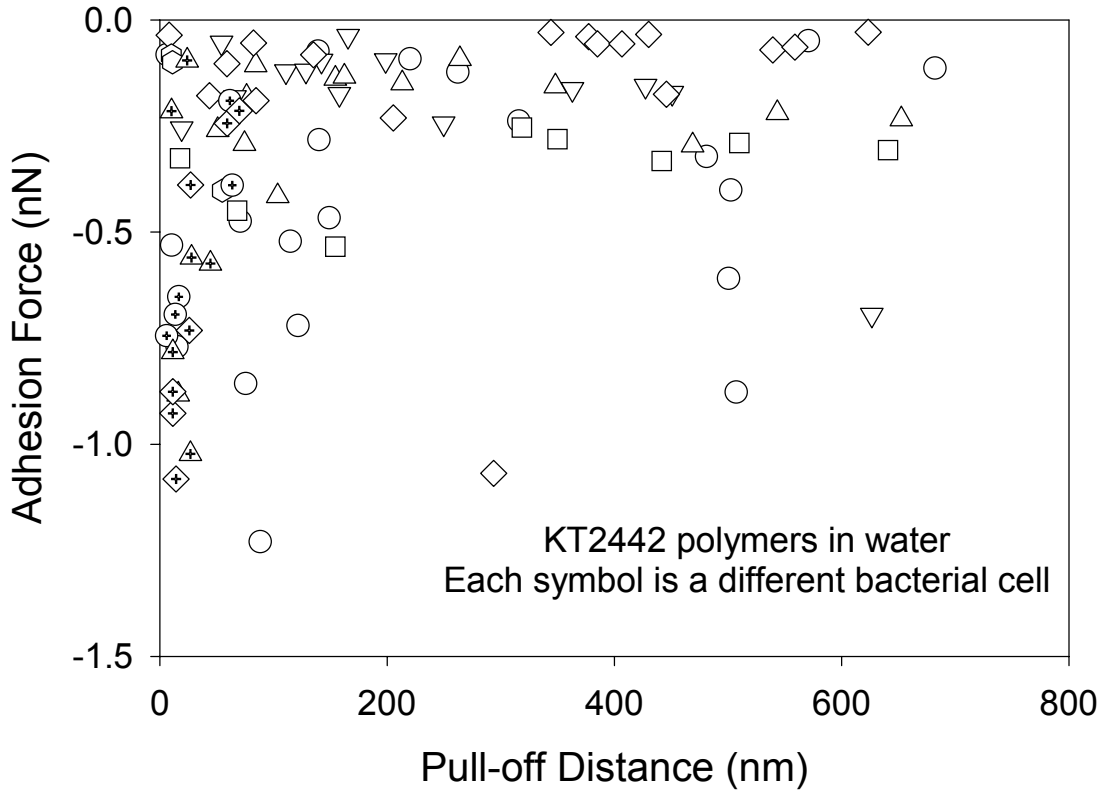
0.0
-0.5
-1.0
-1.5
Adhesion Force (nN)
0
200
400
600
800
Pull-off Distance (nm)
KT2442 polymers in water
Each symbol is a different bacterial cell

Figure 3.3

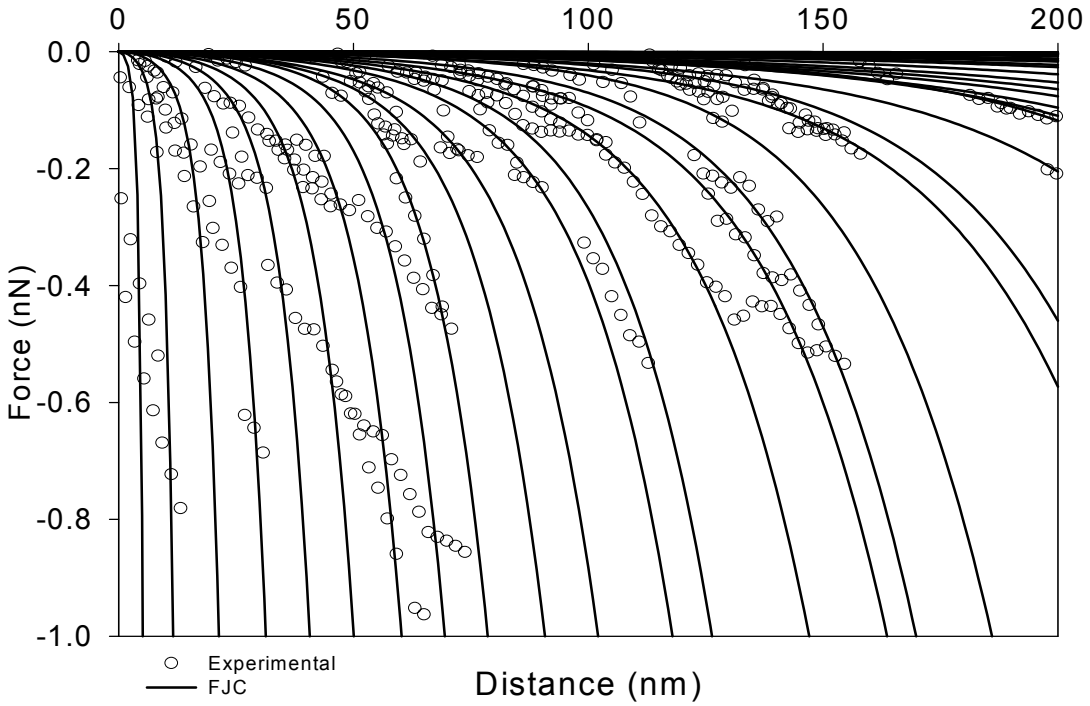
0
50
100
150
200
0.0
-0.2
-0.4
-0.6
-0.8
-1.0
Force (nN)
Experimental
FJC
Distance (nm)

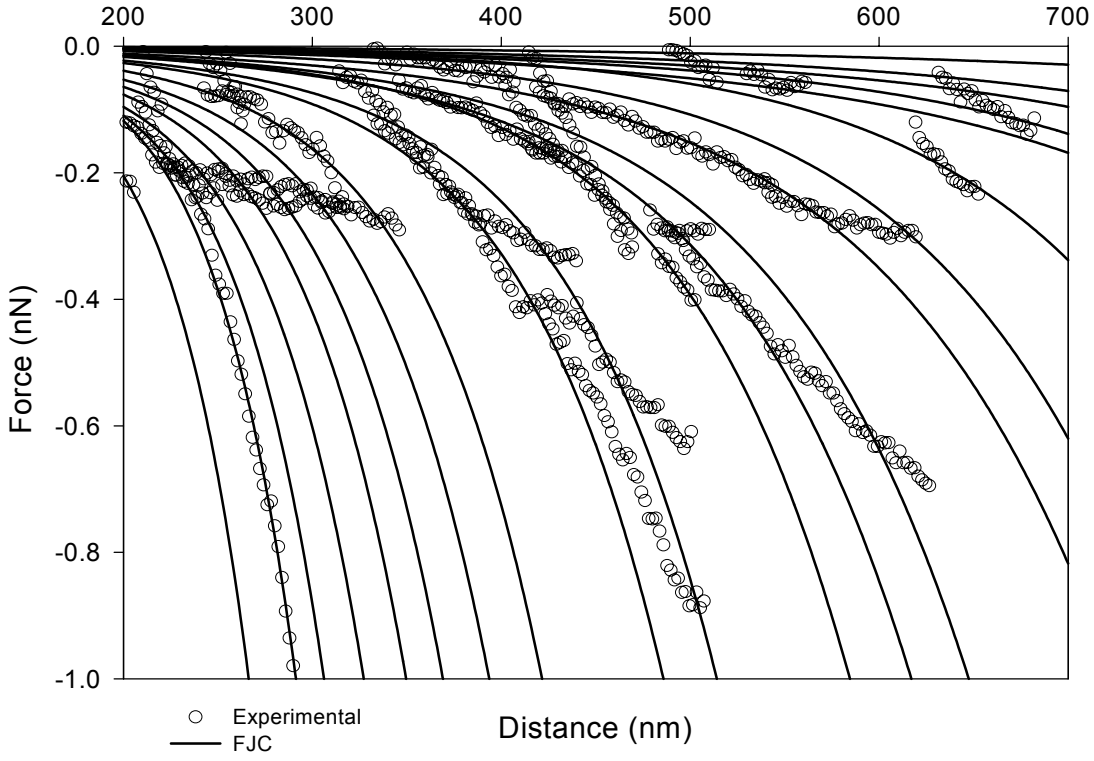
200
300
400
500
600
700
0.0
-0.2
-0.4
-0.6
-0.8
-1.0
Force (nN)
Experimental
FJC
Distance (nm)

Figure 3.4

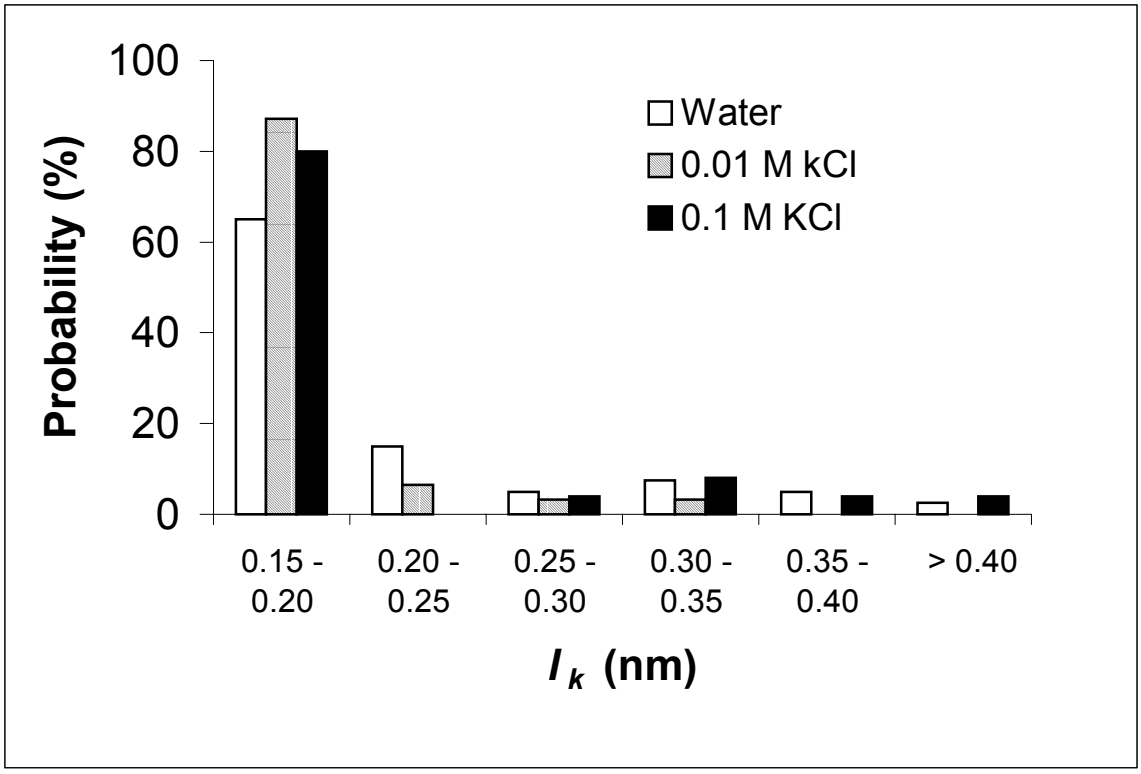
100
80
60
40
20
0
Probability (%)
Water
0.01 M kCl
0.1 M KCl
0.15 - 0.20
0.20 - 0.25
0.25 - 0.30
0.30 - 0.35
0.35 - 0.40
> 0.40
l_k (nm)

Figure 3.5

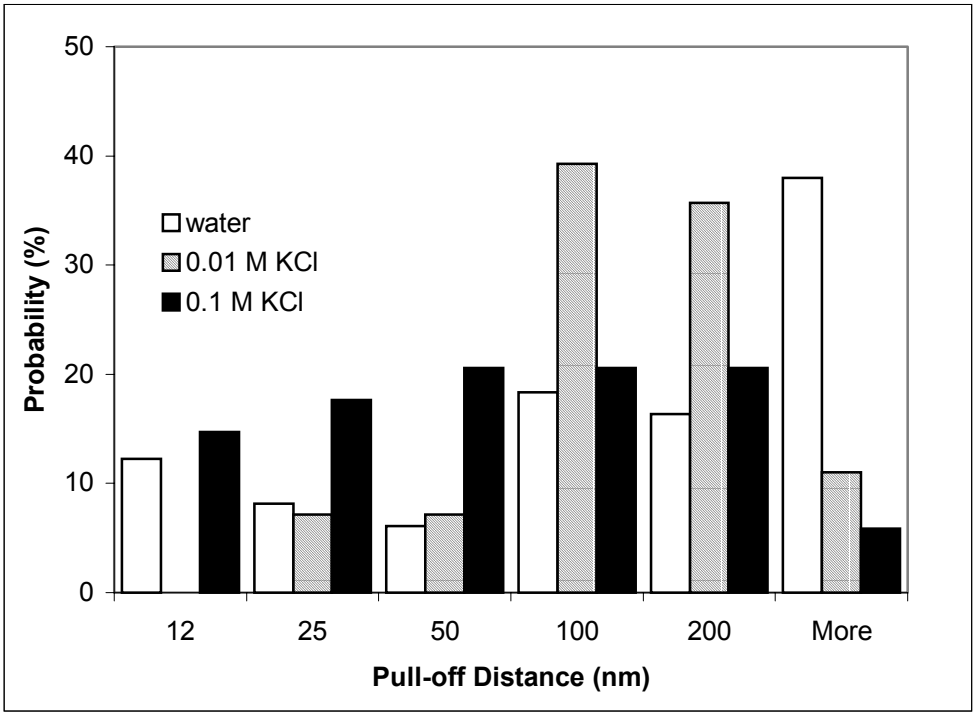
50
40
30
20
10
0
Probability (%)
water
0.01 M KCl
0.1 M KCl
12
25
50
100
200
More
Pull-off Distance (nm)

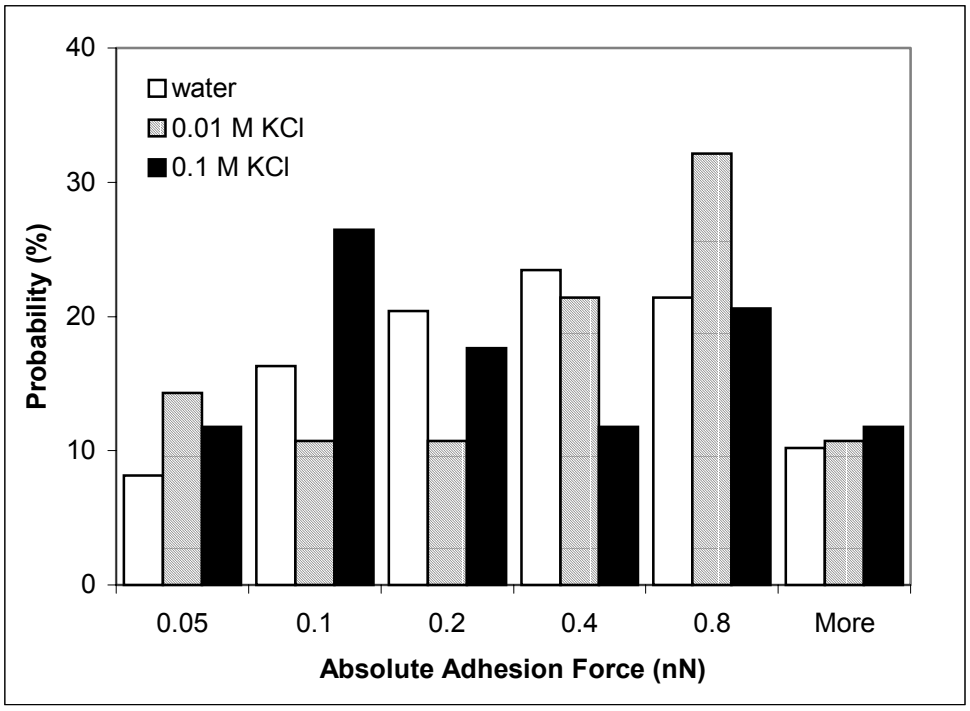
40
30
20
10
0
Probability (%)
water
0.01 M KCl
0.1 M KCl
0.05
0.1
0.2
0.4
0.8
More
Absolute Adhesion Force (nN)

Figure 3.6

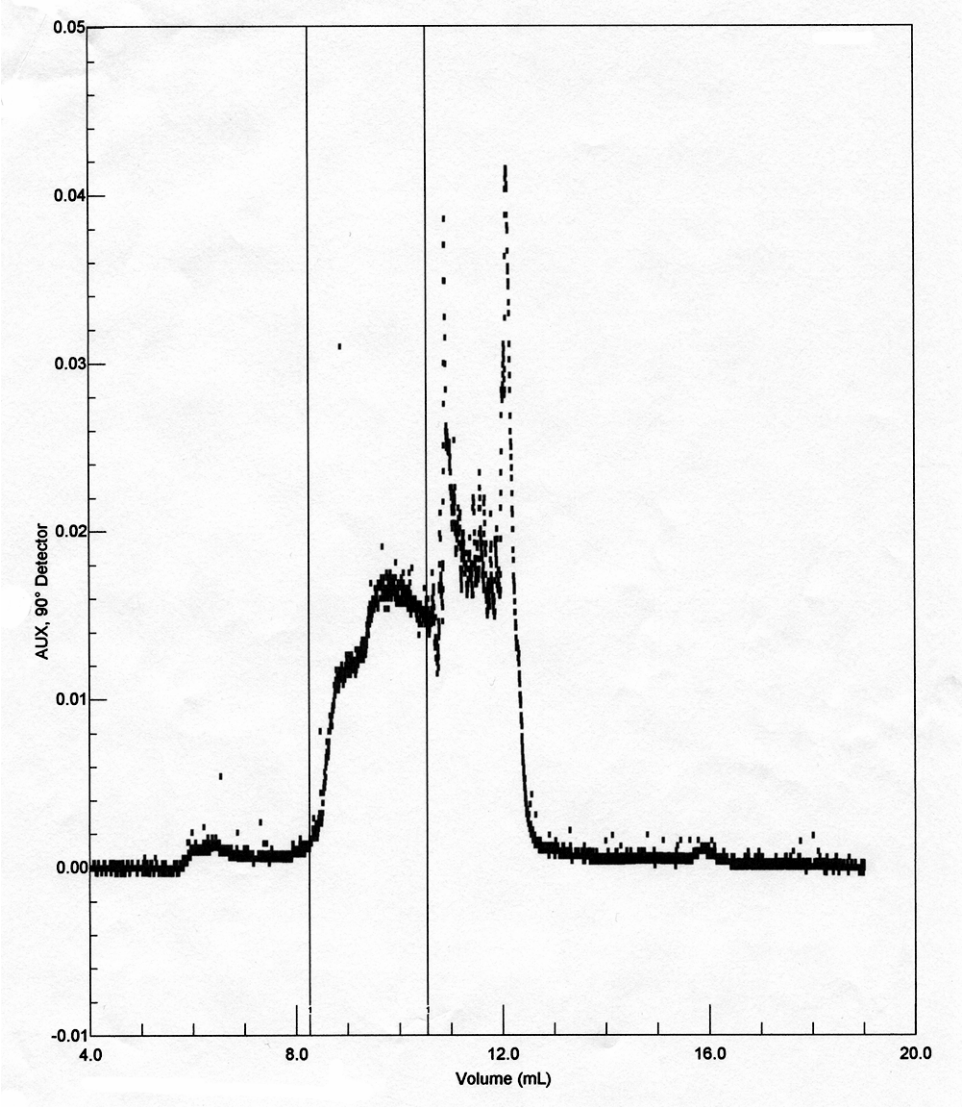
0.05
0.04
0.03
0.02
0.01
0.00
-0.01
AUX, 90° Detector
4.0
8.0
12.0
16.0
20.0
Volume (mL)

Figure 3.7

Chapter 4

Role of Ionic Strength on the Relationship of Biopolymer Conformation, DLVO Contributions, and Steric Interactions to Bioadhesion of *Pseudomonas putida* kT2442

Abstract

Biopolymers produced extracellularly by *Pseudomonas putida* KT2442 were examined via atomic force microscopy (AFM) and single molecule force spectroscopy (SMFS). Surface biopolymers were probed in solutions with added salt concentrations ranging from that of pure water to 1 M KCl. By studying the physicochemical properties of the polymers over this range of salt concentrations, we observed a transition in the steric and electrostatic properties and in the conformation of the biopolymers that were each directly related to bioadhesion. In low salt solutions, the electrophoretic mobility of the bacterium was negative and large theoretical energy barriers to adhesion were predicted from soft-particle DLVO theory calculations. The brush layer in low salt solution was extended due to electrostatic repulsion, and therefore steric repulsion was also high (polymers extended 440 nm from surface in pure water). The extended polymer brush layer was "soft", characterized by the slope of the compliance region of the AFM approach curves (-0.014 nN/nm). These properties resulted in low adhesion between biopolymers and the silicon nitride AFM tip. As the salt concentration increased to $\geq$ 0.01 M, a transition was observed towards a more rigid and compressed polymer brush layer, and the adhesion forces increased. In 1 M KCl, the polymer brush extended 120 nm from the surface and the rigidity of the outer cell surface was greater (slope of the compliance region = -0.114 nN/nm). A compressed and more rigid polymer layer, as well as a less negative electrophoretic mobility for the bacterium, resulted in higher adhesion forces between the biopolymers and the

AFM tip. Scaling theories for polyelectrolyte brushes were also used to explain the behavior of the biopolymer brush layer as a function of salt concentration.

4.1 Introduction

The presence and physicochemical properties of biopolymers on the surface of a bacterium are known to influence bioadhesion to surfaces including soil [1-3], biomaterials such as endotracheal tubes [4], and mammalian cells [5]. Bacterial adhesion and biofilm formation have applications in a number of engineering, scientific, and medical disciplines.

The initial adhesion of a microbe to a surface was suggested to be controlled by electrostatic and van der Waals interactions [6], as could be modeled by the classical Derjaguin-Landau-Verwey-Overbeek (DLVO) theory of colloidal stability [7]. Bulk investigations of bacterial attachment to a similarly charged surface show that ionic strength usually affects the attachment probability, with less attachment seen in low ionic strength solutions due to increased long-range electrostatic repulsion [8]. According to DLVO theory, increasing the solution's ionic strength should monotonically decrease the long-range repulsion between a negatively charged bacterium and a negatively-charged surface. There have been a few cases where the expected trend with ionic strength was not seen. For example, cell adhesion or flocculation was seen at a finite salt concentration despite predictions of energy barriers that should have been too large to permit adhesion/flocculation [9, 10] or bacterial adhesion was indifferent to electrolyte concentration [10-12]. One contributing factor to this discrepancy between bacterial attachment and model predictions involves bacterial motility, since the rotation of the flagella of *Escherichia coli* in solutions with low ionic strength (0.02 M phosphate buffer) was found to provide sufficient energy to assist in attachment [13]. The increased adhesion was attributed to faster transport of motile cells towards the surface or the use of the flagella as an anchor to tether the bacteria to the surface. Another explanation that has been suggested is charge regulation. A recent modeling effort explained that weakly charged groups on the bacterial surface are

involved in an equilibrium process by which they exchange between associated and dissociated states [14], and this charge regulation gives rise to a non-monotonic decrease in the repulsion between like-charged colloids with decreasing cell-substrate separation. In some cases charge regulation can lead to a regime of *increased* repulsion at higher salt concentrations. Poortinga et al. recently provided evidence that charge transfer is an important part of bacterial adhesion, and that bacteria with a thicker ion-penetrable layer adhere to a greater extent onto a similarly charged substrate [11]. Flagellar rotation, charge regulation, and ion-penetrability are important effects that are not typically addressed by DLVO theory. Additional factors also contribute to the discrepancy between the prediction and observation of bacterial adhesion as a function of ionic strength, particularly for microbes with substantial extracellular polymer layers.

For charged polymers on bacterial surfaces, the solution ionic strength will change the conformation and adhesion behavior of these macromolecules, as well as changing the "softness" of the polymer brush layer, each in ways that cannot be fully described by classical DLVO or extended DLVO theories [15]. By viewing the biopolymer as a polyelectrolyte brush layer, the properties of the macromolecules in the brush layer can be characterized using polyelectrolyte scaling relationships.

Recent advances in the application of analytical techniques to microbial systems, such as through single-molecule force spectroscopy (SMFS) [16, 17], atomic force microscopy (AFM) [18-22], total internal reflection aqueous fluorescence microscopy [23], or other optical trapping/evanescent wave techniques [24], make it possible to probe the molecular components of the microbial adhesion process.

We chose *Pseudomonas putida* KT2442 as a model polysaccharide-producing microorganism, a strain for which we already had some information on surface properties. For

example, this microbe is fairly hydrophilic, based on a water contact angle of 24.5 ± 3.4° [25], is negatively charged, and has a very low isoelectric point (2.3), indicating that the surface consists of anionic polysaccharides with phosphate and/or carboxylic group moieties [26]. Previous AFM studies of *P. putida* KT2442 demonstrated that the extracellular biopolymers were heterogeneous in terms of elastic properties, contour lengths, and adhesion affinities for silicon nitride [27]. The biopolymers were flexible in all solvents studied (water, methanol, formamide, 0.1 M KCl), based on application of the freely-jointed chain model to polymer stretching data [17]. Two studies demonstrated that ionic strength only slightly affected the adhesion affinities or interaction forces between *P. putida* KT2442 biopolymers and silicon nitride (from water to 0.01 M KCl [17] or from 0.01 to 100 mM MOPS buffer [26]). We hypothesized that the lack of a substantial effect of the ionic strength on the observed interaction forces or adhesion affinities was due to the fact that at the ionic strengths tested, the concentration of bulk ions was not great enough to counterbalance the ion concentration in the polyelectrolyte brush layer surrounding the microbes.

The current study provides a more thorough and systematic investigation of the role of ionic strength on the physiochemical properties of biopolymers on the surface of *Pseudomonas putida* KT2442. Solutions with a wider range of salt concentrations were chosen, including solutions with much higher salt concentrations than had been previously studied (from pure water to 1 M KCl). For each solution studied, the interaction forces during the approach of a silicon nitride AFM tip to the bacterium were measured, as well as the adhesive forces after the two had been in contact. Direct interaction force measurements were compared with energy predictions based on soft-particle DLVO theory calculations. A steric model for polymer brushes was applied to probe the changing conformation of the brush layer as a function of ionic

strength. Physicochemical properties of the polymers such as the Kuhn and contour lengths were characterized by applying polymer statistical models. The brush layer thickness and density were correlated with salt concentration using scaling models for polyelectrolytes at solid/liquid interfaces. Biopolymer conformation and steric/electrostatic properties were correlated with bioadhesion as a function of salt concentration.

4.2 Materials and Methods

4.2.1 Bacterial Culture Preparation. Our work focused on *Pseudomonas putida* KT2442, which produces a cellulose-like EPS [27]. *P. putida* KT2442 can be found in soil, freshwater, and the rhizospheres of agriculturally important plants [28, 29], and can degrade chlorinated benzenes [30-33]. It is a soil microorganism and a wealth of information is available regarding its genetic [28, 29] and physicochemical properties [17, 25-27]. KT2442 cultures were grown in M9 buffer containing a mineral salt mixture supplemented with 5mM benzoate and 50 μg/L rifampicin [25].

4.2.2 Electrophoretic Mobility. The electrophoretic mobility of *P. putida* KT2442 was measured using a zeta potential analyzer (Zeta PALS, Brookhaven). Measurements were performed three times and averaged, on late-exponential phase bacterial cells resuspended in KCl solutions of varying ionic strengths (10^{-3} -0.15 M KCl; pH=8.0).

4.2.3 Preparing Bacterial Samples for AFM Work. Glass slides were cleaned by soaking in a 3:1 HCl/HNO_3 solution for 25 minutes followed by copious rinsing in deionized (DI) water. This step was followed by soaking in 4:1 H_2SO_4/H_2O_2 solution for 25 minutes, rinsing in DI water, and storage of the slides in a beaker of water that had been sterile-filtered through a 0.2 μm syringe filter until use. KT2442 cells were covalently bonded to clean, silanized glass slides, as described elsewhere [26]. The bonding protocol involves

immobilization of bacteria using the zero-length crosslinker 1-ethyl-3-(3-dimethylaminopropyl)carbodiimide (EDC), stabilized by sulfo-hydroxysuccinimide (sulfo-NHS). The zero-length crosslinkers modify amino-acid side groups (on the glass slide) to permit crosslink formation, but they do not remain as part of the linkage, nor do they modify the bacterial surface. Prior research on pure polymers suggests that the main effect of the EDC/NHS concentration is to change the structure and density of the polymer layer being formed, which would change the observed interaction forces [34]. However, we always have much less than a monolayer of bacteria attached to the slide, and so the EDC/NHS treatment has should not affect the observed interaction forces. Prior work has also shown that biological activities are not disrupted by these chemicals when used in similar bonding protocols [35, 36]. After the bonding reaction, slides were transferred to a Petri dish containing the desired solvent (water or a KCl solution).

4.2.4 Force Analysis Using AFM. Forces were measured between hydrated individual bacterial cells and silicon nitride cantilevers using an AFM (Digital Instruments Dimension 3100 with Nanoscope III controller). Silicon nitride tips were purchased from Digital Instruments (DNPS tips). The spring constant for these tips was 0.13 ± 0.02 N/m, measured using the Cleveland method [37] and the correlation equations given in the Digital Instruments software. The tips were cleaned just prior to use by exposure to ozone generated by ultraviolet light irradiation in an oxygen atmosphere for 1 minute, which removes any organic carbon contamination covering the tip apex [38]. To select a cell for analysis, an image was obtained in tapping mode of a portion of the glass slide. The tip was then positioned over the center of a bacterium, the rastering of the cantilever stopped, the tapping turned off, and a force measurement performed. At least five measurements were performed on a single area of a

bacterial cell and such measurements were performed on at least five bacteria for a given salt solution. Forces were recorded while the tip approached and was retracted from the sample.

The data files were treated as described previously [26] to convert cantilever deflection to force, using the constant compliance region of the curves to "zero" the force curves [39]. Although the method used to determine the origin of the force curves was developed for hard silica spheres, these principles can be applied to other colloidal particles such as soft biological cells and fibrous materials [39], as has been successfully done in many cases [21, 40-43]. This method is appropriate as long as the cantilever is the most compliant component of the system [44]. In addition, Boulbitch et al. recently proved through theoretical relations that the deformation of the envelope of a gram-negative bacterium from a force-displacement relation measured on the top of the bacterium is accurately approximated by a linear dependence [45], suggesting that non-elastic components of the force do not limit our ability to specify the origin of each force-distance relationship. In our study, force measurements were made on clean glass before and after force measurements on bacterial cells, to ensure that the tip was not contaminated during the course of the experiment. The measurements on glass were always practically identical, confirming that no biopolymers remained on the tip after a force measurement.

4.2.5 Determination of Polymer Brush Layer Thickness. A model developed for grafted polymers at relatively high surface coverage was used to model steric interactions between the AFM tip and cell surface polymers. The force per unit area between two surfaces, $F_{St,}$ only one of which is coated with polymer, has been modeled following the work of Alexander [46] and de Gennes [47]. This model was modified by Butt et al. [48] to describe the

forces between a spherical AFM tip and a flat surface by integrating the force per unit area over the tip surface, to produce the interaction force

$$F_{St} = 50\, k_B\, T\, a_1\, L\, \Gamma^{3/2}\, e^{-2\pi h/L} \tag{4.1}$$

where k_B is Boltzmann constant, T is temperature, a_1 the tip radius, Γ the grafted polymer density in the brush layer (m^{-2}) and reflects how much of the surface is covered by polymers, h the distance between the two surfaces, and L the equilibrium height of the polymer brush layer. For these calculations, the tip radius was assumed to be 250 nm based on a previous demonstration that these tips interact as spheres with radii between 100 and 400 nm [49, 50].

4.2.6 Calculation of Surface Potential for Soft Particles. Recent work suggested that for soft particles, such as bacteria, the zeta potential is not an accurate measure of surface potential [12, 51-53]. Therefore, soft-particle DLVO theory was used to evaluate the electrostatic interactions between *P. putida* KT2442 and silicon nitride. This theory assumes the presence of an ion-penetrable, charged polyelectrolyte layer around a rigid core [53]. The approximate mobility formula for soft particles [13, 51, 52, 54, 55] is expressed as:

$$\mu = \frac{\varepsilon_o \varepsilon}{\eta} \frac{\Psi_o / K_m + \Psi_{DON} / \lambda_s}{1/Km + 1/\lambda_s} + \frac{eZN}{\eta \lambda_s^{\,2}} \tag{4.2}$$

Where ε is the permittivity of a vacuum and ε_o is the relative permittivity of the solvent, Ψ_o is the surface zeta potential, K_m the Debye-Hückel parameter for the polymer layer, Ψ_{DON} the Donnan Potential of the polymer layer, Z the valance of the charged groups in the polymers, e the electron charge, N the density of the charged groups, and λ_s the softness parameter, which has dimensions of reciprocal length. The parameters K_m, Ψ_o, and Ψ_{DON} are all functions of ionic strength [53]. The expressions for determining these parameters are provided in the Appendix.

4.2.7 Calculation of Interaction Energies. Derjaguin-Landau-Verwey-Overbeek (DLVO) interaction energy profiles between the bacterium and silicon nitride were calculated. Bacterium/AFM tip interactions were treated using sphere-sphere geometry. The total DLVO interaction energy (E_t) between the bacterium and the silicon nitride tip was calculated as the sum of London-van der Waals and electrostatic interactions [56] .

$$E_t = E_e + E_v \tag{4.3}$$

Where E_e is the electrostatic energy and E_v is the interaction energy due to London-van der Waals forces. The electrostatic interactions were calculated using the linearized version of the Poisson-Boltzmann expression [56].

$$E_e = \frac{2\pi a_1 a_2 n\ k_B T}{(a_1 + a_2)\kappa^2}(\Phi_1^2 + \Phi_2^2)\left(\frac{2\Phi_1\Phi_2}{\Phi_1^2 + \Phi_2^2} ln\left(\frac{1+exp(-\kappa h)}{1-exp(-\kappa h)}\right) + ln[1-exp(-2\kappa h)]\right) \tag{4.4}$$

Where a_2 is the radius of the bacterium, Φ_1, Φ_2 the reduced potentials of tip and the bacterium, respectively, which relate to their surface potentials ψ_1 and ψ_2 according to $\Phi = ze\psi/k_BT$ [56].

For bacterial cells, the soft-particle potential (Ψ_o) calculated from eq. 3 was used as the surface potential ψ. For the silicon nitride tip, the surface potential was taken to be the zeta potential, based on applying the Smoluchowski expression [57] to electrophoretic mobility values obtained from the literature [58, 59].

The van der Waals interaction energy between two dissimilar spheres was calculated using a Hamaker expression, corrected for retardation effects [60].

$$E_v = -\frac{-Aa_1a_2}{6h(a_1 + a_2)(1 + 11.12h/\lambda_c)} \tag{4.5}$$

Where A is the Hamaker constant for the interacting media and λ_c is the "characteristic wavelength" of the interaction, often assumed to be 100 nm. A value of 10^{-20} J was used for the

Hamaker constant describing bacterial-silicon nitride interactions in water, using a value previously developed for the interactions between *Pseudomonas aeruginosa* and glass [61]. This is a reasonable approximation since the zeta potentials and water contact angles of *P. putida* and *P. aeruginosa* are very similar. The water contact angles for both strains indicate hydrophilic surfaces, and are 24.5 ± 3.4 [26] and 33.5 ± 1.2 [62] for *P. putida* and *P. aeruginosa*, respectively. The zeta potentials of *P. putida* and *P. aeruginosa* are -17.31 ± 0.06 mV [17] and -17.59 mV [62], respectively. In addition, we have previously shown that interaction profiles in bacterium-glass systems are similar to those in bacterium-silicon nitride systems [63].

4.2.8 Polymer Elastic Properties. The freely jointed chain model was applied to the adhesion peaks of AFM retraction curves to estimate the Kuhn lengths (l_k). In the freely jointed chain (FJC) model, the polymer is considered to be composed of independent rigid segments, each of length l_k, and connected by freely rotated pivots with equal probabilities for rotation in all directions. The chain gets more flexible as the Kuhn length gets smaller. The force needed to stretch a FJC to a length h is given by [64]:

$$F_{chain} = \frac{-k_B T}{l_k} \mathcal{L}^{-1}\left(\frac{h}{l_c}\right) \tag{4.6}$$

Where k_B is the Boltzmann constant, T is absolute temperature, l_c the contour length of the portion of the chain that was stretched, and $\mathcal{L}^{-1}$ the inverse Langevin function, approximated by the first four terms of its series:

$$\mathcal{L}^{-1}\left(\frac{h}{l_c}\right) = 3\left(\frac{h}{l_c}\right) + \frac{9}{5}\left(\frac{h}{l_c}\right)^3 + \frac{297}{175}\left(\frac{h}{l_c}\right)^5 + \frac{1539}{875}\left(\frac{h}{l_c}\right)^7 \tag{4.7}$$

4.2.9 Scaling Relationships for Polyelectrolyte Brushes. Considerations of tethered polyelectrolytes based on self-consistent field theory [65] predict a roughly parabolic segment density profile that extends further with increasing charge density of decreasing salt

concentration [66, 67]. For many cases, simpler scaling relations can be used to describe the behavior of polyelectrolyte brushes. In this study, the effects of added salt concentration on the dimensions of the biopolymer brush layer were predicted using scaling theories developed for grafted brushes of polyelectrolytes. Available theories characterize the brush layer by relating the changes in the brush height (L), polymer grafting density (Γ), contour length (L_c), and Kuhn length (l_k) to the salt concentration of the solvent (C_s) [68-73]. The contour length is in turn related to the brush height. For the purpose of these scaling calculations, we assumed that the polymer contour length would be related to the brush height, and the relationship $L_c=1.25L$ was used. We could not use the l_c values estimated from application of the FJC model because these "contour lengths" (l_c values) represent the contour length of some region of the polymer chain that was stretched. The AFM tip may have come into contact with the polymer chain anywhere along its length (i.e. not necessarily at the end), and these contour length values will most likely represent the lengths of short sections of the chains, rather than the whole chain molecules. The arbitrary factor that we assumed (1.25) affects only the values of the constants in the scaling relations, and does not affect the observed relationships between contour length, density, Kuhn length, and salt concentration.

For uncharged brushes, scaling theories predict that the brush layer height is proportional to $\Gamma^{1/3}$ [46]. The behavior of charged brushes deviates substantially from this relationship, especially at low ionic strengths. To account for the behavior of charged brushes, electrostatic blob models were developed [72, 74, 75]. Blob models account for excluded volume effects resulting from chain expansions due to interactions between the charged chains (electrostatic, van der Waals, and steric), and some blob models can also be made to account for the elasticity of the biopolymers. For polyelectrolytes, the brush layer thickness was related to the excluded

volume (v) and segment length (l_k) through the relation $L \sim L_c(v\Gamma/l_k)^{1/3}$. The excluded volume interaction parameter accounts for chain interactions. A version of the Daoud-Cotton model that was corrected for polymers attached to a spherical surface was used to calculate the excluded volume parameter [70]

$$\left(\frac{L}{a_2}+1\right)^{5/3} = 1+\frac{KL_c}{a_2}\left(\frac{v\Gamma}{l_k}\right)^{1/3} \tag{4.8}$$

where K is a constant whose value is close to unity. Values of l_k were obtained via application of the FJC model to the AFM retraction curves, where an average l_k value was found for each added salt concentration. L and Γ were obtained from applying the steric model (eq. 1) to AFM approach curves.

Several models have been proposed to relate the brush layer height to salt concentration, each with the general form $L \sim C_s^{-m}$ [70], where m is a fractional exponent. Pincus suggested that chain stiffening could be ignored, or that the Kuhn length is equal to that of an equivalent uncharged chain. In this case and for a semi-dilute solution, the layer thickness was related to salt concentration as $L \sim C_s^{-1/3}$ [76]. Zhulina et al. developed relations for salted and unsalted brushes based on the sum of electrostatic and non-electrostatic forces, in which $L \sim L_c\Gamma^{1/3}C_s^{-1/3}$ for the salted brush [68, 73]. The electrostatic wormlike chain model was developed for the case where chain stiffening occurs, or the Kuhn length changes as the salt concentration in solution is modified [77-79]. The electrostatic WLC model predicts the scaling relation $L \sim C_s^{-1/2}$. Each model was tested for its ability to describe the relationship between brush layer height and salt concentration.

4.3 Results

4.3.1 Biopolymer Electrostatic Properties and Predicted Energy Barriers to Attachment Based on Soft-Particle DLVO Theory. The electrophoretic mobility of *P. putida* KT2442 reached a non-zero asymptotic value as the salt concentration increased (Figure 4.1), which is characteristic of "soft" particles [53]. We applied the soft-particle DLVO theory [51-53, 80] to our electrophoretic mobility data as a function of ionic strength, and determined that ZN = -0.072 M and $1/\lambda$ = 1 nm. These values are similar to ones reported for *Nitrosomonas europaea* and *Escherichia coli* IFO-3301 [53]. Using the soft-cell potentials, the total interaction energy between the tip and the bacterium was calculated as a function of added salt concentration (Figure 4.2, Table 4.1). At salt concentrations < 0.05 M, repulsion was observed between the bacterium and the tip. However, at salt concentrations > 0.05 M, attraction was always observed between the bacterium and the tip.

Although an attempt was made to use the extended-DLVO model (accounting for acid-base interactions), this approach was discarded because it produced unrealistically high repulsive energy barriers at short separation distances (data not shown). These energy barriers of 100s of k_BTs were present at all salt concentrations tested, even though experiments indicated that adhesion occured at an appropriately high salt concentration. The use of conventional-DLVO theory, modified to account for the behavior of "soft" particles, produced predictions that were closest to experimental evidence of adhesion.

4.3.2 Biopolymer Conformation

4.3.2.1 Thickness of the Polymer Brush Layer. The presence of bacterial polymers caused steric repulsion between the bacterium and the tip. These forces were quantified using the Alexander and de Gennes models for steric interactions between a grafted polymer layer and

a bare surface, as modified by Butt et al. when the "surface" is a rounded AFM tip (eq. 4.1) [46-48] (Figure 4.3). The height of the brush layer decreased with increasing salt concentration (Table 4.2). The grafting density increased with increasing C_s, while the total amount of biopolymer on the bacterial surface (estimated as ΓL) was nearly constant and not dependent on C_s. Bacterial cells were always grown under the same conditions, and therefore the total amount of polymer should not have changed when the final suspension solution was changed.

4.3.3. Elastic Properties of the Biopolymers. The biopolymer layer on the surface of KT2442 undergoes changes in its conformation that are dependent upon the salt concentration in solution. In low ionic strength solutions, the polymer brush layer is most extended (L =440 nm). This extension results in the surface of the bacterium appearing as "soft". When the salt concentration increased, the biopolymer brush layer collapsed onto the cell membrane, as evidenced by the decreasing values of L.

The slope of the compliance region of the AFM approach curves provides corroborating evidence of this transition in cell softness. This slope represents the amount that the AFM tip could be compressed into the polymer layer. The value of the slope decreased from -0.114 to -0.014 nN/nm as the salt concentration increased from that of pure water to 1 M KCl (Figure 4.3, Table 4.2), indicating that the surface was more compliant in lower salt solutions.

On a microscopic basis, the biopolymers were flexible in all salt solutions studied, as modeled using the freely jointed chain model. The Kuhn lengths ranged from 0.154 to 0.65 nm in all solutions (Figure 4.4). In a previous study, we reported the range of Kuhn lengths for these biopolymers in water, 0.01 M and 0.1 M KCl. The average values here are in the middle of the ranges we reported previously [17]. Statistical tests confirmed that l_k in water was significantly different from l_k in all other salt solutions. However the l_k values in all salt solutions except

water were not statistically significantly different from one another. All statistical analyses were based on the Dunn rank sum test ($p > 0.05$).

4.3.4 Scaling Relations. The brush layer height can be correlated with $\Gamma^{1/3}$ for an uncharged brush [46]. To maintain dimensionless numbers, we compared L/l_k vs. $(\Gamma l_k^2)^{1/3}$, but this scaling relationship was not satisfactory for our data (Figure 4.5A). An alternate relationship for a polyelectrolyte brush [72, 74, 75] was applicable (Figure 4.5B). In the latter model, L is correlated with $L_c(\Gamma v)^{1/3} l_k^{-1/3}$. The polyelectrolyte model accounts for excluded volume interactions between adjacent "blobs" of the polymer chain and also accounts for the elastic properties of the polymers. The validity of the polyelectrolyte scaling relationship confirms that the polymer brush layer on the surface of *P. putida* KT2442 is charged.

Scaling relationships for polyelectrolytes can also be used to determine the relationship between the brush height (L) and the salt concentration (C_s). Several models have been proposed for this relationship and are based on Monte Carlo simulations [81], mean field calculations [72, 75], and self-consistent field theories [66, 73]. For *P. putida* KT2442, the dependence of the brush layer height on the added salt concentration was investigated through application of the general power law formula $L \sim C_s^{-m}$ [70]. The exponent that best represented our data was -0.51 (Figure 6), which was practically the same as the scaling relation predicted for an electrostatic wormlike chain in a dilute solution ($L \sim C_s^{-1/2}$), where chain stiffening causes l_k to change with salt concentration [77, 78, 82]. The other relationships predict that $L \sim C_s^{-1/3}$ for a salted brush in the regime where added salt far exceeds the counterion concentration [73] or $L \sim C_s^{-2/3}$ in an alternate model to account for local chain stiffening and excluded volume effects [75]. Although the exponent -0.51 provided the best correlation with our data, all of the models to relate L and C_s fit the data well. We therefore cannot conclusively distinguish between these three models.

We used one of the models (the electrostatic WLC) to also determine the maximum compression of the brush layer (L_o), which was found to be 105 nm (Figure 4.6A). If we continue to increase the salt concentration in solution, the most we could compress the brush layer is to a height of 105 nm. We measured a maximum compression of the brush layer as 120 nm in 1 M KCl (Table 4.2), but the model implies that even as salt concentration is increased further, the brush layer could not collapse to a height < 105 nm (Figure 4.7).

4.3.5 Effect of Ionic Strength on Biopolymer Adhesion. A distribution of adhesion peaks between the AFM tip and the bacterial surface polymers was observed in all solvents (Figure 4.8), which mainly reflects the heterogeneity of the bacterial surface. If an average value for the force over all the measured adhesion events was used to represent the adhesion force at a given salt concentration, then a comparison could be made between the adhesion force and C_s (Figure 4.9). Pairwise statistical tests were used to determine if the different "treatments" were significantly different from one another. All combinations of pairs among the six salt concentrations were tested. The average adhesion force at a given C_s was significantly different from the adhesion forces at all other salt concentrations except for the adhesion forces in water and 0.01 M KCl. The latter two treatments (water and 0.01 M KCl) were not significantly different from one another according to the Dunn rank sum test ($p > 0.05$).

4.4 Discussion

4.4.1 Effect of Ionic Strength on Biopolymer Conformation. For neutral polymer brushes on a solid surface, short-range intermolecular repulsion causes the chains to partially stretch in the direction normal to the grafting surface [46, 47]. Polyelectrolyte brushes also stretch in the direction normal to the grafting surface, but the stretching is caused primarily by electrostatic interactions in the layer instead of short-range repulsion between individual units of

the molecule [68, 72]. Since electrostatic interactions are long-range in nature, the chains can become stretched at lower grafting densities, below the overlapping threshold [68, 69]. Scaling relationships to describe the conformational behavior of grafted polyelectrolytes have been developed for planar and curved surfaces [69-72]. To our knowledge such models have not been previously applied to macromolecules grafted to a microbial cell.

The microscopic (single molecule) investigation of polymer rigidity showed that the polymers were flexible under all conditions tested, and we did not observe a trend in the Kuhn length as a function of ionic strength. This implies that for the polymers on the surface of *P. putida* KT2442, interactions between neighboring particles did not lead to electrostatic stiffening of the chains. This finding is consistent with the behavior of polyelectrolytes with a flexible backbone [69]. Previous experimental evidence also indicated that these biopolymers are flexible in many solvents [17, 27].

4.4.2 Polyelectrolyte Theories. The observed scaling relationship of the brush layer height (L) with $L_c\left(\frac{\Gamma v}{l_k}\right)^{1/3}$, as well as the failure of the relation for an uncharged brush $L/l_k \sim (\Gamma l_k^2)^{1/3}$, implies that the biopolymer layer is charged, consistent with the behavior of a polyelectrolyte brush. Neutral and charged polymers can be described using the "blob" model [47], in which a chain at an interface is viewed as a succession of non-interacting blobs. A chain within one blob assumes a conformation that is equivalent to that in a dilute polymer solution. Monomers can interact with adjacent and distant segments in their blob, but not with segments from other blobs. Interactions in a blob can be described by the segment or Kuhn length (l_k) and the reduced excluded volume (v/l_k^3). For neutral polymers, the segment length is independent of

polymer-solvent affinity, but for polyelectrolytes, both the segment length and the excluded volume may be affected by electrostatic interactions.

The concept of an electrostatic wormlike chain has been developed, in which changes in ionic strength affect the local chain stiffness and the excluded volume. Fixman et al. [77, 78] accounted for electrostatic effects within a segment by modeling the backbone of the polymer as a charged torus and solving the non-linear Poisson-Boltzmann expression for the electrostatic field. Electrostatic and steric hindrances were balanced against the kinetic energy of the chain, and expressions were developed to describe the relationship between salt concentration and chain conformation. Hariharan et al. [70] showed that adoption of the electrostatic wormlike chain theory provides the scaling relationship $L \sim C_s^{-1/2}$. In our study, the brush layer height scaled with $C_s^{-1/2}$, but other relationships could not be ruled out. An alternate treatment of local chain stiffening and excluded volume effects by Argillier and Tirrell suggested that polyelectrolytes scale according to the relationship $L \sim C_s^{-2/3}$ [75]. A theory developed by Zhulina et al. [73] that is applicable to both salted and unsalted polyelectrolyte brushes expresses the free energy function as the sum of entropic interactions at a given temperature and the energy caused by excluded volume interactions, and incorporates both electrostatic and non-electrostatic effects. For the salted brush, the scaling relationship obtained is $L \sim L_c \Gamma^{1/3} C_s^{-1/3}$. Both of these latter two relationships described our data nearly as well as that of the electrostatic wormlike chain model.

Although each of the scaling theories (electrostatic wormlike chain, Argillier and Tirrell's treatment of chain stiffening, and Zhulina et al.'s models for a salted brush) reasonably explained the relationship between the brush layer height and the salt concentration, other evidence suggests that the electrostatic wormlike chain model is not applicable to these biopolymers. The

Kuhn length was nearly insensitive to salt concentration, and so chain stiffening does not appear to have been a factor in influencing biopolymer conformation.

4.4.3 Balance of Attractive and Repulsive Forces. A transition in the adhesion force was seen between a C_s of 0.1 and 0.5 M (Table 4.3). Above a critical salt concentration, the net concentration of ions in the solvent exceeds the net concentration of ions in the polymer brush. A theoretical investigation of how the energy barriers change with salt concentration based on the use of soft-particle DLVO theory showed that for a salt concentration > 0.05 M, the total interaction energy was attractive (Table 4.1, Figure 4.2).

Adhesion between two bodies is primarily caused by van der Waals interactions when the bodies are uncharged. The adhesion between two spherical bodies can be calculated based on van der Waals interactions as

$$F_v = \frac{A}{6H_o^2}\left(\frac{a_1 a_2}{a_1 + a_2}\right) \tag{4.9}$$

where H_o the distance of closest approach, usually assumed to be 0.3 nm [83]. It is not necessary to consider retardation effects at this short distance. Application of eq (4.12) provides an adhesion force of 3.09 nN at all salt concentrations (Table 4.3), since van der Waals interactions are typically considered to be independent of ionic strength [7].

The attraction of the polymer for the tip is balanced by electrostatic and Born repulsion, as well as the stretching energy of the chain as the AFM tip is retracted. We estimated the amount of electrostatic repulsive forces between the bacterium and the tip at 0.3 nm by applying the relation $\frac{dE_e}{dh} = -F_e$ where E_e was calculated in eq 4.8. The electrostatic force between two dissimilar spheres at a separation distance H_o can be written as

$$F_e = -\frac{4\pi a_1 a_2 n k_B T}{(a_1 + a_2)\kappa}(\Phi_1^2 + \Phi_2^2)[e^{-2\kappa H_o} - \frac{2\Phi_1\Phi_2}{\Phi_1^2 + \Phi_2^2} e^{-\kappa H_o}][\frac{1}{1 - e^{-2\kappa H_o}}] \quad (4.10)$$

The electrostatic forces as a function of C_s are tabulated in Table 4.3.

Born repulsion is a strong short-range repulsion that originates from the repulsive forces between atoms as their shells interpenetrate each other. A Hamaker-type integration for all molecules in the systems was developed by Feke et al. [84] for the Born repulsive energy between two spheres. Detailed expressions are provided in the Appendix.

We previously ignored Born repulsion in the calculation of DLVO energy profiles between the bacterium and the tip because such forces are only important at very short separations. But when we consider the closest possible separation distance of 0.3 nm, Born repulsion must be included. The calculated Born repulsive force for $h = H_o = 0.3$ nm was 2.20 nN, irrespective of the salt concentration.

The net interaction force at each salt concentration was calculated as the sum of van der Waals attractions, electrostatic repulsion, and Born repulsion. The sum of these forces was compared with the measured adhesion force in each salt solution (Table 4.4). In water and 0.01 M KCl, the predicted adhesion was higher than the average experimentally measured adhesion. In the other four solutions, the predicted and measured adhesion values were similar.

Our simple force balance comes surprisingly close to predicting the measured adhesion forces, but is not without limitations. One complicating factor is that the polyelectrolyte layer itself can increase the ionic strength of the solution in the area between the bacterium and the surface. Boonaert et al. [85] suggested that extracellular material released by *Lactococcus lactis* increased cellular adhesion to polystyrene and glass by increasing the ionic strength of the solution in the region confined between the cells and the substrate. If the local ionic strength was higher, electrostatic repulsion would be less than we predicted.

The forces we calculated in the force balance also did not include hydrogen bonds and the energy of the chain stretching, which would also each contribute to measured adhesion. The actual adhesion force reflects a combination of van der Waals attraction, Born repulsion, chain stretching energy, hydrogen bonding, and electrostatic repulsion. The difficulty in making the force balance reemphasizes the complex nature of the bacterial surface and further necessitates the need for detailed molecular studies of bacterial surface properties.

4.4.4 Critical Salt Concentrations Influencing Biopolymer Conformation and Adhesion. For each physicochemical property that was probed, a transition occurred that was dependent on the salt concentration (Table 4.4). In pure water, the biopolymer layer was extended, "soft", showed low adhesion, exhibited a highly negative electrophoretic mobility and large energy barrier to adhesion, and corresponded to a random conformation. As the salt concentration increased, these physical properties were modified.

Above 0.01 M, the bacterial surface layer transitioned towards a more rigid and ordered structure, the electrophoretic mobility began to reach a plateau, and the predicted energy profile (at C_s > 0.05 M) changed from repulsive to attractive. The magnitude of the adhesion force underwent a transition between 0.1 and 0.5 M KCl, shifting towards higher adhesion between the biopolymers and the AFM tip. Most physical properties were similar in 0.5 and 1 M KCl. At these two latter salt concentrations, the polymer brush layer can be considered rigid (although individual polymers are still flexible), the adhesion forces are high, the electrophoretic mobility is less negative and not dependent on C_s, and attractive energy profiles are predicted.

Similar effects for some of these properties have been observed in other systems. For example, the exopolymer produced by *Pseudomonas* 'gingeri' Pf9 became more rigid at higher ionic strengths because screening of negative charges on the polysaccharide chain promoted a

transition towards a more rigid conformation [86]. Compression to a rigid fibrillar layer upon the addition of 0.1 M KCl was observed by van der Mei et al. when the surface of a fibrillated *Streptococcus salivarius* strain was probed via AFM [80]. In addition to experimental measurements, modeling has shown that the predicted DLVO energy profiles between wild type *Escherichia coli* and glass decreased from an energy barrier of ~ 420 k_BT in 0.02 M phosphate buffer to an attractive profile in 0.2 M phosphate buffer [13]. No other study addressed the combined effects of biopolymer conformation, brush layer properties, and DLVO forces on bacterial adhesion.

The conformation of biopolymers on a bacterial surface has not been greatly studied, but many studies addressed the role of salt concentration on conformation in systems of pure polysaccharides. For example, the anionic polysaccharide succinoglycan undergoes a salt-induced conformational transition from single chains in low salt solutions to dimers of associated single helices in higher salt solutions [87-89]. Xanthan undergoes a similar transition in that the triple helix can unravel if sufficient salt is not present in solution [90-92]. It is therefore not surprising to see conformational changes in the biopolymers on the surface of *P. putida* KT2442, based on the many studies of pure polysaccharides in solution.

Our studies suggest that electrostatic interactions affect the behavior of charged biopolymers in ways beyond what can be described by DLVO theory. Electrostatic interactions affect the conformation of the biopolymers and the softness of the bacterial polymer layer, and these properties in turn affect adhesion. Understanding the interplay of electrostatic and steric interactions in influencing the adhesion of bacteria to surfaces will be critical to the development of improved models predicting bacterial adhesion.

4.5 Summary

The biopolymers on the surface of *P. putida* KT2442 undergo a salt-induced conformational change from a soft, random structure in low ionic strength solutions to an ordered, rigid structure in the presence of salt. This conformational change occurs between 0.01 and 0.05 M KCl. Accompanying this conformational change, the adhesion behavior of the polymer changes. Greater adhesion forces are observed between the biopolymer and silicon nitride for the softer and more charged brush layer in high ionic strength solutions. The change from repulsive to attractive interactions upon the addition of salt was predicted by soft-particle DLVO theory. This study provides evidence that conformational changes in biopolymers that occur due to the salt concentration in solution are important factors in influencing adhesion, and therefore they need to be included in predictive models of bioadhesion.

4.6 Acknowledgments

We thank Patrick Guenoun for helpful discussions that provided the impetus for this study.

This publication was made possible in part by a CAREER Award from the National Science Foundation (grant number BES-0238627).

4.7 Glossary

a_1: Tip radius (250 nm)
a_2: The radius of the bacterium (500 nm)
A: Hamaker constant for the interacting media (10^{-20} J)
C_s: Salt concentration of the solvent (M KCl)
e: Electron charge (1.602×10^{-19}C)
E_b: Born repulsive energy (k_BT)
E_e: Electrostatic interactions (k_BT)
E_t: Total interaction energy (estimated by DLVO theory) (k_BT)
E_v: London-van der Waals interactions (k_BT)
F_{chain}: Force required to stretch FJC chain to length h (nN)
F_e: Electrostatic force between dissimilar spheres (nN)
F_{st}: Steric force (nN)
F_v: van der Waals Interactions (nN)
h: Separation distance between tip and biopolymers (nm)
H_o: Distance of closest approach (0.3 nm)
k_B: Boltzmann constant (1.381×10^{-23} J/K)
K: constant with value of 1
K_m: Debye-Hückel parameter for the polymer layer
L: Equilibrium height of the polyelectrolyte brush layer (m)
$\mathcal{L}^{-1}$: Inverse Langevin function
L_c: Contour length ($1.25L$) used in scaling relationships (nm)
l_c: Contour length obtained from FJC model (nm), represents a portion of whole chain length
l_k: Kuhn length (nm)
L_o: Maximum compressed brush thickness (105 nm)
m: Fractional exponent in polymer scaling model (–0.51)
n: Concentration of bulk ions (M)
N: Density of the charged groups
R: Center-to-center distance between two dissimilar spheres, made dimensionless by dividing by a_1
T: Temperature (298 K)
Z: Valance of the charged groups in the polymers
z: Valence of bulk ions
Γ: Grafting density of bacterial surface biopolymers in brush layer (m^{-2})
ε: Permittivity of a vacuum (8.85×10^{-12} C^2/J·m)
ε_o: Relative permittivity of solvent (78 for water)
η: Solvent viscosity (8.9×10^{-4} kg/m·s)
κ: Debye screening length (nm)
λ: Ratio between the sphere diameters (a_2/a_1)
λ_c: Characteristic wavelength of the van der Waals interaction (100 nm)
λ_s: Softness parameter (nm^{-1})
μ: Electrophoretic mobility (m^2/V·s)
ν: Excluded volume (m^3)
σ: Collision diameter (0.5 nm)
Φ_1: Reduced potential of tip ($\Phi_1 = ze\psi_1/k_BT$)

Φ_2: Reduced potential of bacterium ($\Phi_2 = ze\psi_2/k_BT$)
ψ_1 or ψ_{tip}: Surface potential of tip (V)
ψ_2 or $\psi_{bacterium}$: Surface potential of bacterium (V)
Ψ_{DON}: Donnan potential of polymer layer (V)
Ψ_o: Surface zeta potential (V)

Table 4.1. Summary of Parameters for DLVO Interaction Energy Calculations

C_s (M)[1]	Ψ_{tip} (mV)	$\Psi_{bacteria}$ (mV)	E_{max} (k_BT)
0.01	-16	-31.7	125
0.05	-14	-9.2	1.45
0.1	-12	-4.6	All attraction
0.5	-10	-3.0	All attraction
1	-8	-3.0	All attraction

[1] C_s is the added salt concentration, Ψ_{tip} the surface potential of the tip as estimated by conventional zeta potential theory, $\Psi_{bacteria}$ the surface potential of the bacteria estimated from soft-particle DLVO theory (eq 4.3), and E_{max} the calculated energy barrier based on DLVO theory (eq 4.7).

Table 4.2. Physical Properties of Brush Layer as a Function of Salt Concentration

C_s[1] (M KCl)	L (nm)	Γ x 10^{15} (molecules/m^2)	$L\,\Gamma$ x 10^{-8} (molecules/m)	R^2 for steric model	Slope of compliance region (nN/nm)	l_k (nm)	Average Adhesion Force (nN)
Water[2]	440	1.6	7.04	0.99	-0.014	0.208	-0.33
0.01	280	1.7	4.76	0.99	-0.010	0.202	-0.46
0.05	180	2.5	4.50	0.95	-0.054	0.205	-0.60
0.1	160	3.0	4.80	0.98	-0.035	0.200	-0.66
0.5	130	3.4	4.42	0.98	-0.109	0.186	-1.04
1.0	120	5.2	6.24	0.98	-0.114	0.180	-1.85

[1] C_s is the added salt concentration, L the brush thickness, Γ the grafting density of the polymer brush, l_k the Kuhn length estimated by the use of FJC model (eq 4.10).
[2] While the solvent was pure water, we estimated that the salt concentration with the polymer in solution was 0.0027 M. This estimate was based on extension of the line in Figure 4.6A and extrapolation of the salt concentration at a brush layer thickness of 440 nm.

Table 4.3. Comparison of Measured Adhesion Forces with DLVO Predictions as a Function of Added Salt Concentration

C_s (M)	Predicted Electrostatic Repulsion[1] (nN)	Predicted Force (electrostatic+van der Waals[2] + Born repulsion[3]) (nN)	Average Adhesion Force (Measured) (nN)
Water	3.85	2.96	-0.33
0.01	2.07	1.18	-0.46
0.05	0.46	-0.43	-0.60
0.10	0.15	-0.74	-0.66
0.50	0.04	-0.85	-1.04
1.00	0.05	-0.84	-1.85

By convention for AFM data, attractive forces are negative and repulsive forces are positive in sign.
[1]Predicted based on sphere-sphere interaction force calculated at a separation distance of 0.3 nm.
[2]van der Waals interactions were calculated for sphere-sphere geometry, assuming a separation distance of 0.3 nm, and were -3.09 nN, insensitive to salt concentration.
[3]Born repulsive forces were calculated for sphere-sphere geometry, assuming a separation distance of 0.3 nm, and were 2.20 nN, insensitive to salt concentration (C_s).

Table 4.4. Summary of Physical Property Transitions as a Function of Added Salt Concentration

Transition occurs between water and 0.01 M KCl
---Kuhn length (l_k is significantly different between water and 0.01 M KCl; l_k's are not significantly differently between 0.01 M KCl and all higher salt concentrations)
Transition occurs between 0.01 and 0.05 M KCl
---Electrophoretic mobility
---Softness of the bacterial surface (the slopes of the compliance regions in water and 0.01 M KCl were not significantly different from one another but they are each different from the rest of the data)
Transition occurs between 0.05 and 0.10 M KCl
---Predicted energy barrier based on soft-particle DLVO theory (attraction observed at > 0.05 M KCl)
Transition occurs between 0.1 and 0.5 M KCl
---Magnitude of the average adhesion force between biopolymers and AFM tip

4.8 Figure Captions

Figure 4.1. The electrophoretic mobility of *P. putida* KT2442 as a function of added salt concentration. Each point represents an average of three experimental measurements (pH= 8.0) while the line is the fit of these data points to soft-particle DLVO theory (eq 4.2, R^2=0.97).

Figure 4.2. The total interaction energy between the silicon nitride AFM tip and *P. putida* KT2442 cells, based on soft-particle DLVO theory calculations (electrostatic and van der Waals interactions). The interactions were calculated based on sphere-sphere geometry, where a_1= 250 nm, a_2 = 500 nm, A = 10^{-20} J [61]. The surface potentials for the tip and bacterium are summarized in Table 4.1.

Figure 4.3. Summary of the average AFM approach curves for *P. putida* KT2442 in different salt solutions. A) Water, B) 0.01 M KCl, C) 0.05 M KCl, D) 0.1 M KCl, E) 0.5 M KCl, F) 1 M KCl, and G) A comparison between average approach curves in all salt solutions. In plots A-F, the symbols represent experimental data and the solid lines are best fits based upon the steric model (eq 4.1). Steric model results and the slopes of the compliance regions are given in Table 4.2.

Figure 4.4. Representative data and modeling results for the application of the freely jointed chain model (eq 10) to AFM retraction curves. While hundreds of chains were examined, we present representative data for a few chains. The model fit the chains equally well in all experiments. Experimental conditions were as follows: A) 0.05 M KCl, estimated L_c (nm), l_k (nm) and R^2 values for the chains from left to right are: (11, 0.154, 0.93), (54, 0.247, 0.97), (102, 0.184, 0.99), and (172, 0.154, 0.98). B) 0.5 M KCl, estimated L_c (nm), l_k (nm) and R^2 values for the chains from left to right are: (17, 0.154, 0.96), (63, 0.195, 0.96), (111, 0.154, 0.98), (183, 0.193, 0.99), and (245, 0.155,1.0). C) 1.0 M KCl, estimated L_c (nm), l_k (nm) and R^2 values for the

chains from left to right are: (10, 0.245, 0.97), (36, 0.154, 0.99), (86, 0.165, 0.97), (143, 0.154, 0.98), (187, 0.154, 0.99), and (285, 0.154, 1.0).

Figure 4.5. Application of scaling theories for polyelectrolyte brushes. A) The scaling results for an uncharged brush. B) The scaling relation for a charged polyelectrolyte brush. In A) and B), symbols are experimental values (or calculated values based on experimental data) and the lines are best fits. The excluded volume was estimated using eq. 12. The steric model was applied to the data in Figure 3 to obtain the values of Γ. The Kuhn lengths were estimated from application of the freely jointed chain model to the data in Figure 4.

Figure 4.6. Scaling relationships between L and C_s for polyelectrolytes. A) The general power law relationship ($L \sim C_s^{-m}$) to describes the dependence of brush thickness on added salt concentration, where m = 0.51. Plots B - E represent different relationships that have been proposed for polyelectrolytes. B) Pincus model [72], C) Zhulina et al. [73] model, D) Argillier and Tirrel [75] model, and E) Electrostatic WLC model [77, 78].

Figure 4.7. Conceptual representation of the conformation of bacterial surface biopolymers at low and high salt concentrations.

Figure 4.8. The distribution of adhesion forces observed between the silicon nitride AFM tip and *P. putida* KT2442 biopolymers as a function of ionic strength. Each data point represents an adhesion event between the tip and bacterial surface biopolymers as measured in the retraction portion of a force-displacement curve. Each retraction curve captured may have single or multiple adhesion events. The magnitude of the adhesion force is taken as the maximum value of each adhesion peak. Adhesion peaks were collected from the retraction portions of 25 different force-displacement curves, measured on five different bacterial cells for each salt concentration studied. The magnitude of each adhesion peak is shown in this figure. In some

subsequent calculations, an average value was used to characterize the adhesive interaction at a given salt concentration.

Figure 4.9. The relationship between measured adhesion force and added salt concentration. Each point represents an average of all the adhesion peaks for a given salt concentration (all individual data points are shown in Figure 4.8).

4.9Appendix

4.9.1 Soft-Particle DLVO Theory

The equations below show the dependence on ionic strength of several parameters, which appear in the electrophoretic mobility expression (eq 4.2).

$$\Psi_o = \frac{k_B T}{ze}\left(ln\{\frac{ZN}{2zn} + [(\frac{ZN}{2zn})^2 + 1]^{1/2}\} + \frac{2zn}{ZN}\{1 - [(\frac{ZN}{2zn})^2 + 1]^{1/2}\}\right) \quad (4A.1)$$

$$K_m = \kappa\,[\,1 + (\frac{ZN}{2\,zn})^2\,]^{1/4} \quad (4A.2)$$

$$\kappa = (\frac{1}{\varepsilon_o \varepsilon k_B T}\sum_{i=1}^{N} z_i^2 e^2 n)^{1/2} \quad (4A.3)$$

$$\Psi_{DON} = \frac{K_B T}{ze} ln\{\frac{ZN}{2zn} + [(\frac{ZN}{2zn})^2 + 1]^{1/2}\} \quad (4A.4)$$

Where z is the valence of bulk ions, n the concentration of bulk ions, and κ the Debye screening length. The parameter ZN represents spatial charge density in the polyelectrolyte region and the term $1/\lambda_s$ characterizes the softness of the bacterial surface. The electrophoretic mobility is measured as a function of salt concentration and this data is used to fit the parameters ZN and $1/\lambda_s$ from eq 4.2 in the text.

4.9.2 Born Repulsive Interactions

Born repulsion is a strong short-range repulsion that originates from the repulsive forces between atoms as their shells interpenetrate one another. A Hamaker-type integration for all molecules in the systems was developed by Feke et al. [84] for the Born repulsive energy between two spheres. The equations describing such interactions are as follows:

$$E_b = A_1 A_2 \quad (4A.5)$$

$$A_1 = 4A(\frac{\sigma}{a_1})^{n-6}\frac{(n-8)!}{(n-2)!}\frac{1}{R} \tag{4A.6}$$

and

$$A_2 = [\frac{-R^2-(n-5)(\lambda-1)R-(n-6)[\lambda^2-(n-5)\lambda+1]}{(R-1+\lambda)^{n-5}}+$$

$$\frac{-R^2+(n-5)(\lambda-1)R-(n-6)[\lambda^2-(n-5)\lambda+1]}{(R+1-\lambda)^{n-5}}+$$

$$\frac{R^2+(n-5)(\lambda+1)R+(n-6)[\lambda^2+(n-5)\lambda+1]}{(R+1+\lambda)^{n-5}}+$$

$$\frac{R^2-(n-5)(\lambda+1)R+(n-6)[\lambda^2+(n-5)\lambda+1]}{(R-1-\lambda)^{n-5}}] \tag{4A.7}$$

Where R is the center-to-center separation distance made dimensionless on a_1 ($R = \frac{a_1+h+a_2}{a_1}$), $\lambda = \frac{a_2}{a_1}$, and σ is the collision diameter (assumed to be 0.5 nm). The most common form of the expression is where n = 12. Using this value for n, the repulsive force was calculated by taking the negative derivative of the energy. The full expression for the Born repulsive forces between two spheres can be derived based on these equations (n =12) as:

$$F_B = -\frac{dE_b}{dh} = \frac{1}{a_1}\frac{dE_b}{dR} = \frac{1}{a_1}[A_1\frac{dA_2}{dR}+A_2\frac{dA_1}{dR}] \tag{4A.8}$$

Where

$$\frac{dA_1}{dR} = \frac{-4A}{151200R^2}(\frac{\sigma}{a_1})^6 \tag{4A.9}$$

$$\frac{dA_2}{dR} = [\frac{A_7^7(-2R-7(\lambda-1))-7A_3A_7^6}{A_7^{14}}+$$

$$\frac{A_8^7(-2R+7(\lambda-1))-7A_4A_8^6}{A_8^{14}}+$$

$$\frac{A_9^7(2R+7(\lambda+1))-7A_5A_9^6}{A_9^{14}}+$$

$$\frac{A_{10}^7(2R-7(\lambda+1))-7A_6A_{10}^6}{A_{10}^{14}}] \tag{4A.10}$$

$$A_3=-R^2-7(\lambda-1)R-6(\lambda^2-7\lambda+1) \tag{4A.11}$$

$$A_4=-R^2+7(\lambda-1)R-6(\lambda^2-7\lambda+1) \tag{4A.12}$$

$$A_5=R^2+7(\lambda+1)R+6(\lambda^2+7\lambda+1) \tag{4A.13}$$

$$A_6=R^2-7(\lambda+1)R+6(\lambda^2+7\lambda+1) \tag{4A.14}$$

$$A_7=R-1+\lambda \tag{4A.15}$$

$$A_8=R+1-\lambda \tag{4A.16}$$

$$A_9=R+1+\lambda \tag{4A.17}$$

$$A_{10}=R-1-\lambda \tag{4A.18}$$

4.10 References

1. Williams, V., Fletcher, M., *Pseudomonas fluorescens adhesion and transport through porous media are affected by lipopolysaccharide compostion.* Applied and Environmental Microbiology, 1996. **62**: p. 100-104.
2. DeFlaun, M.F., Oppenheimer, S.R., Streger, S., Condee, C.W., Fletcher, M., *Alterations in adhesion, transport, and membrane characteristics in an adhesion-deficient Pseudomonad.* Applied and Environmental Microbiology, 1999. **65**: p. 759-765.
3. Simoni, S.F., Harms, H., Bosma, T.N.P., and A.J.B. Zehnder, *Population heterogeneity affects transport of bacteria through sand columns at low flow rates.* Environmental Science & Technology, 1998. **32**: p. 2100-2105.
4. Triandafillu, K., Balazs, D.J., Aronsson, B.-O., Descouts, P., Tu Quoc, P., van Delden, C., Mathieu, H.J., Harms, H., *Adhesion of Pseudomonas aeruginosa strains to untreated and oxygen-plasma treated poly(vinyl chloride) PVC from endotracheal intubation devices.* Biomaterials, 2003. **24**: p. 1507-1518.
5. Henriksson, A., Szewzyk, R., Conway, P.L., *Characteristics of the adhesive determinants of Lactobacillus fermentum 104.* Applied and Environmental Microbiology, 1991. **57**: p. 499-502.
6. Marshall, K.C., Stout, R., Mitchell, R., *Mechanism of the initial events in the sorption of marine bacteria to surfaces.* Journal of General Microbiology, 1971. **68**: p. 337-348.
7. Israelachvili, J.N., *Intermolecular & Surface Forces (2nd edition)*. 1992, New York: Academic Press.

8. Rijnaarts, H.H.M., Norde, W., Lyklema, J., and A.J.B. Zehnder, *DLVO and steric contributions to bacterial deposition in media of different ionic strengths.* Colloids and Surfaces B: Biointerfaces, 1999. **14**: p. 179-185.

9. Zita, A., Hermansson, M., *Effects of ionic strength on bacterial adhesion and stability of flocs in a wastewater activated sludge system.* Applied and Environmental Microbiology, 1994. **60**: p. 3041-3048.

10. Smets, B.F., D. Grasso, M.A. Engwall, and B.J. Machinist, *Surface physicochemical properties of Pseudomonas fluorescens and impact on adhesion and transport through porous media.* Colloids and Surfaces B: Biointerfaces, 1999. **14**(1-4): p. 121-139.

11. Poortinga, A.T., R. Bos, and H.J. Busscher, *Electrostatic interactions in the adhesion of an ion-penetrable and ion-impenetrable bacterial strain to glass.* Colloids and Surfaces B: Biointerfaces, 2001. **20**(2): p. 105-117.

12. Abu-Lail, N.I. and T.A. Camesano, *The role of lipopolysaccahrides in the adhesion, retention, and transport of E.coli JM109.* Environmental Science & Technology, 2003. **In Press**.

13. McLaine, J.W., Ford, R.M., *Reversal of flagellar rotation is important in initial attachment of Escherichia coli to glass in a dynamic system with high- and low-ionic strength buffers.* Applied and Environmental Microbiology, 2002. **68**: p. 1280-1289.

14. Dan, N., *The effect of charge regulation on cell adhesion to substrates: salt-induced repulsion.* Colloids and Surfaces B:Biointerfaces, 2003. **27**: p. 41-47.

15. van Oss, C.J., *Interfacial Forces in Aqueous Media*. 1994, New York: Marcel Dekker.

16. Van der Aa, B.C., Michel, R.M., Asther, M, Zamora, M.T., Rouxhet, P.G., and Y.F. Dûfrene, *Stretching cell surface macromolecules by atomic force microscopy.* Langmuir, 2001. **17**: p. 3116-3119.

17. Abu-Lail, N.I., Camesano, T.A., *Elasticity of Pseudomonas putida KT2442 biopolymers probed with single-molecule force microscopy.* Langmuir, 2002. **18**: p. 4071-4081.

18. Lower, S.K., Tadanier, C.J., Hochella, M.F., Jr., *Measuring interfacial and adhesion forces between bacteria and mineral surfaces with biological force microscopy.* Geochimica et Cosmochimica Acta, 2000. **64**: p. 3133-3139.

19. Lower, S.K., Tadanier, C.J., Hochella, M.F. Jr., *Dynamics of the mineral-microbe interface: Use of biological force microscopy in biogeochemistry and geomicrobiology.* Geomicrobiology Journal, 2001. **18**: p. 63-76.

20. Lower, S.K., Hochella, M.F., Jr., and T.J. Beveridge, *Bacterial recognition of mineral surfaces: nanoscale interactions between Shewanella and -FeOOH.* Science, 2001. **292**: p. 1360-1363.

21. Ong, Y.-L., Razatos, A., Georgiou, G., Sharma, M.M., *Adhesion forces between E. coli bacteria and biomaterial surfaces.* Langmuir, 1999. **15**: p. 2719-2725.

22. Bowen, W.R., Lovitt, R.W., and C.J. Wright, *Direct quantification of Aspergillus niger spore adhesion in liquid using an atomic force microscope.* Journal of Colloid and Interface Science, 2000. **228**: p. 428-433.

23. Vigeant, M.A.S., Ford, R.M., Wagner, M., Tamm, L.K., *Reversible and irreversible adhesion of motile Escherichia coli cells analyzed by total internal reflection aqueous fluorescence microscopy.* Applied and Environmental Microbiology, 2002. **68**: p. 2794-2801.

24. Prince, J.L., Dickinson, R.B., *Kinetics and forces of adhesion for a pair of capsular/unencapsulated Staphylococcus mutant strains.* Langmuir, 2003. **19**: p. 154-159.

25. Camesano, T.A., Unice, K.M., and B.E. Logan, *Blocking and ripening of colloids in porous media: Implications for bacterial transport.* Colloids and Surfaces A: Physicochemical and Engineering Aspects, 1999. **160**: p. 291-307.

26. Camesano, T.A., Logan, B.E., *Probing bacterial electrosteric interactions using atomic force microscopy.* Environmental Science & Technology, 2000. **34**: p. 3354-3362.

27. Camesano, T.A., Abu-Lail, N.I., *Heterogeneity in bacterial surface polysaccharides, probed on a single-molecule basis.* Biomacromolecules, 2002. **3**: p. 661-667.

28. Ramos-Diaz, M.A., Ramos, J.L., *Combined physical and genetic map of the Pseudomonas putida KT2440 chromosome.* Journal of Bacteriology, 1998. **180**: p. 6352-6363.

29. Eberl, L., Ammendola, A., Rothballer, M.H., Givskov, M., Sternberg, C., Kilstrup, M., Schleifer, K.-H., Molin, S., *Inactivation of gltB abolishes expression of the assimilatory nitrate reductase gene (nasB) in Pseudomonas putida KT2442.* Applied and Environmental Microbiology, 2000. **182**: p. 3368-3376.

30. Pérez-Pantoja, D., Guzmán, L., Manzano, M., Pieper, D.H., González, B., *Role of C(I)D(I)E(I)F(I) and tfdD(II)C(II)E(II)F(II) gene modules in catabolism of 3-chlorobenzoate by Ralstonia eutropha JMP134(pJP4).* Applied and Environmental Microbiology, 2000. **66**: p. 1602-1608.

31. Klemba, M., Jakobs, B., Wittich, R.-M., Pieper, D., *Chromosomal integration of tcb chlorocatechol degradation pathway genes as a means of expanding the growth substrate*

range of bacteria to include haloaromatics. Applied and Environmental Microbiology, 2000. **66**: p. 3255-3261.

32. van der Meer, J.R., van Neerven, A.R.W., De Vries, E.J., De Vos, W.M., Zehnder, A.J.B, *Cloning and characterization of plasmid-encoded genes for the degradation of 1,2-dichlorobenzene, 1,4-dichlorobenzene, and 1,2,4-trichlorobenzene of Pseudomonas sp strain P51.* Journal of Bacteriology, 1991. **173**: p. 6-15.

33. Nüßlein, K., Maris, D., Timmis, K., Dwyer, D.F., *Expression and transfer of engineered catabolic pathways harbored by Pseudomonas spp. introduced into activated sludge microcosms.* Applied and Environmental Microbiology, 1992. **58**: p. 3380-3386.

34. Vermette, P. and L. Meagher, *Immobilization and characterization of poly(acrylic acid) graft layers.* Langmuir, 2002. **18**: p. 10137-10145.

35. Wissink, M.J.B., M.J.A. Van Luyn, R. Beernink, F. Dijk, A.A. Poot, G.H.M. Engbers, T. Beugling, W.G. Van Aken, and J. Feijen, *Endothelial cell seeding on crosslinked collagen: effects of crosslinking on endothelial cell proliferation and functional parameters.* Thrombosis and Haemostasis, 2000. **84**(2): p. 325-331.

36. Lee, J.M., H.H.L. Edwards, C.A. Pereira, and S.I. Samii, *Crosslinking of tissue-derived biomaterials in 1-ethyl-3-(3-dimethylaminopropyl)carbodiimide (EDC).* Journal of Materials Science, 1996. **7**(9): p. 531-541.

37. Cleveland, J.P., Manne, S., Bocek, D., Hansma, P.K, *Nondestructive method for determining the spring constant of cantilevers for scanning force microscopy.* Review of Scientific Instruments, 1993. **64**: p. 403-405.

38. Tomitori, M. and T. Arai, *Tip cleaning and sharpening processes for noncontact atomic force microscopy in ultrahigh vacuum.* Applied Surface Science, 1999. **140**: p. 432-438.

39. Ducker, W.A., Senden, T.J., and R.M. Pashley, *Direct measurement of colloidal forces using an atomic force microscope.* Nature, 1991. **353**: p. 239-241.

40. Dufrêne, Y.F., Boonaert, C.J.P., van der Mei, H.C., Busscher, H.J., and P.G. Rouxhet, *Probing molecular interactions and mechanical properties of microbial cell surfaces by atomic force microscopy.* Ultramicroscopy, 2001. **86**: p. 113-120.

41. Boonaert, C.J.P., Rouxhet, P.G., and Y.F. Dufrêne, *Surface properties of microbial cells probed at the nanometer scale with atomic force microscopy.* Surface and Interface Analysis, 2000. **30**: p. 32-35.

42. Van der Aa, B.C. and Y.F. Dûfrene, *In situ characterization of bacterial extracellular polymeric substances by AFM.* Colloids and Surfaces B: Biointerfaces, 2002. **23**: p. 173-182.

43. Lower, S.K., C.J. Tadanier, and M.F. HochellaJr., *Measuring interfacial and adhesion forces between bacteria and mineral surfaces with biological force microscopy.* Geochimica et Cosmochimica Acta, 2000. **64**(18): p. 3133-3139.

44. Hutter, J.L. and J. Bechhoefer, *Calibration of atomic-force microscope tips.* Review of Scientific Instruments, 1993. **64**: p. 1868-1873.

45. Boulbitch, A., *Deformation of the envelop of a spherical gram-negative bacterium during the atomic force microscopic measurements.* Journal of Electron Microscopy, 2000. **49**(3): p. 459-462.

46. Alexander, S., *Adsorption of chain molecules with a polar head a scaling description.* J. Phys. II (Paris), 1977. **38**: p. 983-987.

47. de Gennes, P.G., *Polymers at an interface: A simplified view.* Advances in Colloid and Interface Science, 1987. **27**: p. 189-209.

48. Butt, H.-J., Kappl, M., Mueller, H., Raiteri, R., *Steric forces measured with the atomic force microscope at various temperatures.* Langmuir, 1999. **15**: p. 2559-2565.

49. Drummond, C.J., Senden, T.J., *Examination of the geometry of long-range tip-sample interaction in atomic force microscopy.* Colloids and Surfaces A: Physicochemical and Engineering Aspects, 1994. **87**: p. 217-234.

50. Senden, T.J., Drummond, C.J., *Surface chemistry and tip-sample interactions in atomic force microscopy.* Colloids and Surfaces A: Physicochemical and Engineering Aspects, 1995. **94**: p. 29-51.

51. Ohshima, H.K., *Approximate analytical expression for the electrophoretic mobility of colloidal particles with surface-charge layers.* Journal of Colloid and Interface Science, 1989. **130**: p. 281-282.

52. Bos, R., van der Mei, H.C., Busscher, H.J., *"Soft-particle" analysis of the electrophoretic mobility of a fibrillated and non-fibrillated oral streptococcal strain: Streptococcus salivarius.* Biophysical Chemistry, 1998. **74**(3): p. 251-255.

53. Hayashi, H., Tsuneda, S., Hirata, A., Sasaki, H., *Soft particle analysis of bacterial cells and its interpretation of cell adhesion behaviors in terms of DLVO theory.* Colloids Surf. B: Biointerfaces, 2001. **22**: p. 149-157.

54. Morisaki, H., S. Nagai, H. Ohshima, E. Ikemoto, and K. Kogur, *The effect of motility and cell-surface polymers on bacterial attachment.* Microbiology, 1999. **145**(10): p. 2797-2802.

55. Takashima, S., Morisaki, H., Colloids and Surfaces B: Biointerfaces, 1997. **9**: p. 205-212.

56. Hogg, R., Healy, T.W., Fuerstenau, D.W., *Mutual coagulation of colloidal dispersions.* Transactions of the Faraday Society, 1966. **62**: p. 1638-1651.

57. Elimelech, M., Gregory, J., Jia, X., Williams, R.A., *Particle deposition & aggregation: Measurement, modelling and simulation*. 1995, Woburn, MA: Butterworth-Heinemann.

58. Zhmud, B.V., Sonnefeld, J., Bergstrom, L., *Influence of chemical pretreatment on the surface properties of silicon nitride powder.* Colloids and Surfaces A: Physicochemical and Engineering Aspects, 1999. **158**: p. 327-341.

59. Larson, I., Pugh, R.J., *Qualitative adsorption measurements with an atomic force microscope.* Langmuir, 1998. **14**: p. 5676-5679.

60. Schenkel, J.H., Kitchener, J.A., *A test of the Derjaguin-Verwey-Overbeek theory with a colloidal suspension.* Transactions of the Faraday Society, 1960. **56**: p. 161-173.

61. Martin, R.E., Bouwer, E.J., Hanna, L.M., *Application of clean-bed filtration theory to bacterial transport in porous media.* Environmental Science & Technology, 1992. **26**: p. 1053-1058.

62. Grasso, D., Smets, B.F., Strevett, K.A., Machinist, D.B., van Oss, C.J., Giese, R.F. and W. Wu, *Impact of physiological state on surface thermodynamics and adhesion of Pseudomonas aeruginosa.* Environmental Science & Technology, 1996. **30**: p. 3604-3608.

63. Abu-Lail, N.I., Camesano, T.A., *The role of lipopolysaccharides in the adhesion, retention, and transport of Escherichia coli JM109.* Environmental Science & Technology, 2003. **In press.**

64. Butt, H.-J., *Measuring local electrostatic, van der Waals, and hydration forces in electrolyte solution with an atomic force microscope.* Biophysical Journal, 1992. **60**: p. 777-785.

65. Milner, S.T., Witten, T.A., Cates, M.E., Macromolecules, 1988. **21**: p. 2610-2619.

66. Miklavic, S.J. and S. Marcelja, *Interaction of Surfaces Carrying Grafted Poly-Electrolytes.* Journal of Physical Chemistry, 1988. **92**(23): p. 6718-6722.

67. Misra, S., Varanasi, S., Varanasi, P.P., *A polyelectrolyte brush theory.* Macromolecules, 1989. **22**: p. 4173-4179.

68. Borisov, O.V., T.M. Birshtein, and E.B. Zhulina, *Collapse of Grafted Polyelectrolyte Layer.* Journal de Physique II, 1991. **1**(5): p. 521-526.

69. Borisov, O.V., Zhulina, E.B., Birshtein, T.M., *Diagram of the states of a grafted polyelectrolyte layer.* Macromolecules, 1994. **27**: p. 4795-4803.

70. Hariharan, R., C. Biver, J. Mays, and W.B. Russel, *Ionic strength and curvature effects in flat and highly curved polyelectrolyte brushes.* Macromolecules, 1998. **31**(21): p. 7506-7513.

71. Hariharan, R., C. Biver, and W.B. Russel, *Ionic strength effects in polyelectrolyte brushes: The counterion correction.* Macromolecules, 1998. **31**(21): p. 7514-7518.

72. Pincus, P., *Colloid stabilization with grafted polyelectrolytes.* Macromolecules, 1991. **24**: p. 2912-2919.

73. Zhulina, E.B., O.V. Borisov, and T.M. Birshtein, *Structure of Grafted Polyelectrolyte Layer.* Journal de Physique II, 1992. **2**(1): p. 63-74.

74. Pincus, P.A., G. Rossi, and M.E. Cates, *Conformons - Self-Localized Electrons in Soluble Conjugated Polymers.* Europhysics Letters, 1987. **4**(1): p. 41-46.

75. Argillier, J.F. and M. Tirrell, *Adsorption of Water-Soluble Ionic Hydrophobic Diblock Copolymer on a Hydrophobic Surface.* Theoretica Chimica Acta, 1992. **82**(5): p. 343-350.

76. Witten, T., Pincus, P., *Structure and viscosity of interpenetrating polyelectrolyte chains.* Europhysics Letters, 1987. **3**: p. 315-320.

77. Fixman, M., Skolnick, J., *Polyelectrolyte excluded volume paradox.* Macromolecules, 1978. **11**: p. 863-866.

78. Fixman, M., *Polyelectrolyte Bead Model .1. Equilibrium.* Journal of Chemical Physics, 1990. **92**(10): p. 6283-6293.

79. Biver, C., R. Hariharan, J. Mays, and W.B. Russel, *Neutral and charged polymer brushes: A model unifying curvature effects from micelles to flat surfaces.* Macromolecules, 1997. **30**(6): p. 1787-1792.

80. van der Mei, H.C., Busscher, H.J., Bos, R., de Vries, J., Boonaert, C.J.P., and Y.F. Dufrêne, *Direct probing by atomic force microscopy of the cell surface softness of a fibrillated and nonfibrillated oral streptococci strain.* Biophysical Journal, 2000. **78**: p. 2668-2674.

81. Vongoeler, F. and M. Muthukumar, *Polyelectrolyte Brush Density Profiles.* Macromolecules, 1995. **28**(19): p. 6608-6617.

82. Davis, R.M. and W.B. Russel, *On the Theory of Dilute Polyelectrolyte Solutions - Extensions, Refinements, and Experimental Tests.* Journal of Polymer Science Part B-Polymer Physics, 1986. **24**(3): p. 511-533.

83. Rabinovich, Y.I., Adler, J.J., Ata, A., Singh, R.K., Moudgil, B.M., *Adhesion between nanoscale rough surfaces.* Journal of Colloid and Interface Science, 2000. **232**: p. 10-16.

84. Feke, D.L., Prabhu, N.D., Mann, J.A. Jr., Mann, J.A. III, *A formulation of short-range repulsion between spherical colloidal particles.* Journal of Physical Chemistry, 1984. **88**: p. 5735-5739.

85. Boonaert, C.J.P., Y.F. Dufrene, S.R. Derclaye, and P.G. Rouxhet, *Adhesion of Lactococcus lactis to model substrata: direct study of the interface.* Colloids and Surfaces B: Biointerfaces, 2001. **22**(3): p. 171-182.

86. Gianni, R., P. Cescutti, M. Bosco, W.F. Fett, and R. Rizzo, *Influence of substituents on the solution conformation of the exopolysaccharide produced by Pseudomonas 'gingeri' strain Pf9.* International Journal of Biological Macromolecules, 1999. **26**(4): p. 249-253.

87. Balnois, E., Stoll, S., Wilkinson, K.J., Buffle, J., Rinaudo, M., and M. Milas, *Conformations of succinoglycan as observed by atomic force microscopy.* Macromolecules, 2000. **33**: p. 7440-7447.

88. Borsali, R., Rinaudo, M., and L. Noirez, *Light scattering and small-angle neutron scattering from polyelectrolyte solutions: The succinoglycan.* Macromolecules, 1995. **28**: p. 1085-1088.

89. Burova, T.V., Golubeva, I.A., Grinberg, N.V., Mashkevich, A.Y., Grinberg, V.Y., Usov, A., Navarini, L., Cesaro, A., Biopolymers, 1996. **39**: p. 517-529.

90. Camesano, T.A., Wilkinson, K.J., *Single molecule study of xanthan conformation using atomic force microscopy.* Biomacromolecules, 2001. **2**: p. 1184-1191.

91. Holzwarth, G., *Conformation of the extracellular polysaccharide of Xanthomonas campestris.* Biochemistry, 1976. **15**: p. 4333-4339.

92. Holzwarth, G., Prestridge, E.B., *Multistranded helix in xanthan polysaccharide.* Science, 1977. **197**: p. 757-759.

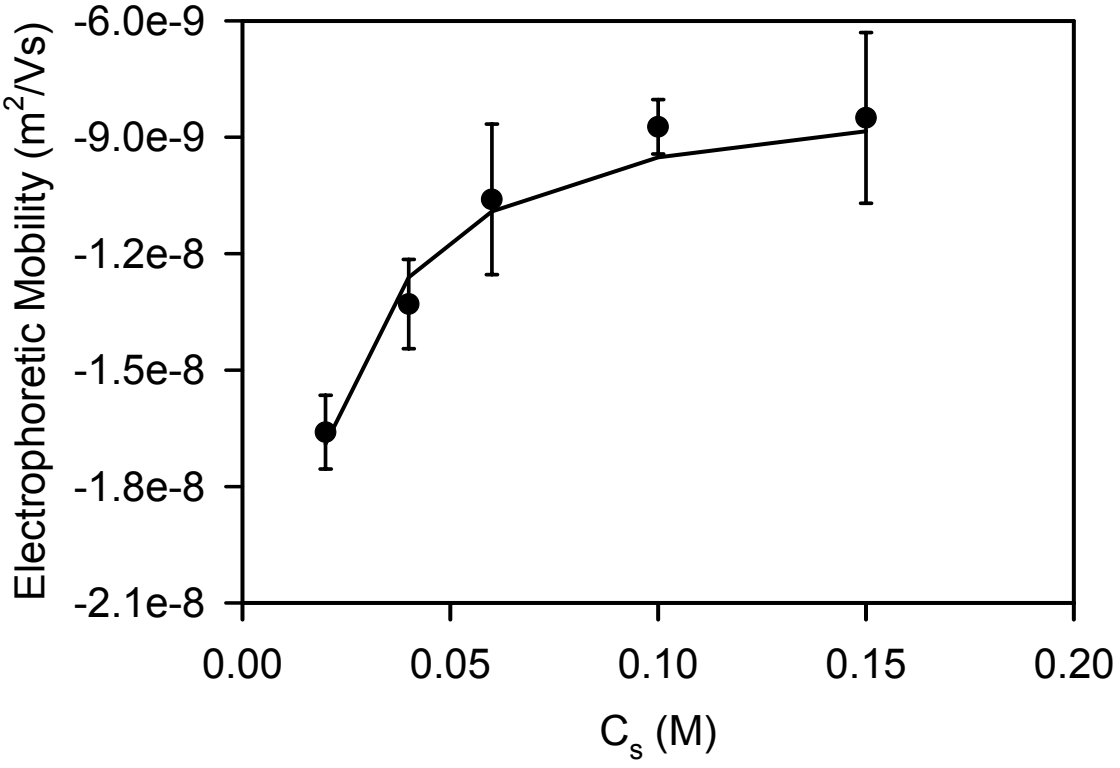
-6.0e-9
-9.0e-9
-1.2e-8
-1.5e-8
-1.8e-8
-2.1e-8
Electrophoretic Mobility (m²/Vs)
0.00
0.05
0.10
0.15
0.20
Cs (M)

Figure 4.1

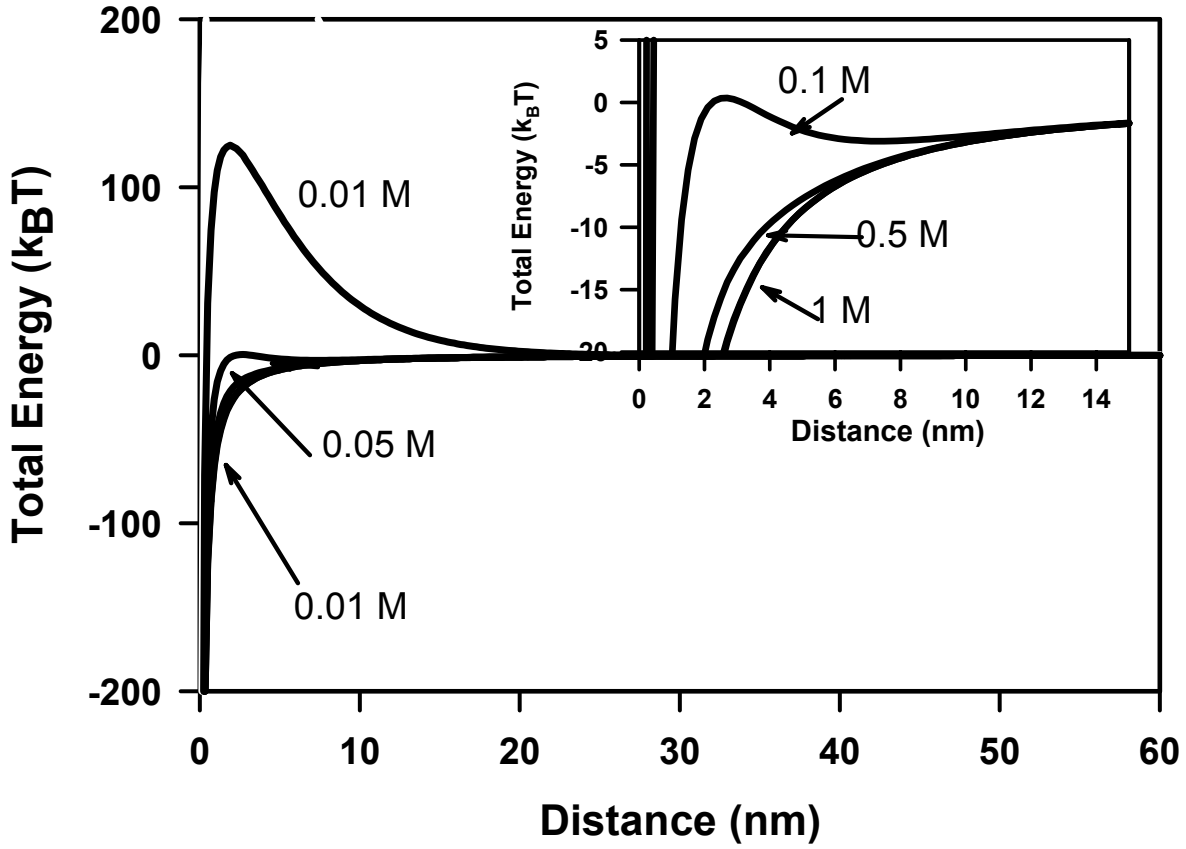
Total Energy (k_BT)
Distance (nm)
0.01 M
0.05 M
0.01 M
0.1 M
0.5 M
1 M
Total Energy (k_BT)
Distance (nm)

Figure 4.2

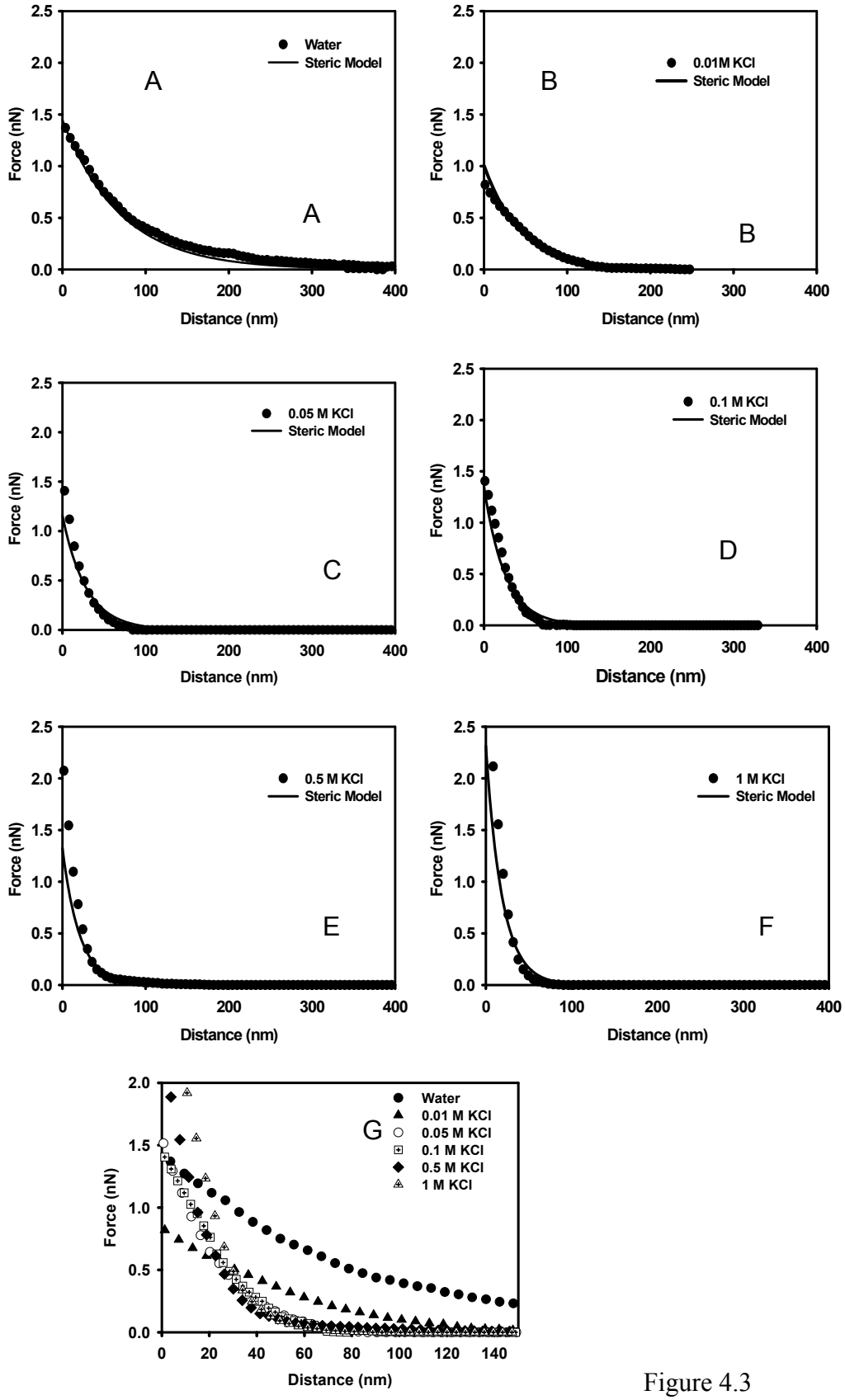
A
Water
Steric Model
B
0.01M KCl
Steric Model
C
0.05 M KCl
Steric Model
D
0.1 M KCl
Steric Model
E
0.5 M KCl
Steric Model
F
1 M KCl
Steric Model
G
Water
0.01 M KCl
0.05 M KCl
0.1 M KCl
0.5 M KCl
1 M KCl
Force (nN)
Distance (nm)

Figure 4.3

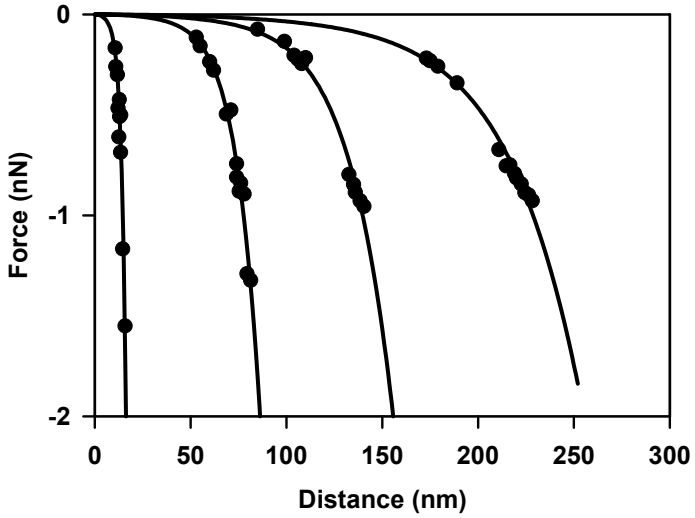

A

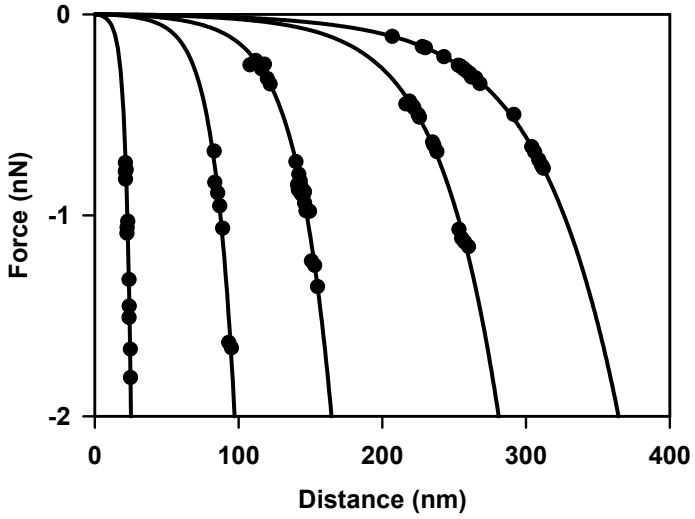

B

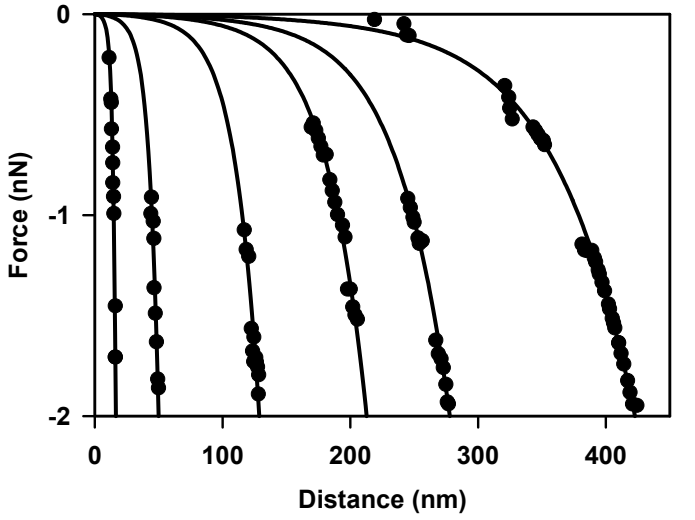

C

Figure 4.4

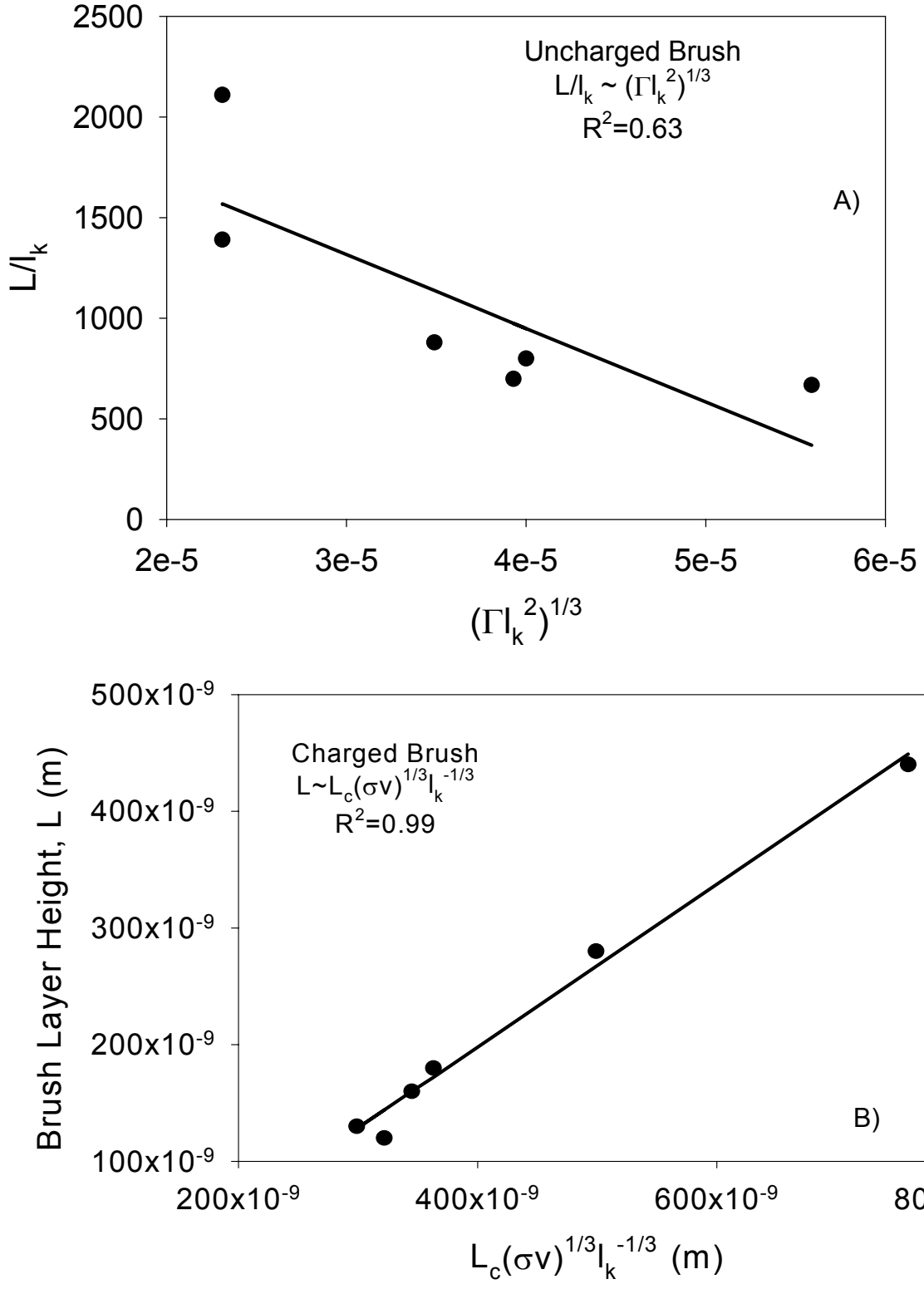
Uncharged Brush
$L/l_k \sim (\Gamma l_k^2)^{1/3}$
R^2=0.63
A)
L/l_k
$(\Gamma l_k^2)^{1/3}$
2500
2000
1500
1000
500
0
2e-5
3e-5
4e-5
5e-5
6e-5
Charged Brush
$L \sim L_c(\sigma v)^{1/3} l_k^{-1/3}$
R^2=0.99
B)
Brush Layer Height, L (m)
$L_c(\sigma v)^{1/3} l_k^{-1/3}$ (m)
500x10^{-9}
400x10^{-9}
300x10^{-9}
200x10^{-9}
100x10^{-9}
200x10^{-9}
400x10^{-9}
600x10^{-9}
800x10^{-9}

Figure 4.5

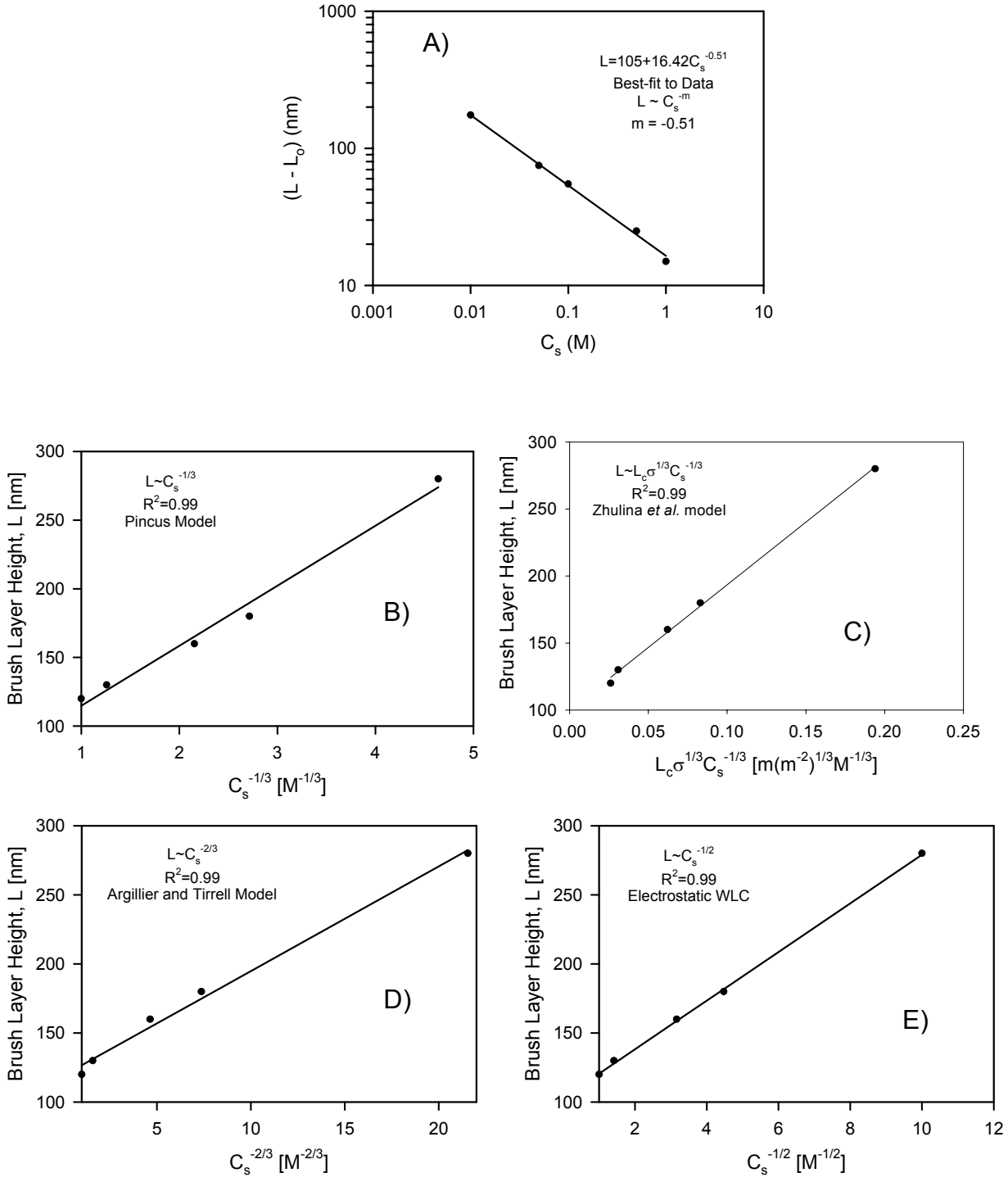
A)
L=105+16.42C_s^-0.51
Best-fit to Data
L ~ C_s^-m
m = -0.51
(L - L_o) (nm)
C_s (M)
B)
L~C_s^-1/3
R^2=0.99
Pincus Model
Brush Layer Height, L [nm]
C_s^-1/3 [M^-1/3]
C)
L~L_cσ^1/3C_s^-1/3
R^2=0.99
Zhulina et al. model
L_cσ^1/3C_s^-1/3 [m(m^-2)^1/3M^-1/3]
D)
L~C_s^-2/3
R^2=0.99
Argillier and Tirrell Model
C_s^-2/3 [M^-2/3]
E)
L~C_s^-1/2
R^2=0.99
Electrostatic WLC
C_s^-1/2 [M^-1/2]

Figure 4.6

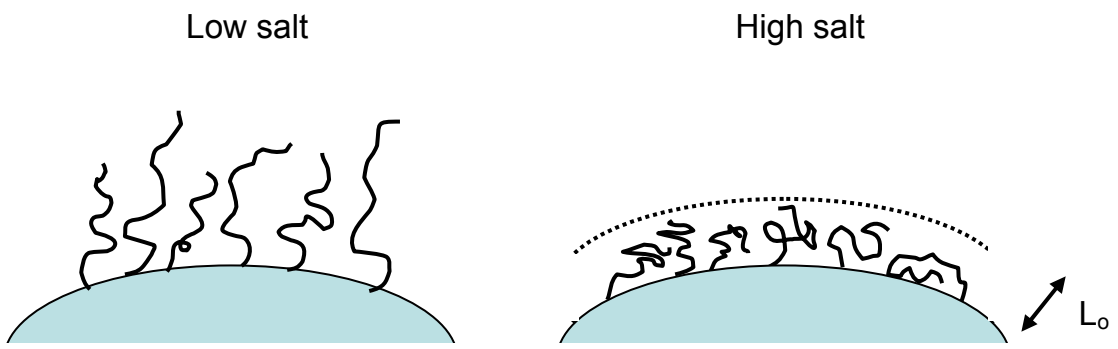

Figure 4.7

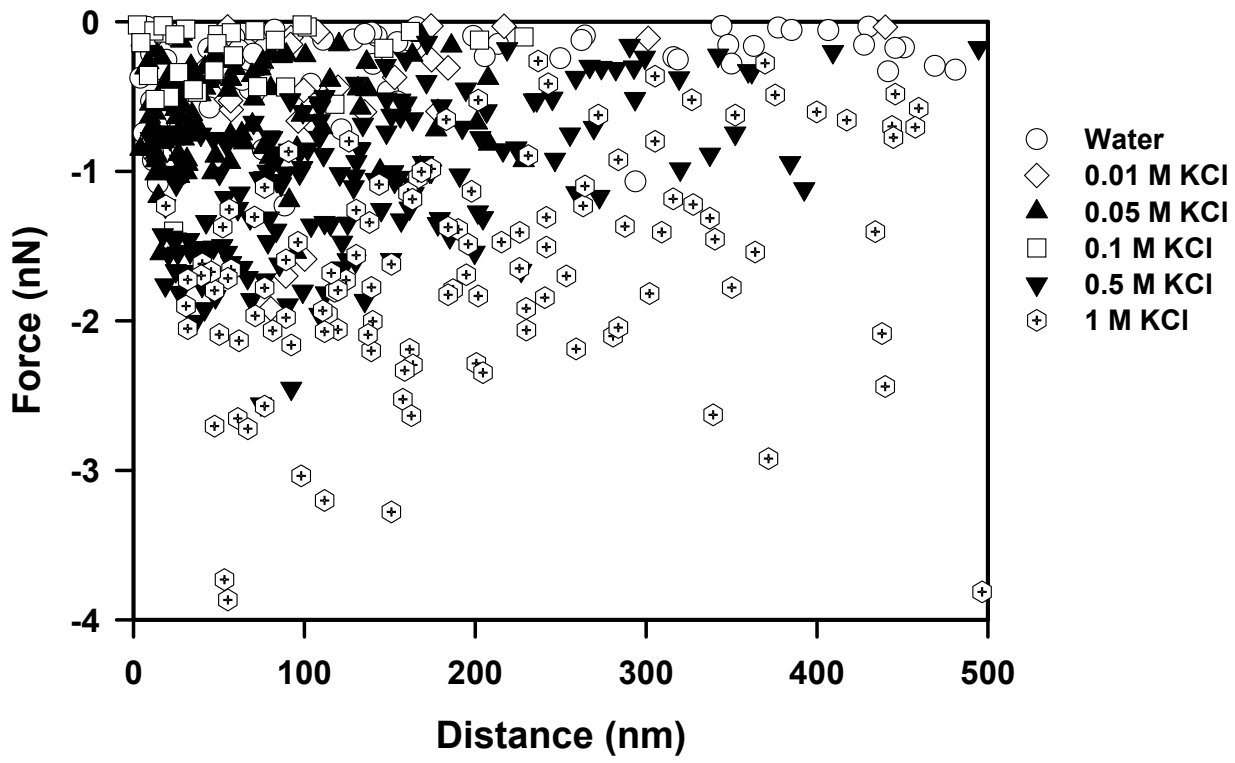
0
-1
-2
-3
-4
Force (nN)
0
100
200
300
400
500
Distance (nm)
Water
0.01 M KCl
0.05 M KCl
0.1 M KCl
0.5 M KCl
1 M KCl

Figure 4.8

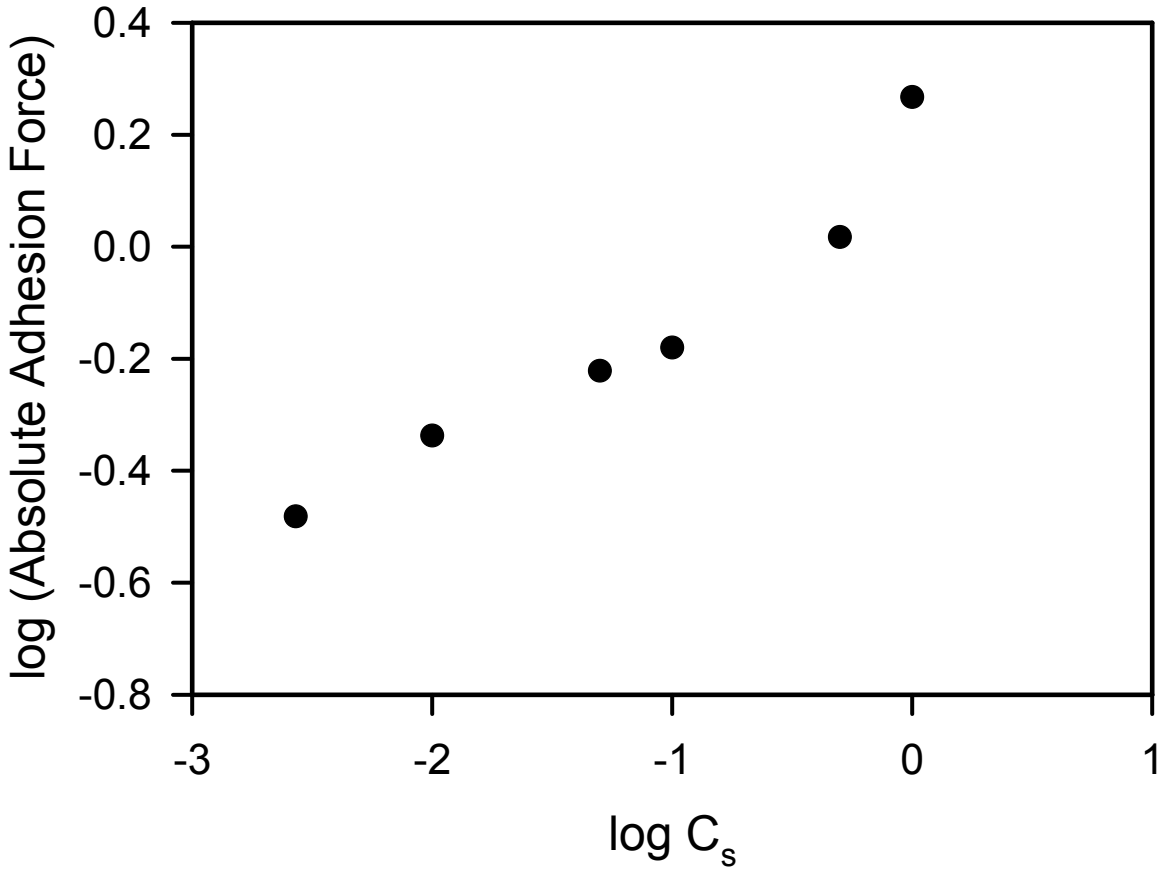

Figure 4.9

Chapter Five

The Role of Lipopolysaccharides in the Adhesion, Retention, and Transport of *Escherichia coli* JM109

Abstract

The role of lipopolysaccharides (LPS) in bacterial adhesion was investigated via atomic force microscopy (AFM). Adhesion between a silicon nitride tip and *Escherichia coli* JM109 was measured in water and phosphate buffered saline (PBS) on untreated cells and on a sample of *E. coli* treated with 100 mM ethylenediaminetetraacetic acid (EDTA), which removes ~ 80% of the LPS molecules. LPS removal decreased the adhesion affinity between the bacterial cells and the AFM tip from -2.1 ± 1.8 nN to -0.40 ± 0.36 nN in water, and from -0.74 ± 0.44 nN to -0.46 ± 0.23 nN in 0.01 M PBS (statistically different, Mann-Whitney rank sum test, $P<0.01$). The distributions of adhesion affinities between *E. coli* LPS macromolecules and the AFM tip could be described by gamma distribution functions. Direct measurements of the adhesive force between *E. coli* and a surface were compared with adhesion in batch and column experiments, and agreement was observed between the influences of LPS on adhesion in each system. Bacterial batch retention to glass or in packed beds to quartz sand decreased after LPS removal. When interaction forces were measured during the approach of the AFM tip to a bacterium, steric repulsive forces were seen for both treated and untreated cells, but the repulsion was greater when the LPS was intact. A model for steric repulsion predicted a reduction of the equilibrium length of the surface polymers from 242 to 64 nm in water, and from 175 to 81 nm in buffer, after removal of a portion of the LPS. DLVO calculations based on conventional and soft-particle DLVO theories predicted higher energy barriers to adhesion for all surfaces after LPS removal, consistent with experimental findings. Adhesion forces between the AFM tip and

bacterial polymers were correlated with bacterial attachment and retention, while measurements of interaction forces during the approach of the AFM tip to the bacterium did not correlate with subsequent adhesion behavior to glass or quartz sand.

5.1 Introduction

Understanding molecular-scale interactions between bacteria and surfaces is important to environmental phenomena and applications, such as subsurface soil remediation [1-4], microbial dissolution of minerals [5-8], microbial uptake of trace metals [9-11], cell-to-cell transfer of genetic material [12, 13], and the fate of pathogens in the subsurface [14]. As a group, bacteria are well adapted to life on surfaces and may have a selective advantage while attached to surfaces [15]. In fact, adherent bacteria often outnumber unattached bacteria in saturated groundwater zones [16, 17].

Bacterial adhesion to a surface has typically been described as the balance between attractive and repulsive physicochemical interactions. Long-range forces that can act over tens of nanometers, such as London-van der Waals and electrostatic interactions, have long been recognized as influencing bacterial adhesion [18]. However, often only qualitative or inconsistent correlations are observed between bacterial adhesion and the van der Waals and/or electrostatic properties of the substrate [19-23]. Short-range forces include steric interactions, specific ion effects, non-charge transfer Lewis acid base interactions, hydration forces, hydration pressure, and hydrogen bonding and the hydrophobic effect [24, 25]. Only recently have quantitative means of including non-DLVO interactions in colloidal interactions been proposed [26, 27]. Bacterial adhesion may also involve specific interactions between complementary surfaces such as lectin-like interactions mediated by surface polymers [28, 29]. Techniques that average surface properties over a population of cells do not allow for the determination of the influence of localized structures.

Lipopolysaccharides (LPS) and proteins in the outer membrane of Gram-negative bacteria, as well as extracellular polysaccharides for some strains, are the polymers that may

influence adhesion. The surface of *Escherichia coli* JM109 consists of 75% LPS and 25% proteins [30]. LPS molecules are anchored to the cell outer membrane through their lipid moiety. The core region of the LPS consists of negatively charged groups, such as phosphates and carboxylic groups, which usually give the LPS its negative charge [31]. The outer polysaccharide part of the LPS is the O-antigen, which consists of 20-70 repeating units of three to five sugars and can protrude up to 30 or more nanometers into the cell surroundings. For Gram-negative bacteria, the O-antigen is likely responsible for polymer interactions with surfaces. Outer membrane proteins are less likely to interact with the solid surfaces, since they are hidden behind the O-antigen layer [32].

Research with mutant bacterial strains has provided some information on how LPS macromolecules affect adhesion. Williams and Fletcher isolated mutant strains of *Pseudomonas fluorescens* whose O-antigen portion of their LPS was either missing or truncated [33, 34]. Without the O-antigen, the mutants attached more to hydrophobic polystyrene tissue culture dishes and less to hydrophilic polystyrene dishes than did the parent strain. However, the parent and mutant strains were all adhesive to sand, which suggested that multiple types of biopolymers mediate adhesion. In some cases, the presence of LPS can facilitate adhesion through the formation of hydrogen bonds. DLVO-type repulsion may be overcome when surface polymers possessing high affinities for the solid surfaces anchor the cell to a substratum across a repulsive energy barrier. The considerable strength of these short-range interactions leading to an irreversible bacterial adhesion has been suggested to originate from the formation of the hydrogen bonds [35]. In another study, the adsorption of three different O-antigens isolated from bacterial LPS on TiO_2, Al_2O_3, and SiO_2 was investigated [36]. Infrared spectroscopy showed that these three bacterial O-antigens formed hydrogen bonds with TiO_2, Al_2O_3, and SiO_2 surface

hydroxyl groups or interacted with water bound on these surfaces [36]. While many studies suggest the importance of surface polymers in bacterial adhesion, the characteristics of these biopolymers (chemical composition, size, conformation, adhesion affinities) are not well-known, and there is still a lack of understanding of the relationship between polymer properties and adhesion behavior.

Recent advances in analytical techniques allow for the characterization of biopolymers at the nano-Newton and nanometer level. Atomic force microscopy (AFM) was used to probe the adhesive interactions and biopolymer properties of various fungal and bacterial cells [37-43]. By making contact between the microbe and an AFM tip and pulling on the surface macromolecules, the physical properties of the biopolymers (elasticity, conformation) were determined [40, 42, 43]. The chemical nature of microbial surfaces was determined, aided by the use of functionalized AFM probes [37].

In previous work, Ong et al. [44] studied the interactions between lawns of *E. coli* and model surfaces with the use of AFM. The bacterial strains studied were *E. coli* K-12 strain D21 (the parent) and the mutant strain D21f2, which has a truncated LPS. Attractive forces were observed between D21 and mica in 1 mM Tris, while repulsive interactions were seen between the parent strain and mica under the same conditions. The authors concluded that the presence of LPS caused steric repulsion with the mica surface, and that its truncation allowed for an attraction to be observed. Subsequently, Velegol and Logan [45] studied isogenic *E. coli* K-12 strains (D21, D21f2, and JM109) with three different lengths of LPS, and observed no correlation between the length of the LPS and the amount of steric repulsion measured.

When LPS are present, specific and/or short-range interactions may become dominant, as compared with non-specific, long-range interactions (London-van der Waals, electrostatic, steric

interactions). This study addresses the hypothesis that LPS facilitates the attachment of bacteria to negatively-charged, hydrophilic surfaces, such as glass and quartz, even when steric and electrostatic interactions would predict a high repulsive energy barrier to attachment. We measured the adhesion between *E. coli* JM109 and a model surface (silicon nitride tip) using an AFM, and we relate these adhesion measurements to bacterial retention in a batch system (with a glass substrate), and bacterial transport in porous media (quartz sand) under flow conditions. In some experiments, bacterial lipopolysaccharides were partially removed to determine their influence on bacterial adhesion.

5.2 Materials and Methods

5.2.1 Cultures

Escherichia coli JM109 (a K-12 strain) was provided by Professor Kristin N. Wobbe of the Department of Chemistry and Biochemistry at Worcester Polytechnic Institute (Worcester, MA). Cells were grown in Luria broth [5 g NaCl, 5 g tryptone, 2.5 g yeast extract in 1 liter of milli-Q water (Millipore)] at 37 ºC and 200 rpm until the late exponential phase of growth. The cells were harvested when the absorbance at 600 nm reached 0.9.

5.2.2 Removal of Lipopolysaccharides via EDTA Treatment

EDTA was used to remove the lipopolysaccharides (LPS) on the bacterial cells [30, 46-48]. Cells were grown in Luria broth and after reaching late exponential growth phase, the culture and the media were centrifuged at 6000 rpm (1000 x g) for 10 minutes (25°C, DAMON/IEC HT Centrifuge). Cell pellets were washed in deionized water once and resuspended in 100 mM EDTA solution. The solution was re-incubated at 37 ºC for 40 minutes while shaking gently. The solution was re-centrifuged for the same time and speed and the bacterial pellets were washed twice with distilled water. Cellular viability, growth rate, and the

ability to synthesize RNA and proteins are not affected by removal of the LPS via this technique [46]. Upon exposure to a higher concentration of EDTA or for a longer time, it is possible that cell lysis could occur due to rupture of the cell membrane. However, we confirmed that cells were not lysed after EDTA treatment by verifying that their cylindrical shape was retained (from AFM images).

5.2.3 Protein Assay

The total protein content of the *E. coli* JM109 cells and the total amount of protein released during EDTA treatment was measured using the Lowry protein assay [49]. *E. coli* JM109 cells were grown until the late exponential phase of growth, then centrifuged at 1000 x g for 10 minutes. The bacterial pellet was resuspended in DI water. The protein content was measured on the resuspended cells and on the remaining supernatant. Protein standards of bovine serum albumin (Sigma; 10 – 500 ppm solutions) were also assayed. Protein content was measured spectrophotometrically at an absorbance of 660 nm (Thermo Spectronic, Genesys 20). Replicates of each sample and of the standards were tested and averaged. Although both proteins and LPS might be removed during EDTA treatment, each has unique force spectra when probed with AFM. We can verify that the force spectra correspond to LPS, rather than proteins, by examining the shape of these curves and the magnitude of the interaction forces.

5.2.4 Electrophoretic Mobility Measurements

The surface potential of *E. coli* JM109 cells and surface polymers was measured using a zeta potential analyzer (Zeta PALS, BIC). A small portion of surface polymers was removed using the following technique [43]. This technique did not grossly alter the morphology of the cell or disrupt the cell membrane, as indicated by AFM imaging of the cells after polymer removal. The resolution of this imaging is expected to be on the order of a few nm.

The polymers were separated from the bacterial cells by centrifugation for 15 minutes at 1000 x g. After separation, the polymers were freeze-dried and kept in the refrigerator until use [43]. The zeta potential of the extracted polymers was measured by using a 1000 ppm solution of the freeze-dried polymers in 0.1 mM MES buffer (pH=6.7). The zeta potential of late-exponential phase *E. coli* JM109 cells was measured in 0.10 mM MES buffer (pH=6.7) and as a function of ionic strength (0.02, 0.04, 0.06, 0.10, and 0.15 M KCl, pH = 7.0). In all cases, zeta potential measurements were performed three to five times and averaged.

5.2.5 Atomic Force Microscopy Experiments

All AFM experiments were performed with a Dimension 3100 Nanoscope III (Digital Instruments/Veeco) and silicon nitride tips (Digital Instruments/Veeco). The spring constants of the tips were 0.13 ± 0.02 N/m, measured by the Cleveland method [50]. Bacterial cells from solution were fixed to cleaned silanized glass slides by covalent bonding [42, 43, 51]. Cells remained hydrated prior to AFM measurements, and AFM imaging was performed in tapping mode under liquid. Once a bacterial cell had been located and brought to the center of the image, the tapping mode was stopped so that force measurements could be performed. Measurements were made in either water or phosphate buffered saline (PBS).

Force measurements were made on a bacterium-free area of the glass slide before and after making the measurement on a bacterium. Equality of the measurements ensured that the tip was not picking up contamination from the media or sample, and that the tip's properties had not been altered by contact with the sample. Even when using non-contact modes for imaging, care must be taken to ensure that AFM imaging and the collection of force measurements does not introduce artifacts to the sample. Previous work in our lab has shown that the collection of > 100 force measurements in succession on a bacterium does not reveal time dependence in the

measurements. Similarly, imaging the same bacterium over a period of a few hours does not suggest that the cell is changing during the time course of the experiments.

Data were captured during both the "approach" and "retraction" of the AFM tip with the bacterial samples. For each bacterial cell, 7-20 measurements were made (always over the center of the cell), and 5-7 cells were examined for a given treatment. The approach curves could be averaged, while the retraction curves had to be considered individually due to the complex interaction between bacterial surface polymers and the AFM tip after contact.

5.2.6 Modeling of Approach Curves with a Steric Model: Determination of Polymer Brush Thickness

A model developed for grafted polymers at relatively high surface coverage was used to model steric interactions between the AFM tip and cell surface polymers. The force per unit area between two surfaces, $F_{St,}$ only one of which is coated with polymer, has been modeled following the work of Alexander [52] and de Gennes [53]. This model was modified by Butt et al. [54] to describe the forces between a spherical AFM tip and a flat surface by integrating the force per unit area over the tip surface, to produce the interaction force

$$F_{St} = 50 k_B T a L_o \Gamma^{3/2} e^{-2\pi h/Lo} \quad (5.1)$$

where k_B is the Boltzmann constant, T is temperature, a the tip radius, Γ the grafted polymer density (m^{-2}), h the distance between the two surfaces, and L_o the equilibrium thickness of the polymer layer, referred to as the polymer brush. For these calculations, the tip radius was assumed constant at 250 nm. This estimate was based on previous work, which demonstrated that while the nominal radius of these tips is smaller, they interact as spheres with radii between 100 and 400 nm [55, 56].

5.2.7 Classical DLVO Theory Calculations of Interaction Energies

Derjaguin-Landau-Verwey-Overbeek (DLVO) interaction energy profiles between the bacterium and either silicon nitride or sand were calculated. Bacterium/AFM tip interactions were treated using flat plate-sphere geometry, with the bacterium as the plate and the tip as a sphere. Bacterium/sand or Bacterium/glass interactions were also treated with flat plate-sphere geometry, but in this case the sand collector or glass slide was treated as the flat plate and the bacterium was modeled as a sphere. The total DLVO interaction energy (E_t) between bacteria and the sand particles is calculated as the sum of London-van der Waals and electrostatic interactions [57] .

$$E_t = E_e + E_v \tag{5.2}$$

Where E_e is the electrostatic energy and E_v is the interaction energy due to London-van der Waals forces. The electrostatic interactions are calculated using the linearized version of the Poisson-Boltzmann expression.

$$E_e = \pi\varepsilon_o\varepsilon a\left(2\psi_1\psi_2\, ln\left(\frac{1+exp(-\kappa h)}{1-exp(-\kappa h)}\right) + \left(\psi_1^2+\psi_2^2\right) ln\left[1-exp(-2\kappa h)\right]\right) \tag{5.3}$$

where ε_o is the permittivitty of vacuum, ε the relative dielectric permittivity of water, a the radius of the sphere (either the silicon nitride tip or the bacterium, depending on the system), ψ_1 the surface potential of the sphere, ψ_2 the surface potential of the flat plate, κ the inverse Debye screening length, and h the separation distance between the sphere and the plane. This expression is valid in 1:1 electrolytes, for potentials less than 60 mV [57], and assuming that both surface potentials were kept constant during their approach.

The van der Waals interaction energy was calculated using the retarded Hamaker expression [58]. An approximation suggested by Gregory [59] was used, which is in excellent agreement with the full expression at short separations (up to 20% of the particle radius).

$$E_V = -\frac{Aa}{6h(1 + 14\ h\ /\ \lambda_c)} \tag{5.4}$$

Where A is the Hamaker constant for the interacting media and λ_c is the "characteristic wavelength" of the interaction, often assumed to be 100 nm.

The potentials for the quartz sand, silicon nitride, and glass were taken as their zeta potentials (ζ) estimated using the Smoluchowski formula.

$$\mu = \varepsilon_o \varepsilon \zeta / \eta \tag{5.5}$$

where η is the viscosity of the medium. Zeta potentials from the literature for quartz sand, glass, and silicon nitride were taken to be -16 mV [60], -29 mV [61], and -16 mV [62], respectively (measurements in 0.01 M KCl for sand and silicon nitride, 0.01 M KNO_3 for glass, all at pH =7.0).

5.2.8 Soft Particle DLVO Theory

Recent work has suggested that for soft particles, such as bacteria, the zeta potential is not an accurate measure of potential [61, 63, 64]. Therefore, soft particle DLVO theory was used to evaluate the electrostatic interactions between *E. coli* JM109 and either sand or silicon nitride. This theory assumes the presence of an ion-penetrable, charged polyelectrolyte layer around a rigid core[65]. Since the outer bacterial membrane is composed of lipopolysaccharides, proteins, and phospholipids[66], the surface has a non-uniform distribution of charge. The approximate mobility formula for soft particles[67-71] is expressed as:

$$\mu = \frac{\varepsilon_o \varepsilon}{\eta} \frac{\Psi_o / K_m + \Psi_{DON} / \lambda}{1/K_m + 1/\lambda} + \frac{eZN}{\eta \lambda^2} \tag{5.6}$$

Where Ψ_o is the surface zeta potential, K_m the Debye-Hückel parameter for the polymer layer, Ψ_{DON} the Donnan Potential of the polymer layer, Z the valance of the charged groups in the polymers, e the electron charge, N the density of the charged groups, and λ the softness parameter, which has dimensions of reciprocal length. The parameters K_m, Ψ_o, and Ψ_{DON} are all functions of ionic strength [65].

$$\Psi_o = \frac{K_B T}{ze}\left(ln\left\{\frac{ZN}{2zn} + \left[\left(\frac{ZN}{2zn}\right)^2 + 1\right]^{1/2}\right\} + \frac{2zn}{ZN}\left\{1 - \left[\left(\frac{ZN}{2zn}\right)^2 + 1\right]^{1/2}\right\}\right) \quad (5.7)$$

$$K_m = \kappa \left[1 + \left(\frac{ZN}{2\,zn} \right)^2 \right]^{1/4} \quad (5.8)$$

$$\kappa = \left(\frac{1}{\varepsilon_0 \varepsilon_r K_B T} \sum_{i=1}^{N} z_i^2 e^2 n_i^{\infty}\right)^{1/2} \quad (5.9)$$

$$\Psi_{DON} = \frac{K_B T}{ze} ln\left\{\frac{ZN}{2zn} + \left[\left(\frac{ZN}{2zn}\right)^2 + 1\right]^{1/2}\right\} \quad (5.10)$$

Where z is the valence of bulk ions, n the concentration of bulk ions, and the parameter ZN represents spatial charge density in the polyelectrolyte region and the term $1/\lambda$ characterizes the softness of the bacterial surface.

For calculations of energy barriers using soft particle DLVO theory, the cell surface potentials were estimated at pH 7.0 in 0.02 M KCl (eq. 5.7) using ZN values obtained from fitting eq. 6 to a plot of zeta potential as a function of ionic strength. Energy barrier calculations for classical DLVO theory used the Smoluchowski eq. (eq. 5.5) to estimate values of the cell surface potentials. The zeta potentials available in the literature for the substrates were available only in 0.01 M solution, while the bacterial potentials were measured in 0.02 M and higher ionic strength solutions. To account for this discrepancy, a sensitivity analysis was made to show the

effect of the silicon nitride surface potential on the predicted energy profiles. The zeta potential of silicon nitride was allowed to vary between -10 and -60 mV.

5.2.9 Modeling of Retraction Curves: Statistical Distributions of Adhesion Affinities

The adhesion affinities between the AFM tip and bacterial polymers (pull-off forces) were distributed over a wide range due to the heterogeneous nature of the macromolecules. Normal and gamma probability distribution functions were applied to the adhesion affinity data.

The normal distribution is a continuous function whose x values range between $-\infty$ and ∞. The normal distribution of the adhesion force (F) is described by:

$$f(F) = \frac{1}{\sqrt{2\pi\sigma^2}} exp\left(\frac{-(F-\overline{F})^2}{2\sigma^2}\right) \tag{5.11}$$

Where F is the pull-off or adhesion force, $\overline{F}$ is the average force value, and σ^2 is the variance of the force distribution.

The second distribution used was the gamma distribution. It is a density function described by two parameters, c and b, which are functions of the average and the standard deviation. The density function is described by:

$$f(F) = \frac{F^{c} exp\left(-\frac{c}{b}F\right)}{\gamma(c+1)\left(\frac{b}{c}\right)^{(c+1)}} \tag{5.12}$$

Where $\gamma(c+1)$ is the gamma function of $(c+1)$. The parameter b describes the mode size, while the parameter c determines whether the distribution is wide or narrow. Large values of c give narrow distributions [72, 73].

5.2.10 Batch Retention Assays

For the untreated cells, bacterial solutions grown to exponential phase were diluted to 5.8 x 10^6 cells/ml and resuspended in water or 0.01 M PBS (after being centrifuged at 1000 x g for 15 minutes). A second batch of cells was treated with EDTA as described above, diluted to 7.7 x 10^6 cells/ml and resuspended in water or 0.01 M PBS. Aqueous-phase cell counts were obtained by staining a 1 mL sample of bacterial solution with 100 μl of 0.1 % acridine orange solution, and viewing on a 0.2 μm black filter [Nucleopore[74]]. Filters were observed using epifluorescence microscopy. At least 10 grid areas were counted and the resulting cell counts were averaged.

For the batch retention assays, glass slides were used as the substrate. Glass slides were cleaned by soaking in 3:1 (volume ratio) HCl (36.5 %–38 %, EM Science)/HNO_3 (68 % – 70 %, VWR) solution for 25 minutes followed by copious rinsing in deionized water. This step was followed by soaking glass slides in 4:1 (volume ratio) H_2SO_4 (96.1 %, Fisher)/H_2O_2 (30%, VWR) solution for 25 minutes and rinsing with deionized water. The reactor consisted of a 200 mL beaker containing 20 mL of bacterial solution. A glass slide was immersed into the bacterial solution and removed after 4 hours. The slides were gently rinsed with water or PBS to remove loosely attached cells. Acridine orange stain was applied and the bacterial cells retained on the glass slide were enumerated using epifluorescence microscopy (100X). Typically, 10-30 fields were counted and the number of cells that had attached per mm^2 of the glass slide was calculated.

5.2.11 Bacterial Transport in Porous Media

The porous medium in these studies was quartz sand (Sigma) with a diameter of 327 ± 40 μm determined by image analysis of 50 particles. The sand was cleaned to remove any residual fine particles that could interfere with measuring the bacterial concentration, or that could clog the column tubing. Several grams of sand were placed in a large flask containing

0.01 M PBS. The container was shaken multiple times and the liquid decanted and replaced until the turbidity was < 0.01 NTU. After soaking overnight in buffer, the shaking/decanting procedure was repeated the next day until the turbidity dropped to < 0.005 NTU.

The columns were packed wet with quartz sand (column diameter = 1.0 cm, length = 15 cm). Packed columns were acclimated to either buffer solution or water for ten pore volumes (one PV ≅ 4.5 ml) using a peristaltic pump (Vera Manostat/Barnant). Bacterial solutions in water or buffer were introduced at an approach velocity of 26 m/day for 10 PV, followed by a 10 PV rinse with the suspending phase. The concentration of bacteria injected into the column was between 0.80 and 1.30 x 10^8 cells/ml. Samples of acridine-orange stained bacterial cells were examined via fluorescence microscopy before the column experiments, to verify that aggregation of cells in the influent solution had not occurred. Separate column experiments were run using the untreated bacterial cells, or cells that had been treated with EDTA to remove the LPS. The column effluent was sampled continuously using a fraction collector (Spectra/Chrom CF-1). The absorbance of the samples was measured spectrophotometrically at a wavelength of 600 nm. While replicate column experiments were not performed, this type of bacterial transport experiment in a laboratory-scale column has been previously shown to yield reproducible results, with maximum differences between individual columns < 5%. [75].

The steady-state breakthrough concentration of the bacterial cells was used to estimate the collision efficiency (α) for each experiment. The collision efficiency is the fraction of striking bacteria that attach to the collector surfaces. The one-dimensional colloid filtration equation developed by Yao et al. [76] was used to calculate α, as

$$\alpha = \frac{-2d_c \, ln(C/C_o)}{3(1-\theta)\eta_c L} \tag{5.13}$$

where C and C_o are the effluent and influent bacterial concentrations, respectively, θ is the porosity of the media, and d_c is the collector diameter. In the Rajagopalan and Tien model for the collector efficiency, η_c is taken as the sum of the physical forces affecting collisions: diffusion, effects of neighboring particles, London-van der Waals forces, interception, and gravitational settling [77, 78].

5.3 Results

5.3.1 AFM Adhesion Measurements—Effect of LPS on Adhesion. EDTA treatment on average resulted in lower adhesion between the silicon nitride tip and the biopolymers than for the system without treatment (Figure 5.1). The treatment also changed the nature of the cell surface by decreasing the length of the LPS. This decrease was manifested through the pull-off or rupture distance, which is the distance at which the polymer breaks free from the tip. The pull-off distances give an indication of the length of the polymers, although the actual lengths could be longer or shorter, depending on the location of attachment of the chain to the AFM tip, and whether the chain is sufficiently elastic that the molecules stretch beyond their contour length when exposed to external force. Untreated cells sometimes showed very large pull-off distances that may have corresponded to individual macromolecules, or may have reflected multiple chains entangled or attached to one another. Partial removal of LPS decreased the rupture lengths to < 100 nm for 98% of chains in water and 88% of chains in the buffer solution. The rupture lengths are shorter in buffer than water because polyelectrolytes can take on a more coiled conformation in the presence of salt. Although there is scatter in the data due to the heterogeneity of the sample, EDTA treatment resulted in a significant decrease in both the adhesion forces and rupture lengths for *E. coli*. This was confirmed by statistical tests (Mann-Whitney rank sum test, $P<0.01$).

For untreated (i.e. intact) *E. coli*, the adhesion forces and the distances at which pull-off occurred were similar in water and PBS. The average adhesive interaction was higher in water than in the buffer (-2.1 ± 1.8 nN compared to –0.74 ± 0.44 nN for water and buffer, respectively; statistically different, Mann-Whitney rank sum test, $P<0.01$), but this was probably skewed by a few very high adhesion affinities measured in water (> 3 nN), which were observed in only 6% of the adhesion events. Pull-off distances were similar in both solvents (144.2 ± 95.5 nm compared to 158.9 ± 130.5 nm for water and buffer, respectively). After LPS removal, adhesion in water and buffer were similar (-0.40 ± 0.36 nN and -0.46 ± 0.23 nN in water and buffer, respectively) and the pull-off distances were short, generally less than 100 nm (29.6 ± 25.9 nm and 59.4 ± 60.1 nm for water and buffer, respectively).

The zeta potential of the LPS macromolecules was similar to the charge of the cell suspension ($\zeta_{isolated\ LPS}$ = -31.7 ± 0.88 mV, $\zeta_{cell\ suspension}$ = -34.49 ± 1.19 mV. Despite the negative charge of the extracted LPS, an electrostatic effect on the adhesion affinity was not observed. This may have been because a narrow range of ionic strengths was tested.

5.3.2 Distribution of Adhesion Affinities

A distribution of adhesion affinities between the AFM tip and the biopolymers was observed in both water and buffer (Figure 5.2). Several statistical models were tested for their ability to describe this distribution. The normal and gamma distributions each could describe the distributions, but the coefficient of correlation (R^2) values were always higher for the gamma distribution (Figure 5.2) and the case of treated bacteria in water could not be described well by the normal distribution. Previous studies of bacterial heterogeneity within a single population suggested that there may be a bimodal distribution in bacterial adhesion or in properties of the

biopolymers [79-81]. However, examination of the histograms in Figure 5.2 did not suggest any bimodal relationship, and so this model was not pursued further.

5.3.3 Steric Interactions

The presence of LPS caused steric repulsion between the bacterium and the tip. Repulsive forces between the bacterial surfaces and the AFM tip (during the approach of the tip to the bacterium) were lower after LPS removal (Figure 5.3). While repulsion was observed in all cases, the cells that were treated with EDTA showed significantly less repulsion with the AFM tip (Mann-Whitney rank sum test, $P<0.01$). This effect was quantified with a model accounting for steric interactions (eq. 5.1) [52-54]. According to the model, the equilibrium length of the polymer brush layer was reduced from 242 to 64 nm in water and from 175 to 81 nm in PBS upon removal of LPS (Table 5.1, Figure 5.3). Partial removal of LPS decreased but did not fully eliminate repulsive steric interactions. The polymer brush layer is larger than previous estimates of LPS (30-50 nm) [79]. Previous work with electron microscopy may not have been sensitive enough to accurately measure the polymer lengths. It is also possible that we sometimes probe an entanglement of more than one molecule.

5.3.4 Energy Calculations using DLVO Theory

5.3.4.1 Zeta Potential and Soft-particle Potential of *E. coli* JM109. The electrophoretic mobilities as a function of ionic strength for untreated and EDTA-treated *E. coli* JM109 are shown in Figures 4A and B. The electrophoretic mobility measurements converged to a non-zero value, consistent with soft-particle behavior [61]. Calculated $1/\lambda$ values of 1.04 and 0.91 nm were found for untreated and EDTA-treated cells, consistent with what others have reported. Wild-type *E. coli* has a reported $1/\lambda$ value of 0.62 nm [68], while $1/\lambda$ values for different strains of *Pseudomonas syringae* ranged between 1.5 – 3.84 nm [82]. The spatial

charge density (*ZN*) was calculated to be -0.075 and -0.087 M, for cells with and without EDTA treatment, respectively, and compared well with literature values (-0.092 M for wild-type *E. coli*) [68]. A comparison of the potentials from conventional theory (in which the zeta potential is taken as the surface potential) with that from the soft-particle calculations showed that conventional theory always predicted higher surface potentials for the bacteria (Table 5.2).

5.3.4.2 Interaction Energies between *E. coli* JM109 and Sand. DLVO interaction energy barriers between bacteria and sand were calculated using eqs. 5.2-5.7 (Figures 5.5A and B). The energy barriers were greater using the hard sphere potential as the surface potential compared to soft-particle theory (Table 5.3). Predicted energy barriers were higher for the EDTA-treated *E. coli* JM109 cells because the potentials were slightly more negative. A similar calculation was made for the interactions between bacteria and glass, and this information is available in the supplementary information in the appendix at the end of the thesis.

5.3.4.3 Interaction Energies between *E. coli* JM109 and Silicon Nitride. DLVO interaction energies between bacteria and silicon nitride were calculated (Figures 5.5C and D). The energy barriers were higher using the zeta potential as the surface potential, compared to the soft-particle analysis (Table 5.3). The energy barriers were higher for EDTA-treated cells than for intact cells.

Since there were slight differences between our experiments and the conditions where we could find zeta potentials for silicon nitride reported in the literature, we also made a sensitivity analysis of the effect of tip surface potential on the resulting energy profile. Experimental interaction force data was converted to energy and compared with the soft-particle DLVO simulations for the interaction energies between *E. coli* JM109 and silicon nitride. Allowing the

potential of the tip to vary between -0.01 and -0.06 V still did not bring the simulation close to the experimental data (Figure 5.6). Experimentally-observed interaction energies showed much higher barriers, and the energy extended over a longer distance than could be predicted by DLVO theory. If we had used the zeta potential instead of the soft-particle potential, we still could not have matched the experimental data, as was shown previously [51].

5.3.5 Batch Retention Experiments

The number of cells adhering to glass slides was 1334 ± 304 cells/mm^2 in water and 1410 ± 429 cells/mm^2 in PBS. In both solutions, removal of LPS reduced the retention of *E. coli* to almost half the values for the untreated cells. The number of bacterial cells adhered to the glass slides decreased to 671 ± 153 and 848 ± 398 in water and buffer, respectively. In these experiments, > 30 fields were counted per slide, with each field containing 20-40 bacterial cells. This technique has been shown to give reproducible results [74]. The ionic strength of the suspending phase did not affect the retention in a batch system within experimental variation. This may have been because a wide enough range of ionic strengths was not tested. If the LPS are highly charged, then the concentration of ions in the polymer brush layer is high compared to the ion concentration in the bulk solution. The ionic strength would have to be increased much higher in order for the ions in solution to balance the ions in the brush layer. A similar effect is seen in the study of the conformation of polyelectrolytes [83-85].

5.3.6 Column Transport Experiments

The breakthrough curves indicated that nearly steady-state transport conditions were present in the columns (Figure 5.7). Since steady-state breakthrough concentrations were reached, we used the average C/C_o values to estimate collision efficiencies (eq. 5.13). Bacteria attached less to quartz sand after removal of their LPS, in both water and PBS (Table 5.4). In

water, α decreased from 0.23 to 0.12, while in buffer a decrease in α from 0.16 to 0.07 was observed after LPS removal. The normalized concentrations from the steady-state portions of the breakthrough curves, with and without EDTA-treatment, were compared using the Mann Whitney Rank Sum test, and the results indicated that the treatment was significant ($P<0.001$).

5.4 Discussion

5.4.1 Effect of EDTA Treatment on Cell Surface Macromolecules. The surface structure of *E. coli* JM109 has been well characterized by prior research, which showed that the surface contains 75% LPS and 25 % proteins [30]. The outer membrane of the cell acts as a selective permeable membrane that can protect the cell from drugs, detergents, toxins, or other agents [30].

Treatment with EDTA causes an almost complete extraction of divalent metal ions such as Ca^{+2} and Mg^{+2} from their binding sites within the outer membrane. This depletion weakens the bonds holding LPS and proteins in the membranes, subsequently causing the release of a significant portion of the LPS and proteins from the membrane. Although EDTA treatment increases outer membrane permeability, the use of this procedure on *E. coli* caused little or no injury to the viability, growth rate, or normal rates of RNA and protein synthesis [46].

From the AFM approach curves and use of the steric model, we estimated the amount of cellular material lost during the EDTA treatment. Total amount of polymer was considered to be proportional to the brush layer thickness L_0 times the polymer density Γ. Treatment with EDTA removed ~ 80% of total polymer, in either water or buffer. This treatment should have removed 30-50% of LPS and 80% of cell surface proteins [46-48]. However, our measurement of the amount of protein released from the cells using the Lowry assay showed that slightly less (62.8% ± 1.2% of the cell membrane proteins) were removed. The treatment removed both LPS and

proteinaceous material. Although we did not do an analysis on released material to determine what fraction of it was protein vs. LPS, the ability to distinguish between polysaccharides and proteins from force spectra allows us to be sure that the AFM tip contacted mainly LPS during the SMFS experiments. The characteristic force spectra of proteins differ notably from those of polysaccharides. Proteins are usually globular in shape and unfold when stretched, leading to a regular "sawtooth" pattern in the retraction curves [86, 87]. The forces required to unfold proteins are in the pN range [86-89], about an order of magnitude lower than the forces we measured.

Another consideration with respect to the EDTA treatment is whether the flagella were affected. Microscopic examination revealed that this microbe is motile [90]. Since the EDTA treatment can also remove proteins, flagella may have been disturbed. Although not quantified, bacterial cells were observed under a microscope with and without EDTA treatment. For the treated population of cells, there was a mixture of motile and non-motile bacteria, while the untreated population showed no non-motile cells. Therefore the reduction in motility is another factor which could have affected the bacterial retention and transport results.

5.4.2 Role of Electrostatic Interactions Controlling the Attachment of *E. coli* to Silicon Nitride, Glass, and Quartz Sand

Electrostatic interactions affect how difficult it is to bring like-charged objects together. In the AFM approach curves, the repulsion was higher for the *E. coli* cells in water than buffer, which would be expected for a system of like-charged colloids (Figure 5.3). However, electrostatic interactions did not control the subsequent adhesion forces or the retention of the bacteria. No effect of ionic strength was observed on the adhesion forces measured with AFM, batch retention results, or the attachment of bacteria to quartz sand (Figure 5.7; Table 5.4).

While electrostatic interactions influence the ability to bring the bacteria into contact with the surface, AFM retraction experiments measure the forces required to break the bond already formed between the polymer and the tip. Contact between bacteria and the surfaces could be made in the batch and column studies, through a combination of hydrodynamics, cellular motility, and bridging of polymer macromolecules. After contact, short-range or specific chemical interactions were strong enough to make the adhesion irreversible.

The calculated energy barrier to adhesion based on DLVO theory was higher for EDTA-treated cells than for untreated cells (Figure 5.5, Table 5.3), suggesting that the attachment of bacteria to the AFM silicon nitride tip is more difficult after partial removal of LPS, which apparently exposed more negative charges. This prediction does not agree with the trend from the AFM approach curves, which show higher repulsion for the untreated cells (Figure 5.3). Electrostatic interactions did not control the observed AFM approach curves. Furthermore, the application of either hard-particle (zeta potential as surface potential) or soft-particle forms of DLVO theory could not fit the experimentally measured approach curves. In all cases, experimentally measured forces were of a higher magnitude and decayed more slowly than the predictions from either form of DLVO theory. These discrepancies are attributed to steric interactions, which are much greater in magnitude and can mask the underlying electrostatic interactions [51].

5.4.3 Role of Steric Interactions Produced by Lipopolysaccharides in Bacterial Adhesion

Bacterial surface polymers have often been implicated in bacterial adhesion and attachment studies [24, 33, 42-45, 51, 91-93]. Despite the importance of polysaccharides and/or lipopolysaccharides in influencing adhesion and the fact that these macromolecules lead to steric

repulsion, the presence of steric interactions did not prevent the attachment of bacteria to glass and quartz sand surfaces. Despite the large steric repulsive energy barriers we observed during AFM force measurements, high retention and adhesion occurred. After contact between the bacterium and AFM tip was made, the adhesive forces holding the two together were often strong (0.05 – 4 nN in water, 0.05 – 2 nN in 0.01 M PBS).

Removal of some portion of the LPS resulted in less steric repulsion. While steric interactions affect the approach of a bacterium to a surface, they are not important in influencing whether the bacteria attach irreversibly to the surface. In the AFM experiments, contact between the bacterium (or bacterial surface macromolecules) and a surface is forced to occur through the motion of the AFM tip. After contact, bacteria with intact LPS showed a greater affinity for the surface than bacterial cells that were deficient in LPS.

5.4.4 Interpreting Bacterial Heterogeneity in Adhesion Forces

The LPS on *E. coli* JM109 exhibited a distribution of adhesion affinities for the AFM tip that were well described by statistical distribution functions. The distribution of attachment efficiencies was closest to a gamma distribution. A log-normal or power-law distribution could not model the shape of the distribution.

The distribution of adhesion affinities that we observed for *E. coli* JM109 (which does not produce capsular material) is different than that of *P. putida* KT2442, a bacterium producing multiple extracellular polysaccharides (i.e. chemically distinct macromolecules) [42, 43]. The adhesion affinities between extracellular polysaccharides of *P. putida* KT2442 and an AFM tip could not be described by a normal or gamma distribution (unpublished data) because there were at least three distinct sugar groups present on the surface of the microbe in addition to the membrane-bound LPS, providing a more complicated surface chemistry [94]. The distribution in

the adhesion affinities for *E. coli* JM109 is due to the intrinsic variability of the LPS and to the way the AFM probes these macromolecules. For polysaccharides, we may at some times probe the linear backbone and at other times probe branched side-chains with the tip, and each part of the macromolecule may have a different adhesion affinity for the surface.

5.4.5 Relating Biopolymer Properties to Bacterial Transport

Previously, the collision efficiency in bacterial transport experiments was related to the maximum height of the DLVO-predicted energy barrier for *E. coli* and other bacteria [61]. For *E. coli* IFO-3301, the critical height of the energy barrier below which spontaneous adhesion could occur was 34 k_BT based on soft-particle theory, or 105 k_BT based on conventional analysis. In the present study, we found similar maximum energy barriers and also found that the energy barriers were lower in DLVO calculations using the soft-particle analysis compared to using the zeta potential as the surface potential.

The maximum heights of the energy barriers were related to bacterial transport. Bacterial transport was quantified in terms of the one-dimensional filtration model [76-78], using the deposition coefficient ($k_d = \alpha\lambda_f u$; where α is the collision efficiency, λ_f is the filtration coefficient, and u is the pore velocity). After treatment with EDTA, the deposition coefficients of *E . coli* JM109 decreased from 9.8×10^{-4} to 5.1×10^{-4} s^{-1} in water, and from 6.0×10^{-4} to 2.4×10^{-4} s^{-1} in PBS. This treatment corresponded to an increase in the energy barrier (calculated according to soft-particle DLVO theory) from 49 to 69 k_BT (Table 5.3).

In addition to the transport mechanisms governing the movement of inert colloids (diffusion, interception, and gravitational settling), this strain of *E. coli* is subject to additional forces because it is motile. When bulk fluid flow is not a variable, bacterial attachment to a surface is aided by motility and/or the presence of flagella. For example, the formation of

biofilms of *E. coli* on abiotic surfaces was much less for mutant cells in which the mutation affected flagellar function [95]. By performing experiments at different temperatures, Vatanyoopaisarn et al. showed that the flagella, independent of cellular motility, act to increase adhesion of *Listeria monocytogenes* to stainless steel surfaces [96]. In the batch assays, the reduced adhesion of treated cells was likely due to a combination of loss of motility and loss of LPS.

The loss of motility is less likely to have affected the attachment of the bacterium to sand in the column assays. Several studies have addressed the role of motility on bacterial attachment to glass, sand, or other surfaces under flow. Most studies have shown that motility does not affect the transport of bacteria in soil packed columns, or that motility only plays a role at certain flow velocities. Camper et al. and Korber et al. each found that the attachment rates of motile vs. non-motile *Pseudomonas fluorescens* to sand (in packed-column experiments) were the same [97, 98]. McLaine and Ford showed that the rotation of the flagella on motile *E. coli* species increased cellular attachment to glass at high fluid velocities [68], but the motile and non-motile mutant strain had similar attachment at low fluid velocities. Increased retention to soil in packed column studies was seen for motile *P. fluorescens* P17, compared to a non-motile form, but this effect was also only observed at high fluid velocities. Strain-to-strain differences make it difficult to be more conclusive about the role of motility on the transport of *E. coli* JM109, although this would be an interesting topic for further study.

In summary, our results demonstrate indicate that LPS facilitates adhesion of *E. coli* to negatively-charged surfaces such as silicon nitride, glass, and quartz sand. While AFM force spectra can provide useful information on the magnitude and nature of the interactions between bacterial surfaces macromolecules and substrata, some caution must be applied in interpretation

of the data. Namely, the approach curves often exhibit large degrees of steric and/or electrostatic repulsion that cannot be used to predict whether bacteria will attach to or be retained on a surface when surface polymers are mediating adhesion. These results underscore the need for further study of specific chemical interactions such as hydrodynamic interactions and short-range interactions between bacterial surface macromolecules and substrata surfaces, which will ultimately lead to a better understanding of bacterial adhesion and to more sophisticated models for predicting the distribution of microorganisms in the subsurface.

5.5 Acknowledgments

The authors thank Prof. Bob Thompson, Prof. John Bergendahl and Mr. Ray Emerson for their comments on an earlier version of the manuscript, and Ms. Megan Lindberg for assistance with the batch assays. We also thank the four anonymous reviewers for their helpful suggestions in improving this manuscript.

5.6 References

1. Caccavo, F.J., Das, A., *Adhesion of dissimilatory Fe(III)-reducing bacteria to Fe(III) minerals.* Geomicrobiology Journal, 2002. **19**: p. 161-177.
2. Munakata-Marr, J., McCarty, P.L., Shields, M.S., Reagin, M., Francesconi, S.C., *Enhancement of trichloroethylene degradation in aquifer microcosms bioaugmented with wild type and genetically altered Burkholderia (Pseudomonas) cepacia G4 and PR1.* Environmental Science & Technology, 1996. **30**: p. 2045-2052.
3. Dong, H., Rothmel, R., Onstott, T.C., Fuller, M.E., DeFlaun, M.F., Streger, S.H., Dunlap, R., Fletcher, M., *Simultaneous transport of two bacterial strains in intact cores from Oyster, Virginia: biological effects and numerical modeling.* Applied and Environmental Microbiology, 2002. **68**: p. 2120-2132.
4. Zhang, P., Johnson, W.P., Scheibe, T.D., Choi, K.-H., Dobbs, F.C., Mailloux, B.J., *Extended tailing of bacteria following breakthrough at the Narrow Channel focus area, Oyster, Virginia.* Water Resources Research, 2001. **37**: p. 2687-2698.
5. Hersman, L., Lloyd, T. Sposito, G., *Siderophore-promoted dissolution of hematite.* Geochimica et Cosmochimica Acta, 1996. **59**: p. 3327-3330.
6. Grantham, M.C., Dove, P.M., DiChristina, T.J., *Microbially catalyzed dissolution of iron and aluminum oxyhydroxide mineral surface coatings.* Geochimica et Cosmochimica Acta, 1997. **61**: p. 4467-4477.
7. Lovley, D.R., Phillips, E.J.P., *Organic matter mineralization with reduction of ferric iron in anaerobic sediments.* Applied and Environmental Microbiology, 1986. **51**: p. 683-689.

8. Maurice, P.A., Vierkorn, M.A., Hersman, L.E., Fulghum, J.E., Ferryman, A., *Enhancement of kaolinite dissolution by an aerobic Pseudomonas mendocina bacterium.* Geomicrobiology Journal, 2001. **18**: p. 21-35.

9. Brantley, S.L., Liermann, L, Bau, M., Wu, S., *Uptake of trace metals and rare earth elements from hornblende by a soil bacterium.* Geomicrobiology Journal, 2001. **18**: p. 37-61.

10. Fein, J.B., Daughney, C.J., Yee, N., Davis, T., *A chemical equilibrium model for metal adsorption onto bacterial surfaces.* Geochimica et Cosmochimica Acta, 1997. **61**: p. 3319-3328.

11. Grantham, M.C., Dove, P.M., *Investigation of bacterial-mineral interactions using fluid tapping mode atomic force microscopy.* Geochimica et Cosmochimica Acta, 1996. **60**: p. 2473-2480.

12. Holben, W.E., *Isolation and purification of bacterial community DNA from environmental samples*, in *Manual of Environmental Microbiology*, C.J. Hurst, Editor. 1997, American Society for Microbiology: Washington, D.C. p. 431-436.

13. Trevors, J.T., van Elsas, J.D., *Quantification of gene transfer in soil and the rhizosphere*, in *Manual of Environmental Microbiology*, C.J. Hurst, Editor. 1997, American Society for Microbiology: Washington, D.C. p. 500-508.

14. Jiang, X., Morgan, J., Doyle, M.P., *Fate of Escherichia coli O157:H7 in manure-amended soil.* Applied and Environmental Microbiology, 2002. **68**: p. 2605-2609.

15. Marshall, K.K., *Planktonic versus sessile life of procaryotes*, in *The Prokaryotes: A Handbook on the Biology of Bacteria: Ecophysiology, Isolation, Identification,*

Applications, A. Balows, Truper, H.G., Dworkin, W., Harder, W., Schleifer, K.-H., Editor. 1992, Springer-Verlag: New York, NY. p. 262-275.

16. Kolbel-Boelke, J., Anders, E.-M., Nehrkorn, A., *Microbial communities in the saturated groundwater environment. II. Diversity of bacterial communities in a Pleistocene sand aquifer and their in vitro activities.* Microbial Ecology, 1988. **16**: p. 31-48.
17. Harvey, R.W., Smith, R.L., George, L., *Effect of organic contamination upon microbial distributions and heterotrophic uptake in a Cape Cod, Mass., aquifer.* Applied and Environmental Microbiology, 1984. **48**: p. 1197-1202.
18. Marshall, K.C., Stout, R., Mitchell, R., *Mechanism of the initial events in the sorption of marine bacteria to surfaces.* Journal of General Microbiology, 1971. **68**: p. 337-348.
19. van Loosdrecht, M.C.M., Lyklema, J., Norde, W., Schraa, G., Zehnder, A.J.B., *Electrophoretic mobility and hydrophobicity as a measure to predict the initial steps of bacterial adhesion.* Applied and Environmental Microbiology, 1987. **53**: p. 1898-1901.
20. van Loosdrecht, M.C.M., Lyklema, J., Norde, W., Schraa, G., Zehnder, A.J.B., *The role of bacterial cell wall hydrophobicity in adhesion.* Applied and Environmental Microbiology, 1987. **53**: p. 1893-1897.
21. van Loosdrecht, M.C.M., J. Lyklema, W. Norde, and A.J.B. Zehnder, *Bacterial adhesion: A physicochemical approach.* Microbial Ecology, 1989. **17**: p. 1-5.
22. McEldowney, S., Fletcher, M., *Effect of growth conditions and surface characteristics of aquatic bacteria on their attachment to solid surfaces.* Journal of General Microbiology, 1986. **132**: p. 513-523.

23. Vigeant, M.A.S., Ford, R.M., *Interactions between motile Eschericia coli and glass in media with various ionic strengths, as observed with a three-dimensional-tracking microscope.* Applied and Environmental Microbiology, 1997. **63**: p. 2474-3479.

24. Rijnaarts, H.H.M., Norde, W., Lyklema, J., and A.J.B. Zehnder, *The isoelectric point of bacteria as an indicator for the presence of cell surface polymers that inhibit adhesion.* Colloids and Surfaces B: Biointerfaces, 1995. **4**: p. 191-197.

25. Israelachvili, J.N., *Intermolecular & Surface Forces (2nd edition)*. 1992, New York: Academic Press.

26. Grasso, D., Subramanian, K., Butkus, M., Strevett, K.A., Bergendahl, J., *A review of non-DLVO interactions in environmental colloidal systems.* Re/Views in Environmental Science & Bio/Technology, 2002. **1**: p. 17-38.

27. Boström, M., Williams, D.R.M., Ninham, B.W., *Specific ion effects: Why DLVO theory fails for biology and colloid systems.* Physical Review Letters, 2001. **87**: p. 168103-1 - 168103-4.

28. Bassler, B.L., *How bacteria talk to each other: regulation of gene expression by quorum sensing.* Current Opinion in Microbiology, 1999. **2**: p. 582-587.

29. Winnans, S.C., *Command, control and communication in bacterial pathogenesis.* Trends in Microbiology, 1998. **6**: p. 382-383.

30. Amro, N.A., Kotra, L.P., Wadu-Mesthridge, K., Bulychev, A., Mobashery, S., Liu, G., *High resolution imaging atomic force microscopy studies of Escherichia coli outer membrane: Structural basis for permeability.* Langmuir, 2000. **16**: p. 2789-2796.

31. Wicken, A.J., Knox, K.W., *Bacterial surface amphiphiles.* Biochimica et Biophysica Acta, 1980. **604**(1): p. 1-26.

32. Makin, S.A., Beveridge, T.J., *The influence of A-band and B-band lipopolysaccharide on the surface characteristics and adhesion of Pseudomonas aeruginosa to surfaces.* Microbiology, 1996. **142**: p. 299-307.

33. Williams, V., Fletcher, M., *Pseudomonas fluorescens adhesion and transport through porous media are affected by lipopolysaccharide compostion.* Applied and Environmental Microbiology, 1996. **62**: p. 100-104.

34. Pringle, J.H., Fletcher, M., *Influence of substratum wettability on the attachment of freshwater bacteria to solid surfaces.* Applied and Environmental Microbiology, 1983. **45**: p. 818-825.

35. van Oss, C.J., Good, R.J., Chaudhury, M.K., *The role of van der Waals forces and hydrogen bonds in "hydrophobic interactions" between biopolymer and low energy surfaces.* Journal of Colloid and Interface Science, 1986. **111**(2): p. 378-390.

36. Jucker, B.A., H. Harms, S.J. Hug, and A.J.B. Zehnder, *Adsorption of bacterial surface polysaccharides on mineral oxides is mediated by hydrogen bonds.* Colloids and Surfaces B-Biointerfaces, 1997. **9**(6): p. 331-343.

37. Dufrêne, Y.F., *Direct characterization of the physicochemical properties of fungal spores using functionalized AFM probes.* Biophysical Journal, 2000. **78**: p. 3286-3291.

38. Dufrêne, Y.F., Boonaert, C.J.P., van der Mei, H.C., Busscher, H.J., and P.G. Rouxhet, *Probing molecular interactions and mechanical properties of microbial cell surfaces by atomic force microscopy.* Ultramicroscopy, 2001. **86**: p. 113-120.

39. Dufrêne, Y.F., *Application of atomic force microscopy to microbiological surfaces: from reconstituted cell surface layers to living cells (Review).* Micron, 2001. **32**: p. 152-165.

40. Van der Aa, B.C., Michel, R.M., Asther, M, Zamora, M.T., Rouxhet, P.G., and Y.F. Dûfrene, *Stretching cell surface macromolecules by atomic force microscopy.* Langmuir, 2001. **17**: p. 3116-3119.

41. Boonaert, C.J.P., Rouxhet, P.G., and Y.F. Dufrêne, *Surface properties of microbial cells probed at the nanometer scale with atomic force microscopy.* Surface and Interface Analysis, 2000. **30**: p. 32-35.

42. Abu-Lail, N.I., Camesano, T.A., *Elasticity of Pseudomonas putida KT2442 biopolymers probed with single-molecule force microscopy.* Langmuir, 2002. **18**: p. 4071-4081.

43. Camesano, T.A., Abu-Lail, N.I., *Heterogeneity in bacterial surface polysaccharides, probed on a single-molecule basis.* Biomacromolecules, 2002. **3**: p. 661-667.

44. Ong, Y.-L., Razatos, A., Georgiou, G., Sharma, M.M., *Adhesion forces between E. coli bacteria and biomaterial surfaces.* Langmuir, 1999. **15**: p. 2719-2725.

45. Velegol, S.B., Logan, B.E., *Contributions of bacterial surface polymers, electrostatics, and cell elasticity to the shape of AFM force curves.* Langmuir, 2002. **18**: p. 5256-5262.

46. Leive, L., *Release of lipopolysaccharide by EDTA treatment of E. coli.* Biochemical and Biophysical Research Communications, 1965. **21**: p. 290-296.

47. Leive, L., Shovlin, V.K., Mergenhagen, S.E., *Physical, chemical, and immunological properties of lipopolysaccharide released from Escherichia coli by ethylenediaminetetraacetate.* The Journal of Biological Chemistry, 1968. **243**: p. 6384-6391.

48. Leive, L., *Studies on the permeability change produced in coliform bacteria by ethylenediaminetetraacetate.* The Journal of Biological Chemistry, 1968. **243**: p. 2373-2380.

49. Gerhardt, P., Murray, R.G.E., Wood, W.A., Krieg, N.R. (Eds.), *Methods for General and Molecular Bacteriology*. 1994, Washington, D.C.: American Society for Microbiology.

50. Cleveland, J.P., Manne, S., Bocek, D., Hansma, P.K, *Nondestructive method for determining the spring constant of cantilevers for scanning force microscopy.* Review of Scientific Instruments, 1993. **64**: p. 403-405.

51. Camesano, T.A., Logan, B.E., *Probing bacterial electrosteric interactions using atomic force microscopy.* Environmental Science & Technology, 2000. **34**: p. 3354-3362.

52. Alexander, S., *Adsorption of chain molecules with a polar head a scaling description.* J. Phys. II (Paris), 1977. **38**: p. 983-987.

53. de Gennes, P.G., *Polymers at an interface: A simplified view.* Advances in Colloid and Interface Science, 1987. **27**: p. 189-209.

54. Butt, H.-J., Kappl, M., Mueller, H., Raiteri, R., *Steric forces measured with the atomic force microscope at various temperatures.* Langmuir, 1999. **15**: p. 2559-2565.

55. Drummond, C.J., Senden, T.J., *Examination of the geometry of long-range tip-sample interaction in atomic force microscopy.* Colloids and Surfaces A: Physicochemical and Engineering Aspects, 1994. **87**: p. 217-234.

56. Senden, T.J., Drummond, C.J., *Surface chemistry and tip-sample interactions in atomic force microscopy.* Colloids and Surfaces A: Physicochemical and Engineering Aspects, 1994. **94**: p. 29-51.

57. Hogg, R., Healy, T.W., Fuerstenau, D.W., *Mutual coagulation of colloidal dispersions.* Transactions of the Faraday Society, 1966. **62**: p. 1638-1651.

58. Hamaker, H.C., Physica, 1973. **4**: p. 1058.

59. Gregory, J., *Approximate expressions for retarded van der Waals interaction.* Journal of Colloid and Interface Science, 1981. **83**: p. 138-145.

60. Johnson, P.R., *A comparison of streaming and microelectrophoresis methods for obtaining the zeta potential of granular porous media surfaces.* Journal of Colloid and Interface Science, 1999. **209**(1): p. 264-267.

61. Hayashi, H., Tsuneda, S., Hirata, A., Sasaki, H., *Soft particle analysis of bacterial cells and its interpretation of cell adhesion behaviors in terms of DLVO theory.* Colloids Surf. B: Biointerfaces, 2001. **22**: p. 149-157.

62. Zhmud, B.V., Sonnefeld, J., Bergstrom, L., *Influence of chemical pretreatment on the surface properties of silicon nitride powder.* Colloids and Surfaces A: Physicochemical and Engineering Aspects, 1999. **158**: p. 327-341.

63. Ohshima, H.K., *Approximate analytical expression for the electrophoretic mobility of colloidal particles with surface-charge layers.* Journal of Colloid and Interface Science, 1989. **130**: p. 281-282.

64. Bos, R., van der Mei, H.C., Busscher, H.J., *"Soft-particle" analysis of the electrophoretic mobility of a fibrillated and non-fibrillated oral streptococcal strain: Streptococcus salivarius.* Biophysical Chemistry, 1998. **74**(3): p. 251-255.

65. Hayashi, H.T., S.; Hirata, A.; Sasaki, H., Colloids and Surfaces B: Biointerfaces, 2001. **22**: p. 149.

66. Fletcher, M., in *Bacterial adhesion: ecological and applied microbiology*. 1996, John Wiley & Sons, Inc.: New-York.

67. Ohshima, H.K., T, Journal of Colloid and Interface Science, 1989. **130**: p. 281.

68. McLaine, J.W., Ford, R.M., *Reversal of flagellar rotation is important in initial attachment of Escherichia coli to glass in a dynamic system with high- and low-ionic strength buffers.* Applied and Environmental Microbiology, 2002. **68**: p. 1280-1289.

69. Takashima, S.M., Colloids and Surfaces B: Biointerfaces, 1997. **9**: p. 205.

70. Bos, R.v.d.M., H.C.; Busscher, H.J., Biophysical Chemistry, 1998. **74**: p. 251.

71. Morisaki, H.N., S.; Ohshima, H.; Ikemoto, E.; Kogur, K, Microbiology, 1999. **145**: p. 2797.

72. Kelley, T.L., *Fundamentals of Statistics*. 1947, Cambridge: Harvard University Press.

73. Randolph, A.D., Larson, M.A., *Theory of Particulate Processes: Analysis and Techniques of Continous Crystallization*. 2nd Ed. ed. 1988, San Diego: Academic Press.

74. Hobbie, J.E., Daley, R.J., Jasper, S., *Use of nucleopore filters for counting microcosms.* Applied and Environmental Microbiology, 1977. **59**: p. 2746-2749.

75. Lahlou, M.H., H.; Sprinael, D.; Ortega-Calvo, J.-J., Environmental Science & Technology, 2000. **34**: p. 3649.

76. Yao, K.-M., Habibian, M.T., O'Melia, C.R., *Water and waste water filtration: Concepts and applications.* Environmental Science & Technology, 1971. **5**: p. 1105-1112.

77. Logan, B.E., D.G. Jewett, R.G. Arnold, E.J. Bouwer, O'Melia, C.R., *Closure to "Clarification of clean-bed filtration models".* Journal of Environmental Engineering, 1995. **121**: p. 869-873.

78. Rajagopalan, R., Tien, C., *Trajectory analysis of deep-bed filtration with the sphere-in-cell porous media model.* AIChE Journal, 1976. **22**: p. 523-533.

79. Simoni, S.F., Harms, H., Bosma, T.N.P., and A.J.B. Zehnder, *Population heterogeneity affects transport of bacteria through sand columns at low flow rates.* Environmental Science & Technology, 1998. **32**: p. 2100-2105.

80. Baygents, J.C., Glynn, Jr., J. R., Albinger, O., Biesewmeyer, B.K., Ogden, K.L., and Arnold, R.G., *Variation of surface charge density in monoclonal bacterial populations: implications for transport through porous media.* Environmental Science & Technology, 1998. **32**: p. 1596-1603.

81. Bolster, C.H., Mills, A.L., Hornberger, G.M. and J. Herman, *Effect of intra-population heterogeneity on the long distance transport of bacteria.* Ground Water, 2000. **38**: p. 370-375.

82. Takashima, S., Morisaki, H., Colloids and Surfaces B: Biointerfaces, 1997. **9**: p. 205-212.

83. Hariharan, R., C. Biver, J. Mays, and W.B. Russel, *Ionic strength and curvature effects in flat and highly curved polyelectrolyte brushes.* Macromolecules, 1998. **31**(21): p. 7506-7513.

84. Hariharan, R., C. Biver, and W.B. Russel, *Ionic strength effects in polyelectrolyte brushes: The counterion correction.* Macromolecules, 1998. **31**(21): p. 7514-7518.

85. Biver, C., R. Hariharan, J. Mays, and W.B. Russel, *Neutral and charged polymer brushes: A model unifying curvature effects from micelles to flat surfaces.* Macromolecules, 1997. **30**(6): p. 1787-1792.

86. Lee, G.U., Kidwell, D.A., Colton, R.J., *Sensing discrete streptavidin-biotin interactions with atomic force microscopy.* Langmuir, 1994. **10**: p. 354-357.

87. Florin, E.-L., Moy, V.T., Gaub, H.E., *Adhesive forces between individual ligand-receptor pairs.* Science, 1994. **264**: p. 415-417.

88. Oberdörfer, Y., Fuchs, H., Janshoff, A., *Conformational analysis of native fibronectin by means of force spectroscopy.* Langmuir, 2000. **16**(26): p. 9955-9958.

89. Oesterhelt, F., Rief, M., Gaub, H.E., Science, 1995.

90. Vigeant, M.A.S., Personal Communication.

91. Rijnaarts, H.H.M., Norde, W., Bouwer, E.J., Lyklema, J., and A.J.B. Zehnder, *Reversibility and mechanism of bacterial adhesion.* Colloids and Surfaces B: Biointerfaces, 1995. **4**: p. 5-22.

92. Rijnaarts, H.H.M., W. Norde, E.J. Bouwer, J. Lyklema, A.J.B. Zehnder, *Bacterial deposition in porous media related to the clean bed collision efficiency and to substratum blocking by attached cells.* Environmental Science & Technology, 1996. **30**: p. 2869-2876.

93. Rijnaarts, H.H.M., Norde, W., Lyklema, J., and A.J.B. Zehnder, *DLVO and steric contributions to bacterial deposition in media of different ionic strengths.* Colloids and Surfaces B: Biointerfaces, 1999. **14**: p. 179-185.

94. Winter, W., Personal Communication.

95. Pratt, L.A., Kolter, R., *Genetic analysis of Escherichia coli biofilm formation: roles of flagella, motility, chemotaxis and type I pili.* Molecular Microbiology, 1998. **30**(2): p. 285-293.

96. Vatanyoopaisarn, S., Nazli, A., Dodd, C.E.R., Rees, C.E.D., Waites, W.M., *Effect of flagella on initial attachment of Listeria monocytogenes to stainless steel.* Applied and Environmental Microbiology, 2000. **66**(2): p. 860-863.

97. Camper, A.K., J.T. Hayes, P.J. Sturman, W.L. Jones, and A.B. Cunningham, *Effects of motility and adsorption rate coefficient on transport of bacteria through saturated porous media.* Applied and Environmental Microbiology, 1993. **59**: p. 3455-3462.

98. Korber, D.R., J.R. Lawrence, Caldwell, D.E., *Effect of motility on surface colonization and reproductive success of Pseudomonas fluorescens in dual-dilution continuous culture and batch culture systems.* Applied and Environmental Microbiology, 1994. **60**: p. 1421-1429.

99. Hamaker, H.C., *The London-van der Waals attraction between spherical particles.* Physica, 1937. **4**: p. 1058-1072.

5.7 Figure Captions

Figure 5.1. Adhesion forces between *E. coli* and silicon nitride after contact has been made between the bacterium and the tip. Each datum represents a single adhesion event. Multiple bacterial cells were probed under each condition. Measurements were made in A) Water and B) PBS.

Figure 5.2. Statistical relationships used to represent distribution of adhesion affinities between AFM tip and bacterial polymers. Solid lines represent Gamma distributions; dashed lines represent Normal distributions. A) Water, untreated bacteria. Normal distribution: $R^2 = 0.78$, Gamma distribution: $R^2 = 0.87$. B) Water, EDTA-treated bacteria. Normal distribution: $R^2 = 0.26$, Gamma distribution, $R^2 = 0.99$. C) 0.01 M PBS, untreated bacteria. Normal distribution: $R^2 = 0.71$, Gamma distribution: $R^2 = 0.94$. D) PBS, EDTA-treated bacteria. Normal distribution: $R^2 = 0.93$, Gamma distribution, $R^2 = 0.96$.

Figure 5.3. A model for steric repulsion was applied to the approach curves for *E. coli* JM109 under several conditions (eq. 5.1) [52-54]. Symbols are experimental data, averaged from ~ 25 individual measurements per condition. Lines are the results from fitting the steric model to the data. The resulting model parameters are shown in Table 1. The supplementary information file contains a Figure demonstrating the reproducibility in the approach curves from cell-to-cell and on a single cell.

Figure 5.4. Electrophoretic mobility measurements of *E. coli* JM109 as a function of ionic strength at a pH of 7.0. The circles represent the average of three experimental measurements and the lines represent the theoretical mobility curve fitted using eq. 6. A) Untreated cells ($R^2 = 0.99$). B) Treated cells ($R^2 = 0.96$).

Figure 5.5. Total interaction energy based on DLVO calculations. Solid lines are calculations based on the Smoluchowski expression for the bacterial potential (eq. 5.5). Dashed lines are calculations based on the soft-particle expression for the surface potential of the bacteria (eq. 5.6). Parameters used in the calculations were: $A = 10^{-20}$ J [99], pH = 7.0, $T = 298$ K, $\zeta_{sand} = -16$ mV [60], $\zeta_{silicon\ nitride} = -16$ mV [62] , $a_{bacterium} = 0.5$ μm, $a_{silicon\ nitride\ tip} = 250$ nm, ionic strength = 0.02 M. A) *E. coli* JM109-sand (sphere-plate), $\zeta_{bacterium,conv.} = -22.9$ mV, $\zeta_{bacterium,soft} = -20.2$ mV. B) Treated *E. coli* JM109-sand (sphere-plate), $\zeta_{bacterium,conv.} = -23.7$ mV, $\zeta_{bacterium,soft} = -22.6$ mV. C) *E. coli* JM109-silicon nitride (plate-sphere), $\zeta_{bacterium,conv.} = -22.9$ mV, $\zeta_{bacterium,soft} = -20.2$ mV. D) Treated *E. coli* JM109-silicon nitride (plate-sphere), $\zeta_{bacterium,conv.} = -23.7$ mV, $\zeta_{bacterium,soft} = -22.6$ mV.

Figure 5.6. The experimentally measured interaction energy for *E. coli* JM109 compared to the energy profiles predicted by soft-particle DLVO calculations. Parameters used in calculating the soft-particle DLVO interaction energies were: $A = 10^{-20}$ J [99] , pH = 7.0, $T = 298$ K, $\zeta_{bacterium,soft} = -20.2$ mV, $\zeta_{silicon\ nitride} = -16$ mV, and ionic strength = 0.02 M. Symbols are experimental data from force measurements that were converted to energy and lines are model predictions. Inset: Sensitivity analysis to demonstrate effect of tip surface potential on the energy profile. $\zeta_{silicon\ nitride}$ was varied (values in the direction of the arrow were -10, -16, -20, -40, and -60 mV). All other parameters were the same as the main figure.

Figure 5.7. Normalized breakthrough curve for the bacterial transport column experiments conducted in 0.01 M PBS, on untreated *E. coli* and *E. coli* treated with EDTA to remove the LPS. Horizontal line shows the steady-state" C/C_o, which was used in eq. 5.13 to calculate α. A similar set of breakthrough curves was obtained in water, which are not shown here, but the average C/C_o values and calculated collision efficiencies are reported in Table 5.4.

Table 5.1. Application of Steric Model to AFM Approach Curves for *E. coli* JM109[a]

Conditions	L_o *(nm)*	Γ (molecules/μm^2)	R^2
Water, untreated *E. coli*	242	3500	0.94
Water, EDTA-treated *E. coli*	64	2800	0.92
PBS, untreated *E. coli*	175	3500	0.99
PBS, EDTA-treated *E. coli*	81	1500	0.85

[a]Eq. 5.1 [52-54] was applied to the approach curves shown in Figure 5.3.

Table 5.2. Evaluation of the Surface Potentials of *E. coli* JM109 using Both Conventional Smoluchowski Theory (Zeta Potential) and Soft-Particle Theory

Ionic Strength (M KCl)	Cell Surface Potential (mV) Untreated		Cell Surface Potential (mV) EDTA-treated	
	Smoluchowski (eq. 5)	Soft-particle (eq. 6)	Smoluchowski (eq. 5)	Soft-particle (eq. 6)
0.02	-22.9	-20.2	-23.7	-22.6
0.04	-17.3	-11.3	-19.2	-12.9
0.06	-14.7	-7.8	-14.9	-9.0
0.10	-13.4	-4.8	-13.3	-5.5
0.15	-12.9	-3.2	-10.8	-3.7

Table 5.3. Summary of E_{max} Values for Calculations of Interaction Energy between *E. coli* and Different Substrates

EDTA treatment	Substrate	E_{max} (k_BT)[a]	E_{max} (k_BT)[b]
No	Sand	72	49
Yes	Sand	79	69
No	Silicon nitride AFM tip	36	24
Yes	Silicon nitride AFM tip	40	35
No	Glass	290	224
Yes	Glass	309	282

[a]Calculated with Smoluchowski expression for zeta potential as the surface potential (eq. 5.5).
[b]Calculated using soft-particle expression for surface potential (eq. 5.6).
All calculations made in water at pH 7, ionic strength = 0.02 M.

Table 5.4. Bacterial Transport Experiments in Quartz Sand Packed Columns

Conditions	Steady-State C/C_o	α
Water, untreated *E. coli*	0.71	0.23
Water, EDTA- treated E. *coli*	0.84	0.12
PBS, untreated *E. coli*	0.75	0.16
PBS, EDTA-treated *E. coli*	0.89	0.07

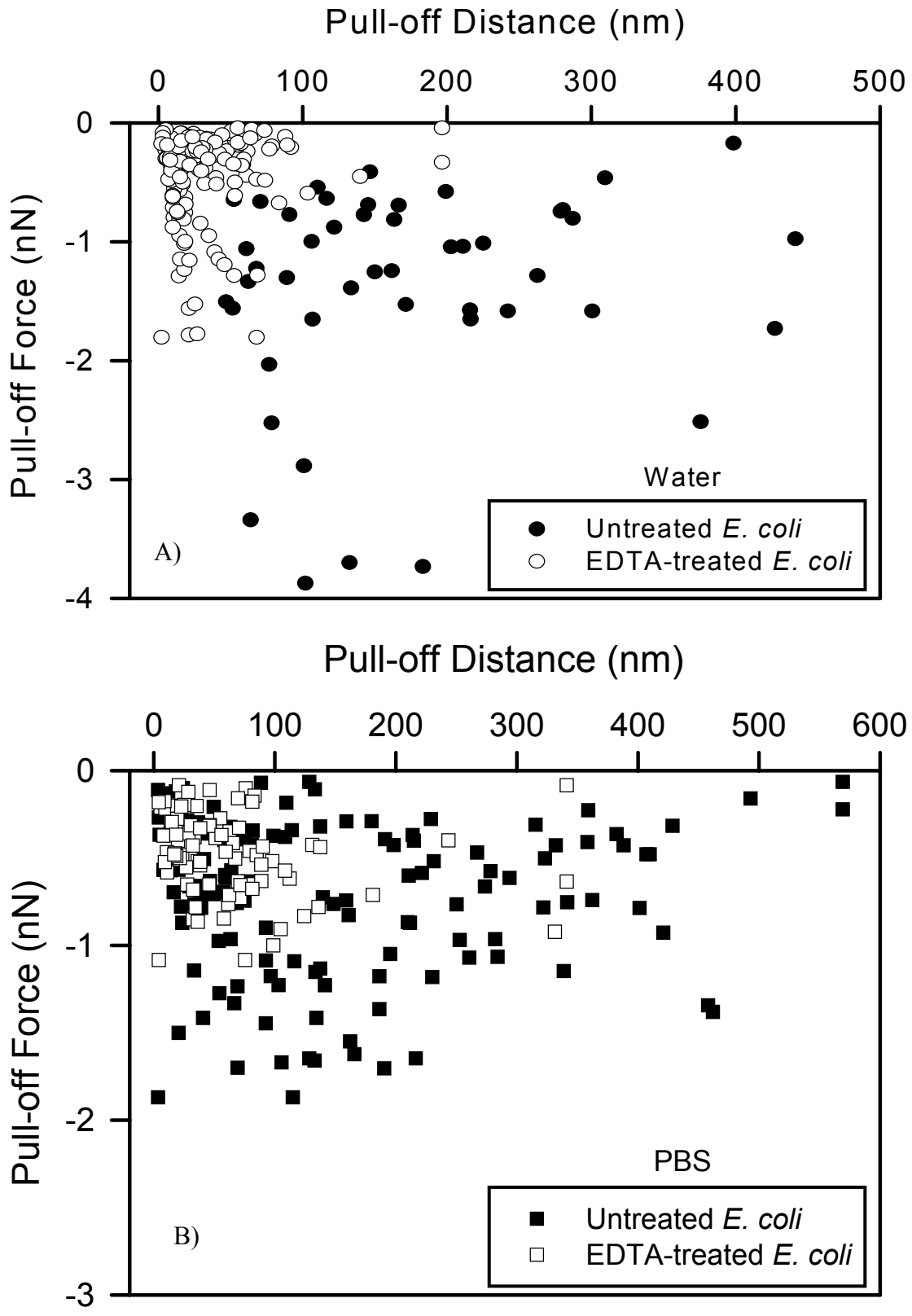
Pull-off Distance (nm)
0
100
200
300
400
500
Pull-off Force (nN)
0
-1
-2
-3
-4
Water
Untreated E. coli
EDTA-treated E. coli
A)
Pull-off Distance (nm)
0
100
200
300
400
500
600
Pull-off Force (nN)
0
-1
-2
-3
PBS
Untreated E. coli
EDTA-treated E. coli
B)

Figure 5.1

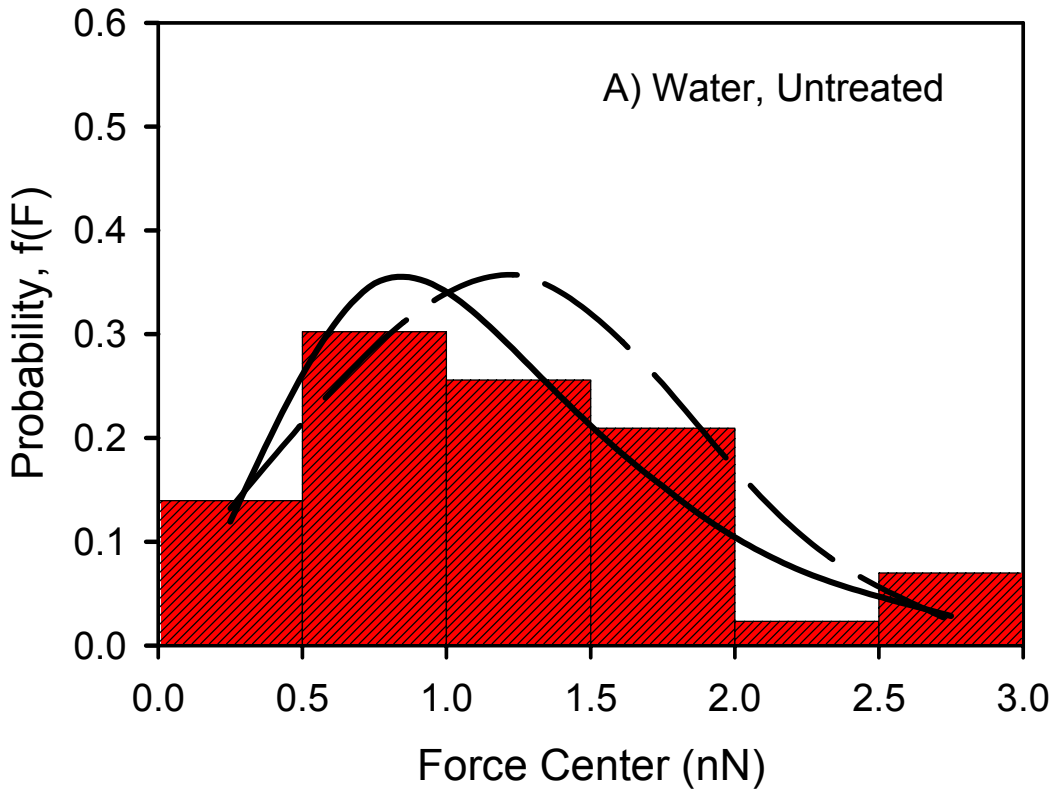
A) Water, Untreated
Probability, f(F)
0.0
0.1
0.2
0.3
0.4
0.5
0.6
0.0
0.5
1.0
1.5
2.0
2.5
3.0
Force Center (nN)

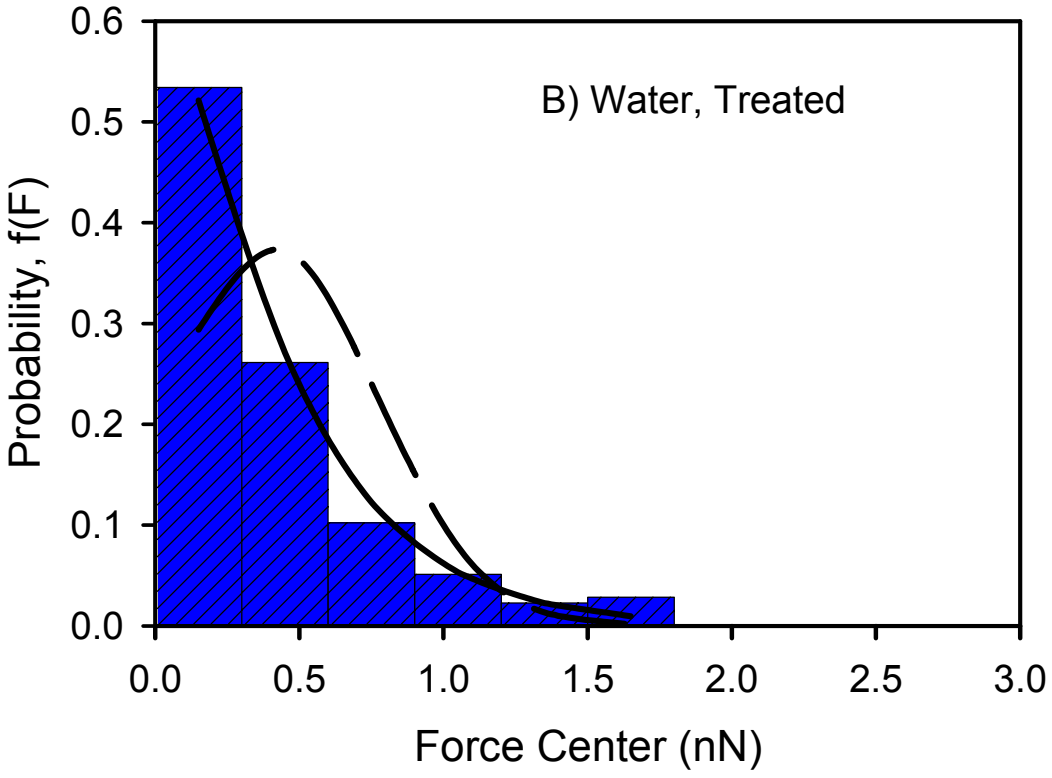
B) Water, Treated
Probability, f(F)
0.0
0.1
0.2
0.3
0.4
0.5
0.6
0.0
0.5
1.0
1.5
2.0
2.5
3.0
Force Center (nN)

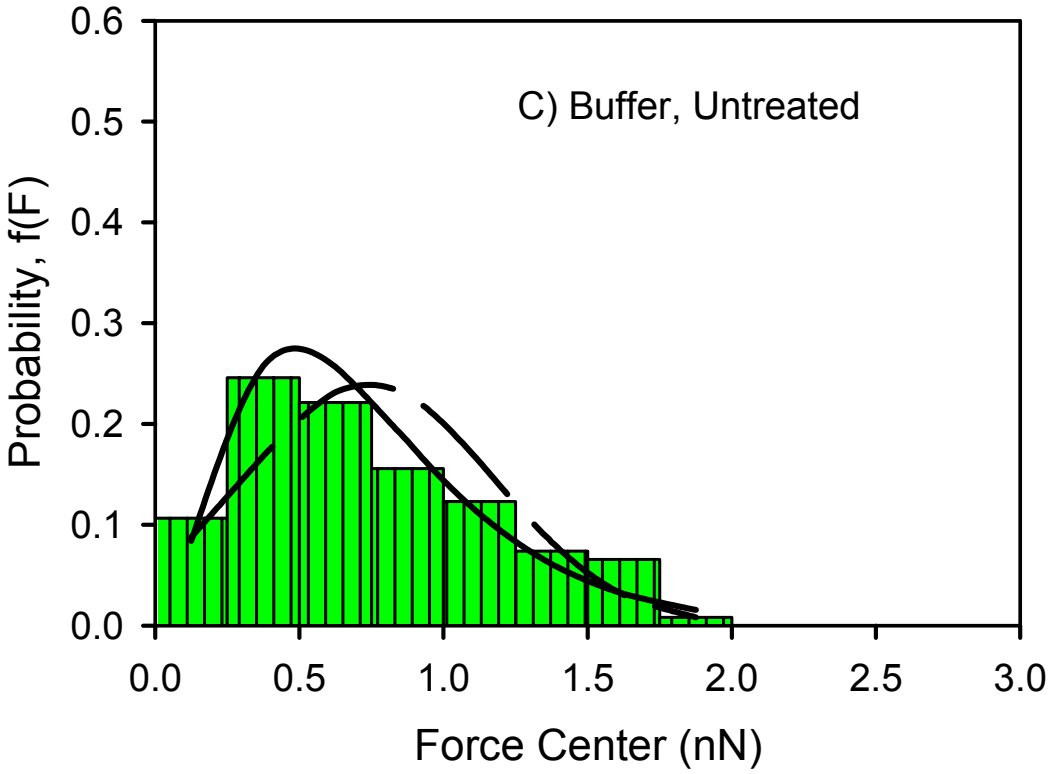
C) Buffer, Untreated
Probability, f(F)
0.0
0.1
0.2
0.3
0.4
0.5
0.6
0.0
0.5
1.0
1.5
2.0
2.5
3.0
Force Center (nN)

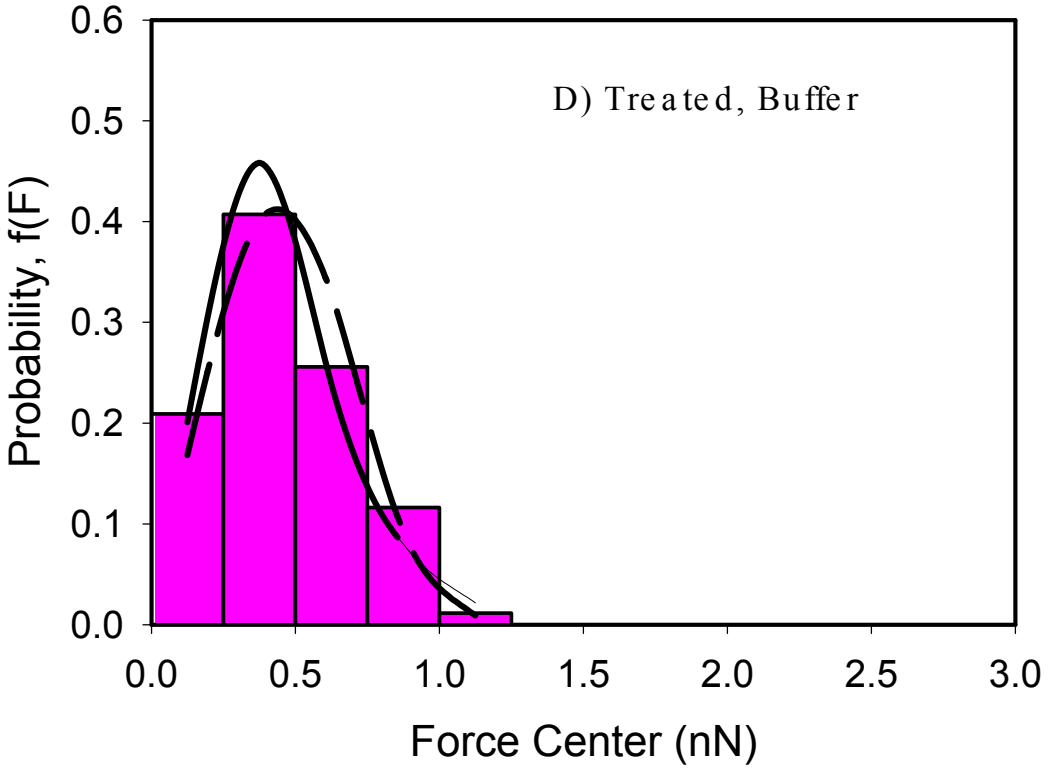
D) Treated, Buffer
Probability, f(F)
0.0
0.1
0.2
0.3
0.4
0.5
0.6
0.0
0.5
1.0
1.5
2.0
2.5
3.0
Force Center (nN)

Figure 5.2

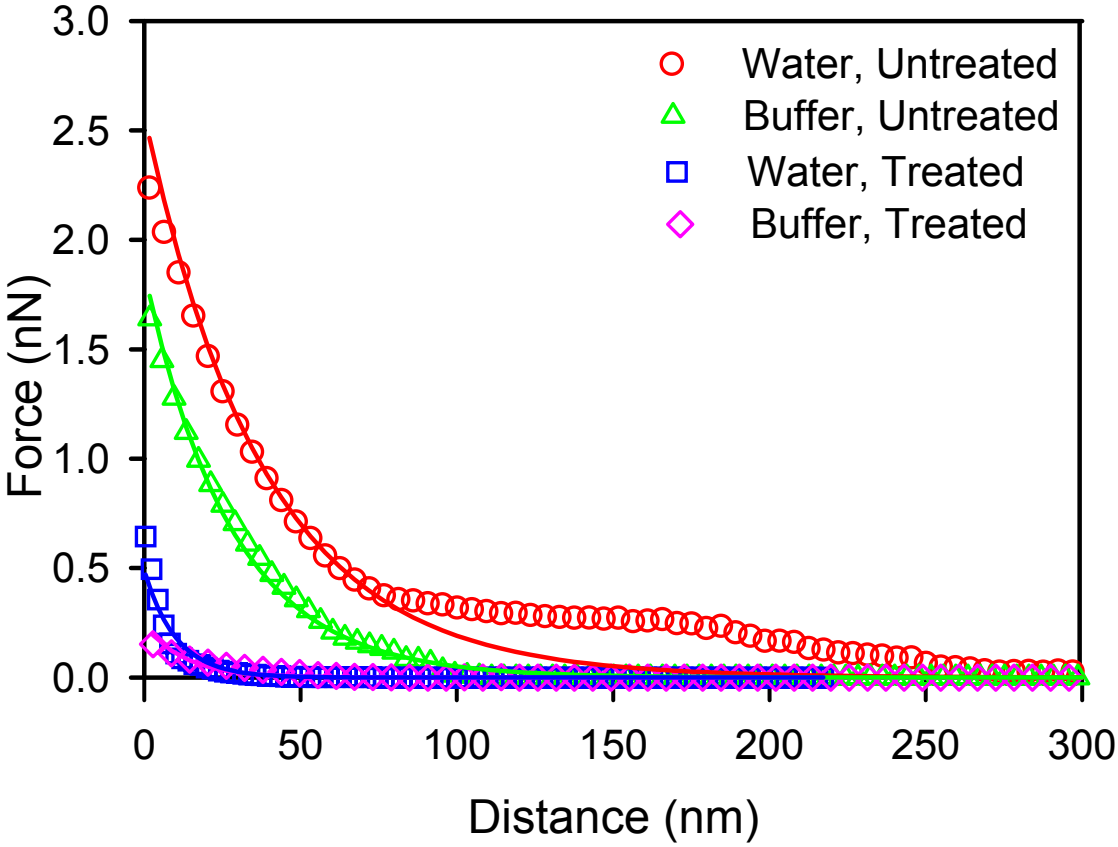
3.0
2.5
2.0
1.5
1.0
0.5
0.0
Force (nN)
0
50
100
150
200
250
300
Distance (nm)
Water, Untreated
Buffer, Untreated
Water, Treated
Buffer, Treated

Figure 5.3

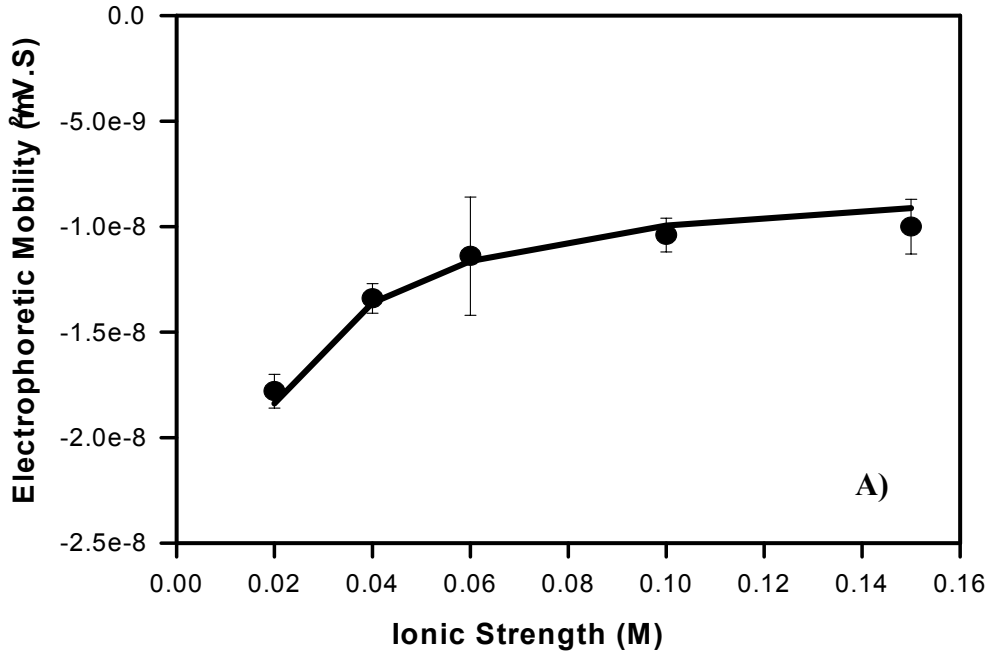
0.0
-5.0e-9
-1.0e-8
-1.5e-8
-2.0e-8
-2.5e-8
Electrophoretic Mobility (m²/V.S)
0.00
0.02
0.04
0.06
0.08
0.10
0.12
0.14
0.16
Ionic Strength (M)
A)

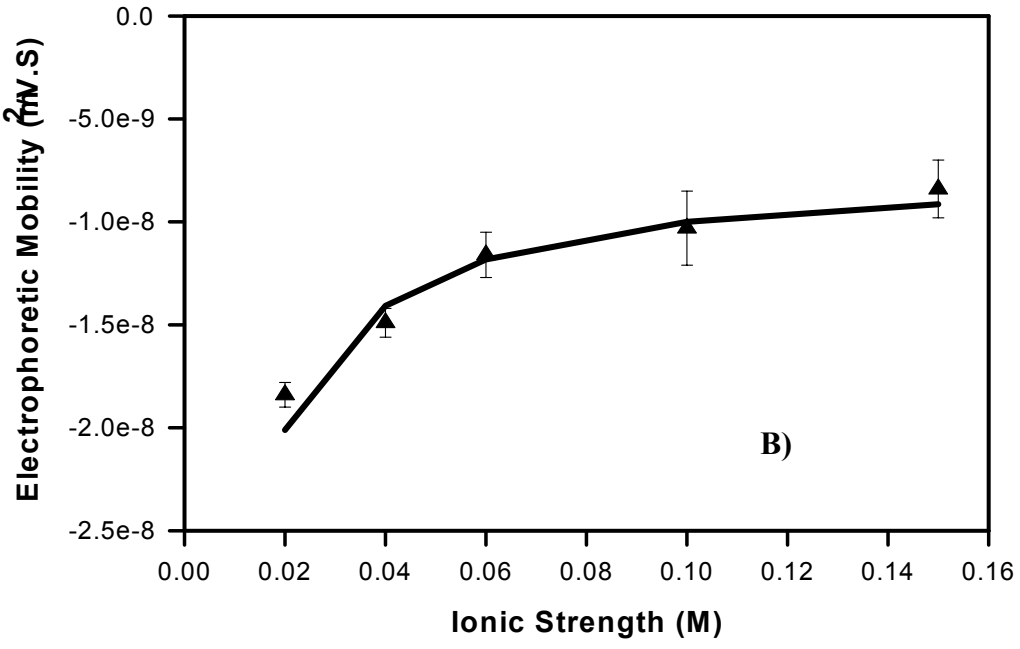
0.0
-5.0e-9
-1.0e-8
-1.5e-8
-2.0e-8
-2.5e-8
Electrophoretic Mobility (m²/V.S)
0.00
0.02
0.04
0.06
0.08
0.10
0.12
0.14
0.16
Ionic Strength (M)
B)

Figure 5.4

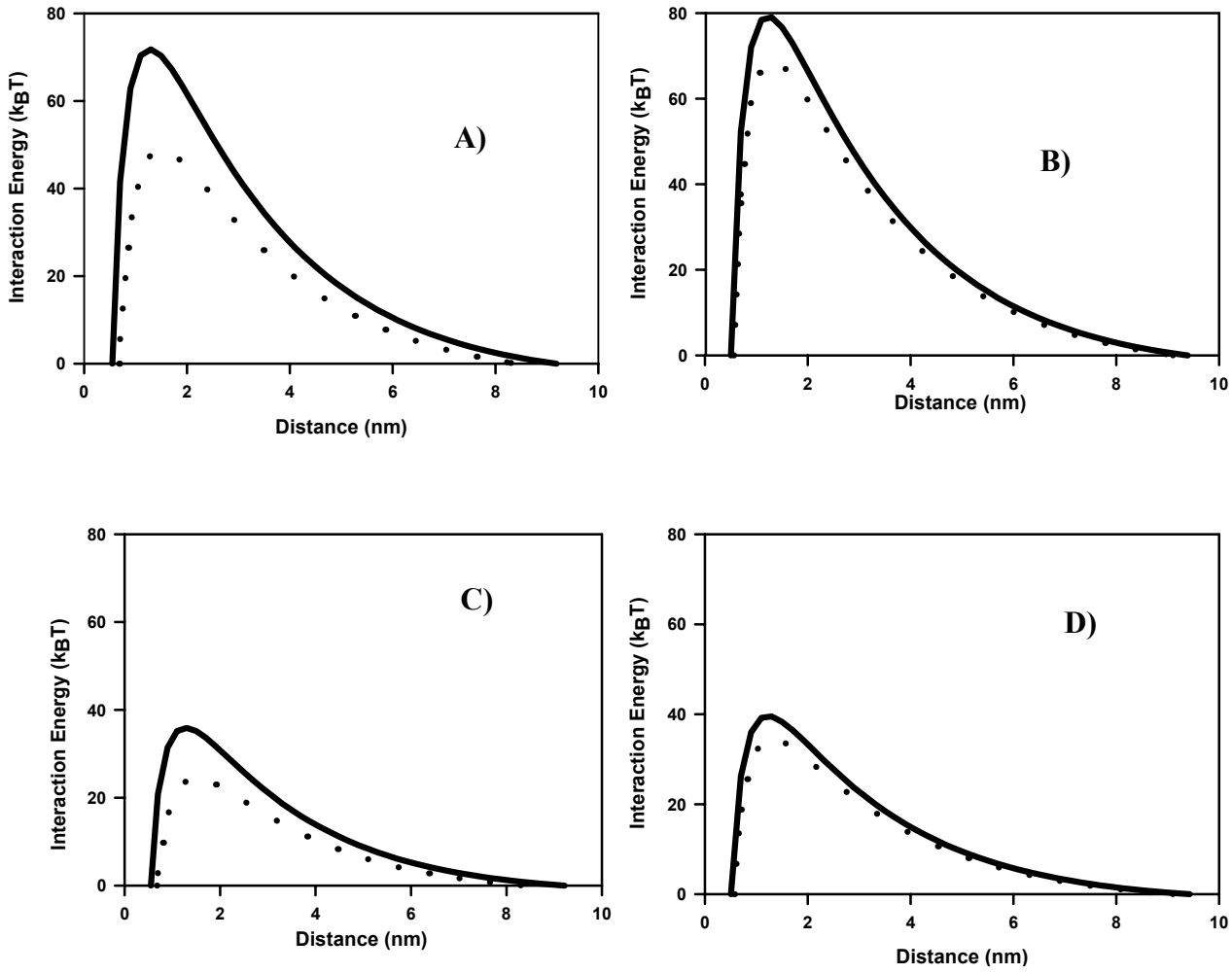
A)
B)
C)
D)
Interaction Energy (kBT)
Distance (nm)
0
20
40
60
80
0
2
4
6
8
10

Figure 5.5

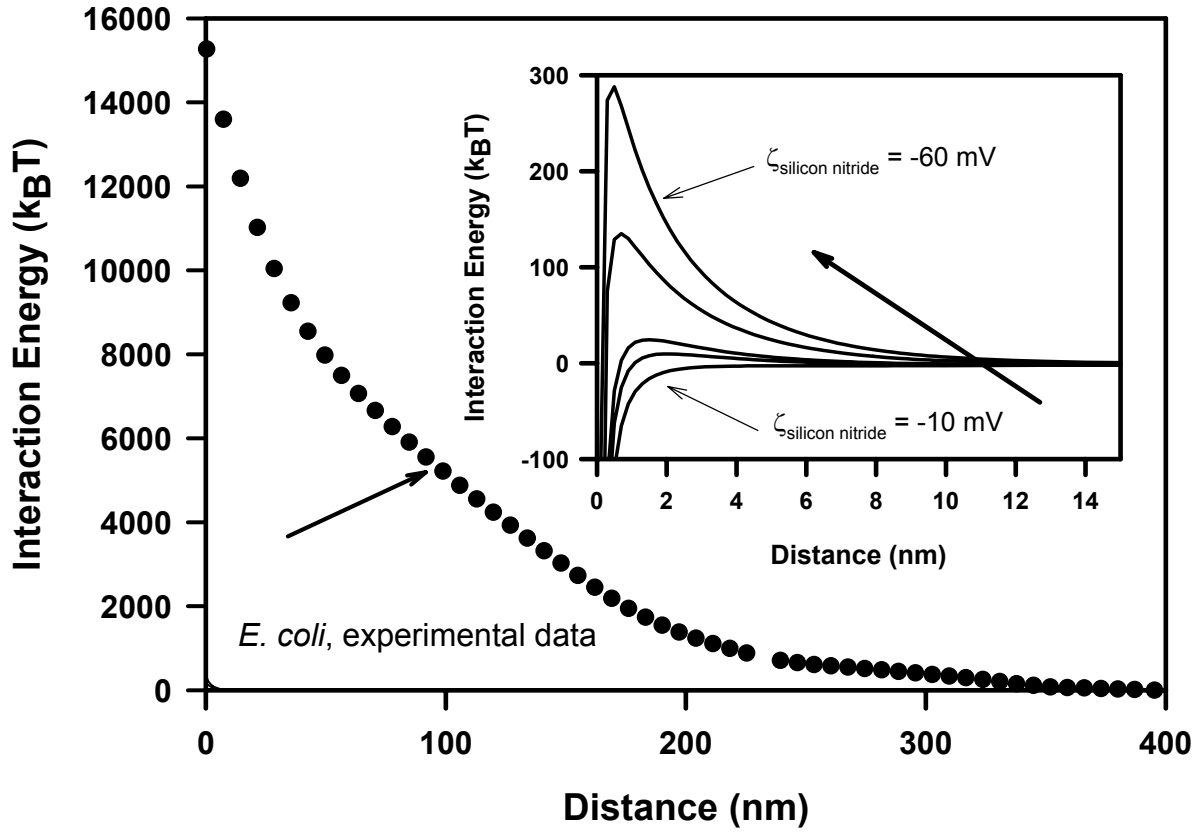
Interaction Energy (kBT)
16000
14000
12000
10000
8000
6000
4000
2000
0
0
100
200
300
400
Distance (nm)
E. coli, experimental data
Interaction Energy (kBT)
300
200
100
0
-100
0
2
4
6
8
10
12
14
Distance (nm)
ζsilicon nitride = -60 mV
ζsilicon nitride = -10 mV

Figure 5.6

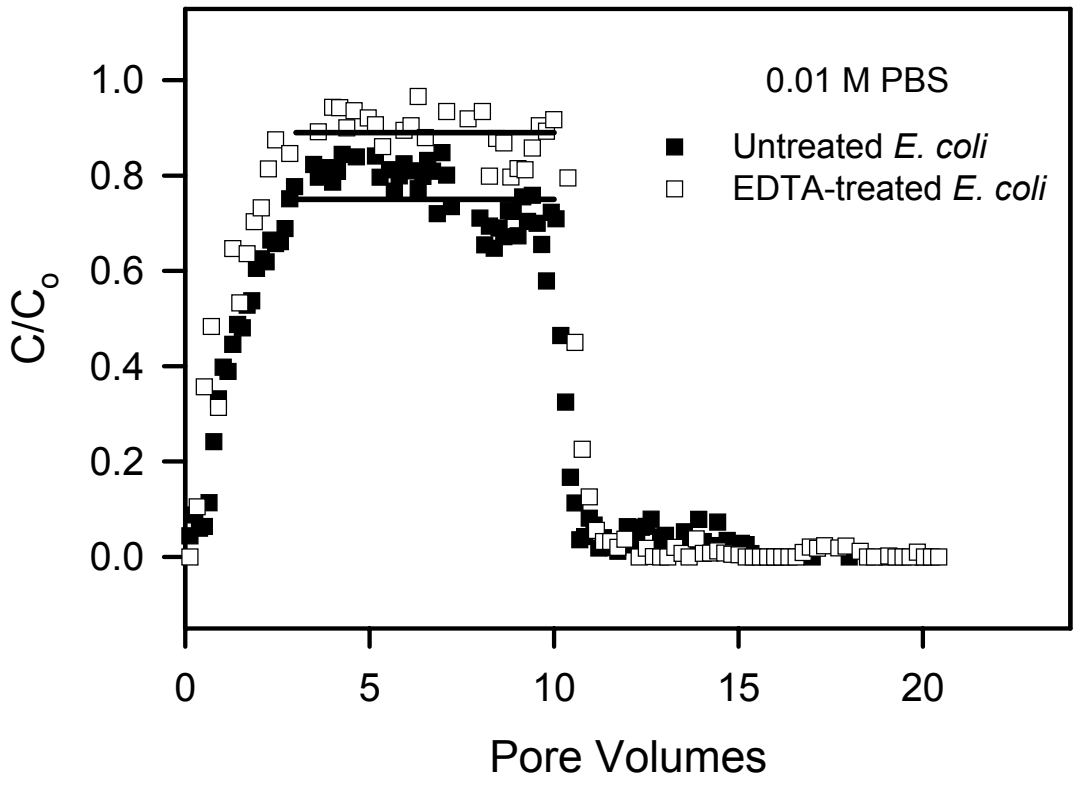
0.01 M PBS
Untreated E. coli
EDTA-treated E. coli
C/C$_o$
1.0
0.8
0.6
0.4
0.2
0.0
0
5
10
15
20
Pore Volumes

Figure 5.7

Chapter 6

Nature of the Interaction Forces between *Escherichia Coli* JM109 and a Model Surface

Abstract

The nature of interactions between *Escherichia coli* JM109 and a model surface (silicon nitride) was investigated via atomic force microscopy (AFM) in solvents of varying polarity (formamide, water, and methanol). The Young's modulus of elasticity for the bacterial surface was estimated by fitting Hertzian deformation theory to force-indentation curves. Young's moduli were a function of solvent polarity, with higher values in methanol (2.2 ± 1.2 MPa), compared to water (0.6 ± 0.4 MPa) or formamide (1.6 ± 0.9 MPa), indicating a stiffer bacterial surface in the low polar solvent (methanol). A biopolymer brush thickness of 546 nm in formamide, 331 nm in water, and 44 nm in methanol was estimated by fitting a steric model to the measured approach curves between the silicon nitride tip and the bacterial surface (statistically different, Kruskal-Wallis test, $P < 0.05$). This lower value in methanol indicates that the polymers are more flexible in the low polarity solvent, since presumably they became coiled to result in lower brush thickness. The average adhesion force in each solvent was negatively correlated with the dielectric constant of the solvent, suggesting hydrophilic biopolymers (statistically different, Mann-Whitney rank sum test, $P< 0.051$). Contact angle measurements with these solvents on bacterial lawns confirmed the hydrophilic nature of the bacterial surface. Specific and non-specific interaction forces between the AFM tip and the biopolymers were further characterized by applying a Poisson statistical analysis to the discrete adhesion data. The relation between the mean and the variance of the

adhesion force was found to be linear in all solvents. The specific and non-specific interaction forces were the highest in methanol (-4 and -1.48 nN respectively). These values are in accordance with the high adhesion magnitudes measured with AFM in methanol. Several models for calculating adhesion forces between elastic bodies were also discussed (Hertz, Derjaguin et. al., and JKR models).

6.1 Introduction

The use of Atomic force microscopy (AFM) to probe the physical properties of microbial surfaces [1, 2] is in a continuous progress. This progression has evolved from the AFM ability to image the microbial surface with sub-nanometer lateral resolution and the ability to directly measure the biological interaction forces under physiological conditions [3]. The force measurements are used to gain an insight on bacterial surface properties, such as hydrophobicity [4], elasticity [5], biopolymer flexibility [4], biopolymer heterogeneity [6], and identification of the discrete interactions which govern bacterial adhesion [7].

An understanding of the fundamental nature of the interaction forces between a bacterium and a surface is sought for many environmental [8, 9], and biomedical applications [10, 11]. For example, bacterial adhesion is important for soil bioremediation of aromatic hydrocarbons [12], controlling drinking water quality [13], and controlling the adherence of bacteria to tissues and biomedical devices [14, 15]. Many of the factors that affect bacterial adhesion are physicochemical in nature, such as the structure and conformation of bacterial surface biopolymers [16-18], the elasticity of the bacterium (represented by Young's modulus) [5], heterogeneity of the biopolymers [6], solvent ionic strength [4, 17], pH [7], polarity [4], and the charge of both the bacterium and the interacting substrate [19-22]. Biological properties of the bacterium also play a role in adhesion, including bacterial motility [23-26], growth phase [27, 28], and metabolic activities [28]. Since these factors combined affect bacterial adhesion, it can be difficult to separate the independent role of each on bacterial adhesion.

However, several recent efforts have focused on studying the role of individual factors on adhesion and on relating micro- and nanoscopic measurements of adhesion and interaction forces to macroscopic properties of the bacterium-substrate system. For example, the repulsive forces probed with AFM upon approach of the tip to the surface of *Streptococcus mitis* were correlated to the activation energy barrier that governs the initial attachment of the bacterium to the glass [29]. Furthermore, the maximum distances at which the attractive forces were probed with an AFM tip upon retraction were in good agreement with the area blocked by an adhering bacterium. A correlation between the equilibrium lengths of the bacterial surface biopolymers and the area blocked by an adhering bacterium was also observed [29]. Earlier studies in our lab addressed the role of lipopolysaccharides (LPS) on bacterial adhesion of *E. coli* JM109 to AFM silicon nitride tips, sand particles, and glass surfaces [16]. The adhesion of the bacterium to these substrates was reduced after the removal of ~ 80% of the LPS from the bacterial surface. Also, the effect of ionic strength on the conformation of *Pseudomonas putida* KT2442 biopolymers and the relation between physiochemical properties and adhesion was also investigated [17]. Similarly, the effect of capsular polysaccharides on adhesion of *E. coli* to different substrates was studied by using isogenic uropathogenic *E. coli* strains that differed in colanic acid expression. The adhesion was studied with AFM and parallel-plate flow cell studies. The results of the study pointed out that the capsular polysaccharide colanic acid does not enhance bacterial adhesion but rather blocks the establishment of specific binding as well as time-dependent interactions between uropathogenic *E. coli* and inert substrates [30].

Statistical analysis of the AFM force measurements can provide a lot of information on the microscopic and macroscopic quantities that affect bacterial adhesion. The individual strength of bonds formed between the AFM tip and bacterial surface biopolymers during contact in liquid media can be estimated from the discrete pull-off forces. Several approaches that rely either on a quantized distribution of discrete single-bond contact forces or on the histogram of the distribution of rupture forces have been used to determine individual bond forces between ligand-receptor interactions, and self-assembled monolayers of carboxylic groups [31-33]. These approaches require several hundreds to thousands of force measurements to be performed and hence require a long measurement time and might damage the sample surface due to repetitive contact [34].

Another approach, which does not require as many measurements and can be used to quantify the individual strength of bond forces, is derived based on Poisson statistics [34-40]. The method is based on statistically analyzing the AFM pull-off events. Applying a Poisson distribution to the data can lead to an accurate estimation of the individual bond strengths and can provide detailed information on the magnitude of specific and non-specific forces [34-40] that are involved in the interaction between the tip and the bacterial surfaces.

Combining the knowledge of the magnitude of the specific forces, non-specific forces, and solvent properties, with different adhesion models [41-43], the significance of different interaction forces in controlling bacterial adhesion can be determined. Depending on the solvent type, the specific forces may include van der Waals interactions, hydrogen bonding, and chemical interactions such as ligand-receptor bonds

[40]. Non-specific force are long-range colloidal forces, such as electrostatic interactions [38].

The current study provides a detailed investigation of the interaction forces that affect the adhesion of *E. coli* JM109 to a model surface, a silicon nitride AFM tip. The interaction forces during the approach of the AFM tip to the bacterium as well as the adhesion forces after contact between the tip and bacterial surface biopolymers were measured in solvents with varying polarity. The force curves were fit with theoretical models to determine the Young's moduli of the cells, the individual bond strengths between the tip and the bacterial surface biopolymers, and to probe the changes in the brush conformation as a function of solvent polarity. The work of adhesion between the tip and the bacterial surface biopolymers was estimated with the use of the established adhesion models such as those proposed by Derjaguin and colleagues [42, 44], Johnson, Kendall, and Roberts (JKR) [41, 45], or models for the elastic deformation of a sphere (Hertz model; [41]). The importance of specific and non-specific forces in controlling bacterial adhesion was discussed.

6.2 Materials and Methods

6.2.1 Experimental Procedures

6.2.1.1 Cultures

Escherichia coli JM109 (a K-12 strain) was provided by Professor Kristin N. Wobbe of the Department of Chemistry and Biochemistry at Worcester Polytechnic Institute (Worcester, MA). Cells were grown in Luria broth [5 g NaCl, 5 g tryptone, 2.5 g yeast extract in 1 liter of milli-Q water (Millipore)] at 37 ºC and 200 rpm until the late

exponential phase of growth. The cells were harvested when the absorbance at 600 nm reached 0.9.

6.2.1.2 Atomic Force Microscopy Experiments

All AFM experiments were performed with a Dimension 3100 Nanoscope III (Digital Instruments/Veeco) and silicon nitride tips (Digital Instruments/Veeco). The spring constants of the tips were 0.13 ± 0.02 N/m, measured by the Cleveland method [46]. Bacterial cells from suspension were attached to cleaned, silanized glass slides by covalent bonding between bacterial carboxylic groups and amino groups of the aminosilane compound [4, 47]. Cells remained hydrated prior to AFM measurements, and AFM imaging was performed in tapping mode under liquid. Once a bacterial cell had been located and brought to the center of the image, the tapping mode was stopped so that force measurements could be performed. Measurements were made in formamide, water, or methanol.

Force measurements were made on a bacterium-free area of the glass slide before and after making the measurement on a bacterium. Equality of the measurements ensured that the tip was not picking up contamination from the media or sample, and that the tip's properties had not been altered by contact with the sample [16].

Data were captured during both the "approach" and "retraction" of the AFM tip with the bacterial samples. For each bacterial cell, 7-20 measurements were made (always over the center of the cell), and 5-6 cells were examined for a given treatment. The approach curves could be averaged, while the retraction curves had to be considered individually due to the complex interaction between bacterial surface polymers and the AFM tip after contact.

6.2.1.3 Contact Angle Measurements

Contact angles of deionized water (polar), formamide (polar), and diiodomethane (apolar) were measured on *E. coli* JM109 lawns, at 26 ± 1 ^{o}C using a Rame-Hart NRL Contact Angle Goniometer (Model #100, Mountain Lakes, NJ). A 2 ml sample of ~ 10^{8} cells/ml was filtered on a 0.45-μm silver membrane filter (Osmonics Inc). At least 20 separate readings with each liquid (2 μL) were taken on both sides of each liquid droplet and averaged (Table 6.1).

6.2.2 Modeling

6.2.2.1 Statistical Description of AFM Data

For each type of AFM experiment, we have data for 3 solvents (water, methanol, and formamide). We used statistical tests to determine if a given parameter, for example, the rupture force, was different among these 3 groups. We used the statistics advisor in Sigma Stat 2.03 (Jandel Scientific) to help select the most appropriate statistical tests for a given data set.

Group comparisons test two or more different groups for a significant difference in the mean or median values, beyond what can be attributed to random sample variation. Two non-parametric tests were applied to the data, namely the Mann-Whitney rank sum (MW) test, and the Kruskal-Wallis analysis of variance on ranks (KW) test. Non-parametric tests do not assume that the samples were drawn from a normal population. Instead, they perform a comparison on ranks of the observations. Rank sum tests automatically rank numeric data, and then compare the ranks rather than the original values. The MW test demonstrates if there is difference between two groups. The null hypothesis is that the two samples were not drawn from populations with different

medians. The KW test compares several different experimental groups. The design is essentially the same as MW test, except that there are more than two experimental groups. The null hypothesis is that there is no difference in the distribution of values among the groups.

6.2.2.2 Analysis of the Adhesion Force Data from AFM Retraction Curves

Retraction curves under different solvents were analyzed to quantify and characterize the adhesion events. In each curve, at least one adhesion event was observed, which represents a physical attachment between the AFM silicon nitride tip and a bacterial surface biopolymer (or biopolymers), after making contact. As the tip is further retracted, it eventually breaks free from the attached biopolymer(s). The point at which this separation occurs is called the pull-off distance, and the force at this location is referred to as a pull-off force or rupture force.

6.2.2.3 Application of Poisson Distribution Function to AFM Pull-off Force Data to Characterize Bonds Formed

Beebe et al. developed a method for characterizing AFM pull-off force data using a Poisson distribution function [34, 38, 40]. The idea behind their approach was to detect the strength of individual chemical bond forces. In one of the first studies performed by their group, an estimation of the individual bond force between a functionalized glass surface with organosilanes and a SiO_2 coated tip with organosilanes also was quantified from analyzing AFM force measurements by Poisson method. The advantages of this approach are that the technique is applicable to any tip size or type, i.e. assumptions are not needed about the surface energies or tip-surface contact area, and that the method does not require a large number of force measurements (< 100 force curves), compared to

the > 4000 needed to analyze discrete adhesive interactions [31], or several hundreds when the unbinding forces of discrete complexes were considered [33]. Measurement time and sample damage due to repetitive contact are reduced.

The two main assumptions that lie behind applying the Poisson distribution methodology to analyze the AFM force data are 1) the total adhesive force (F) develops as the sum of any possible discrete chemical bonds and any possible non-covalent bond interactions such as hydrogen bonding and van der Waals forces [48] and 2) these bonds form randomly with a small probability and all have similar force values (F_i), as will be specified later. As a result of the first assumption, the distribution of the pull-off force measurements within a fixed contact area should follow a Poisson distribution. Beebe et al. demonstrated that this is a valid technique for measuring single bond forces between functionalized surfaces of organosilanes and surfaces functionalized with carboxylic groups [38-40].

6.2.2.4 Poisson Statistical Analysis

The probability function that is used to describe the Poisson distribution of the forces formed at the pull-off point can be expressed as [49]

$$P(F) = (F_{av})^{n} \frac{\exp(-F_{av})}{n!} \qquad (6.1)$$

Where: P (F) represents the possibility that an event with an adhesive force (F) will form, $F_{av.}$ is the average of the pull-off events under a certain set of conditions, and n is the number of occurrences of a certain pull-off event.

An important feature of the Poisson distribution is the equality of the mean and the variance of the distribution, i.e. $\mu_F = \sigma_F^2$. The adhesive force, F, measured as a pull-

off force event in force-distance curve, is related to the number of bonds ruptured during the pull-off event by

$$F = n_i F_i \tag{6.2}$$

where F_i represents the average individual-bond rupture force in the system, and n_i represents the number of individual bonds. The first step in obtaining F_i, is to calculate the mean, $\mu_{F,}$ and the variance, $\sigma_{F,}^2$ of many pull-off events. On the basis of the relationship between the measured force and the number of bonds ruptured (Equation 6.2), one can derive the following equations

$$\mu = \mu_F F_i \tag{6.3}$$

$$\sigma^2 = \sigma_F^2 F_i^2 \tag{6.4}$$

Since $\mu_F = \sigma_F^2$ for a Poisson distribution, the magnitude of F_i can be determined from easily measured quantities as

$$F_i = \sigma^2 / \mu \tag{6.5}$$

where μ and σ^2 represent the mean and the variance of the total adhesive pull-off forces, respectively.

The analysis presented thus far is limited to describing specific interactions. If non-specific interactions, $F_{o,}$ are also important, the previous analysis is modified, as follows

$$\mu = \mu_F F_i + F_o \tag{6.6}$$

$$\sigma^2 = \sigma_F^2 F_i^2 = \mu_F F_i - F_i F_o \tag{6.7}$$

To obtain the values for the individual force and the non-specific interactions, a plot of the variance versus the mean of the pull-off force from several sets of measurements, and a linear regression is applied. The slope and the intercept of this line

are the individual bond-rupture force, F_i, and the product $-F_iF_o$, respectively. The product quantity can be used to determine the non-specific interactions, F_o.

6.2.2.5 Elasticity of Microbial Cells

Quantitative information on the elasticity of the bacterial cell can be obtained from the AFM measurements. To quantify the elasticity of a bacterium, a force curve was recorded on the center of the cell. The measured force curve was converted from a cantilever deflection-distance curve to a force-indentation curve. Cantilever vertical deflection, d, was plotted versus the separation distance, h. The curve was calibrated by subtracting the deflection offset, d_o, from all deflection values. This offset is the deflection value when the cantilever is far from the sample surface. Similarly, an offset in the distance, h_o, is subtracted from all distance values. The value of this offset is considered as the initial value at which the tip starts to contact the sample surface [5]. After the cantilever deflection- distance curve is calibrated, the curve is converted to a force-indentation curve. On a stiff sample, the slope of the compliance region of the force-indentation curve is expected to be 1, but since the force curve is measured on a soft biological cell, the slope is <1. The difference between the separation distance that would be obtained between the tip and the sample on a hard surface and the one that is obtained on a soft surface is equal to the indentation depth of the tip into the sample surface and is defined by [5]

$$\delta = (h-h_o) - (d-d_o) \tag{6.8}$$

The cantilever deflections measured with AFM can be converted into force data using Hooke's law, with the knowledge of the spring constant of the cantilever, K_c, as follows

$$F= K_c\,(d-d_o) \tag{6.9}$$

6.2.2.6 Bacterial Cell Elasticity is Characterized by the Young's Modulus

Young's moduli were evaluated by applying Hertzian models of continuum mechanics of contact to the force-indentation curves [5]. These models are valid for elastic surfaces and do not take into account tip-surface adhesion. The models are applied to AFM approach curves when there is no measured adhesion between the tip and the sample. The Hertzian model describes the indentation of a non-deformable conical indenter (the AFM silicon nitride tip) into an infinitely deformable elastic half space (the bacterial surface). According to the Hertz model, the force-indentation relationship for a conical indenter is given by

$$F_{cone} = \frac{2}{\pi} \tan \alpha E^{*} \delta^{2} \tag{6.10}$$

where α is the half opening angle of the conical tip, taken as 18^{o} based on a study using similar tips [5], E^{*} is the surface elastic constant of the bacterium, defined by

$$E^{*} = \frac{E_2}{1 - \upsilon_2^2} \tag{6.11}$$

where F_{cone} is the theoretical value for the force between a conical indenter (the tip in our case) and the bacterium, E_2 is the Young's modulus or tensile elastic modulus of the bacterium and ν_2 is its Poisson ratio, assumed to be 0.5 for biological materials [5]. The bacterium Young's modulus of the bacterium is obtained by fitting equations 6.4 and 6.5 to the force-indentation curves.

6.2.2.7 Modeling Adhesion Forces between Elastic Surfaces

The adhesion force between two bodies was first investigated between two rigid surfaces (Figure 6.1 A). The adhesion force between the two surfaces is simply related to

the work of adhesion between them. For a rigid sphere interacting with a rigid flat plate, the average adhesion force is described by

$$F_{av} = 2 \pi R W_{ad,Rigid} \quad (6.12)$$

However, real particles are never completely rigid, and when the two bodies come into contact they deform elastically under the combined effect of molecular interactions and any external loading forces [43]. The strength of adhesion between two elastic bodies is dependent not only on the surface energy of the two surfaces, but also on surface roughness, and the liquid media [50]. Several models have been proposed to characterize the adhesion between the two contacting bodies. These models describe the work of adhesion required to separate the two bodies in contact [50].

The Hertz model was the first model to describe the contact between two smooth elastic bodies [43]. Hertz demonstrated that both the size and the shape of the zone of contact followed from the elastic deformation of the bodies. The bodies deform elastically under the influence of any externally applied load as well as the attractive interface forces that pull two surfaces together (Figure 6.1B). This deformation gives rise to a finite contact area even under zero external load [43]. For contact between a sphere (AFM tip) and a plate (the bacterium), the radius of contact (a_H) is a function of the loading force (F_L) and is given by

$$a^3_{Hertz} = \frac{3}{4}\pi(k_1 + k_2)RF_L \quad (6.13)$$

Where k_1 and k_2 are the elastic constants of the tip and the bacterium and given in terms of the Poisson ratio and Young's modulus as [41]

$$k_1 = \frac{1-\upsilon_1^2}{\pi E_1} \qquad \text{and} \qquad k_2 = \frac{1-\upsilon_2^2}{\pi E_2} \quad (6.14)$$

and the applied load, F_L, is given by [51]

$$F_L = \frac{4E_2 R^{1/2}\sqrt{Z^3}}{3(1-\upsilon_2{}^2)} \tag{6.15}$$

In Equation 6.15, Z is the indentation depth of the tip in the bacterium and can be evaluated from the AFM approach curves, by following the approach described in Hyonchol et al.[51]. According to the Hertz model, molecular forces do not change the deformation of the soft particle and therefore the surface energy effects involved in the interactions between the two contacting bodies are ignored [41].

To address the effect of molecular forces on the deformation between two interacting bodies, Derjaguin was the first to consider how the contact deformations influence the sticking of elastic particles [43, 52]. Later on, in an attempt to address the effect of surface forces on the adhesion of elastic bodies, Derjaguin, Muller, and Toporov (DMT) proposed their method [42]. In their (thermodynamic) model, the elastic deformation was assumed to be entirely due to Hertz pressure acting within the contact area, while the adhesive forces are confined to the external zone, i.e. long-range attractive forces are only considered [53]. Due to these assumptions, it is appropriate for contacts involving weak adhesion, small radius of curvature, and large elastic modulus [54]. According to the DMT model, the deformable body does not change its form when approaching the substrate until the point of contact is reached. On the formation of the contact point, the shape of the contacting bodies is defined by Hertz equations. The main defect of the DMT model is it's ignoring to the adhesive forces that act within the contact area [53].

To address the deformation effect on the adhesion between the two particles, the shape of the deformed surface was thought to ultimately determine the attractive forces. According to their model, a finite force F_{av} is required to overcome the attractive forces and pull the surfaces a part. This minimum pull-off force value required to separate the two bodies is given by

$$F_{av} = 2 \pi R W_{ad, DMT} \quad (6.16)$$

where R is the tip radius, and W_{ad} is the work of adhesion required to separate the two interacting bodies. This pull-off force value is equal to the value that would apply to non-deformable solids (Equation 6.12).

The second model that addresses the effect of deformation on adhesion between smooth elastic bodies is the model of Johnson, Kendall, and Roberts (JKR). The JKR model is based on the contact mechanics of the two surfaces. The model suggests that the work of adhesion goes to create a new surface. The energy required to create unit area of new surface can be defined as the free energy of the solid, which can be quantified by measuring the contact angle of a liquid on the solid [41]. According to the model, the attractive forces between the sphere (AFM tip in our case) and the flat plate (the bacterium) (Figure 6.1C) are concentrated primarily in the immediate contact area (couple of atomic layers) and can be neglected outside this area. The second assumption in JKR theory is that the linear elasticity holds over the whole range of deformations involved and this can not be true at the edges and leads to a sharp discontinuity at the edge of the contact zone. Due to these assumptions, the model is appropriate for strong adhesive forces that act at short distances, large radius of curvature, and small elastic modulus [54].

When the two surfaces are pulled apart, the radius of the circle of contact keeps decreasing with the increase in the pulling-off force. This will proceed until the rate of release of mechanical energy in the contact zone is greater than the surface energy requirements (Figure 6.1D). This occurs for a pull-off force given by

$$F_{av} = 1.5\ \pi\ R\ W_{ad,\ JKR} \tag{6.17}$$

In comparison to the DMT model, the required force to separate the two interacting bodies according to the JKR model is ¾ that of the DMT force. According to the JKR model, the radius of the contact area at rupture, a_{JKR}, which results due to pressing the two bodies together by an external load, F_L, can be evaluated as

$$a_{JKR}^{\ 3} = \frac{R}{K}\left(F_L + 3\pi R W_{ad,JKR} + \sqrt{(6\pi R F_L W_{ad,JKR}) + (3\pi R W_{ad,JKR})^2}\right) \tag{6.18}$$

Equation 6.18 reduces to the simple Hertz model (Equation 6.13) when the W_{ad} is zero, i.e. the two bodies are non-adhering. The mean elastic modulus of the contact, K, is given by [41]

$$K = \frac{4}{3\pi(k_1 + k_2)} \tag{6.19}$$

Both DMT and JKR models provide two limiting cases that used to describe the adhesion between elastic surfaces. This fact was not understood till Tabor pointed out that both models are the opposite extremes of the deformation spectrum described by the parameter μ [55]

$$\mu = \left(\frac{R W_{ad}^{\ 2}}{E^{*2} Z_o^{\ 3}}\right)^{1/3} \tag{6.20}$$

The parameter μ can be shown to represent the ratio of the elastic displacement of the surfaces at the point of separation (pull-off) to the effective range of surface forces characterized by the equilibrium distance at separation (Z_o). The JKR theory applies to large, compliant spheres, i.e. at large values of μ (μ>5), while the DMT theory applies more for small, stiffer spheres, i.e. low values of μ (μ<0.1) [53]. μ values in the range between 0.1 – 5 describe elastic deformation and adhesion in the transition area between DMT and JKR models. Although Tabor was the first to describe the adhesion between elastic particles in a comprehensive way, more sophisticated treatments to describe the transition area between DMT and JKR models were provided by Muller et al. [56], Greenwood et al. [57], and Maugis et al. [58].

6.2.2.8 Surface Energy Calculations

For two surfaces at equilibrium and in contact, the net free energy of adhesion between the two surfaces can be described as a function of the apolar (van der Waals) and polar (Lewis acid-base) free energies. Free energies are related to the surface tension components of the two surfaces. The various surface tension components of the bacterial cell can be calculated using the Young-Dupré equation [59, 60]

$$(1+\cos\theta)\gamma_L = 2(\sqrt{\gamma_s^{LW}\gamma_L^{LW}} + \sqrt{\gamma_s^{+}\gamma_L^{-}} + \sqrt{\gamma_s^{-}\gamma_L^{+}}) \qquad (6.21)$$

Where θ is the contact angle; γ_L is the total surface tension of the liquid in J/m^2; γ_i^{LW} is Lifshitz-van der Waals (LW), or a polar surface tension component of condensed material (i) in J/m^2; γ_i^+ and γ_i^- are the electron-acceptor and electron-donor parameters of the Lewis-acid base or the polar components of the surface tension of condensed material in J/m^2 [61].

6.2.2.9 van der Waals Force and Energy Interactions

For consideration of rough surfaces, a different form of the van der Waals expression can be used, in which the roughness of the adhering particle (*E. coli* JM109, in this case) is accounted for. Strictly speaking, the AFM tip also has a roughness associated with it, but the roughness of silicon nitride is at a smaller scale than the microbial cell, with its many surface macromolecules. If we assume that the roughness in the interaction is primarily due to the distribution of biopolymers and other macromolecules on the microbial surface, then the appropriate model for calculating the adhesion force has been derived by Rabinovich et al. as [62, 63]

$$F_{v,\,rough} = -\frac{A_{132}R}{6H_o^2}\left[\frac{1}{1+\left(\frac{32Rk_v rms}{\lambda^2}\right)}+\frac{1}{\left(1+\frac{k_v rms}{H_o}\right)^2}\right] \tag{6.22}$$

where H_o is the distance of closest separation (0.3 nm), k_v is a coefficient equal to 1.817, and the terms *rms* and λ refer to the asperities on the surface. If a line trace is performed on an AFM image of the microbe, the peak distance between asperities is λ, and *rms* is the root-mean square of the surface roughness.

In equation 6.22, A_{132} is the Hamaker constant for the interacting media and calculated as:

$$A_{132} \approx (\sqrt{A_{11}} - \sqrt{A_{33}})(\sqrt{A_{22}} - \sqrt{A_{33}}) \tag{6.23}$$

where A_{132} is defined as the non-retarded Hamaker constant for media 1 (bacterium) and 2 (silicon nitride) interacting across media 3 (solvent) [43]. The individual Hamaker constant for each of the interacting components can be calculated as:

$$A_{ii} = 24\pi l_o^2 \gamma_i^{LW} \quad (6.24)$$

where l_o is the closest separation distance, taken as 1.57 Å [61].

Based on Equation 6.22, an expression to calculate the energy of the interaction can be derived as the negative of the integral of the force with respect to distance. The energy will be:

$$E_{v,Rough} = \frac{-A_{132}R}{6}\left[\frac{1}{H_o}\left(\frac{1}{1+\frac{32Rk_v rms}{\lambda}}\right)+\frac{1}{k_v rms + H_o}\right] \quad (6.25)$$

6.2.2.10 Modeling of Approach Curves with a Steric Model: Determination of Polymer Brush Thickness

A model developed by Alexander [64] and de Gennes [65], and modified by Butt et al. [66] was used to model the steric interactions between the AFM tip (sphere) and cell surface polymers. The force per unit area between two surfaces, $F_{St,}$ is described by

$$F_{St} = 50k_B T R L_o \Gamma^{3/2} e^{-2\pi h/Lo} \quad (6.26)$$

where k_B is the Boltzmann constant, T is temperature, Γ the grafted polymer density, h the distance between the two surfaces, and L_o the equilibrium thickness of the polymer layer, referred to as the polymer brush. For these calculations, the tip radius was assumed constant at 250 nm [16].

6.3 Results

6.3.1 Elasticity and Adhesion Models

6.3.1.1 Elasticity of Bacterium

To quantify the elasticity of the bacterium in different solvents, the deflection-distance curves were converted to force-indentation curves as described by equations 6.8 and 6.9. A typical deflection-distance curve measured on the center of *E. coli* JM109 in

formamide is shown in Figure 6.2A. Using the values of h_o and d_o (-529.7 nm, -96 nm), the curve is converted to a force-indentation curve (Figure 6.2B). Quantitative information on the Young's moduli of the bacterial surface under different solvents was extracted by fitting the force-indentation curves to the Hertz model (equations 6.10 and 6.11). A quasi-quadratic relation was observed between the tip indentation and the force (Figure 6.2B) as will be predicted from the Hertz model for a conical indenter. With the use of the Hertz model, Young's moduli values were calculated for the bacterial surfaces in all solvents. The Young's moduli values were highest in methanol (2.2 ± 1.2 MPa) and lowest in water (0.6 ± 0.4 MPa) (Table 6.2). The large standard deviation of these values reflects the heterogeneity of the biopolymers on the bacterial surface. The bacterial surface is least compliant in methanol (the least polar solvent), compared to water and formamide.

6.3.1.2 Adhesion Models

The DMT and JKR adhesion models were used to calculate the work of adhesion between the bacterial surface and the silicon nitride tip (equations 6.16 and 6.17). Both models were functions of the average adhesion force in the solvent and the tip radius (250 nm). The values of the work of adhesion predicted by the JKR theory were higher than the values predicted by the DMT method for all solvents. The work of adhesion values increased as the polarity decreased. The work of adhesion was highest in methanol (1.86 mJ/m^2, 1.39 mJ/m^2 using JKR and DMT, respectively) and lowest in formamide (1.01 mJ/m^2, 0.76 mJ/m^2 using JKR and DMT, respectively). The values reported for the work of adhesion in water were between those for methanol and formamide (1.36 mJ/m^2, 1.02 mJ/m^2 using JKR and DMT, respectively). This trend qualitatively agrees with the

observed trend in adhesion values observed between *E. coli* JM109 and the tip in all solvents.

The values for the work of adhesion calculated based on both models and the indentation values estimated from the approach curves (Table 6.3) were used to calculate the Tabor parameter given by equation 20. μ values that range between 0.01 to 0.03 were estimated in all solvents.

The contact and adhesion models can also be used to estimate the radius of contact between the tip and the bacterial surface biopolymers in the presence of an external load (equations 6.13 and 6.18). The radii of contact values predicted based on JKR model were higher than the values predicted based on Hertz theory in all solvents. The radius of contact increased with increasing polarity using both models. The values of the radii of contact were the highest in formamide using Hertz and JKR models (215, and 260.1 nm, respectively). The radii of contact in water and methanol were 159 and 60.7 nm, respectively using Hertz model and 214.8, and 104.2 nm, successively using JKR model.

6.3.2 Relationships between Solvent Polarity and Adhesion Other Properties

Pull-off distances and adhesion forces between bacterial surface biopolymers and the silicon nitride tip were compared for all solvents (Figure 6.3A). For the data shown, each retraction curve was considered separately, without any averaging. Three retraction curves each on five different bacterial cells were considered per solvent. Pair-wise comparisons of pull-off forces in all solvents (adhesion forces) showed that the forces are statistically different (Mann Whitney sum rank test, $P<0.051$). A negative correlation between solvent polarity and adhesion was observed. The average of the adhesion peaks

was the highest in the least polar solvent, methanol (-2.19 ± 1.5 nN) and lowest in the highest polar solvent, formamide (-1.18 ± 0.91 nN). The distribution of the pull-off forces in all solvents (Figure 6.3B, 6.3C, and 6.3D) showed that the percentage of the pull-off force less than 2 nN measured with AFM was the highest in the highest polar solvent. These percentages were 87%, 68%, and 50% in formamide, water, and methanol successively.

The effect of polarity was also investigated on the interaction forces measured during the approach of the AFM tip to *E. coli* JM109 in formamide, water, and methanol. The interaction forces upon approach were statistically different from each other (Kruskal-Wallis rank sum tests, $P < 0.05$). Greater repulsion was observed with increasing solvent polarity (Figure 6.4). The steric repulsion between the tip and the bacterial surface biopolymers was modeled using Equation 6.25 [64, 65] (Figure 6.4). The height of the biopolymer brush layer was the lowest in the least polar solvent (methanol) (Table 6.3). The grafting density was the highest in the least polar solvent, indicating a compression of biopolymers on the bacterial surface. The distance over which the force decays to zero was lowest in the least polar solvent (Figure 6.4). The slope of the compliance region in the approach curves was less negative in the highest polar solvent (Table 6.3), indicating that the bacterial surface was softer in the more polar solvent.

A direct relationship was observed between the dielectric constant, a macroscopic quantity that describes solvent polarity, and several microscopic system properties estimated from AFM force measurements. There was an indirect linear relationship between the magnitude of the adhesion force in each solvent and the reciprocal of the

dielectric constant (Figure 6.5A). A direct linear relationship was observed between $1/\varepsilon$ and L_o (Figure 6.5B), and between $\Gamma^{1.5}$ and $1/\varepsilon$ (Figure 6.5C). The linear dependence that was found between$1/\varepsilon$ and both $\Gamma^{1.5}$ and the brush thickness, agrees well with the linear dependence between F and both $\Gamma^{1.5}$ and the brush thickness as described by the steric model. These results indicate that a direct relationship can be obtained between the microscopic quantities measured with AFM and the solvent macroscopic properties such as the dielectric constant.

6.3.3 Specific and Non-specific Forces

The rupture forces between the silicon nitride tip and biopolymers in each solvent were characterized by applying a Poisson distribution function to the distribution of adhesion forces (Figure 6.6). A minimum of five different sets of data (on five different bacterial cells) was analyzed per solvent. Each set consists of the peaks from three to five force curves measured on each bacterial cell. A summary of all the mean values and the standard deviation of the adhesion forces per set per solvent is given in Table 6.4. Plots of the mean versus variance of the force were constructed (Figure 6.7), and a linear regression was applied to the data.

The slopes of these linear regression lines are related to specific interactions between the bacterial surface biopolymers and the tip, the different segments of biopolymers, and the interactions between the bacterial surface biopolymers and the solvents. The intercept of the linear regression line is the product of the specific forces and the non-specific forces. The slope was highest in methanol (-4.00 nN) and lowest in water (-0.42 nN). The magnitude of the non-specific interactions can be deduced from the y-intercept, and was similarly highest in methanol and lowest in water (Table 6.5). In

each solvent, the contribution of the specific interactions to the total force was greater than that of the non-specific interactions. The high specific and non-specific forces estimated from the Poisson distribution for methanol is in agreement with the high values of adhesion measured between methanol and the tip via AFM retraction curves.

With the knowledge of the specific forces, the strength of the hydrogen bond can be estimated. Specific forces are the sum of van der Waals forces and hydrogen bonding. Therefore, the value of the hydrogen bond force can be estimated by subtracting the van der Waals force component (Equation 6.22) from the specific forces. The adhesion between two bodies is primarily controlled by van der Waals interactions at short separations for uncharged particles. The adhesion between the silicon nitride tip and the bacterium was calculated based on a model proposed by Rabinovich et al. for van der Waals forces between a rough sphere and a plate (Equation 6.22). According to this model, an estimation of the rms and the distance between asperities on the bacterial surface is necessary to calculate the van der Waals force component. AFM images on *E. coli* JM109 revealed that the rms values changed depending on the solvent (6.8, 3.7, and 9.8 nm in formamide, water, and methanol, respectively) while the λ value (139.7 nm) was measured on *E. coli* JM109 cells in air, so it was independent of solvent type. Using these values allowed us to calculate the van der Waals forces and energies of adhesion based on the "rough" model of Rabinovich et al. [67, 68]. The van der Waals forces were calculated in all solvents at the distance of closest approach, taken to be 0.3 nm. The Hamaker constant was calculated in all solvents based on contact angle measurements (equations 6.23 and 6.24). The Hamaker constant for the bacterium was calculated to be

6.36×10^{-20} J (Table 6.6). The estimated values of the hydrogen bond forces were the highest in methanol (Table 6.6).

Similarly, the energy of the hydrogen bond can be calculated based on

$$W_{ad,JKR} = 2\ E_v + 2\ E_H \qquad (6.27)$$

where E_v is the van der Waals energy and E_H is the Hydrogen bond energy. The van der Waals energy was calculated by the use of Rabinovich energy model (equation 6.25). The energy per unit area was calculated by dividing the calculated energy per the area occupied by one bond. The area per bond was calculated by dividing the total effective area calculated from JKR method (πa^2) per the number of bonds estimated from Poisson method (# of bonds = Total $F_{avg.}/ F_i$). The energy of hydrogen bond ranged between 0.51 – 0.93 mJ/m^2 in all solvents (Table 6.6).

6.4 Discussion

6.4.1 Effect of Polarity on Biopolymer Conformation and Bacterial Adhesion

The effect of solvent polarity on the adhesion of *E. coli* JM109 to the silicon nitride AFM tip was investigated by studying the nature of the approach and retraction curves of the force measurements. The magnitude of adhesion as measured from AFM retraction curves increased as the polarity of the solvent decreased. The average of the pull-off measurements was highest in methanol and lowest in formamide. This trend suggests that the biopolymers are hydrophilic. Contact angle measurements on *E. coli* JM109 cells also suggest a hydrophilic surface (Table 6.1) since a small contact angle was measured in water and a higher contact angle was measured in diiodomethane. The approach curves showed a greater repulsion between the bacterium and the tip in the higher polar solvents. This observation can be explained by the fact that the polarity

increases when the electronegativity difference between interacting atoms increases. As the electronegativity increases, the partial charge (negative and positive) on the atoms increases [69].

The adhesion of the bacterium to silicon nitride was related to the conformation of the bacterial surface biopolymers in each solvent. Modeling of the approach curves with the steric model showed that the brush thickness was lowest and the grafting density of the bacterial surface biopolymers was highest in the least polar solvent. The modeling results suggest that the biopolymers collapse on the bacterial surface in lower polarity solutions. This hypothesis was supported with the increase in the bacterial surface rigidity as the polarity decrease as measured by the slope of the compliance region in the approach curves. Relating the conformation of the bacterial surface biopolymers to adhesion showed that the adhesion increases as the biopolymers flexibility increase.

The effect of solvent polarity on bacterial adhesion and biopolymer conformation was compared to other studies in the literature. In an earlier study performed in our lab, the bacterial surface biopolymers of *P. putida* KT2442 were more flexible in a higher polar solvent (methanol) compared to lower polar solvents (water and formamide)[4]. The flexibility of *P. putida* KT2442 biopolymers was quantified by estimating their segment lengths with the freely jointed chain model. The changes in the brush height and grafting density reflect conformational changes of the biopolymers. The transition in biopolymer flexibility was associated with an increase in the adhesion between the bacterium and silicon nitride tip. In another study, the effect of solvent polarity on the interaction forces measured between intrachains of Poly (ethylene-glycol) (PEG) was

investigated. As a result of the study, the hydrophobic interactions between intrachains of PEG were eliminated in hexadecane, which is an entirely apolar solvent [70].

In a new way to utilize the AFM data more effectively, the pull-off measurements (AFM data) as a microscopic quantity were related to the dielectric constant, a macroscopic quantity that describes polarity. There was a direct and linear relationship between the dielectric constant and the measured adhesion force. The observed relationship between the force and the inverse of the dielectric constant agrees well with what one would expect based on the theory behind the dielectric constant. The dielectric constant (ε) is generally familiar in the expression for the force (f) between two charges (e, é) separated by a distance (z): $f = e é/ \varepsilon z^2$, in which ε is a constant characteristic of the medium between the two charges [71]. The relation between the dielectric constant and the AFM measurements extends more to the conformation of the biopolymers on the bacterial surface. A direct linear relationship was also found between the brush thickness of the bacterial surface biopolymers and the inverse of the dielectric constant. The relationship between the grafting density$^{1.5}$ and the inverse of the dielectric constant was linear too. The observed relation between ε and both L_o and $\Gamma^{1.5}$ agrees well with what would be expected based on the steric model, i.e. since F and ε are linearly related and the steric model predicts a linear relationship between the Force and both L_o and $\Gamma^{1.5}$, a linear relationship would be expected between ε and both L_o and $\Gamma^{1.5}$.

A similar relationship between solvent dielectric constant and adhesion was observed in a study aimed to determine the rupture forces between self-assembled monolayers of organosilanes. A decrease in the single-molecule-bond-rupture forces was observed as the dielectric constant increased [37]. In another successful effort to relate

the microscopic quantities measured with AFM to macroscopic quantities that characterize bacterial adhesion, the adhesion of *Streptococcus mitis* to a silicon nitride AFM tip was related to different macroscopic quantities. For example, the equilibrium length obtained from the steric model and the maximum distance at which attractive forces are probed with AFM were each related to the area blocked by adhering bacteria. Similarly, the repulsive forces probed by an AFM upon approach of the tip to the bacterial surface were corresponded with an activation barrier that governs the initial macroscopic adhesion of the bacterium to glass [29]. These steps form the initial efforts towards finding direct relations between microscopic properties and macroscopic predictors of adhesion. Continued efforts in this respect will lead to a high resolution and better accuracy in characterizing bacterial adhesion.

6.4.2 The Role of Interaction Forces in Controlling the Adhesion of *E. coli* JM109 to Silicon Nitride

A detailed statistical characterization of the pull-off adhesion forces was used to investigate the role of different interaction forces in controlling the adhesion of *E. coli* JM109 to silicon nitride. The distribution of the pull-off adhesion forces was investigated statistically by direct fitting of Poisson statistical distribution to the distribution of pull-off adhesion forces. The Poisson distribution was chosen to minimize the effect of heterogeneity of the polymers [6, 16] and to predict the single chemical bond forces in different solvents. The later was based on applying the method developed by Beebe et al., based on Poisson statistical distribution [34, 40].

The validity of Poisson distribution to fit the distribution of adhesion affinities between SAMs was well investigated in literature [34, 35, 40, 48]. To our knowledge,

the applicability of the Poisson model to describe adhesion affinities between AFM tip and bacteria has not been investigated previously.

Using the Poisson distribution, we estimated the hydrogen bond strength. In general, when the AFM tip withdraws from contact with the sample surface, an adhesion force develops between the tip and the sample. These adhesion forces, when carried in liquid, can only originate from physical attractions and chemical bonds that form between the tip and the sample because no capillary force between the tip and the sample exists [34]. The interactions are usually divided into specific interactions that include hydrogen bonding, and van der Waals forces and non-specific interactions such as electrostatic interactions.

Applying the Poisson distribution to our data showed that both the specific and non-specific components of the interaction force have significant contributions to the measured interactions. The non-specific forces were ~ 28% of the specific forces (Figure 6.8). The Poisson fit to the mean vs. variance plots of the pull-off forces were linear, with a non-zero, indicating that only discrete and homogeneous bonds [37, 38] were formed between the tip and the bacterial surface biopolymers. If multiple types of interactions took place in a significant fraction of the force measurements, the dispersion in the rupture-forces can introduce a non-linearity in the plot of the mean versus variance [37].

The magnitude for the rupture forces obtained between *E. coli* JM109 and silicon nitride AFM tip were higher than the rupture forces reported for SAMs [37, 40, 48, 72]. This difference is mainly due to the differences in the chemical nature of the systems. When SAMs are considered, the type of interaction forces that act between the tip and the substrate can be predicted. For example, when interaction forces were studied between

Au (111) surfaces and silicon nitride (bare) tips, only van der Waals forces were detected (60 ± 3 pN). When the forces were measured between silicon nitride tips and mica surfaces, hydrogen bonding was observed in addition to the van der Waals forces, as would be expected, with an individual bond force of 181 ± 35 pN [34].

However, when a bacterial surface is considered, the type of interactions cannot be predicted due to the undefined chemistry of the surface. For instance, the surface of *E. coli* JM109 consists of 75% LPS with at least seven different types of oligomers and 25% proteins [73, 74]. The chemistry for each LPS type is different from the other and therefore the type of interactions will be different too. In addition to that, each AFM measurement is taken at a different contact area, so each pull-off measurement consists of different individual bonds. Variations can be recorded as different interactions between individual bonds in a single pull-off event, between force measurements taken at the same location, and between sets of measurements taken at different locations.

When compared to other studies, the number of rupture forces observed between the bacterial surface biopolymers and the tip was lower than the number of rupture forces observed between SAM's. This low number is expected since low number of adhesion events during force measurements was recorded. The less number of multiple adhesion events suggest that also few bond forces are formed. Simple calculation of the number of biopolymers interacting with the tip under different solvents showed that around 7-21 molecules could interact with the tip (Table 6.3). The calculated numbers were based on assuming a homogeneous distribution of biopolymers on the bacterial surface. A lower number of molecules will be expected to interact with the tip due to the dynamic movement of biopolymers. Due to this low number of molecules interacting with the tip,

it is likely that the measured adhesion events are a reflection of measurements between the tip and single molecule or multi-measurements between the tip and different positions of a single biopolymer molecule more than measurements between the tip and multiple different biopolymers.

With the knowledge of specific and non-specific forces, an estimation of hydrogen bond forces is possible. In most biological systems, several different chemical forces are involved, including multiple hydrogen bonds, and van der Waals interactions [35]. In water and salt solutions, electrostatic forces can also be important. Factors such as steric hindrance and direction of approach can play a significant role in the interactions in the biological systems also.

In all solvents, the specific forces were considered as the sum of the hydrogen bonding, and van der Waals forces. Based on this, the hydrogen bond forces were estimated in all solvents by subtracting van der Waals force component. van der Waals forces were calculated at 0.3 nm as the closest separation distance using Rabinovich model for rough surfaces (Equation 6.22) [62, 63]. The rough van der Waals model gives a much better agreement than the traditional van der Waals expression, which predicts a value that is 2-5 times larger. The magnitude for the hydrogen bond forces ranged between 2.6 nN in formamide to 5.1 nN in water. These values indicate that multiple hydrogen bonding are most likely to take place in all solvents given that the hydrogen bond force ranges between 0.094 – 0.377 nN [43]. The values estimated in our study were higher than the hydrogen bond strength values estimated between carboxylic groups modified surface and a bare silicon nitride tip (20 – 70 pN, depending on solvent type) by applying Poisson method to AFM data [40]. Although the estimated hydrogen bond

values were different between the two studies, the same trend between the strength of the hydrogen bond and the solvent polarity was observed. In their study, the hydrogen bond strength decreased linearly as the solvent polarity increased. The relationship found between the polarity and the strength of the hydrogen bond was different from the inverse relation that would be expected based on Coloumb law [43]. The difference between the experimental findings and the expected theoretical trend was attributed to a difference in the dielectric constant of the solvent at bulk and at molecular level, since the dielectric constant is a continuum concept.

The dependence of the hydrogen bond values on solvent polarity results from the dependence of van der Waals forces on solvent properties and also from the dependence of the rupture forces on solvent polarity. The effect of polarity on van der Waals forces was considered by calculating Hamaker constant in each solvent. Negative total Hamaker constant value was obtained in methanol and therefore repulsive van der Waals forces, while positive values for Hamaker constant were obtained in water and formamide and therefore attractive van der Waals forces. The negative value of total Hamaker constant in methanol was obtained since the Hamaker constant for the bacterial cell was higher than the Hamaker constant for the methanol. Negative values for Hamaker constant and therefore repulsive van der Waals forces are often occur between different types of polymers dissolved in organic solvents[43, 61]. Hamaker constant for the bacterial cell was calculated based on contact angle measurements and the value obtained (6.36×10^{-20} J) lies within the same range of Hamaker constants obtained for other bacterial strains types[7, 16].

6.4.3 Elasticity of the cell

The indentation of the tip in the bacterial surface was used to quantify the compliance of the bacterial surface. Young's Moduli values were calculated for the bacterial surface in different polar solvents. The bacterial surface was more rigid in methanol (2.2 ± 1.2 MPa) than water or formamide, where Young's Moduli of 0.6 ± 0.4 and 1.6 ± 0.9 MPa were observed for the two solvents, respectively. This result again supports our conceptual model that the biopolymers are more compressed on the bacterial surface in low polarity solvents. This compression of the polymer layer leads us to measure a more rigid surface.

The large standard deviation of the Young's Moduli reflects the heterogeneity of the bacterial surface, and has been observed for other types of samples. Large variations in estimated Young's moduli of aqueous gelatin gels submerged in dodecane, estimated by applying the Hertz model to AFM force data, were partially attributed to the structural in-homogeneity of the polymer network at length scales < 100 nm [75].

Young's moduli for *E. coli* JM109 in different solvents (1.6 ± 0.9 MPa to 2.2 ± 1.2 MPa) are in range of what others have measured on multiple locations of *Saccharomyces cerevisiae* MUCL 38475 yeast cells (0.6 ± 0.4 MPa to 6.1 ± 2.4 MPa) with AFM in water. Similarly, AFM measurements on *Shewanella oneidensis* yielded a Young's modulus of 0.3 Mpa. These Young's moduli values are 2-3 times lower than the magnitude known for peptidoglycan, the biomolecule that provides a rigid frame work to the cell wall [76]. The large difference observed between the measured Young's modulus on the cells and that of the peptidoglycan molecule is due to the action of the fluidity of the outer membrane in allowing the bacterium to react rapidly to the tip and congregate

reactive membrane macromolecules at points of contact with the tip. This fluidity action was missing when the Young's modulus was estimated for murein sacculi isolated from *E. coli* cells. A Young's modulus of 25 MPa was reported on collapsed murein sacculi isolated from *E. coli* K-12 in the hydrated state using AFM. The high value obtained for the elastic modulus on the peptidoglycan strands in the sacculus was in excellent agreement with theoretical calculations on peptidoglycan network [77]. Measurements on the proteinaceous sheath of the archaebacterium *Methanospirillum hungatei* GP1 gave young's modulus of 20 to 40 GPa using AFM [78].

6.4.4 Adhesion Models

The work of adhesion required to separate the tip from the bacterium was evaluated using DMT, and JKR models. According to both models, the work of adhesion is independent of the elastic properties of the two bodies and depends only on geometrical factors and the magnitude of adhesion forces. The main advantage of applying these models to AFM data to evaluate the work of adhesion is that few AFM data are required. In addition, although the these models are continuum-type theories, they can be used reasonably to predict the contact area at pull-off [39]. However, the main disadvantages that are associated with applying the adhesion models are that detailed information about the tip shape is needed [79], and the bond rupture probabilities are not known [80].

The JKR model predicted higher values for the work of adhesion than what the DMT model did in all solvents, as would be expected form their equations. Higher work of adhesion values were predicted in the lower polar solvent. The higher values may be due to that JKR model consider an effective area of contact between the tip and the cell at

high-applied forces while the DMT model assumes a zero value for the area of contact. The difference in the area allows more molecules to interact with the tip leading to a higher adhesion and hence higher work values. Although both models were used to calculate the work of adhesion, the DMT model was more appropriate to use for our case. This judgment on choosing the more appropriate model from the two models to describe the adhesion between the tip and the bacterium was based on the adhesion map constructed by Johnson et al [53]. Johnson et al. used the Mauges-Dugdale theory to construct an adhesion map with non-dimensional coordinates μ and p, where μ is the elasticity parameter (equation 6.20) defined as the ratio of elastic deformation resulting from adhesion to the effective range of surface forces and P ($F_L/\pi RW_{ad}$) as the load parameter defined as the ratio of the applied load to the adhesive force [53]. By calculating μ and p (Table 6.7), and the use of Johnson et al. map, DMT model was the best model to fit the adhesion in water and methanol, however, Hertz model was the best to describe the adhesion behavior in formamide. Although adhesive forces are present at all contact loads, at a sufficiently high load, the adhesive component may be neglected and the Hertz theory becomes applicable [53].

The applicability of the JKR and DMT models to evaluate the work of adhesion based on AFM measurement has been well investigated for different types of systems in literature [39, 48, 51, 72, 79, 81]. Examples on these systems are evaluation of the work of adhesion between a variety of functionalized tips and surfaces with (CH_3, OH, NH_2, COOH, and $CONH_2$) [79], and the work evaluated between SAMs monolayers of amino groups [48]. The work of adhesion values estimated between *E. coli* JM109 biopolymers and the silicon nitride tip are in good agreement with values reported for some systems

and very different from other systems. For instance, our values were two orders of magnitude higher than the values reported to separate interactions between fibronectin coated-tip and living cell surface of Balb/3T3 fibroblast. The separation work estimated based on AFM measurements and calculated with JKR theory was found to be 0.0069 ± 0.0045 mJ/m^2 [51]. However, values of work of adhesion reported between a wide range of possible combinations of self assembled monolayers were on the same order of magnitude to the obtained work of adhesion values for our system [79]. The large differences between the different estimated values for the work of adhesion between different studies go back to the fact that the work of adhesion is dependent on the radius of the tip. We calculated the work of adhesion based on an assumed tip radius of 250 nm. This assumption was justified since research demonstrated that these tips interact as spheres with radii between 100 and 400 nm [82, 83]. If the tip radius was replaced in our calculations for the work of adhesion by the manufacturer value of the nominal tip radius (30 nm), the reported values of the work of adhesion will increase almost by ten times. Another reason behind this variation in the reported values for the work of adhesion arises from a serious practical limitation in the JKR and Hertz theories. This limitation is that both these theories assume perfectly smooth surfaces while most particle surfaces are rough, and asperities as small as 1-2 nm can significantly lower their adhesion, but there is as yet no satisfactory theory for such real word situations [43].

Another advantage of JKR theory and DMT models lies in the ability of the models to estimate the magnitude of the surface energy of the substrate and compare that to contact angle measurements. The application of the JKR theory to evaluate the surface energy has been found to be correct to within about 25% to a variety of surfaces in vapors

or liquids and to be independent of the elastic modulus [43]. This is feasible for SAMs and defined systems but not for real biological systems. The main reason behind this inability of the JKR theory to estimate the surface energy of the bacterium is explained by the difficulty in determining the exact chemistry of the molecules and hence the molecular weight of the surface macromolecules on the bacterial surface and the heterogeneity of the bacterial surface biopolymers. For SAMs, the exact chemistry of the surfaces is usually well known.

Adhesion models can also be used to estimate the actual contact area between the tip and the bacterial surface biopolymers based on the AFM pull-off measurements. To evaluate the contact radius, Hertz model, and JKR theory were used. Both models take into account the effect of the loading forces, adhesion forces, geometrical factors, and the elastic properties of the two interacting bodies in the calculation of the actual radius of contact. The radius of contact was estimated in the presence of an external applied force. In the presence of an external force, both Hertz model and JKR model can be used to estimate a radius of contact, with the main difference between both of them theory being that the JKR theory takes into account the surface energy effect on the deformation of the interacting bodies while Hertz theory does not. Although the predicted values by both models were close to each other, higher values were reported with JKR theory. This is due to the fact that JKR theory includes the effect of the molecular interactions in addition to the loading force on deformation while Hertz theory considers the loading forces only. The radius of contact values was lowest in the lower polar solvent in all investigated models. When compared together, the radii values calculated when an external load is applied were close to the values that can be calculated based on the

projected area of the actual tip radius (250 nm) [82]. However these radii values are higher than what should be expected, since both JKR and Hertz models are applicable for $a << R$ [84].

The applicability of the JKR theory and Hertz model to estimate the contact area between adhering surfaces or non-adhering surface has been found to be in good agreement with experimentally measured values for the contact area [43].

6.5 GLOSSARY

A_{132}: Hamaker constant for interacting media (J)
a_{Hertz}: Radius of contact according to Hertz theory (nm)
A_{ii}: Individual hamaker constant of each component (J)
a_{JKR}: Radius of contact according to JKR theory under a load force (nm)
d: Cantilever vertical deflection(nm)
d_o: Deflection offset (nm)
E^*: Surface elastic constant of the bacterial surface (Pa)
e: Electric charge of interacting body 1 (Coulombs)
é: Electric charge of interacting body 1 (Coulombs)
E_1: Young's modulus of the tip (Pa)
E_2: Young's modulus of the bacteria (Pa)
E_H: Hydrogen bond energy (J)
$E_{v,Rough}$: van der Waals energy for rough surfaces (J)
E_v: van der Waals energy (J)
F: Adhesion force (nN)
f: Interaction force between two bodies in contact (nN)
F_{av}: Average adhesion force (nN)
F_{cone}: Indentation force for conical tip (nN)
F_e: Electrostatic force (nN)
F_H: Hydrogen bond force (nN)
F_i: Individual bond force (nN)
F_o: Non-specific force (nN)
F_{st}: Steric force (nN)
$F_{v, Rough}$: van der Waals force for rough surfaces (nN)
F_v: van der Waals force (nN)
h: Separation Distance (nm)
H_o: Closest separation distance used to estimate van der Waals forces (nm)
h_o: Offset in separation distance (nm)
K: Mean elastic modulus of contact (Pa^{-1})
k_1: Elastic constant of the tip (Pa^{-1})
k_2: Elastic constant of the bacteria (Pa^{-1})
K_B: Boltzmann Constant (1.381×10^{-23} J/K)
K_c: Cantilever spring constant (0.13 N/m)
k_v: A constant coefficient (1.817)
L_o: Brush thickness (nm)
l_o: Closest separation distance (1.57 A^o)
n: Number of occurrences of certain pull-off event
n_i: # of individual bonds
P: Load parameter in Johnson et al. map
R: Tip radius (nm)
R_c: Bacterial radius (nm)
rms: Root-mean square roughness of the bacterium (nm)
T: Temperature (298 K)
$W_{ad, DMT}$: Work of adhesion according to DMT theory (J/m^2)
$W_{ad, JKR}$: Work of adhesion according to JKR theory (J/m^2)

$W_{ad, Rigid}$: Work of adhesion according between two rigid surfaces (J/m^2)
Z: Depth of indentation (nm)
Z_o: Separation distance at pull-off (nm)
z: Separation distance between two interacting bodies (nm)
α: half opening angle of the conical tip (18^o)
Γ: Grafting density of the bacterial biopolymers ($molecules/m^2$)
γ_L^- : The electron-donor parameter of the Lewis acid-base surface tension component of the liquid (mJ/m^2)
γ_L : Total surface tension of liquid (mJ/m^2)
γ_L^+ : The electron-acceptor parameter of the Lewis acid-base surface tension component of the liquid (mJ/m^2)
γ_L^{LW} : Lifshitz- van der Waals surface tension component of the liquid (mJ/m^2)
γ_s^- : The electron-donor parameter of the Lewis acid-base surface tension component of the bacterium (mJ/m^2)
γ_s^+ : The electron-acceptor parameter of the Lewis acid-base surface tension component of the bacterium (mJ/m^2)
γ_s^{LW} : Lifshitz- van der Waals surface tension component of the bacterium(mJ/m^2)
δ: Indentation depth of the tip in the sample (nm)
δ_a: Closest approach distance according to Hertz model (nm)
ε: Dielectric constant of the solvent
θ: Contact angle
λ: Peak distance between aspirities (nm)
μ: Elasticity parameter in Johnson et al. map
μ_F: Mean of the adhesion forces (nN)
ν_1: Poisson ratio of the tip (0.22)
ν_2: Poisson ratio of the bacteria (0.5)
σ^2_F: variance of the adhesion force (nN^2)

6.6 Figure Captions

Figure 6.1. Schematic diagrams to explain the adhesion models behavior. A) Contact between rigid sphere and rigid flat plate. B) Interaction between elastic rigid sphere and elastic flat plate in the absence of adhesion and in the presence of and external load (Hertz theory). C) Adhesion between rigid sphere and elastic flat plate in the presence of both molecular adhesion and an external load (JKR theory). D) The rigid sphere after separated from the elastic flat plate (after being in an adhesive contact).

Figure 6.2. A) An example on a cantilever deflection-distance curve measured in formamide. B) The corresponding force-indentation curve to the cantilever deflection-distance curve in A. The solid line is the best fit obtained by applying Hertz model to the force-indentation curves to estimate the Young's modulus of the cell (E = 2.99 MPa, R^2 = 0.99).

Figure 6.3. A) A summary of the pull-off forces measured during tip retraction from the bacterium between *E. coli* JM109 cells biopolymers and silicon nitride AFM tips in all solvents. B) The histogram of the pull-off forces in formamide. C) The histogram of the pull-off forces in water. D) The histogram of the pull-off forces in methanol.

Figure 6.4. Symbols are the average of 15 approach curves measured between *E. coli* JM109 and AFM silicon nitride tip in formamide, water, and methanol. Solid lines are the fitting results of applying the steric model to the approach curves (equation 6.26). The fitting parameters used are summarized in Table 6.3.

Figure 6.5. The inverse of the dielectric constant as a function of different microscopic bacterial surface properties. A) As a function of the average adhesion force, R^2 =1. B) As

a function of the brush thickness, R^2 = 0.92. C) As a function of the bacterial surface biopolymers grafting density$^{1.5}$, R^2 = 0.98.

Figure 6.6. Statistical Poisson distribution used to represent the histogram of the distribution of adhesion affinities between the AFM tip and the bacterial surface biopolymers in formamide, R^2 = 0.92.

Figure 6.7. The linear relations between the mean and the variance of the pull-off forces in different solvents. The experimental data points are pairs of the variance and the mean of the pull-off force measurements in different solvents. The solid lines are the linear regression fits to the experimental data. A) In formamide. B) In water. C) In methanol.

Figure 6.8. The relation between the specific and non-specific forces estimated using Poisson method for the interactions between *E. coli* JM109 and the silicon nitride tip in all solvents. The linear regression relationship obtained between the two forces is Y = 0.28 X-0.37, R^2 = 0.98.

6.7 References

1. Dufrêne, Y.F., C.J.P. Boonaert, H.C. van der Mei, H.J. Busscher, and P.G. Rouxhet, *Probing molecular interactions and mechanical properties of microbial cell surfaces by atomic force microscopy.* Ultramicroscopy, 2001. **86**: p. 113-120.
2. Razatos, A., Y.-L. Ong, M.M. Sharma, and G. Georgiou, *Evaluating the interaction of bacteria with biomaterials using atomic force microscopy.* Journal of Biomaterials Science Polymer Ed., 1998. **9**: p. 1361-1373.
3. Dufrêne, Y.F., *Application of atomic force microscopy to microbiological surfaces: from reconstituted cell surface layers to living cells (Review).* Micron, 2001. **32**: p. 152-165.
4. Abu-Lail, N.I. and T.A. Camesano, *Elasticity of Pseudomonas putida KT2442 biopolymers probed with single-molecule force microscopy.* Langmuir, 2002. **18**: p. 4071-4081.
5. Touhami, A., B. Nysten, and Y.F. Dufrene, *Nanoscale mapping of the elasticity of microbial cells by AFM.* Langmuir, 2003. **19**: p. 4539-4543.
6. Camesano, T.A. and N.I. Abu-Lail, *Heterogeneity in bacterial surface polysaccharides, probed on a single-molecule basis.* Biomacromolecules, 2002. **3**(661-667).
7. Camesano, T.A. and B.E. Logan, *Probing bacterial electrosteric interactions using atomic force microscopy.* Environmental Science & Technology, 2000. **34**: p. 3354-3362.

8. Simoni, S.F., H. Harms, T.N.P. Bosma, and A.J.B. Zehnder, *Population heterogeneity affects transport of bacteria through sand columns at low flow rates.* Environmental Science & Technology, 1998. **32**: p. 2100-2105.

9. Williams, V. and M. Fletcher, *Pseudomonas fluorescens adhesion and transport through porous media are affected by lipopolysaccharide composition.* Applied and Environmental Microbiology, 1996. **62**: p. 100-104.

10. Hendricks, S.K., C. Kwok, M. Shen, T.A. Horbett, B.D. Ratner, and J.D. Bryers, *Plasma-deposited Membranes for Controlled Release of Antibiotic to Prevent Bacterial Adhesion and Biofilm Formation.* Journal of Biomedical Materials Research, 2000. **50**: p. 160-170.

11. Truskey, G.A. and T.L. Proulx, *The effect of fluid shear stress upon cell adhesion to fibronectin treated surfaces.* Journal of Biomedical Materials Research, 1990. **24**: p. 1333-1353.

12. Wattiau, P., *Microbial aspects in bioremediation of soils polluted by polyaromatic hydrocarbons.* Focus on Biotechnology, 3A(Biotechnology for the Environment: Strategy and Fundamentals), 2002: p. 69-89.

13. Dawson, D.J. and D.P. Sartory, *Microbiology safety of water.* British Medical bulletin, 2000. **56**(1): p. 74-83.

14. Dunkirk, S.G., S.L. Gregg, L.W. Duran, J.D. Monfils, J.E. Haapala, J.A. Marcy, D.L. Clapper, R.A. Amos, and P.E. Guire, *Photochemical coatings for the prevention of bacterial colonization.* Journal of Biomaterials Applications, 1991. **6**(2): p. 131-156.

15. Bundy, K., U. Schlegel, B. Rahn, V. Geret, and S. Perren, *An improved peel test method for measurement of adhesion to biomaterials.* Journal of Materials Science: Materials in Medicine, 2000. **11**(8): p. 517-521.

16. Abu-Lail, N.I. and T.A. Camesano, *The role of lipopolysaccahrides in the adhesion, retention, and transport of E.coli JM109.* Environmental Science & Technology, 2003. **37**: p. 2173-2183.

17. Abu-Lail, N.I. and T.A. Camesano, *Role of ionic strength on the relationship of biopolymer conformation, DLVO contributions, and steric interactions to bioadhesion of pseudomonas putida KT2442.* Biomacromolecules, 2003. **4**(4): p. 1000-1012.

18. DEFlaun, M.F., S.R. Oppenheimer, S. Streger, C.W. Condee, and M. Flethcher, *Alterations in adhesion, transport, and membrane characteristics in an adhesion-deficient Pseudomonas.* Applied and Environmental Microbiology, 1999. **65**(2): p. 759-765.

19. Dan, N., *The effect of charge regulation on cell adhesion to substrates:salt - induced repulsion.* Colloids and Surfaces B: Biointerfaces, 2003. **27**: p. 41-47.

20. Ahimou, F., F.A. Denis, A. Touhami, and Y.F. Dufrene, *Probing microbial cell surface charges by atomic force microscopy.* Langmuir, 2002. **18**(25): p. 9937-9941.

21. Baygents, J.C., J. Glynn, J. R., O. Albinger, B.K. Biesewmeyer, K.L. Ogden, and R.G. Arnold, *Variation of surface charge density in monoclonal bacterial populations: implications for transport through porous media.* Environmental Science & Technology, 1998. **32**: p. 1596-1603.

22. Poortinga, A.T., R. Bos, and H.J. Busscher, *Measurement of charge transfer during bacterial adhesion to an indium tin oxide surface in a parallel plate flow chamber.* Journal of Microbiological Methods, 1999. **38**: p. 183-189.

23. Camesano, T.A. and B.E. Logan, *Influence of fluid velocity and cell concentration on the transport of motile and non-motile bacteria in porous media.* Environmental Science & Technology, 1998. **34**: p. 2254-3362.

24. Camper, A.K., J.T. Hayes, P.J. Sturman, W.L. Jones, and A.B. Cunningham, *Effects of motility and adsorption rate coefficient on transport of bacteria through saturated porous media.* Applied and Environmental Microbiology, 1993. **59**: p. 3455-3462.

25. Korber, D.R., J.R. Lawrence, and D.E. Caldwell, *Effect of motility on surface colonization and reproductive success of Pseudomonas fluorescens in dual-dilution continuous culture and batch culture systems.* Applied and Environmental Microbiology, 1994. **60**: p. 1421-1429.

26. Witt, M.E., M.J. Dybas, R.M. Worden, and C.S. Criddle, *Motility-enhanced bioremediation of carbon tetrachloride-contaminated aquifer sediments.* Environmental Science & Technology, 1999. **33**: p. 2958-2964.

27. Pohlmann-Dietze, P., M. Ulrich, K.B. Kiser, G. Doring, J.C. Lee, J.-M. Fournier, K. Botzenhart, and C. Wolz, *Adherence of Staphylococcus aureus to endothelial cells: influence of capsular polysaccharide, global regulator agr, and bacterial growth phase.* Infection and Immunity, 2000. **68**(9): p. 4865-4871.

28. Usters, J.G., G.A.W.M. Mulders-Kremers, C.E.M. van Doornik, and B.A.M. van der Zeijst, *Effects of multiplicity of infection, bacterial protein synthesis, and*

growth phase on adhesion to and invasion of human cell lines by Salmonella typhimurium. Infection and Immunity, 1993. **61**(12): p. 5013-5020.

29. Vadillo-Rodriguez, V., H.J. Busscher, W. Norde, J. de Vries, and H.C. van der Mei, *On relations between microscopic and macroscopic physiochemical properties of abcterial cell surfaces: An AFM study on Streptococcus mitis strains.* Langmuir, 2003. **19**: p. 2372-2377.

30. Hanna, A., M. Berg, V. Stout, and A. Razatos, *Role of capsular colanic acid in adhesion of uropathogenic Escherichia coli.* Appl. Environ. Microbiol., 2003. **69**(8): p. 4474-4481.

31. Hoh, J.H., J.P. Cleveland, C.B. Prater, J.-P. Revel, and P.K. Hansma, *Quantized adhesion detected withAFM.* J. Am. Chem. Soc., 1992. **114**: p. 4917-4918.

32. Lee, G.U., D.A. Kidwell, and R.J. Colton, *Sensing discrete streptavidin-biotin interactions with atomic force microscopy.* Langmuir, 1994. **10**: p. 354-357.

33. Moy, V., T., E.-L. Florin, and H.E. Gaub, *Intermolecular forces and energies between ligands and receptors.* Science, 1994. **266**: p. 257-259.

34. Williams, J.M., T. Han, and J.T.P. Beebe, *Determination of single-bond forces from contact force variances in AFM.* Langmuir, 1996. **12**: p. 1291-1295.

35. Lo, Y.-S., N.D. Huefner, W.S. Chan, F. Stevens, J.M. Harris, and J.T.P. Beebe, *Specific interactions between biotin and avidin studied by AFM using the Poisson statistical analysis method.* Langmuir, 1999. **15**: p. 1373-1382.

36. Lo, Y.-S., Y.-J. Zhu, and J.T.P. Beebe, *Loading-rate dependence of individual ligand-receptor bond-rupture forces studied by AFM.* Langmuir, 2001. **17**: p. 3741-3748.

37. Wenzler, L.A., G.L. Moyes, G.N. Raikar, R.L. Hansen, J.M. Harris, J.T.P. Beebe, L.D. Wood, and S.S. Saavedra, *Measurements of single-molecule bond-rupture forces between self-assembled monolayers of organosilanes with the atomic force microscope.* Langmuir, 1997. **13**: p. 3761-3768.

38. Wenzler, L.A., G.L. Moyes, L.G. Olson, J.M. Harris, and T.B. Beebe, *Single-Molecule Bond-rupture force analysis of interactions between AFM tips and substrates modified with organosilanes.* Anal. Chem., 1997. **69**(14): p. 2855-2861.

39. Stevens, F., Y.-S. Lo, J.M. Harris, and J.T.P. Beebe, *Computer modeling of AFM force measurements: comparisons of Poisson, histogram, and continuum methods.* Langmuir, 1999. **15**: p. 207-213.

40. Han, T., J.M. Williams, and J.T.P. Beebe, *Chemical bonds studied with functionalized AFM tips.* Analytica Chimica Acta, 1995. **307**: p. 365-376.

41. Johnson, K.L., K. Kendall, and A.D. Roberts, *Surface energy and the contact of elastic solids.* Proc. R. Soc. London A, 1971. **324**: p. 301-313.

42. Derjaguin, B.V., V.M. Muller, and Y.P. Toporov, *Effect of contact dimensions on the adhesion of particles.* Journal of Colloid and Interface Science, 1975. **53**(2): p. 314-326.

43. Israelachvili, J.N., *Intermolecular & Surface Forces (2nd edition)*. 1992, New York: Academic Press.

44. Muller, V.M., V.S. Yushchenko, and B.V. Derjaguin, *On the influence of molecular forces on the deformation of an elastic sphere and its sticking to a rigid plane.* Journal of Colloid and Interface Science, 1980. **77**(1): p. 91-101.

45. Johnson, K.L., *Contact Mechanics*. 1985, Cambridge: Cambridge University Press.

46. Cleveland, J.P., S. Manne, D. Bocek, and P.K. Hansma, *Nondestructive method for determining the spring constant of cantilevers for scanning force microscopy.* Review of Scientific Instruments, 1993. **64**: p. 403-405.

47. Camesano, T.A. and B.E. Logan, *Imaging modified bacterial cells using atomic force microscopy.* Langmuir, 2000. **16**: p. 4563-4572.

48. Wei, Z.Q., C. Wang, C.F. Zhu, C.Q. Zhou, B. Xu, and C.-L. Bai, *Study on single-bond interaction between amino-terminated organosilane self-assembled monolayers by AFM.* Surface Science, 2000. **459**: p. 401-412.

49. Barlow, R.J., *Statistics. A guide to the use of statistical methods in physical sciences*. 1989, New York: Wiley.

50. Tabor, D., *Surface Forces and Surface Interactions.* Journal of Colloid and Interface Science, 1977. **58**(1): p. 2-13.

51. Hyonchol, K., H. Arakawa, T. Osada, and A. Ikai, *Quantification of fibronectin and cell surafce interactions by AFM.* Colloids and Surfaces B: Biointerfaces, 2002. **25**: p. 33-43.

52. Derjaguin, B.V., Kolloid Z., 1934. **69**: p. 155.

53. Johnson, K.L. and J.A. Greenwood, *An adhesion map for the contact of elastic spheres.* Journal of Colloid and Interface Science, 1997. **192**: p. 326-333.

54. Patrick, D.L., J.F. Flanagan, P. Kohl, and R.M. Lynden-Bell, *Atomistic molecular dynamics simulations of chemical force microscopy.* Journal of the American Chemical Society, 2003. **125**: p. 6762-6773.

55. Tabor, D., Journal of Colloid and Interface Science, 1976. **58**: p. 1.

56. Muller, V.M., B.V. Derjaguin, Y.P. Toporov, and P. Yu, Colloids and Surfaces, 1983. **7**: p. 251.

57. Greenwood, J.A. and K.L. Johnson, Phil. Mag. A, 1981. **43**: p. 697.

58. Maugis, D. and M. Barquins, Journal of Applied Physics D. Applied Physics, 1978. **11**: p. 1989.

59. Grasso, D., B.F. Smets, K.A. Strevett, D.B. Machinist, C.J. van Oss, R.F. Giese, and W. Wu, *Impact of physiological state on surface thermodynamics and adhesion of Pseudomonas aeruginosa.* Environmental Science & Technology, 1996. **30**: p. 3604-3608.

60. Morrow, J.B., B.F. Smets, and D. Grasso, *Perceived substratum characterestics as a function of AFM probe and imaging fluid properties.* Langmuir, 2003. **19**(15): p. 6151-6159.

61. van Oss, C.J., *Interfacial Forces in Aqueous Media*. 1994, New York: Marcel Dekker.

62. Rabinovich, Y.I., J.J. Adler, A. Ata, R.K. Singh, and B.M. Moudgil, *Adhesion between nanoscale rough surfaces 1. Role of Asperity Geometry.* Journal of Colloid and Interface Science, 2000. **232**: p. 10-16.

63. Rabinovich, Y.I., J.J. Adler, A. Ata, R.K. Singh, and B.M. Moudgil, *Adhesion between nanoscale rough surfaces 2. Measurement and Comparison with Theory.* Journal of Colloid and Interface Science, 2000. **232**: p. 17-24.

64. Alexander, S., *Adsorption of chain molecules with a polar head a scaling description.* Journal de Physique (Paris), 1977. **38**(8): p. 983-987.

65. de Gennes, P.G., *Polymers at an interface: A simplified view.* Advances in Colloid and Interface Science, 1987. **27**: p. 189-209.

66. Butt, H.-J., M. Kappl, H. Mueller, and R. Raiteri, *Steric forces measured with the atomic force microscope at various temperatures.* Langmuir, 1999. **15**: p. 2559-2565.

67. Rabinovich, Y.I., J.J. Adler, A. Ata, R.K. Singh, and B.M. Moudgil, *Adhesion between nanoscale rough surfaces I. Role of asperity geometry.* Journal of Colloid and Interface Science, 2000. **232**: p. 10-16.

68. Rabinovich, Y.I., J.J. Adler, A. Ata, R.K. Singh, and B.M. Moudgil, *Adhesion between nanoscale rough surfaces II. Measurement and comparison with theory.* Journal of Colloid and Interface Science, 2000. **232**: p. 17-24.

69. Sanderson, R.T., *Polar Covalence*. 1983, New York: Academic Press.

70. Oesterhelt, F., M. Rief, and H.E. Gaub, *Single molecule force spectroscopy by AFM indicates helical structure of poly(ethylene-glycol) in water.* New Journal of Physics, 1999. **1**: p. 6.1-6.11.

71. Smyth, C.P., *Dielectric Constant and Molecular Structure*. Monograph Series, ed. A.C. Society. 1931, New York: The Chemical Cataloge Company, Inc. 214.

72. Skulason, H. and C.D. Frisbie, *Direct detection by AFM of single bond forces associated with the rupture of discrete charge-transfer complexes.* J. Am. Chem. Soc., 2002. **124**: p. 15125-15133.

73. Amro, N.A., L.P. Kotra, K. Wadu-Mesthridge, A. Bulychev, S. Mobashery, and G. Liu, *High resolution imaging atomic force microscopy studies of Escherichia*

coli outer membrane: Structural basis for permeability. Langmuir, 2000. **16**: p. 2789-2796.

74. Phillips, N.J., T.J. Miller, J.J. Engstrom, W. Melaugh, R. McLaughlin, M.A. Apicella, and B.W. Gibson, *Characterization of chimeric LPS from E. coli strain JM109 Transformed with lipooligasaccharide synthesis genes (lsg) from Haemophilus influenzae.* The Journal of Biological Chemistry, 2000. **275**(7): p. 4747-4758.

75. Uricanu, V.I., M.H.G. Duits, R.M.F. Nelissen, M.L. Bennink, and J. Mellema, *Local Structure and Elasticity of Soft Gelatin Gels Studied with AFM.* Langmuir, 2003: p. In Press.

76. Lower, S.K. and M.F.J. Hochella. *nanoforce and nanomechanical measurements between living microorganisms and minerlas surfaces: evidence of specific biomolecule-mineral recognition.* in *Eleventh Annual V.M. Goldschmidt Conference*. 2001.

77. Yao, X., M. Jericho, D. Pink, and T. Beveridge, *Thickness and elasticity of gram-negative murein sacculi measured by atomic force microscopy.* Journal of Bacteriology, 1999. **181**(22): p. 6865-6875.

78. Xu, W., P.J. Mulhern, B.L. Blackford, M.H. Jericho, M. Firtel, and T.J. Beveridge, *Modeling and measuring the elastic properties of an archael surface, the sheath of Methanospirillum hungatei, and the implication for methane production.* Journal of Bacteriology, 1996. **178**: p. 3106-3112.

79. van der Vegte, E.W. and G. Hadziioannou, *Scanning force microscopy with chemical specificity: An extensive study of chemical specific tip-surface*

interactions and the chemical imaging of surafce functional groups. Langmuir, 1997. **13**(16): p. 4357-4368.

80. Thomas, R.C., J.E. Houston, R.M. Crooks, T. Kim, and T.A. Michalske, *Probing adhesion forces at the molecular scale.* J. Am. Chem. Soc., 1995. **117**: p. 3830-3834.

81. Skulason, H. and C.D. Frisbie, *Contact mechanics modeling of pull-off measurements: effect of solvent, probe radius, and chemical binding probability on the detection of single-bond rupture forces by AFM.* Anal. Chem., 2002. **74**: p. 3096-3104.

82. Drummond, C.J. and T.J. Senden, *Examination of the geometry of long-range tip-sample interaction in atomic force microscopy.* Colloids and Surfaces A: Physicochemical and Engineering Aspects, 1994. **87**: p. 217-234.

83. Senden, T.J. and C.J. Drummond, *Surface chemistry and tip-sample interactions in atomic force microscopy.* Colloids and Surfaces A: Physicochemical and Engineering Aspects, 1994. **94**: p. 29-51.

84. Schwartz, U.D., *A generalized analytical model for the elastic deformation of an adhesive contact between a sphere and a flat surface.* Journal of Colloid and Interface Science, 2003. **261**: p. 99-106.

85. Lide, D.R., *CRC Handbook of Chemistry and Physics*. 77 ed, ed. H.P.R. Frederikse. 1996, New York: CRC Press.

Table 1. Contact Angle Measurements on *E. coli* JM109

Solvent	Contact Angle (θ)	N[a]
Formamide	43.0 ± 1.9	41
Water	17.0 ± 3.8	21
Diiodomethane	50.1 ± 1.0	41

[a] N is the number of contact angle measurements averaged in the reported value

Table 2. Young's Moduli for *E. coli* JM109

Solvent	E (MPa)	R^2
Formamide	1.6 ± 0.9	0.99
Water	0.6 ± 0.4	0.98
Methanol	2.2 ± 1.2	0.71

Table 3. Correlation of Bacterial Surface Properties Obtained from Interaction Force Measurements with Solvent Properties

Solvent	ε [85]	Slope of Compliance Region (nN/nm)	L_o[a] (nm)	Γ[b] (Mol./m^2)	R^2	# of polymers interacting with the tip[c]	Z[d] (nm)	F_L[e] (nN)
Formamide	111	-0.08	546	2.51×10^{15}	0.99	7	242.8	170.2
Water	80.1	-0.06	331	2.68×10^{15}	0.99	8	133.3	25.9
Methanol	33	-0.15	44	7.27×10^{15}	1.0	21	19.4	5.26

[a,b] Fitting parameters obtained by applying equation 26 to the AFM approach curves. [c] This # is calculated based on multiplying the total number of molecules on the cell surface ($\Gamma^* 4\pi R_c^2$) by the ratio of the tip area (πR^2) to the cell surface area. The cell radius R_c was taken as 0.5 μm and the tip radius R was considered as 30 nm (supplied by manufacturer). [d] Z is measured from the approach curve as described in [51]. [e] F_L is estimated based on Hertz model (Equation 15) using the indentation depth Z.

Table 4. Summary of Adhesion Forces Measured by AFM

Solvent	Cell	Avg. F nN	Stdev F nN	Variance F nN^2	Set Size*
Formamide	1	-0.79	0.03	0.00	2
	2	-1.81	1.01	1.01	15
	3	-0.78	0.22	0.05	8
	4	-0.84	0.35	0.13	6
	5	-0.86	0.43	0.19	10
	All	-1.18	0.81		41
Water	1	-2.59	0.93	0.87	8
	2	-1.76	0.81	0.65	21
	3	-0.75	0.27	0.07	5
	4	-0.64	0.30	0.09	4
	5	-0.82	0.45	0.20	4
	All	-1.6	0.97		42
Methanol	1	-2.35	1.53	2.35	13
	2	-6.03	4.32	18.68	3
	3	-2.21	1.77	3.14	12
	4	-2.08	0.87	0.76	46
	5	-1.33	0.46	0.21	3
	6	-1.40	0.50	0.25	3
	7	-1.34	0.35	0.12	4
	All	-2.19	1.5		84

* The number of adhesion peaks observed in three to five force curves measured on each bacterial cell.

Table 5. Summary of Calculated Parameters Based on Fitting Poisson Distribution to Adhesion Force Data

Solvent	Specific Force (F_i) (nN)	Intercept ($-F_iF_o$) (nN^2)	Non-specific interactions (F_o) (nN)	R^2
Formamide	-0.94	0.68	-0.72	0.99
Water	-0.42	0.18	-0.42	0.97
Methanol	-4.0	5.93	-1.48	0.98

Table 6: Summary of Forces and Energies in Different Solvents

Solvent	δ (nm)	A_{132} (J)	F_v (nN)	E_v (J)	F_e^* (nN)	E_v (mJ/m^2)	F_H (nN)	E_H (mJ/m^2)
Formamide	27.3	2.16×10^{-20}	-1.65	-7.5×10^{-20}	0	-4.8	2.6	0.51
Water	152.2	3.80×10^{-20}	-4.71	-2.4×10^{-19}	0.013	-21.2	5.1	0.69
Methanol	224.8	-8.49×10^{-21}	0.47	2.1×10^{-20}	0	0.09	3.5	0.93

* This value is calculated by assuming the water salt concentration as 0.0027 M, the tip and the bacterial surface potentials as -0.016 V and -0.0267 V, respectively [16].

Table 7. Summary of the adhesion map parameters constructed by Johnson et al. [53]

Solvent	P (DMT)	μ (DMT)	Model	P (JKR)	μ (JKR)	Model
Formamide	285	0.01	Hertz	215	0.02	Hertz
Water	32.3	0.02	DMT	24.2	0.03	DMT
Methanol	4.82	0.02	DMT	3.6	0.02	Rigid

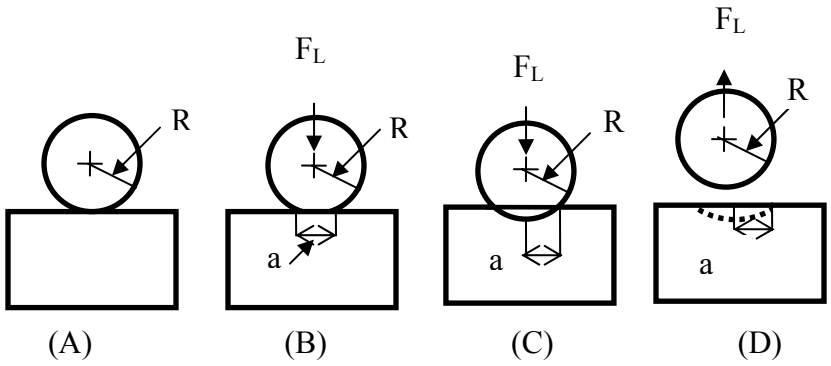

Figure 6.1

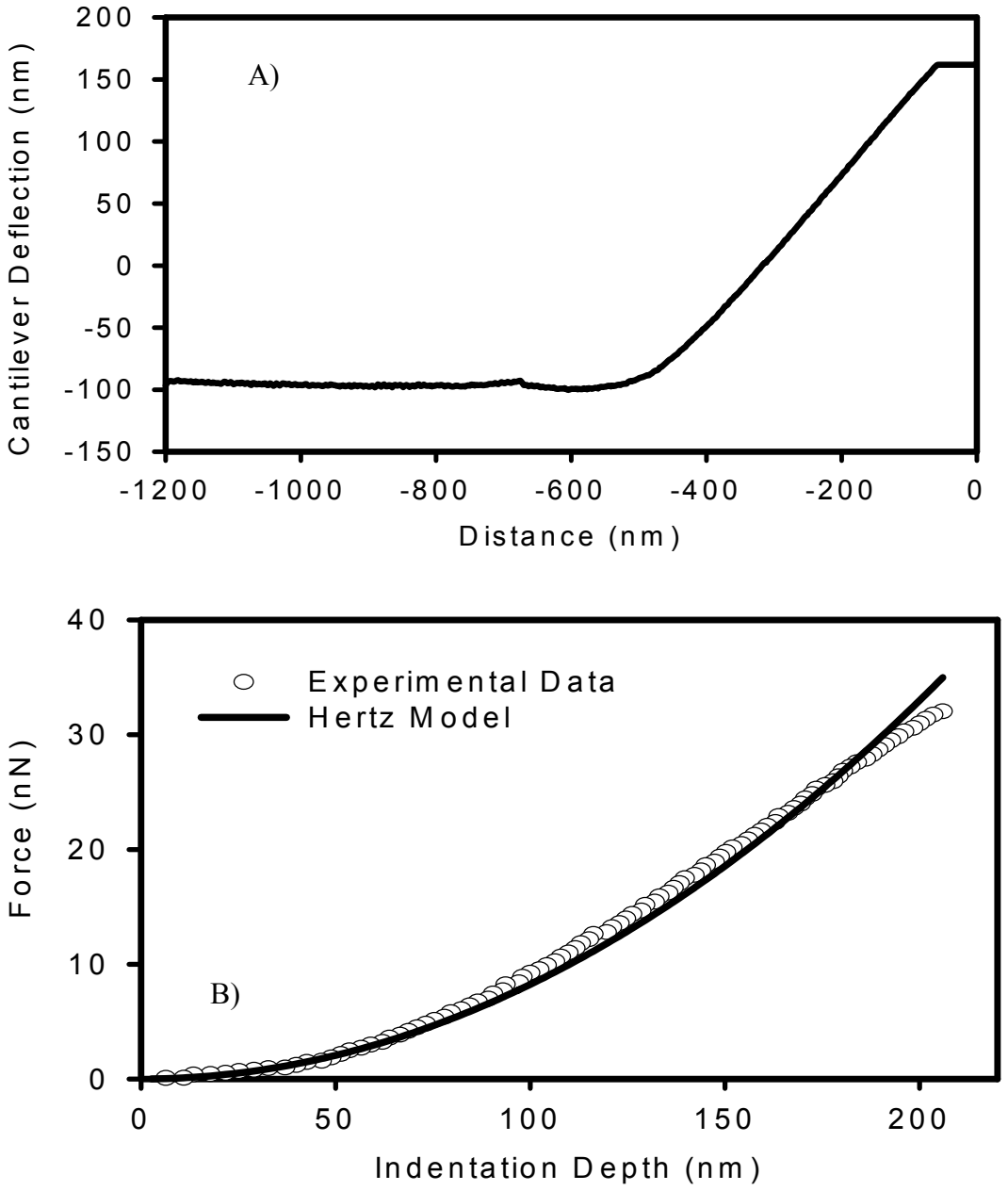
A)
Cantilever Deflection (nm)
200
150
100
50
0
-50
-100
-150
-1200
-1000
-800
-600
-400
-200
0
Distance (nm)
B)
Experimental Data
Hertz Model
Force (nN)
40
30
20
10
0
0
50
100
150
200
Indentation Depth (nm)

Figure 6.2

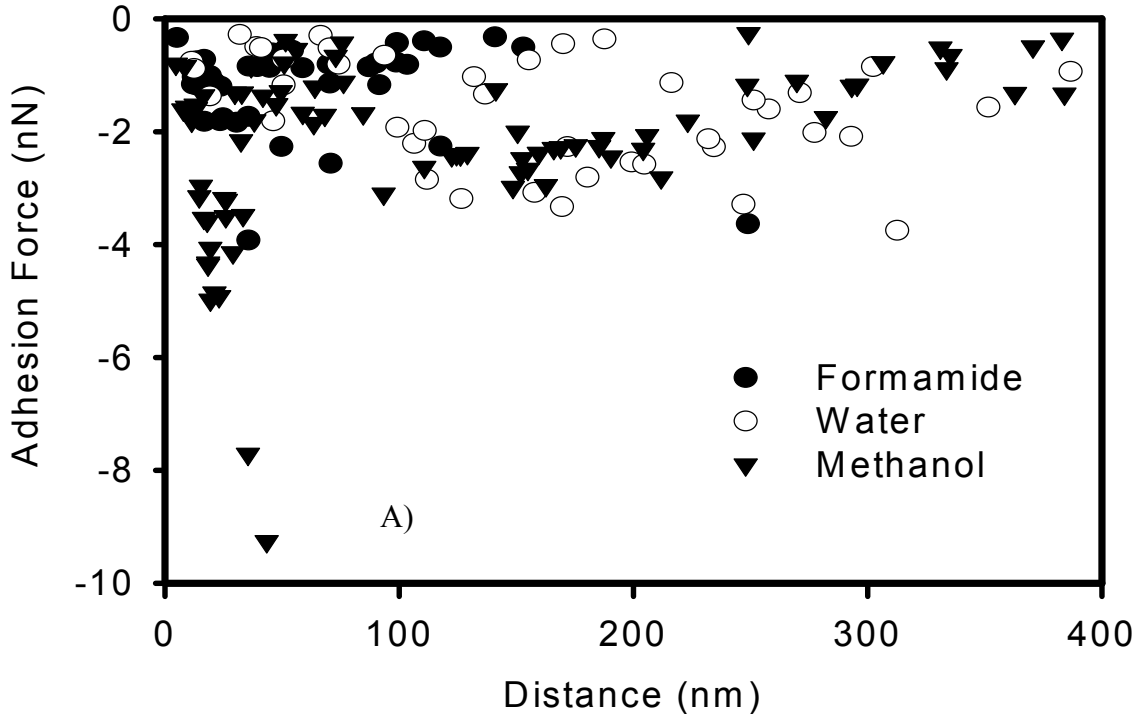
0
-2
-4
-6
-8
-10
Adhesion Force (nN)
0
100
200
300
400
Distance (nm)
Formamide
Water
Methanol
A)

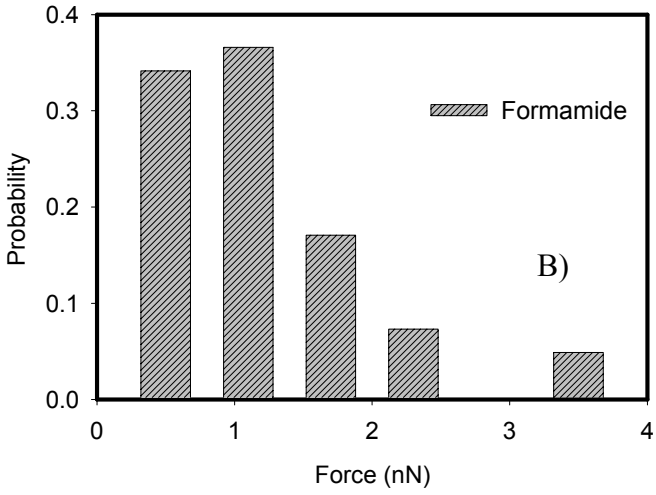
0.4
0.3
0.2
0.1
0.0
Probability
Formamide
B)
0
1
2
3
4
Force (nN)

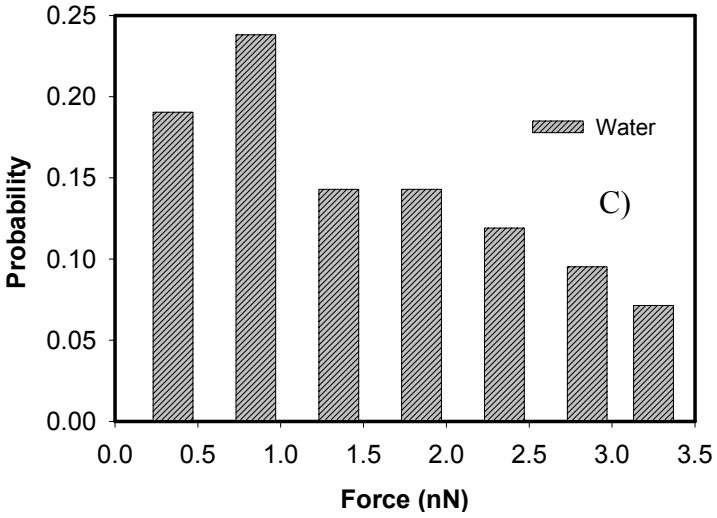
0.25
0.20
0.15
0.10
0.05
0.00
Probability
Water
C)
0.0
0.5
1.0
1.5
2.0
2.5
3.0
3.5
Force (nN)

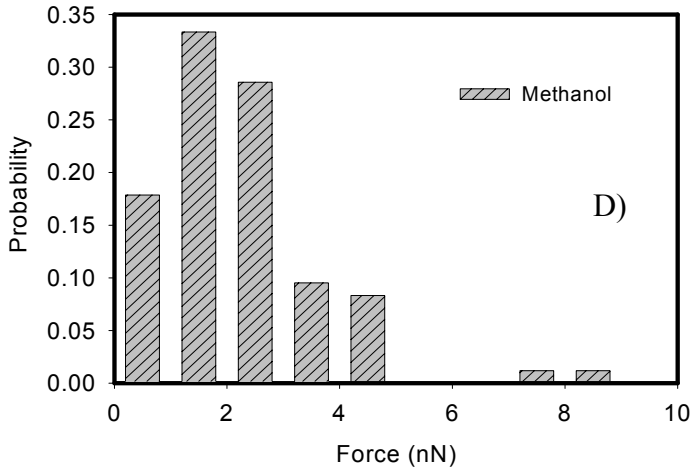
0.35
0.30
0.25
0.20
0.15
0.10
0.05
0.00
Probability
Methanol
D)
0
2
4
6
8
10
Force (nN)

Figure 6.3

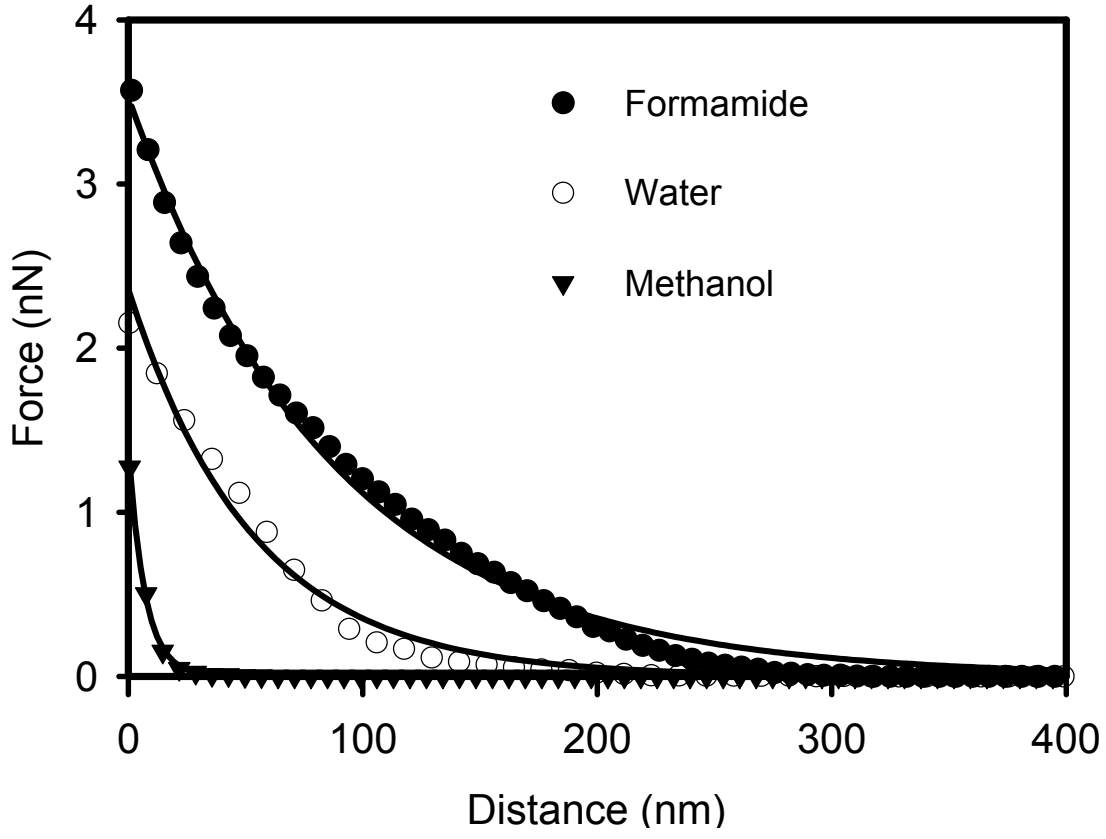
4
3
2
1
0
Force (nN)
0
100
200
300
400
Distance (nm)
Formamide
Water
Methanol

Figure 6.4

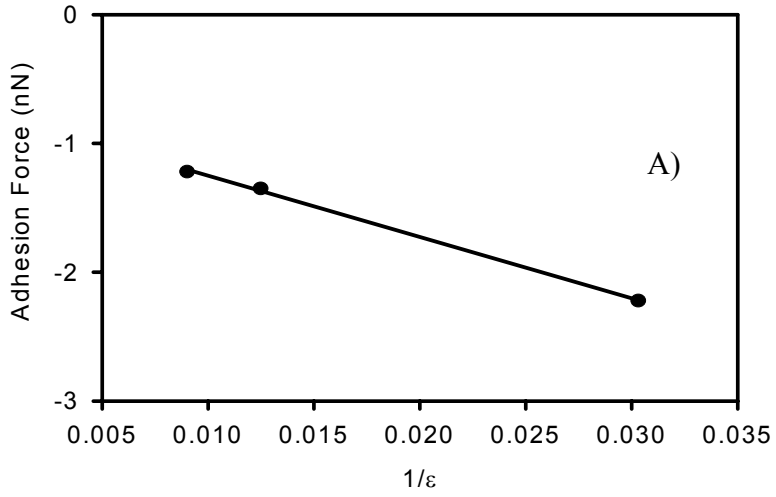
0
-1
-2
-3
Adhesion Force (nN)
A)
0.005
0.010
0.015
0.020
0.025
0.030
0.035
1/ε

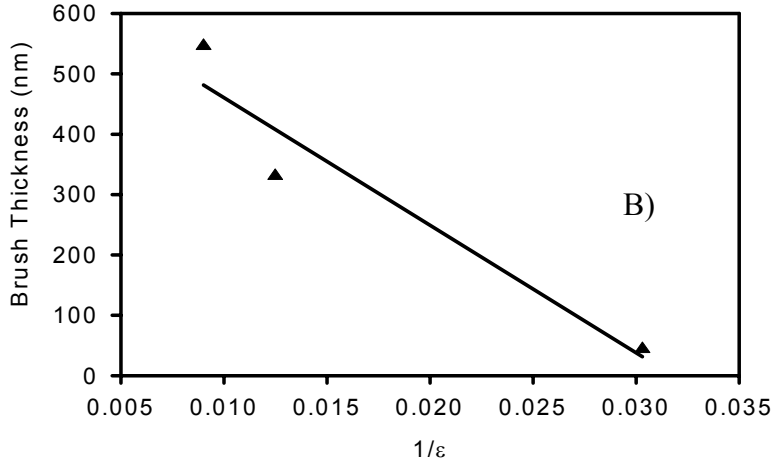
600
500
400
300
200
100
0
Brush Thickness (nm)
B)
0.005
0.010
0.015
0.020
0.025
0.030
0.035
1/ε

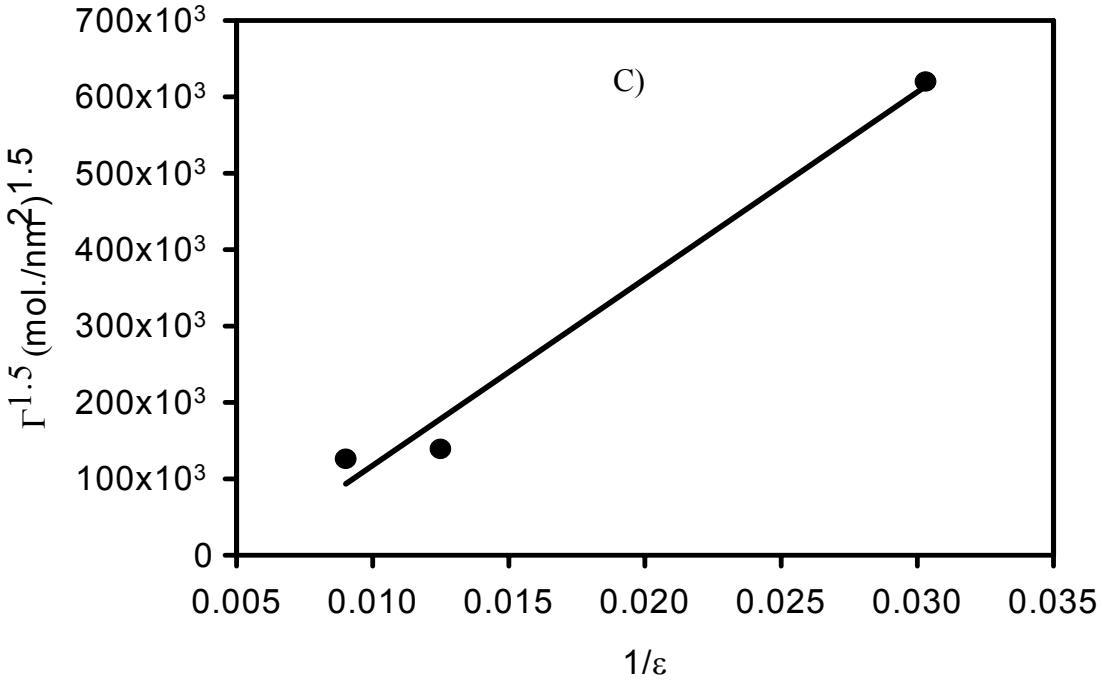
C)
700x10³
600x10³
500x10³
400x10³
300x10³
200x10³
100x10³
0
Γ^1.5 (mol./nm²)^1.5
0.005
0.010
0.015
0.020
0.025
0.030
0.035
1/ε

Figure 6.5

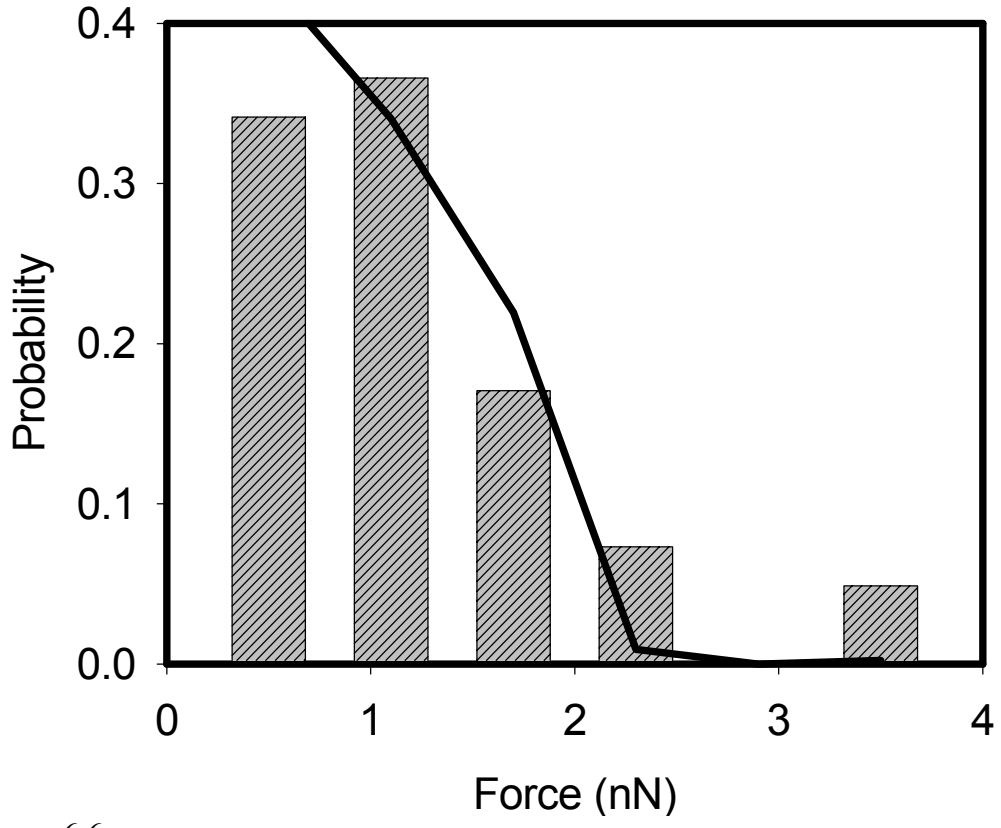

Figure 6.6

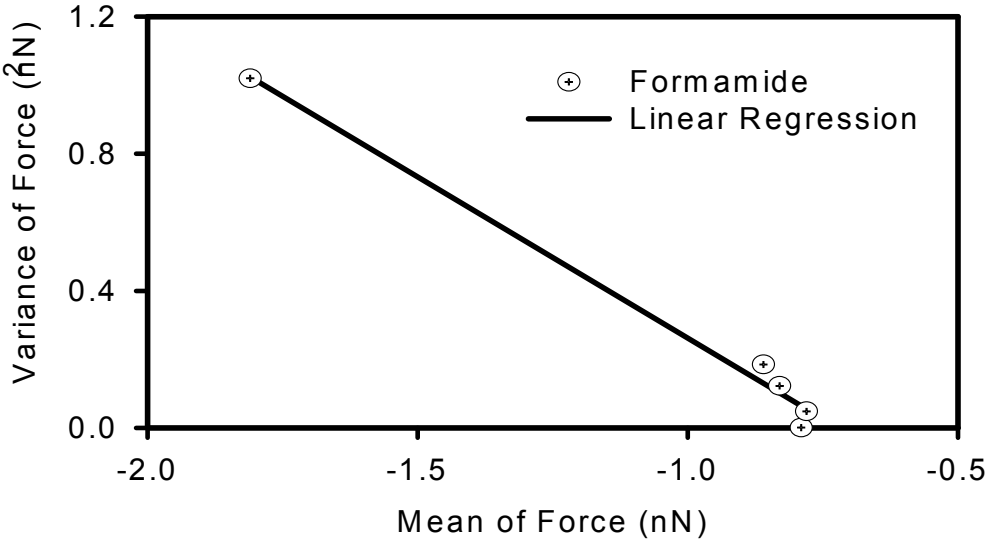
Variance of Force (nN)2
1.2
0.8
0.4
0.0
-2.0
-1.5
-1.0
-0.5
Mean of Force (nN)
Formamide
Linear Regression

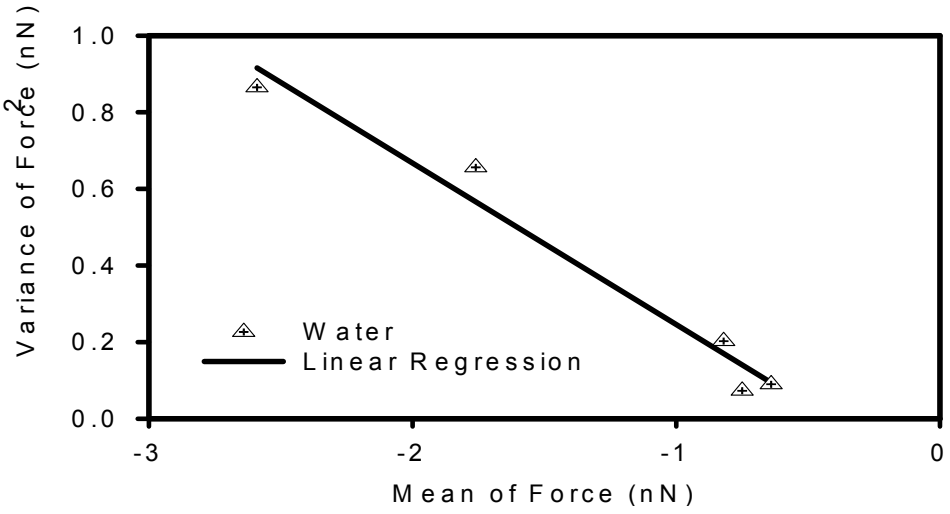
Variance of Force (nN)2
1.0
0.8
0.6
0.4
0.2
0.0
-3
-2
-1
0
Mean of Force (nN)
Water
Linear Regression

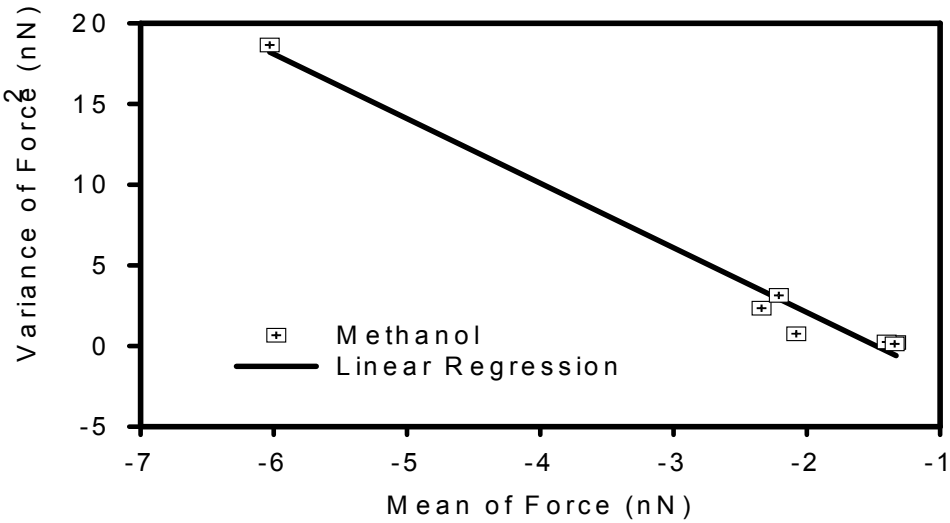
Variance of Force (nN)2
20
15
10
5
0
-5
-7
-6
-5
-4
-3
-2
-1
Mean of Force (nN)
Methanol
Linear Regression

Figure 6.7

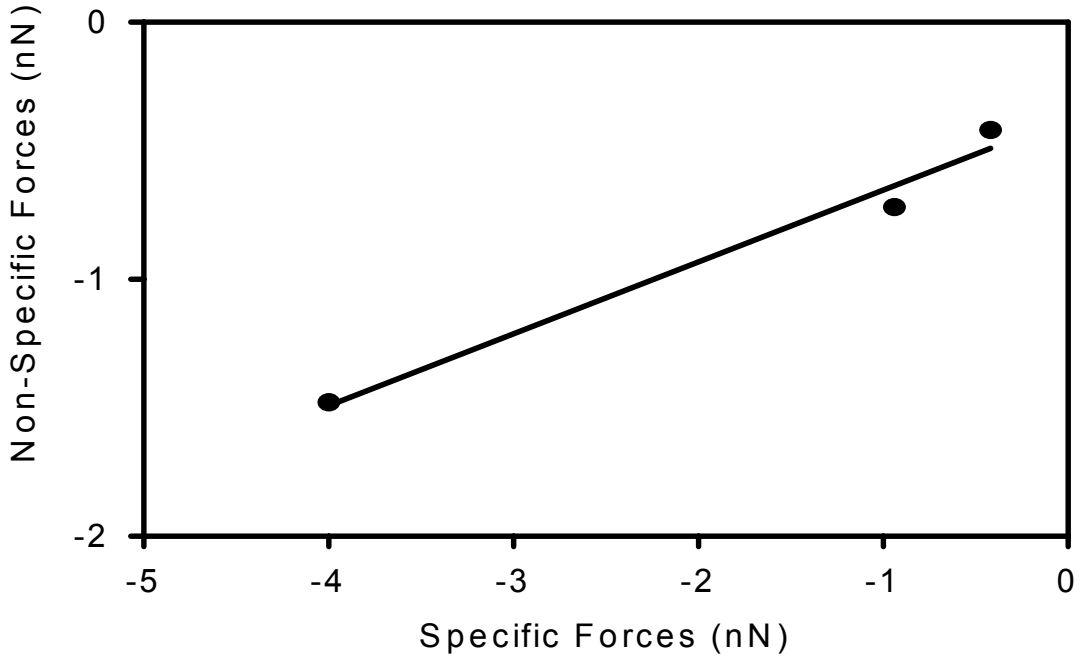

Figure 6.8

Chapter 7

Conclusions and Recommendations

7.1 Conclusions

Since its invention, the use of atomic force microscopy (AFM) to investigate biological surfaces and biological interactions with surfaces has been continuously increasing. Motivated by its high lateral and vertical resolutions, we have successfully used AFM to characterize bacterial surface biopolymers of two bacterial strains, *Pseudomonas Putida* KT2442 and *Escherichia coli* JM109. The effect of these biopolymers on macroscopic bacterial adhesion to different surfaces was further explored and related to microscopic force measurements.

Single-molecule force microscopy was successfully used to probe the elasticity of *Pseudomonas putida* KT2442 surface biopolymers in various solvents. The effect of the elasticity of the surface biopolymers on adhesion of *Pseudomonas putida* KT2442 to an AFM tip in different solvents was also investigated. The effect of ionic strength on the polymer elasticity and adhesion was studied through using salt concentrations that ranged between that of pure water to 1 M KCl solutions. The effect of polarity on polymer elasticity and adhesion was studied using methanol, water, and formamide.

Three different models were used to quantify polymer elasticity from force-extension profiles: the freely-jointed chain (FJC), wormlike chain (WLC), and extensible freely-jointed chain (FJC+) models. The FJC was found to fit the experimental data better than the WLC model. Enthalpic effects were concluded to be unimportant since the FJC+ was not better than the FJC model. The polymers were found to be very flexible, since more than 70% of the total estimated segment or persistence length of the chains was ~0.18 nm, only slightly greater than the C-C bond length (0.154 nm). Although the

polymers were flexible in all solvents, a distribution of segments lengths and persistence lengths was observed. This distribution in the segments values is the result of having different polymer types on the bacterial surface. These polymers are distributed heterogeneously on the bacterial surface, which we demonstrated for the first time using single-molecule detection technique. Adhesion forces between the bacteria and the AFM tip increased as the solvent polarity decreased; indicating that the polymers are hydrophilic.

Biopolymer conformation could also be related to adhesion. The flexibility of the biopolymers increased with decreasing polarity, indicating the more flexible the polymers, the higher the adhesion is. However, when the ionic strength effect is considered, the biopolymers on the surface of *P. putida* KT2442 were found to undergo a salt-induced conformational change from a soft, random structure in low ionic strength solutions to an ordered, rigid structure in the presence of salt. This conformational change occurs between 0.01 and 0.05 M KCl. Accompanying this conformational change, a change in the adhesion behavior of the polymer to the AFM tip was observed. Greater adhesion forces were observed between the biopolymer and silicon nitride for the softer and more charged brush layer in high ionic strength solutions. The change from repulsive to attractive interactions upon the addition of salt was predicted by soft-particle DLVO theory.

This part of my work demonstrated the important role of biopolymer physicochemical properties in governing bacterial adhesion behavior. We pointed out the need for bacterial adhesion models that account for polymer properties, conformation,

and heterogeneity. This work will be useful to those wishing to develop improved models of bacterial adhesion.

In the second part of the study, the role of specific type of biopolymer, Lipopolysaccharides (LPS), on the adhesion of *E. coli* JM109 on adhesion to an AFM silicon nitride tip, glass, and sand was investigated in detail. Adhesion between a silicon nitride tip and *E. coli* JM109 was measured in water and phosphate buffered saline (PBS) on untreated cells and on a sample of *E. coli* treated with 100 mM ethylenediaminetetraacetic acid (EDTA). EDTA removes ~ 80% of the LPS molecules and ~ 70% of the surface proteins.

LPS removal decreased the adhesion affinity between the bacterial cells and the AFM tip in both water and PBS buffer. Direct measurements of the adhesive force between *E. coli* and silicon nitride were compared with adhesion in batch (glass) and column experiments (with quartz sand as the porous media). Agreement was observed between the three systems with regard to the influences of LPS on adhesion. Bacterial batch retention to glass or attachment to sand in packed beds to quartz sand decreased after LPS removal. Steric repulsive forces measured during the approach of the AFM tip to a bacterium were greater when the LPS was intact. A model for steric repulsion confirmed a reduction of the equilibrium length of the surface polymers after removal of a portion of the LPS.

DLVO calculations based on conventional and soft-particle DLVO theories predicted higher energy barriers to adhesion for all surfaces after LPS removal, consistent with experimental findings. Adhesion forces between the AFM tip and bacterial polymers were correlated with bacterial attachment and retention, while measurements of

interaction forces during the approach of the AFM tip to the bacterium did not correlate which subsequent adhesion behavior to glass or quartz. The distribution of adhesion affinities between *E. coli* LPS macromolecules and the AFM tip could be described by normal or gamma distribution functions. We concluded from this part of the study that lipopolysaccharides control both adhesion forces and adhesion of certain types of bacterial cells measured at three scales (nanoscale, batch, and column experiments).

By this time, we had gained a good conceptual understanding of the nature of the polysaccharides on an EPS-producing soil bacterium, *P. putida*, and the subsequent effect on adhesion. But a complete picture of the nature of the interactions for a strain that does not produce EPS, such as *E. coli*, was lacking. Therefore, our final goal was to probe the nature of interactions between *E. coli* JM109 and a model surface (silicon nitride). We also examined the elastic response of the bacterial surface by calculating Young's moduli values. The Hertz model was applied to force-indentation curves to characterize the elastic modulus. Applying a Poisson distribution to the adhesion affinities gave a good estimation of the individual bond strength between the tip and the bacterial surface biopolymers in different solvents. The magnitudes of the specific and non-specific interactions were determined from the Poisson statistics. Changes in the brush conformation as a function of solvent polarity were successfully probed with AFM. The work of adhesion and the contact area between the tip and the bacterial surface biopolymers were determined with the use of thermodynamic and contact mechanics models such as those of Hertz, Derjaguin, Muller, and Toporov (DMT), and Johnson, Kendall, and Roberts (JKR) models. The contribution of DLVO and non-DLVO forces in controlling bacterial adhesion was also compared.

7.2 Recommendations for Further Study

During the course of my study, several unresolved issues that need to be addressed in more details came to my attention. A brief discussion of these issues is presented below.

In addition to these unresolved issues, some interesting preliminary results on complementary topics are also discussed.

7.2.1 Accurate Estimation of the Tip Radius

An important unresolved issue is connected to the accurate estimation of the tip radius. This issue is of great concern since the tip radius is involved in many theoretical models used to evaluate interaction forces, such as models of steric, electrostatic, and van der Waals interactions [1], and Born repulsion forces [2]. The tip radius also used to calculate the surface energy of the substrate in the adhesion models [3], and is important when the force curves need to be normalized with respect to the tip radius for comparison with other studies [4].

There is a discrepancy between the actual radius of the tip (which can be measured using electron micrographs) and the radius of interaction of the tip for the purposes of making energy calculations. For example, the radius of interaction for commonly used microfabricated silicon nitride AFM tips was estimated to range between 100 to 400 nm using a simple method developed by Senden et. al. [5]. The basic idea behind this method is to measure the interactions between a spherical particle of known radius and a planer surface, both coated with an adsorbed surfactant bilayer, in aqueous solution. This standard interaction is then compared with the measurements of the force of interaction between AFM tip and planer surfaces possessing the same adsorbed

surfactant bilayers in aqueous solution [5]. This radius of interaction value is much higher than the values reported by the manufacturer for the nominal tip radius, which is (20-40 nm)[6]. In another method of calculation, the radius of AFM tips can be obtained from one of the adhesion models. We found the radius of silicon nitride tips to range between 104 to 260 nm using JKR theory [7]. Even though it is widely accepted that the radius of interaction will be larger than the nominal tip radius, there is still no easy way to calibrate the tips for routine force measurements in order to choose appropriate values for making energy calculations and force balances.

7.2.2 Estimation of Cantilever Spring Constant

A rapid and reliable way to accurately determine the stiffness of AFM cantilevers is still unavailable. At least four different calibration methods have been published to estimate the cantilever spring constant [8]. The methods are either geometrical methods or thermal methods. The first geometrical method that is commonly used to calibrate the cantilever stiffness is the Cleveland method, based on measuring the resonant frequency of the cantilever before and after adding small end masses [9]. Order of magnitude variability in the spring constant values for a single type of cantilever was observed using this technique [8]. Although the Cleveland method is the most widely used by the tip manufacturers to estimate the cantilever spring constants, the manufacturer reported spring constant values are different from what was estimated for the same tips by different research groups [8].

The thermal methods are based on the acquisition of the cantilever's thermal distribution spectrum. Thermal methods estimate the spring constant of the cantilevers more accurately than the geometrical methods [10]. Their main disadvantage lies in their

sensitivity to the AFM tip quality and that they apply only for a limited resonant frequency [8].

The variation in the cantilever spring constant directly impacts the magnitude of measured force values. Since the force values are linearly related to the stiffness of the cantilever by Hook's law [11], the error in estimating the stiffness of the cantilever appears as an error in all the measured force values. This wide range of estimated values for the cantilever spring constant points to the critical need of finding an accurate method to measure the stiffness of the cantilever, particularly for silicon nitride cantilevers with low resonant frequencies. A paradox here is that the cantilevers which are most reliable for non-destructive probing of biological samples in liquids (i.e. silicon nitride tips with low resonant frequencies) are the tips for which it is most difficult to measure spring constant accurately.

7.2.3 Finding the Zero Separation Distance between the AFM Tip and the Substrate

A third major issue to be resolved involves the accurate estimation of the zero separation distance between the AFM tip and the sample, in this case the bacterium. Different methods have been suggested to determine the zero separation distance in AFM force measurements. The first and most-widely accepted approach was that suggested by Ducker et al. for silica spheres [12]. The "zero" or origin of the force-displacement curve was chosen to occur when the cantilever deflection was linear with respect to sample displacement at high force. The main advantage of this approach is its simplicity; however it is only accurate on hard surfaces. When the interactions are measured on a soft sample, the cantilever deflection is a non-linear function of displacement. On soft

samples, Hertz theory provides an accurate estimate of the zero of the displacement [13]. Although this method provides a non-linear relation between the deflection and the displacement, it is not easy to be applied on regular basis within time limits.

Another approach is developed to determine the origin of the distance separation is used in the special case in which an attraction is observed in the approach curve. The method considers the point at which the tip contacts the surface as the zero distance of separation (Figures 7.1A and B) [14].

Finally, one can use a simple method to determine the zero of the distance is by taking the zero with respect to the distance at the point at which the derivative of the force with respect to the distance changes from zero to higher values. This method is simple, but the problem with the technique is the great scattering in the derivative data, which makes it tough to decide the exact zero point (Figures 7.2 A and B).

These difficulties and uncertainties in determining the zero of the force displacement curve present a challenge for scientists to find an easy and an accurate way to calibrate AFM data.

7.2.4 Bacterial Adhesion Models

The available adhesion and bacterial interaction force models are not without limitations. First, roughness of the interacting surfaces is usually ignored as almost all adhesion models were developed for smooth surfaces, with the exception of few cases [15-17]. A second limitation is that the effect of the biopolymer charge was not counted in the existing bacterial models. Most of the interactions between bacteria and different surfaces were always explained by the use of one of these theories: DLVO theory [18] and soft-particle DLVO theory [19]. Although both theories were used to explain the adhesion of

bacteria to different surfaces, they cannot account for the charge effect when studied on a polymer brush leading to inaccurate prediction for the bacterial adhesion.

The polymer models we used were developed for neutral molecules. Examples of these models are the FJC [11], WLC [20], and steric models of polymer behavior [1]. The lack of understanding of the effect of the charge of the biopolymers and roughness on bacterial adhesion raises the need to develop a comprehensive adhesion model that accounts for all different properties of the two interacting media and for solvent properties.

7.2.5 Chemical Force Microscopy to Probe Bacterial-Natural Organic Matter Interactions

Interactions between bacterial cell surfaces and the natural organic matter (NOM) play an important role in governing adhesion of bacteria to soil [21]. Since NOM coats nearly all soil surfaces [22], an investigation of how bacterial strains adhere to NOM will be useful bioremediation studies.

In a preliminary work, the interactions between two bacterial strains (*Pseudomonas putida* KT2442 *and Escherichia coli* JM109) and a chemically modified AFM silicon nitride tip were measured. The silicon nitride tips were chemically modified with carboxylic groups (Figure 7.3) to mimic the natural organic matter (NOM) in subsurface. Although the procedure for tips modification is simple, a basic problem was associated with it. The problem simply lies in covering the silicon nitride tips with a thin homogeneous gold layer. The gold layer is required to self-assemble the carboxylic groups on the tip surface through covalent bonding between thiol groups and the gold layer (Figure 7.3)[23-25]. AFM control measurements between cleaned glass surface and

gold coated tips (the tips were coated by sputtering a gold layer over the tip under vacuum) showed non-reproducible force measurements (Figure 7.4). A better control on the sputtering process might result in a more homogeneous gold coating. To continue our investigation, gold coated tips were purchased from Bioforce Laboratory. Reproducible control experiments could be obtained between these tips and a clean glass surface (Figure 7.5). Measurements between tips functionalized with carboxylic groups and bacterial cells showed an obvious difference in the magnitude of the repulsive forces compared to bare tips (Figure 7.6). These preliminary results were encouraging to continue this investigation.

A few steps must be taken before measuring the interactions between NOM and bacteria. First, more control experiments between the modified AFM tip and cleaned glass have to be done to make sure that the chemical modification procedure is reproducible. Second, an optimization of several parameters in the chemical modification procedure has to be done. Examples on these parameters are the incubation period for the tips in the 16-mercaptohexadecanoic acid and the acid concentration.

7.2.6 The Use of Peptides as Biosensors

A complementary topic was investigated that can provide the impetus for further study, preliminary data on the use of peptides as biosensors for *E. coli*, in the context of food biosafety was obtained. The capability of biosensors lies in the measurement of proteins binding to other proteins as well as to DNA, RNA, receptors, antibodies, and membranes. Most peptides were shown to be accessible at the cell surface in terms of metal binding [26]. For example, recombinant *Staphylococcus carnosus* and

Staphylococcus xylosus strains were generated with surface exposed chimeric proteins containing polyhistidyl peptides designed for binding to divalent metal ions [27].

In my preliminary study, a known sequence of cys-cecropin P1 peptide was attached to an AFM tip covered by a gold layer. The interactions between this peptide and *E. coli* JM109 proteins were measured in PBS buffer. The successful modification of the tip with the peptide was confirmed by the big difference in the repulsion magnitudes reported in the approach curves (Figure 7.7). An average adhesion force of –1.31 nN was measured between the cells and the peptides. These results are encouraging since a significant adhesion was measured between the peptide and the bacterial surface proteins. Further exploration of the effect of higher peptide concentration, and the time-dependence of the bacterial-peptide interaction is needed.

7.3 References

1. Camesano, T.A. and B.E. Logan, *Probing bacterial electrosteric interactions using atomic force microscopy.* Environmental Science & Technology, 2000. **34**: p. 3354-3362.
2. Abu-Lail, N.I. and T.A. Camesano, *Role of ionic strength on the relationship of biopolymer conformation, DLVO contributions, and steric interactions to bioadhesion of pseudomonas putida KT2442.* Biomacromolecules, 2003. **4**(4): p. 1000-1012.
3. van der Vegte, E.W. and G. Hadziioannou, *Scanning force microscopy with chemical specificity: An extensive study of chemical specific tip-surface interactions and the chemical imaging of surafce functional groups.* Langmuir, 1997. **13**(16): p. 4357-4368.
4. Frank, B.P. and G. Belfort, *Intermolecular forces between extracellular polysaccharides measured with the atomic force microscope.* Langmuir, 1997. **13**: p. 6234-6240.
5. Drummond, C.J. and T.J. Senden, *Examination of the geometry of long-range tip-sample interaction in atomic force microscopy.* Colloids and Surfaces A: Physicochemical and Engineering Aspects, 1994. **87**: p. 217-234.
6. *Dimension^{TM} 3100 Series Scanning Probe Microscope Instruction Manual*. 1998, Digital Instruments: Santa Barabara, CA.
7. Abu-Lail, N.I. and T.A. Camesano, *Nature of Interaction Forces between E. coli JM109 and a Model Surface.* 2003.

8. Burnham, N.A., X. Chen, C.S. Hodges, G.A. Matei, E.J. Thoreson, C.J. Roberts, M.C. Davies, and S.J.B. Tendler, *Comparison of calibration methods for atomic-force microscopy cantilevers.* Nanotechnology, 2003. **14**: p. 1-6.

9. Cleveland, J.P., S. Manne, D. Bocek, and P.K. Hansma, *Nondestructive method for determining the spring constant of cantilevers for scanning force microscopy.* Review of Scientific Instruments, 1993. **64**: p. 403-405.

10. Hutter, J.L. and J. Bechhoefer, *Calibration of atomic-force microscope tips.* Review of Scientific Instruments, 1993. **64**(7): p. 1868-1873.

11. Janshoff, A., M. Neitzert, Y. Oberdorfer, and H. Fuchs, *Force spectroscopy of molecular systems-single molecule spectroscopy of polymers and biomolecules.* Angew. Chem. Int. Ed., 2000. **39**: p. 3212-3237.

12. Ducker, W.A., T.J. Senden, and R.M. Pashley, *Direct measurement of colloidal forces using an atomic force microscope.* Nature, 1991. **353**: p. 239-241.

13. Radmacher, M., M. Fritz, C.M. Kacher, J.P. Cleveland, and P.K. Hansma, *Measuring the viscoelastic properties of human platelets with the atomic force microscope.* Biophysical Journal, 1996. **70**(1): p. 556-567.

14. Ong, Y.-L., Razatos, A., Georgiou, G., Sharma, M.M., *Adhesion forces between E. coli bacteria and biomaterial surfaces.* Langmuir, 1999. **15**: p. 2719-2725.

15. Johnson, K.L., *Contact Mechanics*. 1985, Cambridge: Cambridge University Press. 452.

16. Rabinovich, Y.I., J.J. Adler, A. Ata, R.K. Singh, and B.M. Moudgil, *Adhesion between nanoscale rough surfaces 2. Measurement and Comparison with Theory.* Journal of Colloid and Interface Science, 2000. **232**: p. 17-24.

17. Rabinovich, Y.I., J.J. Adler, A. Ata, R.K. Singh, and B.M. Moudgil, *Adhesion between nanoscale rough surfaces 1. Role of Asperity Geometry.* Journal of Colloid and Interface Science, 2000. **232**: p. 10-16.

18. Israelachvili, J.N., *Intermolecular & Surface Forces (2nd edition)*. 1992, New York: Academic Press.

19. Hayashi, H., S. Tsuneda, A. Hirata, and H. Sasaki, *Soft particle analysis of bacterial cells and its interpretation of cell adhesion behaviors in terms of DLVO theory.* Colloids and Surfaces B: Biointerfaces, 2001. **22**(2): p. 149-157.

20. Ortiz, C. and G. Hadziioannou, *Entropic elasticity of single polymer chains of poly(methylacrylic acid) measured by atomic force microscopy.* Macromolecules, 1999. **32**: p. 780-787.

21. Smets, B.F., D. Grasso, M.A. Engwall, and B.J. Machinist, *Surface physicochemical properties of Pseudomonas fluorescens and impact on adhesion and transport through porous media.* Colloids and Surfaces B: Biointerfaces, 1999. **14**: p. 121-139.

22. Johnson, W.P. and B.E. Logan, *Enhanced transport of bacteria in porous media by sediment-phase and aqueous-phase natural organic matter.* Water Research, 1996. **30**: p. 923-931.

23. Keller, H., W. Schrepp, and H. Fuchs, *Self-assembled organic films on gold and silver.* Thin Solid Films, 1992. **210/211**: p. 799-802.

24. Akari, S., D. Horn, H. Keller, and W. Schrepp, *Chemical imaging by scanning force microscopy.* Advanced Materials, 1995. **7**: p. 849-551.

25. Noy, A., C.D. Frisbie, L.F. Rozsnyai, M.S. Wrighton, and C.M. Lieber, *Chemical force microscopy: Exploiting chemically-modified tips to quantify adhesion, friction, and functional group distribution in molecular assemblies.* Journal of the American Chemical Society, 1995. **117**: p. 7943-7951.

26. Wernerus, H., J. Lehtio, P. Samuelson, and S. Stahl, *Engineering of staphylococcal surfaces for biotechnological applications.* Journal of Biotechnology, 2002. **96**: p. 67-78.

27. Samuelson, P., H. Wernerus, M. Svedberg, and S. Ståhl, Science, 2000. **268**: p. 103.

28. Ong, Y.-L., A. Razatos, G. Georgiou, and M.M. Sharma, *Adhesion forces between E. coli bacteria and biomaterial surfaces.* Langmuir, 1999. **15**: p. 2719-2725.

7.4 Figure Captions

Figure 7.1. A) The relation between cantilever's deflection and distance measured between *E. coli* JM109 and silicon nitride tip in methanol. B) The same curve in A) zeroed on the way suggested by Ong et. al.[28] The solid line in part A corresponds to the zero point in part B.

Figure 7.2. A) The distance-force curve measured between *Pseudomonas Putida* KT2442 and silicon nitride tip in 1 M KCl. B) The corresponding dF/dX versus distance curve for part A. The dotted lines are those showing the scattering range of the data. The solid line refers to where the zero point should be taking according to this technique.

Figure 7.3. Schematic diagram of the tip after being modified with the carboxylic groups.

Figure 7.4. Force measurements between gold coated tips (coated by sputtering under vacuum) and cleaned glass surface in water. Each curve represents a different gold coated tip. The force curves show the irreproducibility of the force measurements due to heterogeneities in the gold layer coating. Each curve is an average of 15 individual force measurements between the gold coated tip and the glass surface.

Figure 7.5. Force measurements between gold coated tips (Bought from Bioforce Laboratory) and cleaned glass surface in water. Each curve represents a different gold coated tip. The force curves show the reproducibility of the force measurements due to homogeneous gold coating. Each curve is an average of 15 individual force measurements between the gold coated tip and the glass surface.

Figure 7.6. Comparison between force measurements performed on *E. coli* JM109 surface with bare tips and carboxylic groups modified tips in water. The solid line is the force measurements with the use of bare silicon nitride tip while the dotted line is the force measurements with the chemically modified tip. Each curve is an average of 15 individual force curves.

Figure 7.7. The average of approach curves measured between a bare tip and a clean glass surface (the solid line), and between the modified tip with cys-cecropin P1 peptide and a clean glass surface (the dotted line).

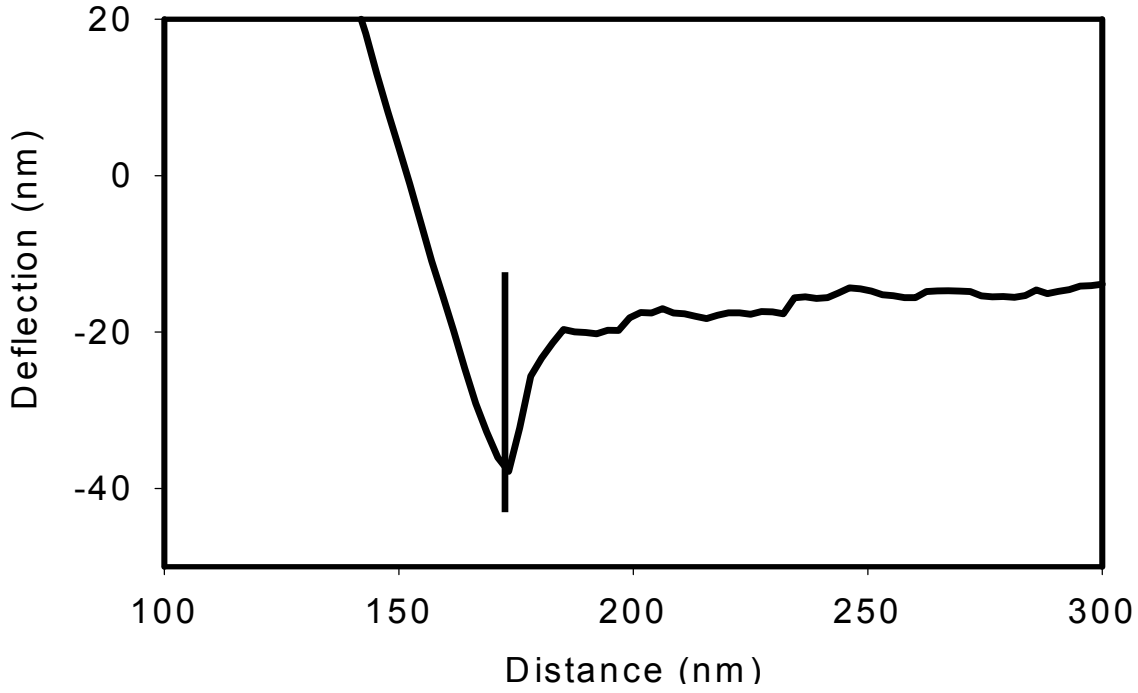
20
0
-20
-40
Deflection (nm)
100
150
200
250
300
Distance (nm)

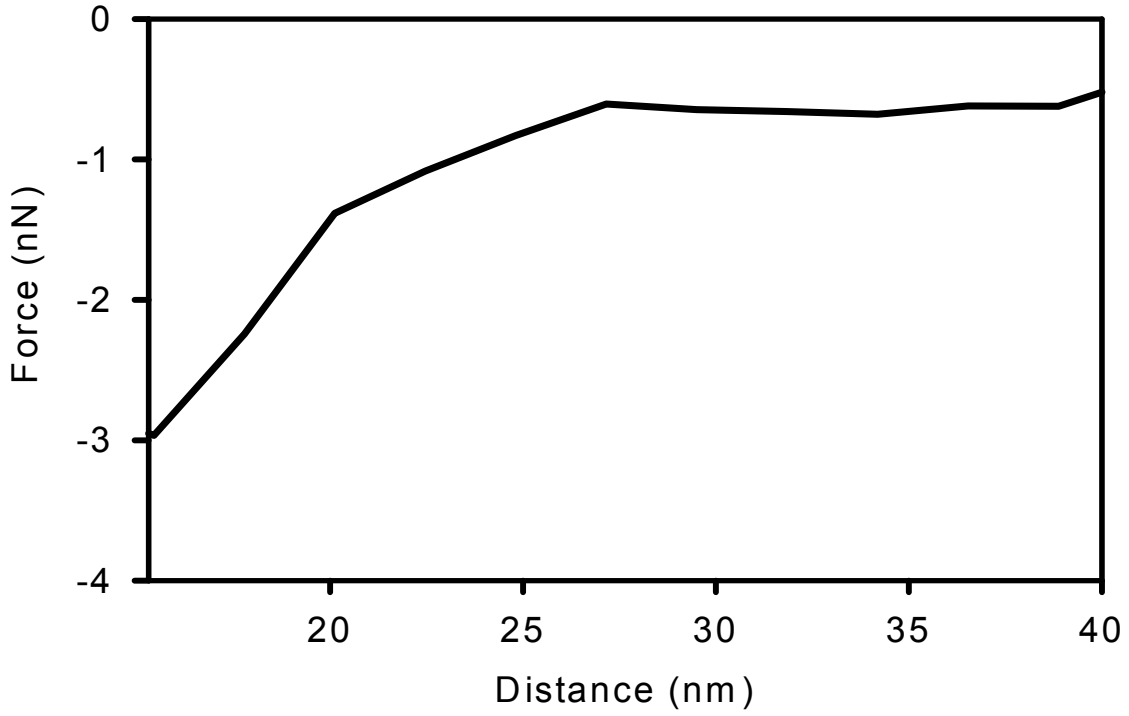
0
-1
-2
-3
-4
Force (nN)
20
25
30
35
40
Distance (nm)

Figure 7.1

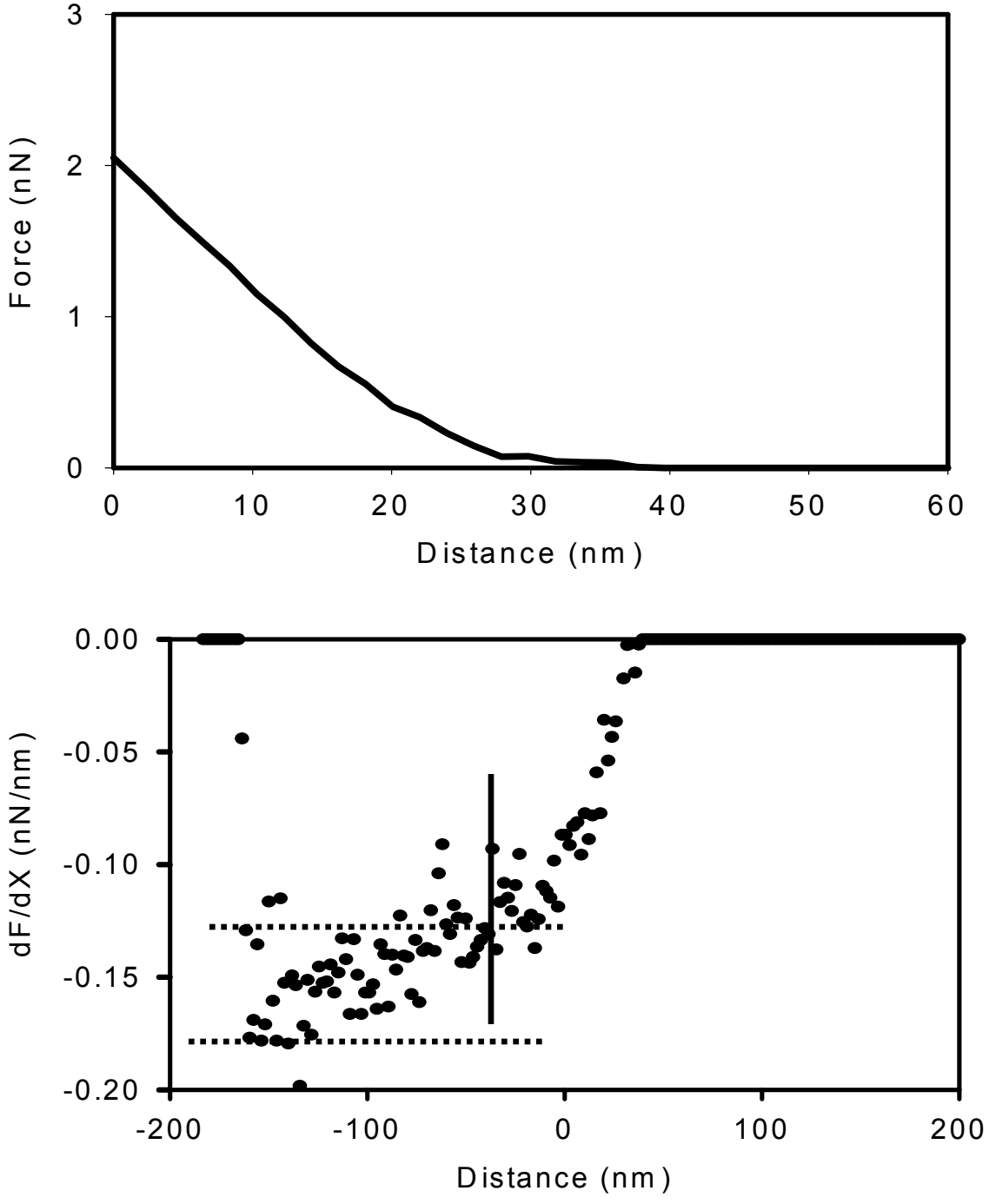
3
2
1
0
Force (nN)
0
10
20
30
40
50
60
Distance (nm)
0.00
-0.05
-0.10
-0.15
-0.20
dF/dX (nN/nm)
-200
-100
0
100
200
Distance (nm)

Figure 7.2

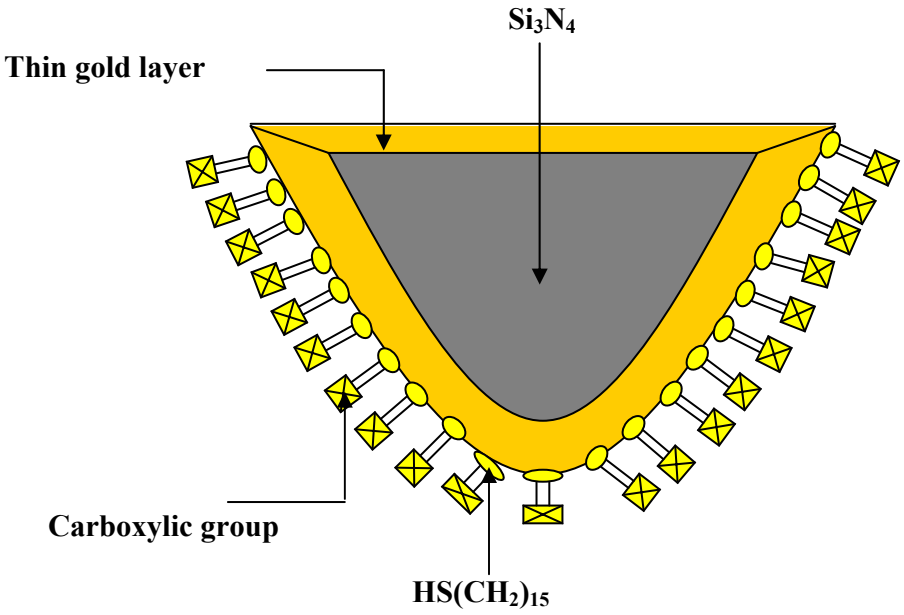

Figure 7.3

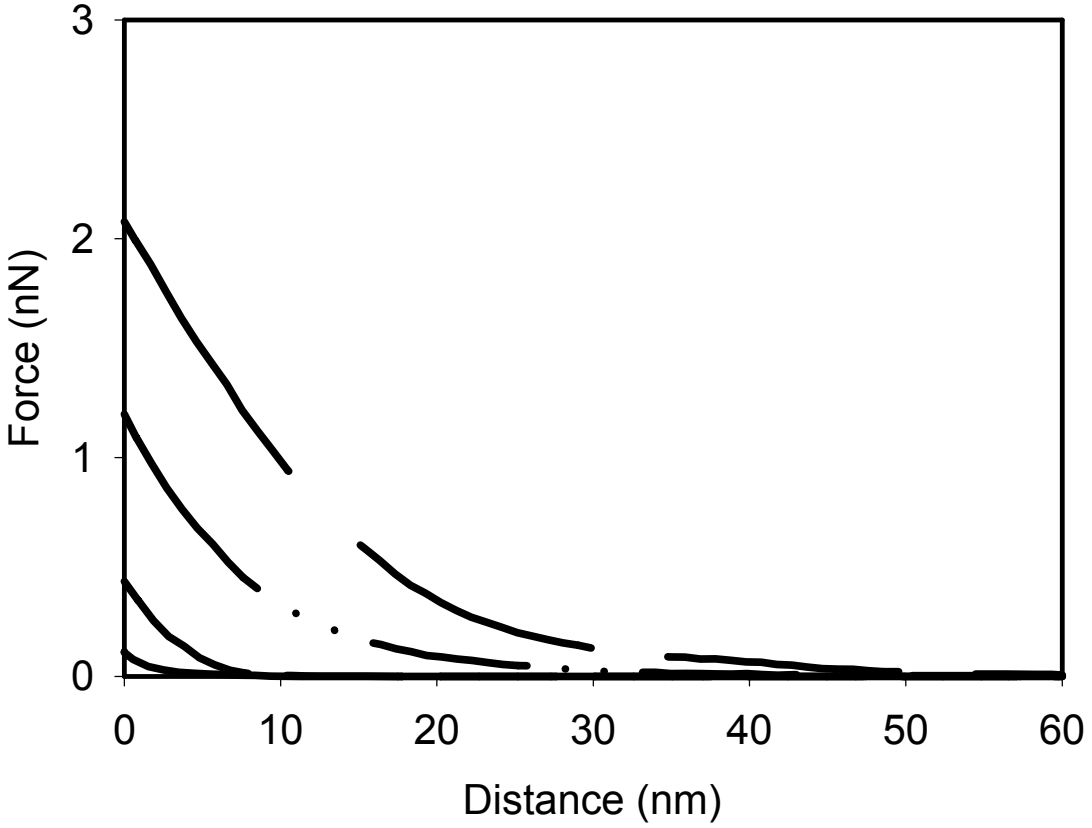

Figure 7.4

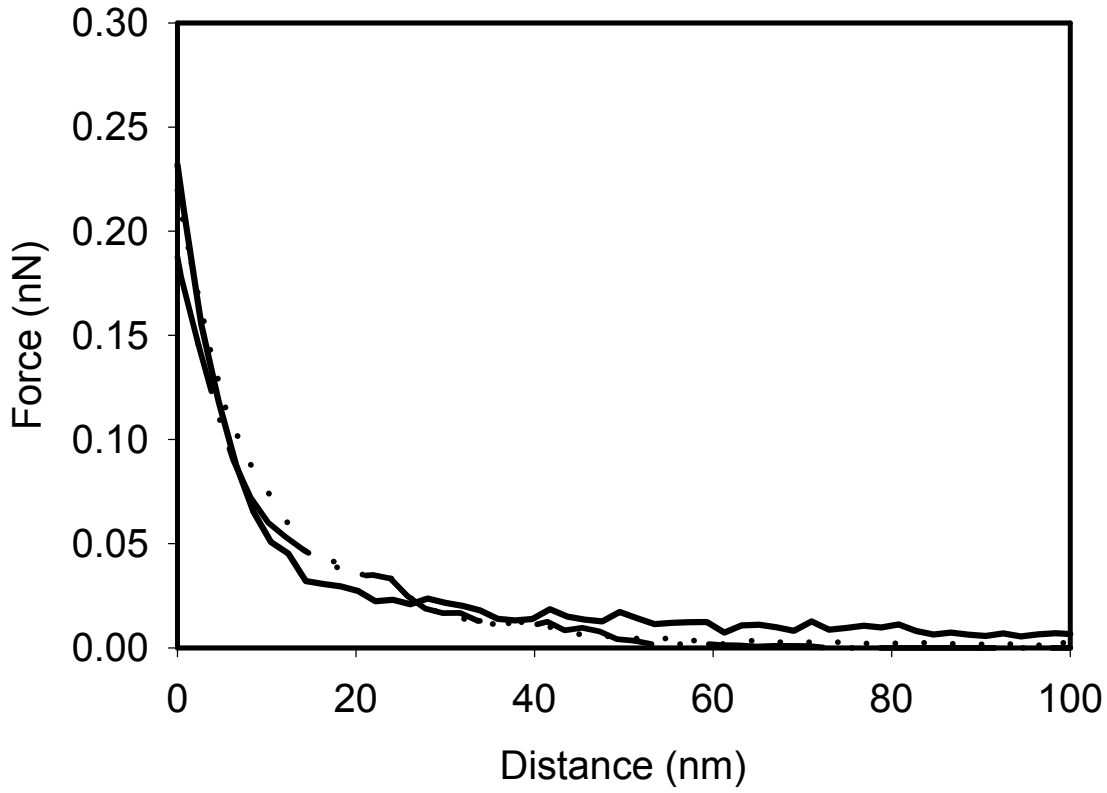
0.30
0.25
0.20
0.15
0.10
0.05
0.00
Force (nN)
0
20
40
60
80
100
Distance (nm)

Figure 7.5

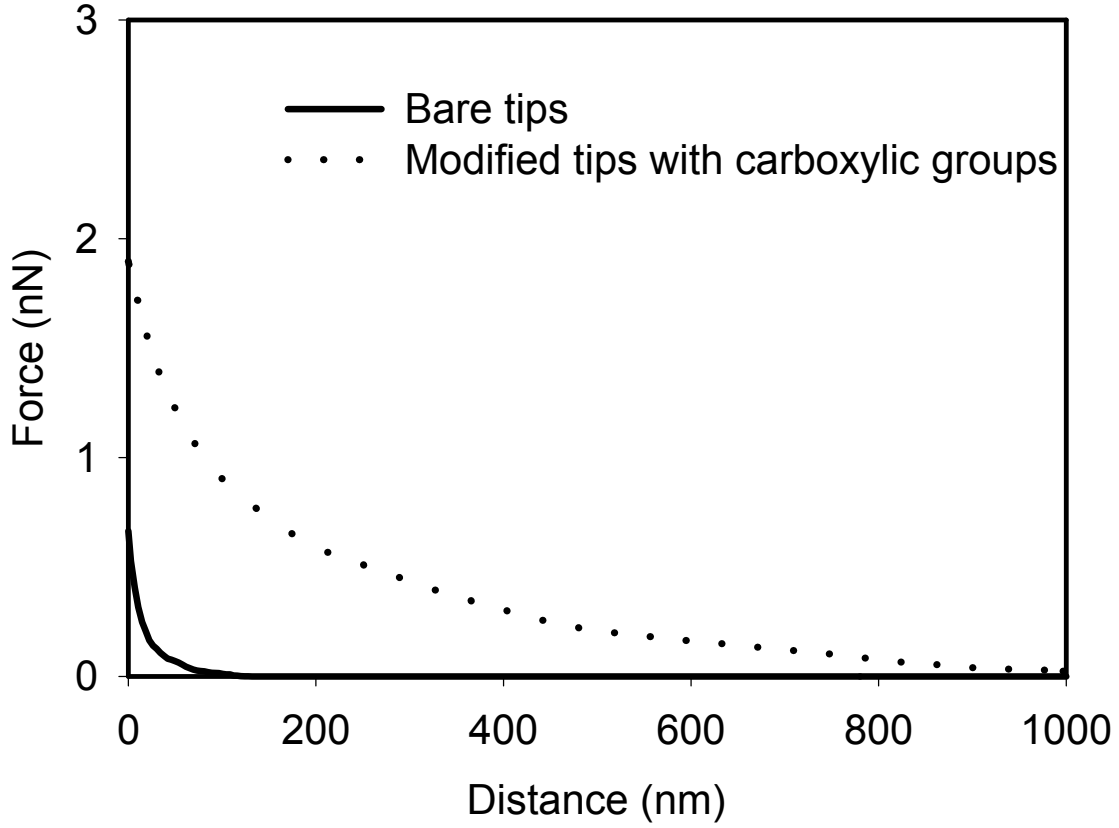
Bare tips
Modified tips with carboxylic groups
Force (nN)
Distance (nm)
0
1
2
3
0
200
400
600
800
1000

Figure 7.6

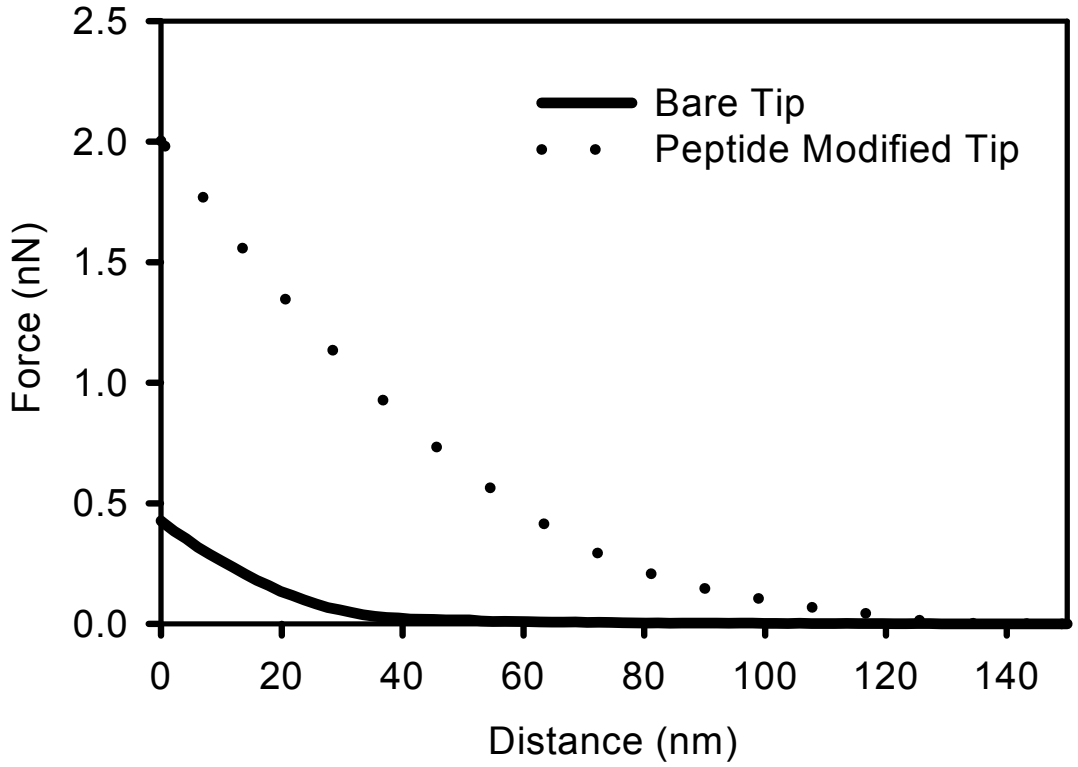
2.5
2.0
1.5
1.0
0.5
0.0
Force (nN)
0
20
40
60
80
100
120
140
Distance (nm)
Bare Tip
Peptide Modified Tip

Figure 7.7

Appendix

Supplementary information to accompany chapter five "The Role of Lipopolysaccharides in the Adhesion, Retention, and Transport of *Escherichia coli* JM109"

A. 1 Energy Calculations using DLVO Theories

DLVO interaction energy barriers between bacteria and glass were calculated using eqs. 5.2-5.7 (Figure S1A, and S1B). The energy barriers were greater using conventional zeta potential theory compared to soft-particle theory. Comparing the energy barriers between the untreated *E. coli* JM109 cells and the EDTA treated *E. coli* JM109 cells showed that the energy barrier was greater for cells treated with EDTA to partially remove their LPS.

A.2 Reproducibility in Force Measurements

The intrinsic heterogeneity of the bacterial cells and their biopolymers affects the interaction and adhesion forces measured with AFM. The best way to deal with the heterogeneity is to make many measurements and to use statistical models to help describe the interaction forces and the biopolymer properties. The symbols in Figure S2 demonstrate five measurements of the forces during the approach of the AFM silicon nitride tip to an *E. coli* bacterium. The solid line is the average of those five measurements on a single cell. The dotted line is the average of 25 measurements on five different bacterial cells under the same experimental conditions.

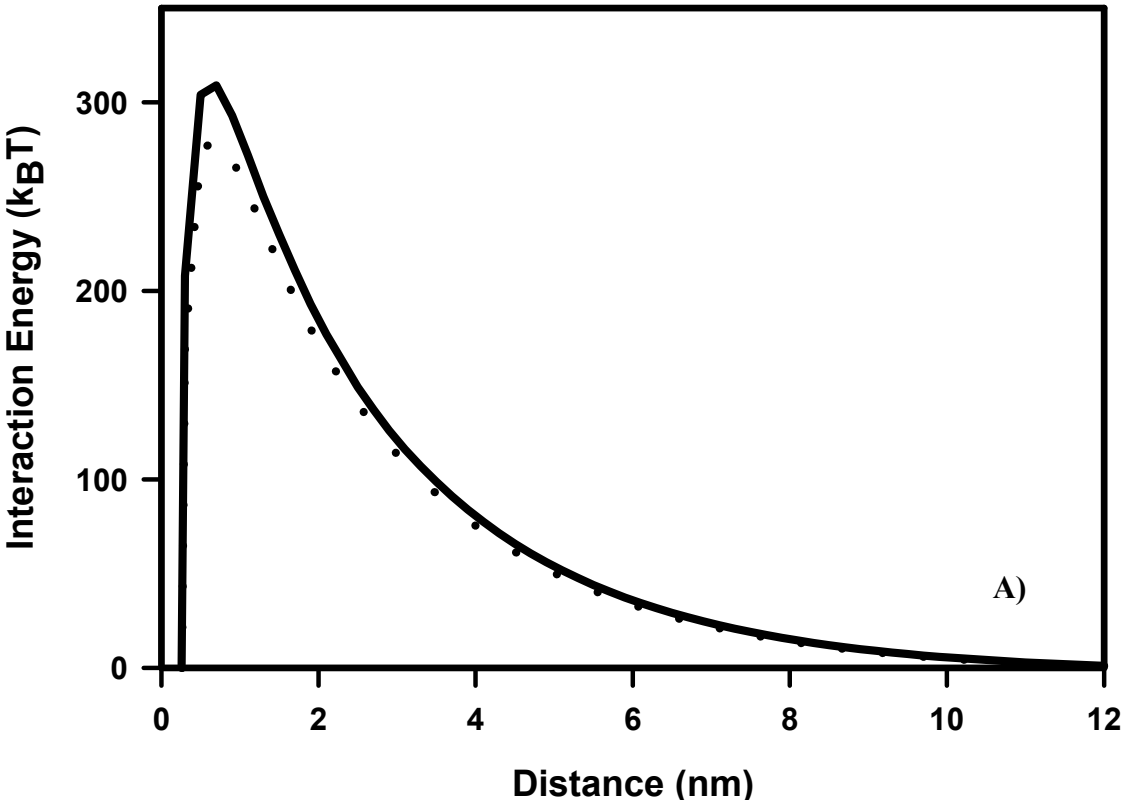
Interaction Energy (k_BT)
300
200
100
0
0
2
4
6
8
10
12
Distance (nm)
A)

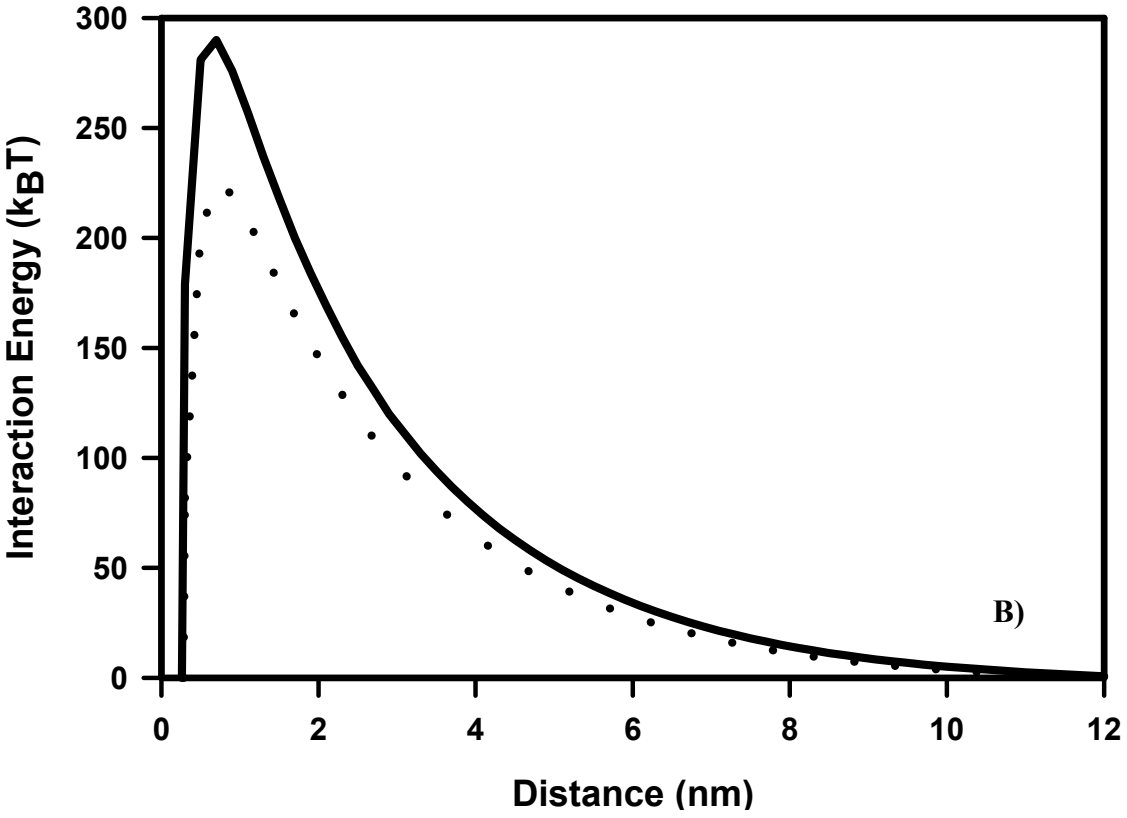
300
250
200
150
100
50
0
Interaction Energy (k_BT)
0
2
4
6
8
10
12
Distance (nm)
B)

Figure S1

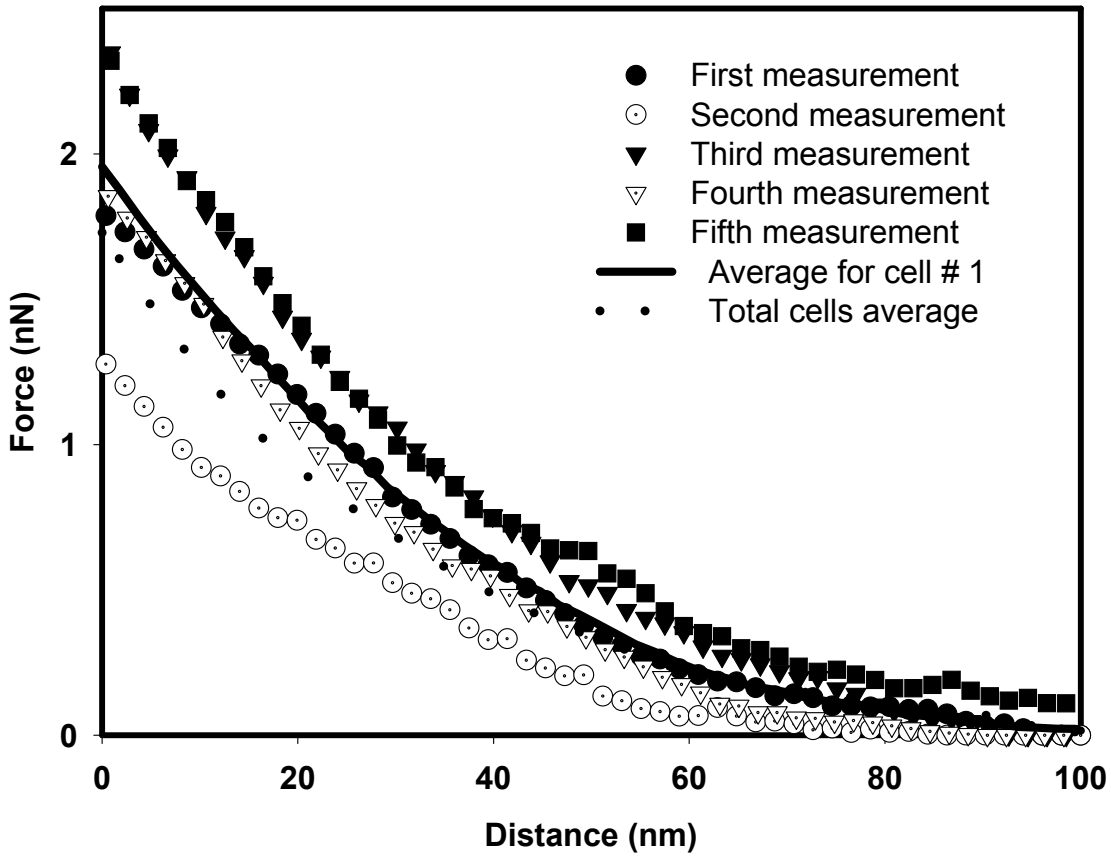
First measurement
Second measurement
Third measurement
Fourth measurement
Fifth measurement
Average for cell # 1
Total cells average
Force (nN)
Distance (nm)
0
1
2
0
20
40
60
80
100

Figure S2

A.3 Figure Captions

Figure S1. Total interaction energy curves based on DLVO theory. A) Between untreated *E. coli* JM109 bacterial cells and glass. B) Between EDTA-treated *E. coli* JM109 bacterial cells and glass. Solid curves represent calculated results based on conventional zeta potentials (eq. 5.5). Dashed lines are calculations based on soft-particle DLVO theory (eq. 5.6). Parameters used in the calculations were: Hamaker constant = 10^{-20} J, pH = 7.0, temperature = 298 K, ionic strength – 0.02 M KCl, ζ_{glass} = -0.29 mV, $a_{bacterium}$ = 0.5 μm. For untreated cells, $\zeta_{bacterium,conv.}$ = -22.9 mV, $\zeta_{bacterium,soft}$ = -20.2 mV, and for treated cells $\zeta_{bacterium,conv.}$ = -23.7 mV, $\zeta_{bacterium,soft}$ = -22.6 mV.

Figure S2. Representative example demonstrating reproducibility in the approach curves. The symbols show five different measurements done on one *E. coli* JM109 bacterium. The solid line represents the average of these five different measurements while the dotted line represents an average for 25 measurements done on five different cells. All measurements were done in PBS using a DNP-S silicon nitride tip.